UCRL 9566

UNIVERSITY OF CALIFORNIA

Ernest O. Lawrence Radiation Laboratory

CHEMISTRY DIVISION ANNUAL REPORT, 1960

TWO-WEEK LOAN COPY

This is a Library Circulating Copy which may be borrowed for two weeks. For a personal retention copy, call Tech. Info. Division, Ext. 5545

UCRL-9566

DISCLAIMER

This document was prepared as an account of work sponsored by the United States Government. While this document is believed to contain correct information, neither the United States Government nor any agency thereof, nor the Regents of the University of California, nor any of their employees, makes any warranty, express or implied, or assumes any legal responsibility for the accuracy, completeness, or usefulness of any information, apparatus, product, or process disclosed, or represents that its use would not infringe privately owned rights. Reference herein to any specific commercial product, process, or service by its trade name, trademark, manufacturer, or otherwise, does not necessarily constitute or imply its endorsement, recommendation, or favoring by the United States Government or any agency thereof, or the Regents of the University of California. The views and opinions of authors expressed herein do not necessarily state or reflect those of the United States Government or any agency thereof or the Regents of the University of California.

Research and Development

UCRL-9566
UC-4 Chemistry-General
TID-4500(16th Ed.)

UNIVERSITY OF CALIFORNIA
Lawrence Radiation Laboratory
Berkeley, California

Contract No. W-7405-eng-48

CHEMISTRY DIVISION ANNUAL REPORT, 1960

February 1961

Printed in USA. Price $4.50. Available from the
Office of Technical Services
U. S. Department of Commerce
Washington 25, D.C.

CHEMISTRY DIVISION ANNUAL REPORT, 1960

Contents

INTRODUCTION 11

A. RADIOACTIVITY AND NUCLEAR SPECTROSCOPY

1. States of Even-Even Nuclei in the Near-Harmonic Region: Spectra of Rn^{218}, Rn^{220}, and Rn^{222} (Stephens, Asaro, and Perlman). 12
2. Analysis of Long-Range Alpha-Emission Data (Griffioen and Rasmussen). 17
3. The Energy Levels of Uranium-233 (Albridge, Gallagher, Hamilton, and Hollander) 19
4. The Decay of Neptunium-238 (Albridge and Hollander). . . . 22
5. Coulomb Excitation of Vibrational Levels in Uranium-238 and Thorium-232 (Elbek, Igo, Stephens, and Diamond) 25
6. The Alpha Decay of Fermium-255 (Asaro, Stephens, Thompson, and Perlman) 28
7. The Isomers of Americium-242 (Asaro, Perlman, Rasmussen, and Thompson). 32
8. Alpha Decay of Long-Lived Americium-242 (Asaro, Michel, Thompson, and Perlman) 32
9. Decay Scheme of Einsteinium-253 (Asaro, Thompson, Stephens, and Perlman) 39
10. Alpha-Particle and Gamma-Ray Studies and Half-Life Determinations of Members of the Uranium-229 and Uranium-228 Families (Ruiz, Asaro, and Perlman) 42
11. Search for Electric Monopole Transition Following Alpha Decay of Plutonium-239 (Bjørnholm and Asaro) . . . 46
12. Alpha-Decay Studies in the Rare Earth Region (Macfarlane) 46
13. Alpha Decay to Beta Vibrational States in Even-Even Nuclei (Asaro and Perlman) 50
14. High-Energy Gamma Rays in the Decay of 27-hour Holmium-166 (Horen and Chiao) 53
15. Anomalous Electric Dipole Conversion Coefficient in Odd-Mass Isotopes of the Heavy Elements (Asaro, Stephens, Hollander, and Perlman) 57

*Preceding reports (semiannual): UCRL-9093, UCRL-8867

16. Absolute Measurements of Internal-Conversion Coefficients, Particularly of E2 Character, by the Method of Internal-External Conversion (Hollander, Horen, and Hultberg) 57

17. Theory of E0 Transition Probabilities of Deformed Nuclei (Rasmussen) 62

18. Odd-Even Shift in the K=0 Band of Odd-Odd Deformed Nuclei (Newby) 63

19. Tensor-Force Effects in Odd-Odd Spherical Nuclei (Newby) 64

20. Theoretical Calculations of Magnetic Moments of Spheroidal Nuclei (Chiao and Rasmussen) 65

21. Nuclear Orientation of Iodine by Electric hfs Alignment (Shirley, Johnson, and Schooley) 70

22. Nuclear Orientation of Terbium-160 (Shirley, Johnson, and Schooley) 73

23. Nuclear Alignment of Neodymium-147 (Westenbarger and Shirley) 75

24. Nuclear Orientation of Dysprosium-155 and Dysprosium-157 (Navarro and Shirley) 79

25. Nuclear Orientation of Promethium-144 (Schooley, Shirley and Rasmussen) 80

26. Nuclear Moment of Cerium-137m by Nuclear Alignment (Haag, Johnson, Shirley, and Templeton) 84

27. The Mössbauer Effect in Gold-197 (Shirley, Axel, and Kaplan) 89

28. The Neutron-Deficient Chain Strontium-80–Rubidium-80 (Hoff, Hollander, and Michel) 95

29. New Neutron-Deficient Iridium Isotopes: Iridium-182, -183, and -184 (Diamond, Hollander, Horen, and Naumann) 96

B. FISSION

1. Ternary Spontaneous Fission of Californium-252 (Brown, Gibson, Scheer, and Thompson). 99

2. Fission of Gold by Carbon Ions (Gordon, Larsh, and Sikkeland) 101

3. Mass-Yield Curve for Fission in the Reaction C^{12}(112 Mev) + U^{238} → fission (Haines) 106

4. Angular Distributions for Heavy-Ion-Induced Fission Reactions (Viola) 109

5. The Effect of Angular Momentum on Fission Probability (Gilmore, Perlman, and Thompson) 111

6. Fission of Uranium-238 by Carbon Ions (Sikkeland, Larsh, and Gordon) 115

7. Composition-Dependent Surface Energy of Heavy Nuclides and Spontaneous Fission (Brandt and Thompson) . . . 120

8. Fission Barrier Heights in Elements Lighter Than Radium (Burnett and Thompson) 124

C. NUCLEAR REACTIONS

1. Total Reaction Cross Sections (Wilkins and Igo) 126

2. Theoretical Reaction Cross Sections for Alpha Particles with the Optical Model (Huizenga and Igo) 128

3. The Reaction $C^{12}(\alpha, d)N^{14}$ (Cerny and Harvey) 133

4. The Reactions $Li^{6}(\alpha, d)Be^{8}$ and $N^{14}(\alpha, d)O^{16}$ (Cerny, Harvey, and Pehl) 138

5. The Two-Nucleon Stripping Reaction (Glendenning) 143

6. Recoil Studies of Nuclear Reactions Induced by Heavy Ions (Alexander and Winsberg) 145

7. Recoil Properties of Fission Products (Alexander and Gazdik) 145

8. The n, α Reaction Induced by Thermal Neutrons (Griffioen) 147

9. Studies in Low-Level Liquid Scintillation Counting (Kaufman, Nir, and Parks) 152

10. On Some Applications of the α, n Reactions on Oxygen-18 (Nir) 152

11. Heavy-Ion Elastic Scattering (Alster and Conzett) 153

12. Elastic Scattering of 31-Mev He^{3} Ions (Gonzalez-Vidal, Igo, and Markowitz) 158

13. Ranges and Range Straggling of Terbium-149, Astatine, and Polonium (Winsberg and Alexander) 174

14. Polarization in p-He^4 Scattering at 22 Mev (Conzett, Igo, and Nir) 174

15. Survey of Tritium-Producing Nuclear Reactions (Gonzalez-Vidal and Wade) 177

16. Self-Transfer of Californium-252 (Gatti, Phillips, Bowman, and Thompson) 184

D. PHYSICAL CHEMISTRY

1. Reactions of Accelerated Carbon-14 Ions with Benzene (Lemmon, Mullen, and Reynolds) 189

2. The Radiolysis of Biacetyl Vapor (Mains and Newton) . . . 190

3. The Mercury-Sensitized Radiolysis and Photolysis of Methane (Mains and Newton) 193

4. The Radiation Chemistry of the Symmetrical Dichloroethylenes (Futrell and Newton) 196

5. Crystal and Molecular Structure of the Compound of Triethyl Phosphine and Carbon Disulfide (Margulis and Templeton) 198

6. Crystal Structure of Hydrogen Peroxide Dihydrate (Olovsson and Templeton) 200

7. Crystal Structure of Vanadyl Bisacetylacetonate: Geometry of Vanadium in Fivefold Coordination (Dodge, Templeton, and Zalkin) 203

8. Single-Crystal Tungsten Ribbon (Reynolds). 204

9. Mechanisms of Ion Exchange (Whitney and Diamond) . . . 208

10. Submicrogram Methods Used in Studies of the Synthetic Elements (Cunningham) 210

11. Preparation and Crystal Structure of Americium Metal (McWhan, Wallmann, and Cunningham) 218

12. Atomic Beam Research (Marrus) 219

13. Hyperfine Structure and Nuclear Moments of Protactinium-233 (Marrus, Nierenberg, and Winocur) 220

14. The Magnetic Dipole and Electric Quadrupole Interaction Constants of Bismuth-210 (Alpert, Lipworth, White, and Smith) 220

15. Nuclear Moments of Iodine-133 (Alpert, Lipworth, and White) 221

16. Nuclear Moments of Iodine-132 (White, Alpert, Garvin, and Lipworth) 221

17. Nuclear Spin and Hyperfine Structure of Lutetium-176m (White, Alpert, and Lipworth) 222

18. Nuclear Spins of Promethium-149, Promethium-151, and Terbium-160 (Cabezas, Lindgren, Marrus, and Rubinstein) 222

19. Electronic Energy Levels and Crystal Quantum States of Thulium(IV) (Gruber and Conway) 222

20. Evaluation of Electrostatic Energy Levels of f^6 (Gruber and Conway) 228

21. Theory of Zeeman Effect in the Ground Multiplets of Rare Earth Atoms (Judd) 235

22. Crystal-Field Splitting of Energy Levels of Thulium Ethylsulfate (Gruber and Conway) 237

23. Paramagnetic Resonance Hyperfine Structure of Tetravalent Pa^{231} in Cs_2ZrCl_6 (Axe, Stapleton, and Jeffries) 245

24. Paramagnetic Resonance in Tetravalent Protactinium-231 (Axe, Kyi, and Stapleton) 246

25. Nuclear Quadrupole Resonance Studies (Reddoch) 247

E. INSTRUMENTATION

1. Use of Silicon p-n Junction Detectors in Studies of Nuclear Reactions Induced by Heavy Ions (Larsh, Gordon, Sikkeland) 248

2. A Modification of the Super-Snapper Pulse-Height Analyzer (Mosier and Leres) 254

3. Energy Resolution in Semiconductor Particle Detectors (Hansen and Goulding) 256

4. A Multiplex Punched-Tape Pulse-Height Analyzer (Wydler) 258

5. Summary of 1960 Hilac Operations (Hubbard) 260

F. CHEMICAL ENGINEERING

1. Conductivities in Emulsions (Meredith and Tobias) 264
2. Fractional Crystallization from Melts (Wilcox and Wilke) 264
3. Diffusion Coefficients in Multicomponent Solvents (Holmes, Olander, and Wilke) 265
4. Free and Forced Convection in a Diaphragm-Type Diffusion Cell (Holmes, Olander, and Wilke) 267
5. Coalescence and Dispersion Rates in Agitated Liquid-Liquid Systems (Vanderveen and Vermeulen) 269
6. Downflow Boiling and Nonboiling Heat Transfer in a Uniformly Heated Tube (Sani and Bromley) 270
7. Resistance to Potential Flow through a Cubical Array of Spheres (Meredith and Tobias) 272
8. Nonequilibrium Thermodynamic Theory for Concentration Profiles in Liquid Extraction (Hennico and Vermeulen) 272
9. Longitudinal Dispersion in Two-Phase Continuous-Flow Operations: Solution and Tables for Cocurrent Flow (Miyauchi, McMullen, and Vermeulen) 273
10. A Digital Computer Program for Tributyl Phosphate Solvent-Extraction Column Design (Olander) 276

G. THESIS ABSTRACTS 278

1. Electronic and Nuclear Properties of Some Radioactive Rare-Earth Elements (Cabezas). 279
2. A Mass-Spectrometric Investigation of Sulfur Vapor as a Function of Temperature (Zietz) 283
3. The Electronic Structure of Octrahedrally Coordinated Protactinium IV (Axe) 284
4. I. Beta-Spectroscopic Studies in the Promethium Region. II. The Coriolis Interaction in Deformed Nuclei (Marshall) 285
5. Chemical Properties of Astatine (Appelman) 286
6. Fission and Spallation in Nuclear Reactions Induced by Heavy Ions (Gordon) 287
7. Coincidence Measurements in Nuclear Decay-Scheme Studies (Unik) 288

8. Fission of Gold with 112-Mev C^{12} Ions: A Yield-Mass and Charge-Distribution Study (Blann) 289

9. Some Low-Temperature Nuclear Orientation Studies (Schooley) 291

10. Perturbation of Alpha-Gamma Angular Correlations in Transuranium Isotopes (Flamm) 292

11. Some Problems of Crystallography (Johnson) 293

12. The Cross Sections for the Formation of Astatine Isotopes Made by the Bombardment of Bismuth-209 with Helium-3 (Strom) 294

13. $N^{15}(p, p2n)N^{13}$ Reaction Induced by Protons of Energy 0.4 to 6.2 Bev (Sah) 295

14. Oxidation Potential of the Ce(III)-Ce(IV) Couple as a Function of Temperature in Perchloric Acid Solutions: Thermodynamic Properties (Conley). 296

15. Ionic Mass Transport by Free Convection to Horizontal Electrodes (Fenech) 297

16. Longitudinal Dispersion in Beds of Finely Divided Solids (Robinson) 298

17. Charged-Particle-Induced Fission: A Mass Spectrometric Yield Study (Chu) 299

18. Some Nuclear and Electronic Ground-State Properties of Protactinium-233, Americium-241, and 16-hr Americium-242 (Winocur) 301

19. Nuclear Spectroscopic Studies in the Heaviest-Element Regions; An Accelerating Electron Spectrograph (Albridge) 303

H. AUTHOR INDEX OF UCRL REPORTS FOR 1960 304

AUTHOR INDEX 329

CHEMISTRY DIVISION ANNUAL REPORT, 1960*

Lawrence Radiation Laboratory
University of California
Berkeley, California

February 1961

INTRODUCTION

Jack M. Hollander, Frederick L. Reynolds, and James C. Wallmann

This report presents a review of the research progress made during the 1960 calendar year by the Nuclear Chemistry Division of the Lawrence Radiation Laboratory. Though the report is not exhaustive, an effort has been made to give a balanced view of the widely ranging research interests and problems of the Division. Contributors to this report include staff members of the Radiation Laboratory, graduate students, and visiting post-doctoral chemists and physicists from many laboratories, domestic and foreign.

Nineteen Ph. D. theses were awarded during 1960 to graduate students who did their research work in this Division, and six Master's theses were given. Abstracts of these theses are included in this report.

In previous progress reports issued semiannually, Lawrence Radiation Laboratory work in the areas of high-temperature chemistry and inorganic materials appeared along with material presented in this report. Such work will now be covered in a separate report.

*This work was done under the auspices of the U. S. Atomic Energy Commission.

A. RADIOACTIVITY AND NUCLEAR SPECTROSCOPY

1. STATES OF EVEN-EVEN NUCLEI IN THE NEAR-HARMONIC REGION: SPECTRA OF RADON-218, RADON-220, AND RADON-222 (*)

Frank S. Stephens, Frank Asaro, and I. Perlman

Gamma-ray singles and coincidence spectra have been measured in the α decay of Ra^{222}, Ra^{224}, and Ra^{226}. Excluding the prominent transitions from the first excited states, the energies (and abundances relative to total α emission) of the observed radiations were:

Ra^{222}: 325 kev (8.4×10^{-5}), 475 kev (7×10^{-5}), 525 kev (2×10^{-5}), and 798 kev (2.5×10^{-4});

Ra^{224}: 290 kev (9×10^{-5}), 410 kev (4×10^{-5}), 650 kev (6×10^{-5});

Ra^{226}: 260 kev (0.9×10^{-4}), 420 kev (7×10^{-6}), 450 kev (3×10^{-6}), 610 kev (1.0×10^{-5}). The observed γ-γ coincidences were

Ra^{222}: 325-325 kev, 325-475 kev, and 325-525 kev;

Ra^{224}: 241-290 kev and 241-410 kev;

Ra^{226}: 188-260 kev and 188-420 kev. It was not strictly determined that the Ra^{222} radiations were not due to other members of the Th^{226} family. These data have been used to deduce the levels, spins, and parities in the daughter Rn nuclides as shown in Figs. A.1-1, A.1-2, and A.1-3. The 2+ states in Rn^{220} and Rn^{222} have been previously assigned by Scharff-Goldhaber.[1] These results are incorporated in a general energy-level systematics of even-even nuclei in the heavy-element region, as shown in Fig. A.1-4.

---

*Brief version of published paper, Phys. Rev. 119, 796 (1960).

[1] G. Harbottle, M. McKeown, and G. Scharff-Goldhaber, Phys. Rev. 103, 1776 (1956); G. Scharff-Goldhaber, Phys. Rev. 103, 837 (1956).

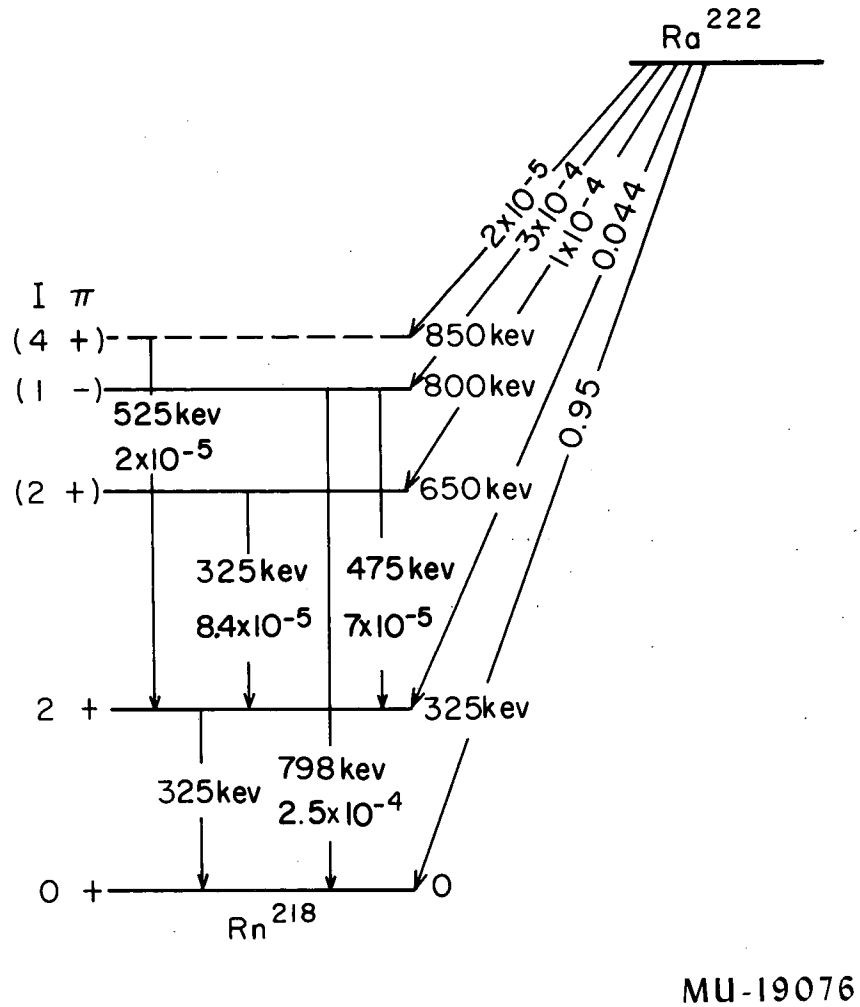

Fig. A. 1-1. Decay scheme of Ra^{222}.

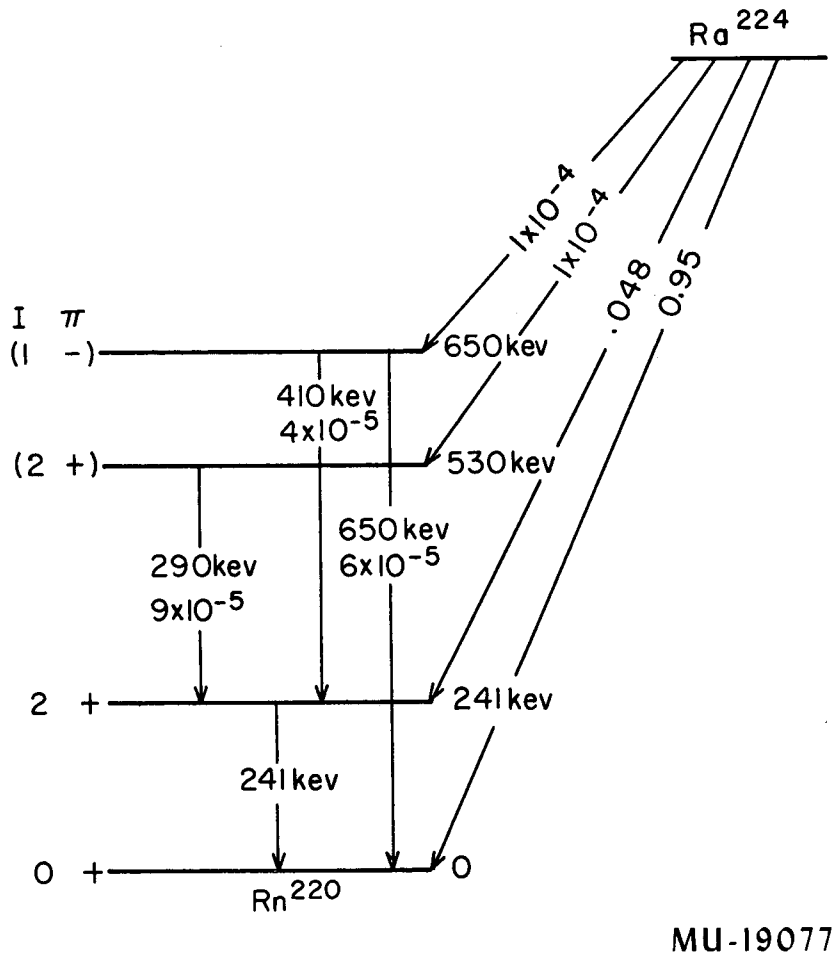

Fig. A. 1-2. Decay scheme of Ra^{224}.

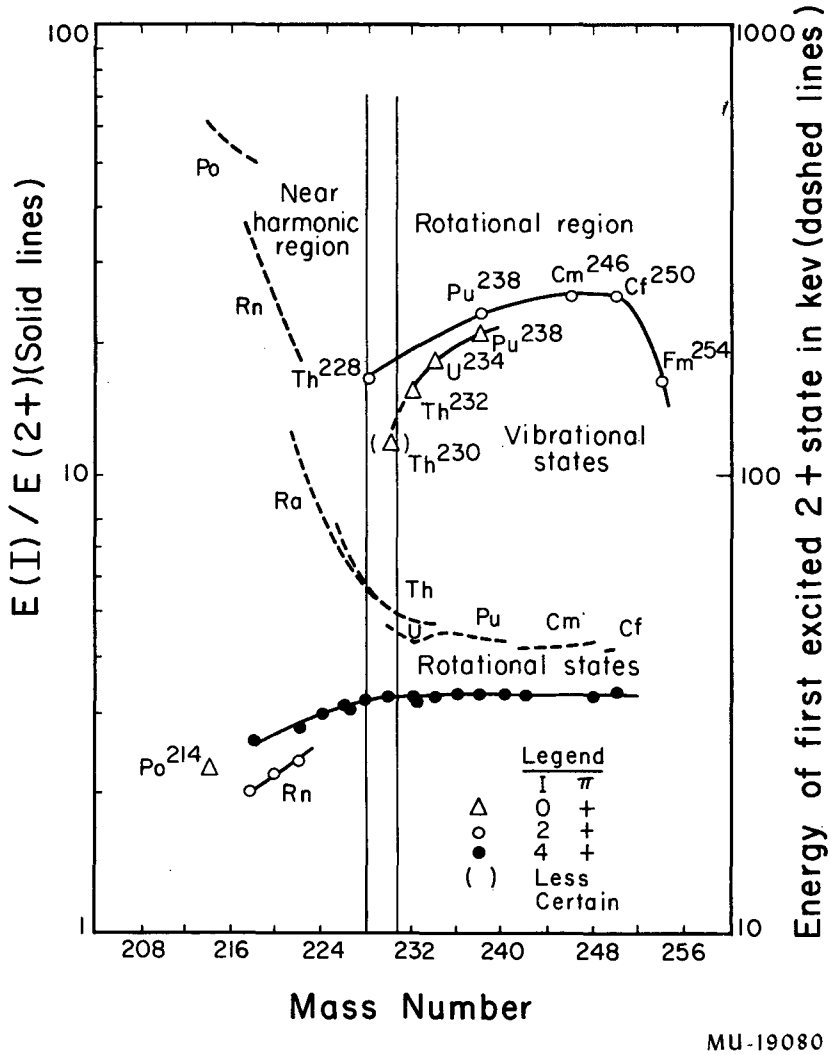

Fig. A. 1-4. Even-parity states in even-even nuclides.

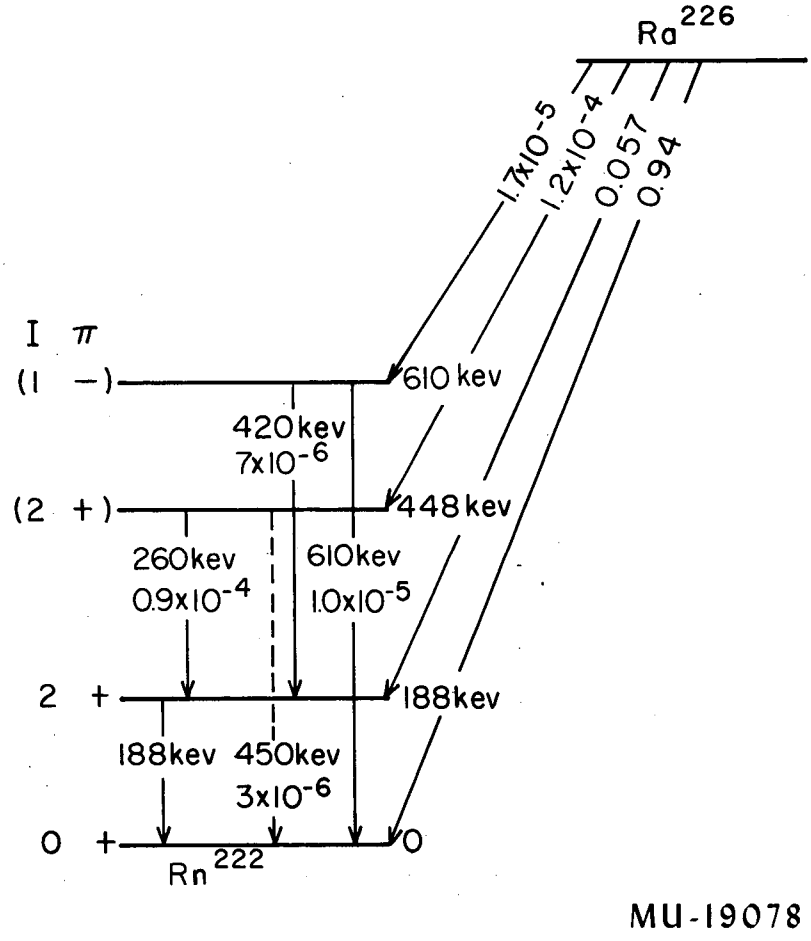

Fig. A. 1-3. Decay scheme of Ra^{226}.

2. ANALYSIS OF LONG-RANGE ALPHA-EMISSION DATA (*)

Roger D. Griffioen and John O. Rasmussen

INTRODUCTION

Rasmussen has reported α-decay barrier-penetration calculations made with use of an exponential nuclear potential.[1,2] Details of the calculation were discussed[1] and numerical results for all measured α transitions of even-even[1] and odd-mass[2] nuclei were given. The α-nuclear potential used was the real part of a potential given by Igo to fit α-elastic-scattering data:[4]

$$V(r) = -\ 1100 \exp \left\{ \frac{1.17\, A^{1/3} - r}{0.574} \right\} \text{Mev.}$$

This potential is used here to calculate, with the IBM 650 computer, the α-decay barrier-penetration factors for the long-range α particles from the excited states of Po^{212} and Po^{214}. The centrifugal potential for the angular momentum of the α particle, as determined from the decay schemes, is included in these calculations. The penetration factors are used to calculate the partial half lives of the levels for α decay, with the assumption that the decay is unhindered with respect to the ground-state decay. The relative α particle and γ-ray abundances are then used to calculate partial half lives for the gamma transitions from these same states.

Po^{214}

In the case of Po^{214}, two different proposed level schemes and decay schemes are used. The first of these, due to Bishop,[4] assumes that all the long-range α groups arise from transitions to the ground state of Pb^{210}. The second, due to Hauser,[5] proposes that three of the long-range α groups arise from transitions to excited states of Pb^{210}. This proposal was made to account for the fact that γ rays from the levels corresponding to some of the α groups have not been detected.

The α barrier-penetration factor, P, is calculated for each of the states, assuming spins and parities as indicated by the two decay schemes. This penetration factor is then used to calculate the partial α half life for each level:

$$t_{\alpha,\ \text{excited state}} = t_{\alpha,\ \text{ground state}} \left(P_g / P_e \right) ,$$

where P_g and P_e are penetration factors for the ground-state and excited-state α decay.

---

*Brief version of a paper (UCRL-9368) submitted to Physical Review.

[1] J.O. Rasmussen, Phys. Rev. 113, 1593 (1959).

[2] J.O. Rasmussen, Phys. Rev. 115, 1675 (1959).

[3] G. Igo, Phys. Rev. Letters 1, 72 (1958).

[4] G.R. Bishop, Nuclear Phys. 5, 358 (1958).

[5] U. Hauser, Z. Physik 150, 599 (1958).

This partial α half life and the relative α and γ abundances lead to partial γ half lives which are compared with single-particle γ half lives calculated from the formulae given by Moszkowski.[6] The value obtained by Nierhaus and Daniel[7] of 19% of the β transitions in Bi^{214} going directly to the ground state of Po^{214} was used. The γ-ray intensities in both cases are taken from the work of Bishop[4] and of Dzhelepov et al.[8]

No α group has been detected from the 1378-kev level. By analogy with the E2 transitions from the 1281-and 1416-kev levels the partial gamma half life of the 1378-kev γ ray is assumed to be five times the single-particle value. This assumption gives a value of 2.7 α particles from this level per 10^6 ground-state transitions. This number could easily be unresolved from the abundant α group from the 0+ 1416-kev level; thus, the data on this level are consistent with the α-decay data.

The calculations also show that it is reasonable that some of the γ rays from certain α-emitting states have not been detected. On the other hand, the second decay scheme allows one to calculate relative reduced transition probabilities, δ^2 (see Reference 1), for the decay of a few given levels to the first excited state and to the ground state of Pb^{210}. This ratio increases greatly as the energy increases. This would indicate that the transition to the ground state becomes quite hindered as the energy of the initial state increases.

The results of these calculations do not differ appreciably from those of Hauser,[5] who used a simpler potential and experimental level spacings. The calculations on the groups leading to excited states are very interesting. The large variation in reduced transition probabilities indicates that the assumption of α decay to the excited states of Pb^{210} may not be valid.

Po^{212}

The level scheme and decay scheme of Po^{212} due to Emery and Kane[9] and also to Sergeev et al.[10] is used in these calculations. The γ intensities and multipolarities are taken from Emery and Kane and the level energies from Sergeev et al.

Partial α and γ half lives are calculated as in the case of Po^{214}. The results here differ by a factor of about two from those of Emery and Kane,[9] who also based their calculations on the ground-state decay while using a simpler potential.

---

[6] S. A. Moszkowski, in Beta- and Gamma-Ray Spectroscopy, K. Siegbahn, Ed. (Interscience Publishers, New York 1955), Chap. XIII.

[7] R. Nierhaus and H. Daniel, Z. Naturforsch. 12A, 1 (1957).

[8] B. Dzhelepov, S. Shestopalova, and I. Uchevatkin, Nuclear Phys. 5, 413 (1958).

[9] G. T. Emery and W. R. Kane, Phys. Rev. 118, 755 (1960).

[10] A. G. Sergeev, E. M. Krisyuk, G. D. Latyshev, Yu. N. Trofimov, and A. S. Remennyi, Soviet Phys.--JETP 6, 878 (1958).

Ratios of single-particle half lives to experimental half lives[11, 12, 13] for first excited (2+) states in even-even nuclei are known for many isotopes in the vicinity of this mass region. The ratios calculated here for Po^{212} and Po^{214} agree well with the general trend, indicating that the assumption of unhindered alpha decay is probably good for these first excited states.

[11] D. Strominger, J. M. Hollander, and G. T. Seaborg, Revs. Modern Phys. 30, 585 (1958).

[12] R. H. Davis, A. S. Divatia, D. A. Lind, and R. D. Moffat, Phys. Rev. 103, 1801 (1956).

[13] F. K. McGowan and P. H. Stelson, Phys. Rev. 99, 112 (1956).

3. THE ENERGY LEVELS OF URANIUM-233

Royal G. Albridge, Jr., C. J. Gallagher, J. H. Hamilton, and J. M. Hollander

The energy levels of U^{233} have been studied by means of the decay of the 27-day β emitter Pa^{233}. High-resolution conversion-electron and γ-ray spectrometry were employed, with use of permanent field 180-deg electron spectrographs,[1] an iron-free double-focusing β spectrometer (Uppsala),[2] and a 2-meter curved-crystal γ-ray diffraction spectrometer (Pasadena),[3] as well as lower-resolution β- and γ-ray techniques. Sources of Pa^{233} were prepared by irradiation of Th^{232} in high-flux reactors.

A summary of the conversion-electron and photon energies is given in Table I, together with the multipolarities of the transitions, which were determined from the total conversion coefficients and subshell conversion ratios.

From analyses of transition energies, intensities, and multipolarities, the decay scheme of Fig. A. 3-1 has been constructed. The assigned quantum states indicate that the ground-state β transition proceeds largely by the "unique" $\Delta I = 2$, yes, type of decay, since $\Delta I = 1$ transitions are K-forbidden ($\Delta K = 2$). In addition, the first-forbidden transition to the ground state is "hindered," in the notation of Alaga,[4] since a selection rule on the asymptotic quantum number Λ is violated. These considerations are consistent with the observed log ft of 9.16 for the ground-state β transition.

[1] W. G. Smith and J. M. Hollander, Phys. Rev. 101, 746 (1956).

[2] K. Siegbahn and K. Edvarson, Nuclear Phys. 1, 137 (1956).

[3] J. W. M. DuMond, in Beta- and Gamma-Ray Spectroscopy, edited by K. Siegbahn (Interscience Publishers, Inc., New York, 1955).

[4] G. Alaga, Phys. Rev. 100, 432 (1955); Nuclear Phys. 4, 625 (1957).

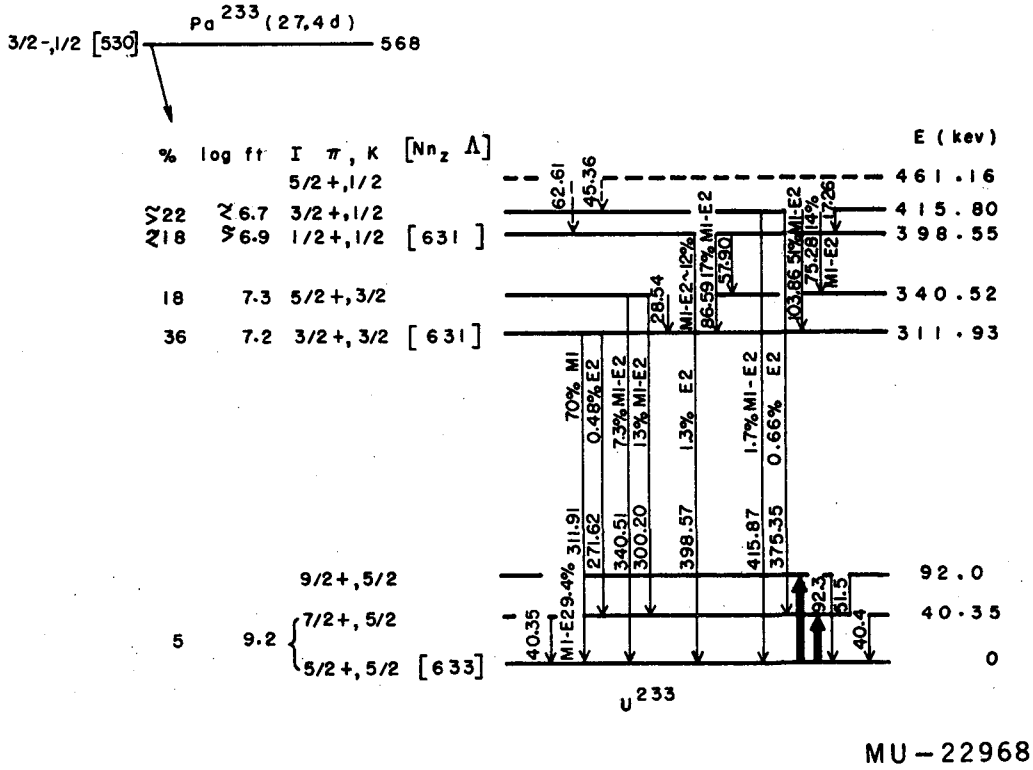

Fig. A. 3-1. The energy levels of U^{233}.

Table I. Decay data for Pa^{233}

Transition energy (kev)		Multipolarity		Total transition intensity (in % β decay)
from conversion-electron data	from photon data	M1 (%)	E2 (%)	
17.26		----		----
28.54		98	2	≈12
40.29	40.35	70	30	9.4
57.90				
75.13	75.28	98	2	14
86.45	86.59	97	3	17
103.6	103.86	95	5	5.1
	145.4			
271.5	271.6		100	0.48
299.8	300.2	90	10	13
311.7	311.9	100		70
340.3	340.5	95	5	7.3
375.5	375.4		100	0.66
398.3	398.6		100	1.3
415.6	415.9	22	78	1.7

From the measured M1-E2 mixing ratio of the 40.3-kev transition and the known magnetic and quadrupole moments of U^{233}, the g factors for the odd particle and for the "core" in U^{233} are calculated to be, respectively,

$$g_{\Omega} = 0.157, \qquad g_R = 0.320.$$

Newton has previously reported values for g_R of 0.17 or 0.28.[5] From theory, g_R is expected to have the value $g_R \approx Z/A \approx 0.4$.[6]

The levels in U^{233} at 311 and 340 kev are interpreted as the 3/2 and 5/2 members of a rotational band based on the Nilsson level 3/2+[631].[7] The experimental log ft values for β decay to these states are consistent with first-forbidden "nonunique" decay (ΔI = 0 or 1, yes) and hence in agreement with the assigned spins and parities. There are some quantitative differences between the observed and predicted[4] branching ratios for beta decay to these states, however.

The levels at 398 and 416 kev are assigned as the 1/2+ and 3/2+ members of a K = 1/2 rotational band based on the Nilsson level 1/2+ [631]. Evidence

5. J.O. Newton, Nuclear Phys. 5, 218 (1958).

6. A. Bohr and B.R. Mottelson, Kgl. Danske Videnskab Selskab., Mat.-fys. Medd. 27, No. 16 (ed 2, 1957).

7. B.R. Mottelson and S.G. Nilsson, Mat.-fys. Skr. Danske Videnskab Selskab. 1, No. 8 (1959).

for this assignment comes mainly from the pure E2 character of the 375- and 398-kev transitions, and from the partial M1 character of the 416-kev transition.

In a comparison of the intensities of transitions depopulating the 3/2+ 416-kev level, the intensity ratio of the E2 components of the 375- and 416-kev radiations is in agreement with theory, while the ratio of the M1 components of the 75- and 103-kev radiations differs by a factor of at least two from theory. This latter discrepancy may possibly be due to admixture of state 1/2+[640] with the K = 1/2 or K = 3/2 bands.

A full description of this work has been submitted for publication in Nuclear Physics.

4. THE DECAY OF NEPTUNIUM-238 (*)

Royal G. Albridge, Jr. and Jack M. Hollander

A study has been made of the energy levels of Pu^{238} which are populated by Np^{238} β decay, by an examination of the Np^{238} internal-conversion electron spectrum in high-resolution 180-deg permanent-field electron spectrographs. The level scheme of Pu^{238}, as presently well understood, is shown in Fig. A. 4-1.

In earlier studies of Np^{238}, two prominent transitions at around 1030 kev had not been completely resolved and the γ transition between the K = 2, I = 2+ state and the K = 0, I = 4+ state had not been seen; therefore it had not been possible to make a complete comparison of the experimental transition intensities with those predicted by the Bohr-Mottelson theory.[1] In this work, the composite transition at approx 1030 has been resolved into transitions of 1027.4 kev and 1029.9 kev, with relative intensities which disagree with the results of Baranov and Shlyagin,[2] who reported that the lower component (1027) was more intense than the higher-energy component (1030). We find the opposite to be the case.

The experimental transition intensities are compared in Table I with the theoretical values,[1] for various K values of the initial states. The results support the value K = 2 for the upper rotational band, but because of the relatively poor agreement of experimental and theoretical ratios, admixtures of other K values cannot be ruled out.

---

*Brief version of a paper (UCRL-8034 Rev.) submitted to Nuclear Physics.

[1] Alaga, Alder, Bohr, and Mottelson, Kgl. Danske Videnskab. Selskab Mat.-fys. Medd. 29, No. 9 (1955).

[2] S. A. Baranov and K. N. Shlyagin, Atomnaya Energ. 1, 52 (1956).

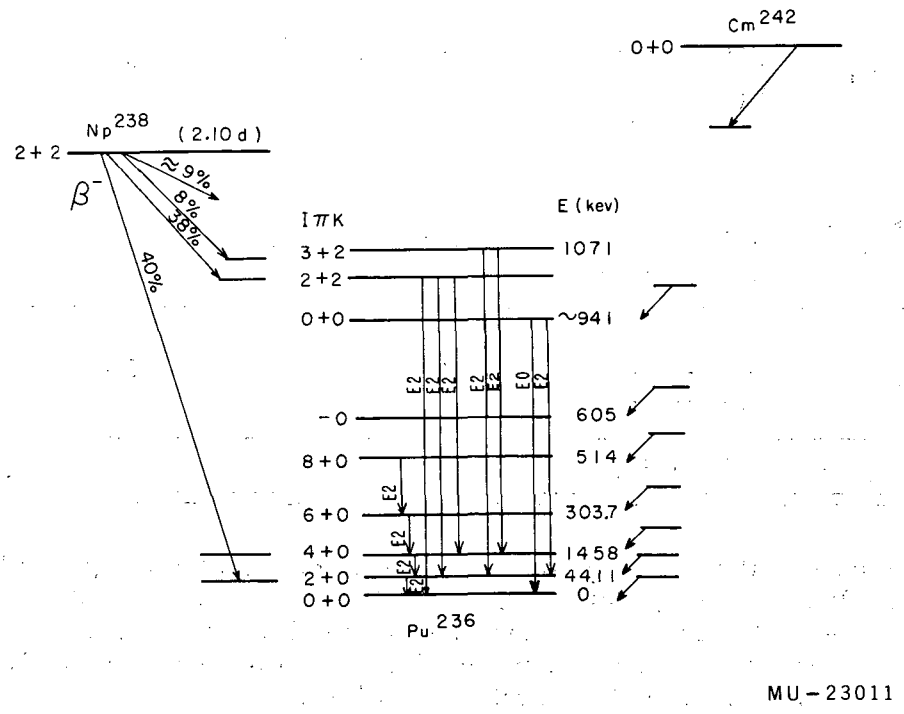

Fig. A. 4-1. Level scheme of Pu^{238}.

Table I. Comparison of experimental and theoretical relative reduced transition probabilities in the decay of Np^{238}

Initial state (kev)	E_γ/E'_γ	$\frac{B(I_i \rightarrow I_f)}{B(I_i \rightarrow I_f')}$	Experimental	Theoretical[a] $K_i = 0$	$K_i = 1$	$K_i = 2$
1030	$\frac{986}{1030}$	$\frac{B(2 \rightarrow 2)}{B(2 \rightarrow 0)}$	1.5	1.4	0.36	1.4
	$\frac{885}{1030}$	$\frac{B(2 \rightarrow 4)}{B(2 \rightarrow 0)}$	0.15	2.6	1.1	0.071
1071	$\frac{1027}{925}$	$\frac{B(3 \rightarrow 2)}{B(3 \rightarrow 4)}$	1.0		0.4	2.5

[a] From Alaga et al. (Ref.1).

A number of other transitions were observed, at energies 119.8, 221.0, 292.6, 870.6, 940.4, 943.1, 989.1, 1033.8 and 1095.3 (only the 940 had been reported previously). These transitions cannot be fitted uniquely into the level scheme, but a tentative interpretation of some of them is given in terms of levels at 914.7, 943.1, 984.5, and 1033.5 kev.

Although it is not possible to make a unique assignment of the 940.4- and 943.1-kev transitions, it is tempting to postulate that the 943.1-kev is the same transition as the 941.1±2-kev E0 transition reported by Asaro and Perlman[3] from the α decay of Cm^{242}. This transition defines the base state (0+) of the K = 0 β vibrational band. It is suggested here that the 940.4-kev transition is the E0, which proceeds between the 2+ state of the β vibrational band to the 2+ state of the ground (K=0) band. The ground-state transition of 984 kev would be an E2, with a small conversion coefficient, and would not be seen. Note that these states are populated by Np^{238} β decay only to the extent of $\leq 0.1\%$.

The log ft values of the various Np^{238} β- decay groups were also investigated. From comparison of experimental and theoretical branching ratios it is concluded that:

(a) Beta decay to the K=2 γ vibrational band proceeds largely by an L=1 transition.

(b) The Russian result[2] of 3% β decay to the I=4+ state of the ground rotational band is incorrect.

3. F. Asaro and I. Perlman, Paper A.13, this report.

(c) Unfortunately no unique parity assignment can be made to Np^{238} on the basis of these data.

From the known spin (2) of Np^{238}, it is possible to say that the odd proton occupies the 5/2+ [642] intrinsic orbital, and the neutron occupies either the 1/2+ [631] or the 1/2- [501] orbital.

5. COULOMB EXCITATION OF VIBRATIONAL LEVELS IN URANIUM-238 AND THORIUM-232.

Bent Elbek, George Igo, Frank S. Stephens Jr., and Richard M. Diamond

By use of O^{16} ions, members of the rotational bands based on the first β, γ, and octupole vibrations in U^{238} and Th^{232} have been Coulomb excited. De-excitation γ-ray spectra taken in coincidence with those O^{16} ions that cause an excitation and are backscattered through 120 to 160 deg into a gas scintillation counter showed the presence of groups of transitions at about 0.78 and 1.02 Mev in Th^{232} and 0.66 and 1.06 Mev in U^{238}. (Such spectra have lower background than straight singles spectra.) From the work of Stelson and McGowan,[1] Class et al.,[2] and Bernstein,[3] it is known the 0.78-Mev group in Th^{232} contains the 2+ → 0+ ground-state transitions from the β- and γ-vibrational bands, but the other transitions are new.

During the course of this work, Class has determined that the 1.06-Mev group in U^{238} involves the β band, by observing the electrons of the electric monopole transition (2+ → 2+). By similar conversion-electron studies, we have confirmed this assignment and have also observed the K-conversion electron lines of the 2+ → 0+ and 2+ → 4+ transitions as well as the 0+ → 0+ and 4+ → 4+ monopole lines. We have also observed the 2+ → 0, 2+ → 2+, and 4+ → 2+ lines from the γ band in U^{238}, as shown in the energy-level diagram, Fig. A.5-1.

In Th^{232}, we have confirmed the assignment of the 2+ → 2+ monopole transition, and have also observed the 0+ → 0+, 2+ → 0+, 2+ → 4+, and 4+ → 4+ transitions from the β-band, as well as the 2+ → 0+ and 2+ → 2+ transitions from the γ-band. These are shown in Fig. A.5-2.

Excitation functions of the γ-ray yield show that the 0.78 Mev group in Th^{232} and the 1.06-Mev group in U^{238} are E2 excitations, but that the 1.02-Mev group in Th^{232} and the 0.66-Mev group in U^{238} are E3 excitations. In the U^{238} case, we have further confirmation that we are dealing with octupole

1. F.K. McGowan and P.H. Stelson, Bull. Am. Phys. Soc. Ser. II, 2, 207 (1957).

2. D.H. Rester, F.E. Durham, and C.M. Class, Bull. Am. Phys. Soc. Ser. II, 4, 98 (1959); F.E. Durham, D.H. Rester, and C.M. Class, Bull Am. Phys. Soc. Ser. II, 5, 110 (1960).

3. E.M. Bernstein, Bull. Am. Phys. Soc. Ser. II, 4, 9 (1959).

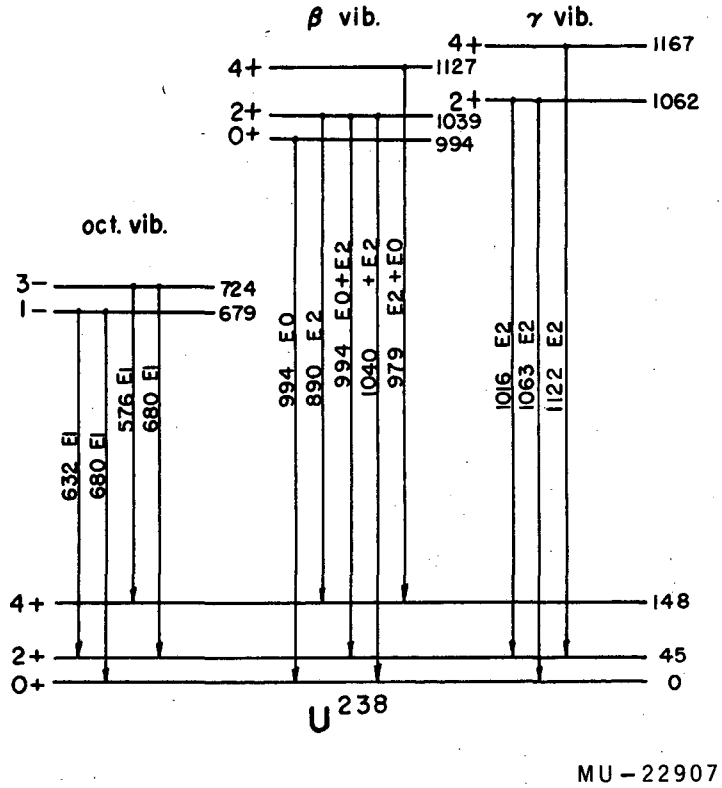

Fig. A. 5-1. Spectra of transitions observed in Coulomb excitation of U^{238} by O^{16}.

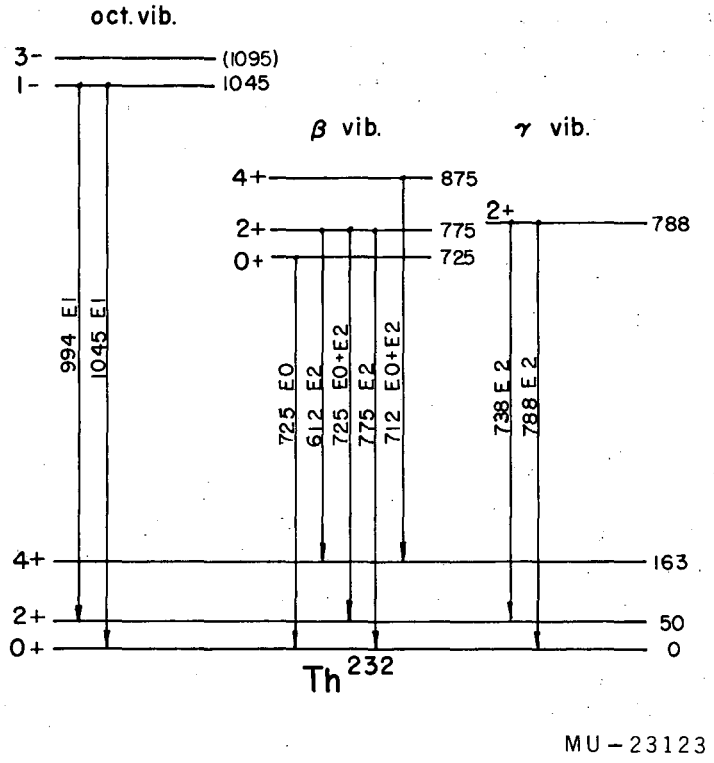

Fig. A. 5-2. Spectra of transitions observed in Coulomb excitation of Th^{232} by O^{16}.

excitations to the odd-parity states. A comparison of the γ spectrum taken in coincidence with backward-scattered particles shows that the 0.66-Mev peak disappears in the former case, as would be expected of an E3 excitation. Octupole excitations are more strongly correlated with particles scattered backwards than are E1 or E2 excitations. Furthermore, a comparison of the yield of this γ-ray group with the intensities of K-conversion electrons we have observed for the same transitions gives conversion coefficients for these de-excitation transitions. These conversion coefficients indicate E1 transitions. Finally, with the electron spectrometer we observe three electron lines which correspond to the four E1 decays from the 1- and the 3- levels of the odd-parity band to the ground-state band, as indicated in Fig. A.5-2. (Two of the transitions have approximately the same energy).

6. THE ALPHA DECAY OF FERMIUM-255 (*)

Frank Asaro, Frank S. Stephens Jr., Stanley G. Thompson, and I. Perlman

Abstract

The study of Fm^{255} α decay leads to identification of odd-mass energy levels in the region above the 152-neutron subshell. Alpha groups of 7.09 (0.4%), 7.03 (94%), 6.97 (5%) and 6.90 Mev (0.8%) were observed. The data indicate that the most likely spin for Fm^{255} is 7/2 or 9/2, which corresponds to the 7/2+ [613] or 9/2+ [615] Nilsson orbitals.

Extensive correlations[1,2] have been made between odd-mass energy levels and the theoretical Nilsson orbitals.[3] Because of a lack of experimental data, however, these have not been extended to orbitals above the 152-neutron subshell. The work presented here concerns the α decay of Fm^{255}, which gives some insight to the classification of the 153rd and 155th neutron states.

Measurements with a magnetic α-particle spectrograph showed four Fm^{255} groups with α-particle energies and intensities of 7.09 (0.4%), 7.03 (94%), 6.97 (5%), and 6.90 Mev (0.8%). The partial half life of the most intense group was longer by only a factor of 1.2 than the theoretically unhindered value.[4] Such a small hindrance factor indicates that the transition is probably of the "favored" type;[5] i.e., the state in Cf^{251} populated by the 7.03-Mev α particle has the same configuration as the parent Fm^{255} state

---

*Paper given at International Conference on Nuclear Structure, Kingston, Ontario, 1960.

1. B.R. Mottelson and S.G. Nilsson, Kgl. Danske Videnskab. Selskab Mat.-fys. Skr. 1, No. 8 (1959).

2. F.S. Stephens, F. Asaro, and I Perlman, Phys. Rev. 113, 213 (1959).

3. S.G. Nilsson Kgl. Danske Videnskab. Selskab Mat.-fys Medd. 29, No. 16 (1955).

4. Helen V. Michel, Hindrance Factors for Alpha Decay, UCRL-9229, May 1960.

5. A. Bohr, P.O. Froman, and B.R. Mottelson, Kgl. Danske Videnskab. Selskab Mat.-fys. Medd. 27, No. 16 (1953).

(see Fig. A.6-1). The favored decay assignment is confirmed by the intensities of the 6.97-Mev and 6.90-Mev groups, which are in excellent agreement with the calculated values for the other rotational band members, as shown in Table I. It should be noted that the calculation is not very sensitive to K; hence, additional data are needed to establish the spins.

From the Bohr-Mottelson theory[6] the spins of the band members may be calculated from the equation

$$E = \frac{\hbar^2}{2\mathcal{J}}\left\{I(I+1) + (-1)^{I+1}(I+1)\,\delta_{K^{1/2}}\right\} .$$

With the energy separations 60.1±.6 and 72.6± 1.3 kev between the band members, the calculated value of the base spin of the band (K in this case) is $3.8\pm^{0.7}_{0.5}$. This value is most consistent with $K = 7/2$, although $K = 9/2$ is within the experimental error. Further information on the spin assignment can be obtained from the absolute value of the level spacings. For even-parity levels near the region of 152 neutrons, the values of $\frac{\hbar^2}{2\mathcal{J}}$ range from 6.2 to 6.5 kev. The 6.1±.6-kev separation corresponds to values of $\frac{\hbar^2}{2\mathcal{J}}$ of 6.7±.1 kev for $K = 7/2$ and 5.5±.1 kev for $K = 9/2$, again in somewhat better agreement with $K = 7/2$. Inspection of a Nilsson diagram shows that the only odd-parity state in this region with about the right spin is an $\frac{11}{2}$- level. This assignment seems unlikely from the relative energy spacings, but it cannot be completely ruled out. The most probable Nilsson assignments, $K\pi[Nn_z\Lambda]$[1,3] for states with the foregoing spins are $\frac{7}{2}+[613]$, $\frac{9}{2}+[615]$, and $\frac{11}{2}-[725]$.

In order to measure the decay energy of Fm^{255}, an α spectrum was taken with a grid chamber having about 50% counting geometry. In this type of chamber the energies of coincident electrons entering the counting volume add to the energy of the α particle. Only about 15% of the α emission was at 7.03 Mev, the remainder being distributed at higher energies up to 7.12 Mev, roughly consistent with previous measurements.[7,8] This gives very roughly 90 kev as the energy of the state populated by the 7.03-Mev α group, as shown in Fig. 9.

Alpha-gamma and α-L x-ray coincidence measurements gave further information on the de-excitation of the approx 90-kev level. Low-intensity

---

6. A. Bohr and B.R. Mottelson, Kgl. Danske Videnskab, Selskab Mat.-fys. Medd. 27, No. 16 (1953).

7. Albert Ghiorso, unpublished data; Ghiorso, Thompson, Higgins, Seaborg, Studier, Fields, Fried, Diamond, Mech, Pyle, Huizenga, Hirsch, Manning, Browne, Smith, and Spence, Phys. Rev. 99, 1048 (1955).

8. Jones, Schuman, Butler, Cowper, and Eastwood, Phys. Rev. 102, 203 (1956).

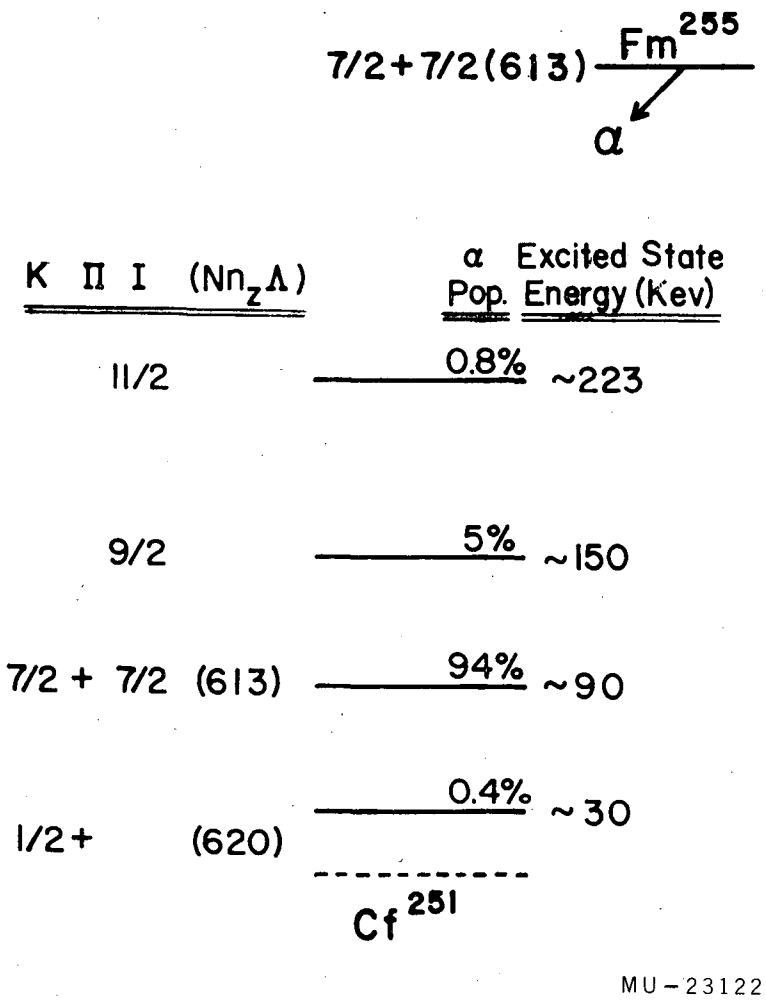

Fig. A.6-1. Decay scheme of Fm^{255}. The notation $K\pi I(Nn_z\Lambda)$ refers to the Nilsson quantum numbers (Refs. 1, 3).

Table I. Favored alpha decay of Fm^{255} to the $\frac{7}{2}$ + [613] state.

Excited-state energy (kev)	I	Calculated abundances[a] (%) L = 0	L = 2	L = 4	Σ_L	Experimental abundances (%)
X	7/2	83.2	9.8	0.2	93.2	94
X + 60	9/2	----	5.0	0.4	5.4	5
X + 133	11/2	----	0.63	0.29	0.92	0.8
X + 219 est.	13/2	----	----	0.08	0.08	< 0.4
X + 320 est.	15/2	----	----	0.01	0.01	< 0.4

[a] The abundances were calculated from the equation

$$P_E \propto P_{0E} \sum_L c_L \left\{ C^{I_i \quad L \quad I_f}_{K_i \; K_f - K_i \; K_f} \right\}^2 ,$$

where $\sum_E P_E$ = total population to the rotational band,

P_{0E} contains the energy dependence for α decay,

c_L is the inverse of the hindrance factors for Fm^{254} decay[4]

$(c_0 : c_2 : c_4 = 1 : 0.25 : 0.033)$,

and the last factor is a Clebsch-Gordan coefficient.

radiations of 55 → 60 kev (≈ 1%) and 80 kev (≈ 1 %) were observed as well as high-intensity L x rays. The L x-ray intensity, corresponding to 2.3 ± .2 total conversion electrons[9] per Fm^{255} α particle, indicates there are at least two highly converted transitions. These data are consistent with a $K = \frac{1}{2}+$ rotational band at or near the ground state with a decoupling parameter of 0.1 → 0.3, in reasonable agreement with the calculated value for the $\frac{1}{2}$+ [620] Nilsson level, 0.3. Further and more precise experimental data are needed to make the assignments secure.

[9] Valid only for transitions over the L binding energies.

7. THE ISOMERS OF AMERICIUM-242 (*)

Frank Asaro, Isadore Perlman, John O. Rasmussen
and Stanley G. Thompson

Contrary to earlier evidence, new measurements on the Am^{242} isomers show that the 16-hr activity is the ground state and the 152-yr activity is the upper isomers, as shown in Fig. A.7-1. By electrostatic collection techniques some 16-hr americium activity was separated from an aged sample containing the 152-yr isomer, as indicated in Figs. A.7-2 and A.7-3. Careful study of the conversion-electron spectrum of the sample containing 152-yr Am^{242m} revealed eleven conversion lines of a 48.6-kev transition converted in americium, and the relative M-subshell conversion intensities are consistent only with an E4 assignment. This information, coupled with the recent atomic beam measurement of spin 1 for the 16-hr activity, leads to a spin assignment of 5 for Am^{242m}.

Detailed analysis of the experimental information on these isomers is given in terms of the Bohr-Mottelson model. This leads to the surprising conclusion that the spin-1 ground state has a K-quantum number of zero, and hence a negative spectroscopic quadrupole moment. Consideration of the data on levels and decay of the low-spin isomers of Ho^{166} and Ta^{180} lead to the conclusion that there is generally an energy displacement between odd- and even-spin members of K = 0 rotational bands in odd-odd spheroidal nuclei.

*Brief version of published paper, Phys. Rev. 120, 934 (1960).

8. ALPHA DECAY OF LONG-LIVED AMERICIUM-242 (*)

Frank Asaro, Maynard C. Michel, Stanley G. Thompson,
and Isadore Perlman

Abstract

The α decay of Am^{242m} (157 yrs) permits the investigation of strong-coupling energy levels of odd-odd nuclei in a region where odd-mass level assignments are well known. An unhindered Am^{242m} α group (5.20 Mev) populates a 350-kev excited state in Np^{238} followed by five cascading transitions. The data are interpreted in terms of the adjacent odd-mass energy levels.

The α spectrum of an $Am^{241,242,243}$ source was measured with a high-resolution magnetic spectrograph. This spectrum is shown in Fig. A.8-1. Besides the characteristic spectra of $Am^{241,243}$, there was an additional group at 5.201 Mev which we assigned to long-lived Am^{242m}. This assignment was confirmed by an α grid chamber measurement of a mass-separated Am^{242} sample. The 5.201-Mev group, however, was distributed between 5.2 and 5.4 Mev, indicating a number of coincident conversion electrons. This latter conclusion was reinforced by the γ spectrum in coincidence with the 5.201-Mev α group. A definite E1 γ ray of 48 kev was observed, as well as other radiations which were not well resolved from one another. These

*Abstract of paper given at International Conference on Nuclear Structure, Kingston, Ontario, 1960.

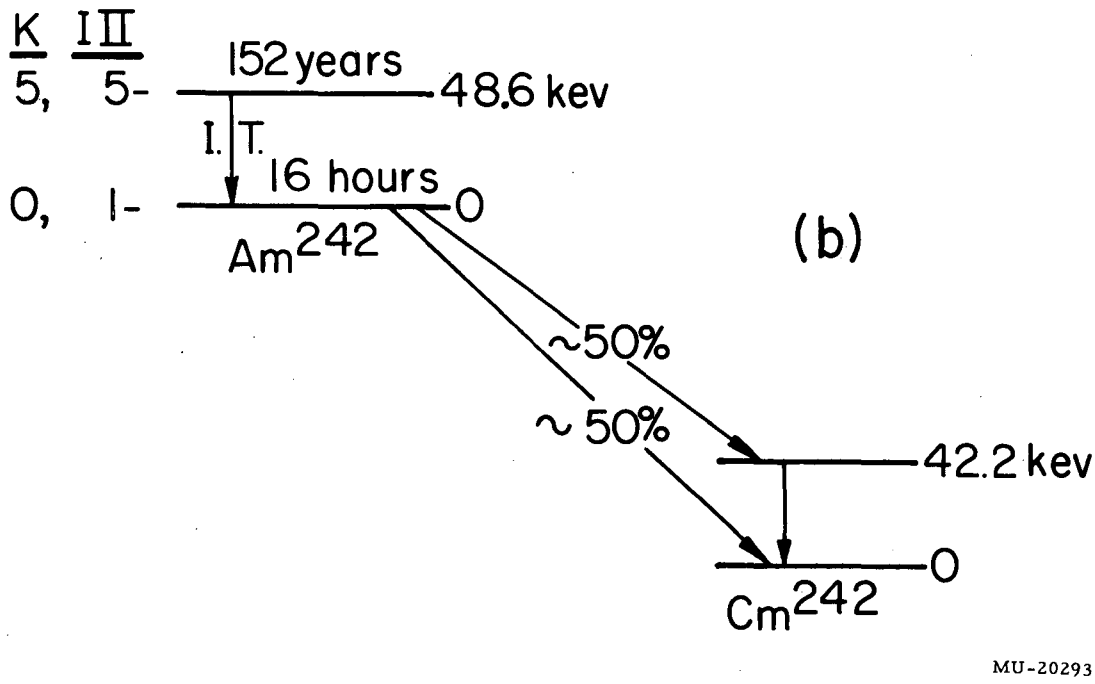

Fig. A. 7-1. Decay scheme of Am^{242} isomers (from this work).

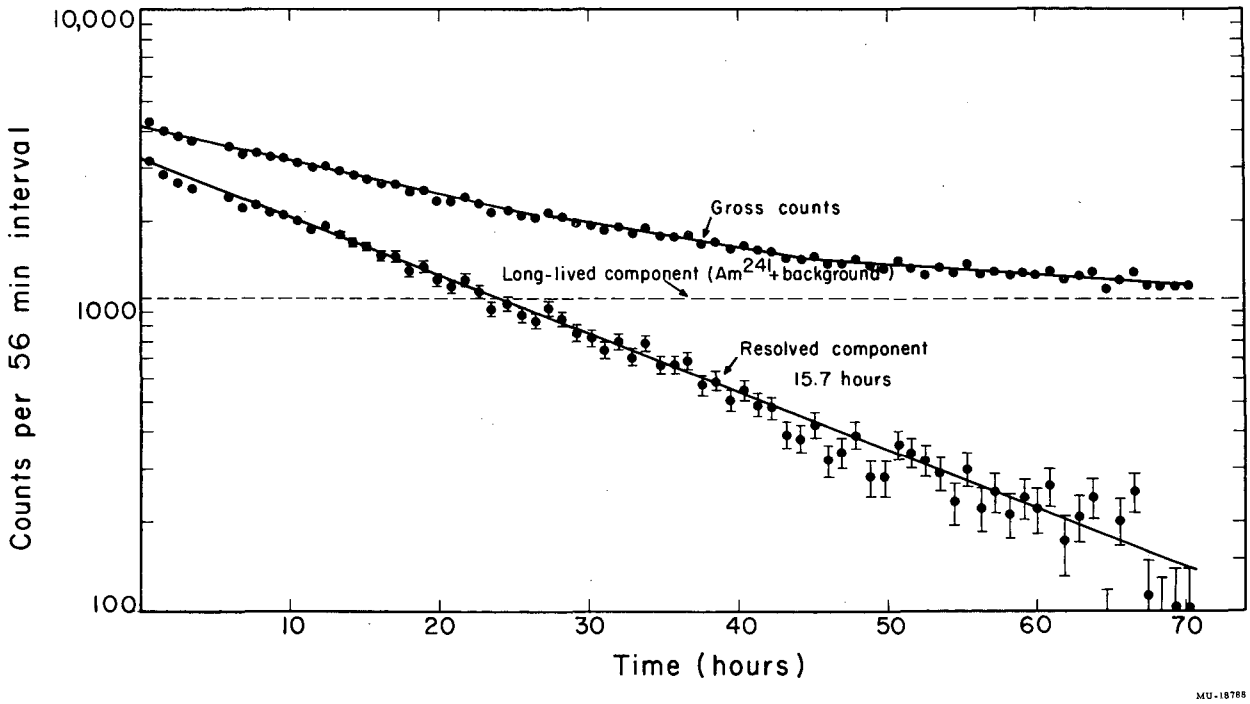

Fig. A.7-2. Decay of purified "recoil" products from americium containing 152-year Am^{242} as measured with a windowless proportional counter.

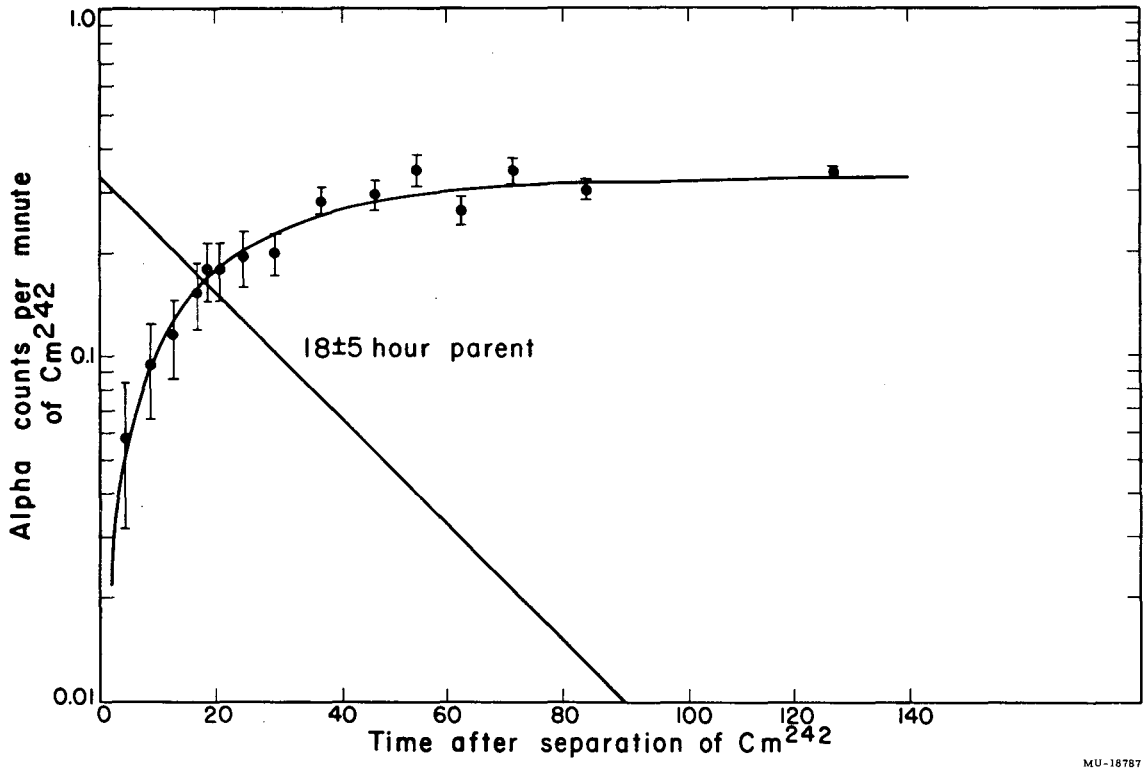

Fig. A. 7-3. Curium-242 growth from the purified americium fraction of a "recoil" sample. One α count per minute equals two α disintegrations per minute.

data are all consistent with a closed-cycle calculation which indicates the 5.201-Mev group populates a state about 340 kev above the ground state of Np^{238}. The best values for the γ-ray energies and intensities are incorporated in Fig. A. 8-2.

The partial α half life of the 5.201-Mev group is 3×10^4 years, very close to the over-all partial α half life measured genetically,[1] and to the theoretical value for this energy, 2×10^4 years. This close agreement between experiment and theory is unusual for odd-odd nuclei and is reminiscent of the "favored" type of α decay[2] observed with odd-mass α emitters. For this type of decay the 340-kev state in Np^{238} would have the same Nilsson quantum numbers, $\Omega\pi[Nn_z\Lambda\Sigma]$,[3,4,5] as the parent state, Am^{242m}; i.e., 5/2-[523↓] for the proton orbital and 5/2+[622↑] for the neutron orbital. Also these orbitals would couple to give a state with K = 5-, as found for Am^{242m}, and a state with K = 0-, as found for 16-hr Am^{242}.[6] It will be useful later to note that in Am^{242} the K = 5-state is 48.6 kev higher than the K = 0- state.[6]

An interesting comparison can be made between the energies of the Nilsson states in the adjacent odd-mass nuclides and the 340-kev state in Np^{238}. The 5/2-[523↓] proton orbital discussed earlier has an energy above the ground state of 59.6 kev in Np^{237} and 74.6 kev in Np^{239}, which averages to 67 kev. The 5/2+[622↑] neutron orbital discussed earlier has an energy above the ground state ≈ 158 kev[7,8] in U^{237} and 286 kev[4,7] in Pu^{239}, which averages to 222 kev. In analogy to Am^{242}, the K = 5- state is assumed to be 49 kev higher than the K = 0- state. When this quantity is added to the sum of the averages, the total energy for the K = 5- state in Np^{238} becomes 338 kev, in good agreement with the experimnetal value, 340 kev. Inherent in the calculation, however, is the arbitrary assumption that the energy splitting of the Np^{238} ground-state coupling is also about 49 kev; hence, the agreement may be fortuitous.

In the free-wheeling spirit of the foregoing calculation we have coupled all the Nilsson orbitals that would result in pertinent (high spin) states with energies less than 340 kev above the ground state of Np^{238}. The resulting hypothetical levels are listed in Fig. A. 8-2. For each pair of states formed

---

[1] Barnes, Henderson, Harkness, and Diamond, J. Inorg. Nuclear Chem. 9, 105 (1959).

[2] A Bohr, P.O. Fröman, and B.R. Mottelson, Kgl. Danske Videnskab. Selskab Mat.-fys. Medd. 29, No.10 (1955); P.O. Fröman, Kgl. Danske Videnskab. Selskab Mat.-fys. Skr. 1, No.3 (1957).

[3] S.G. Nilsson, Kgl. Danske Videnskab. Selskab Mat.-fys. Medd 29, No.16 (1955).

[4] B.R. Mottelson and S.G. Nilsson, Kgl. Danske Videnskab. Selskab Mat.-fys. Skr. 1, No. 8 (1959).

[5] C.J. Gallagher and S.A. Moszkowski, Phys. Rev. 111, 1282 (1958).

[6] F. Asaro, I. Perlman, J.O. Rasmussen, and S.G. Thompson, Phys. Rev. (in press).

[7] F.S. Stephens, F. Asaro, and I. Perlman, Phys. Rev. 113, 212 (1959).

[8] The 145-kev γ in Pu^{241} decay probably de-excites to a 1/2+ 3/2 state, whose energy is estimated at approx 13 kev.

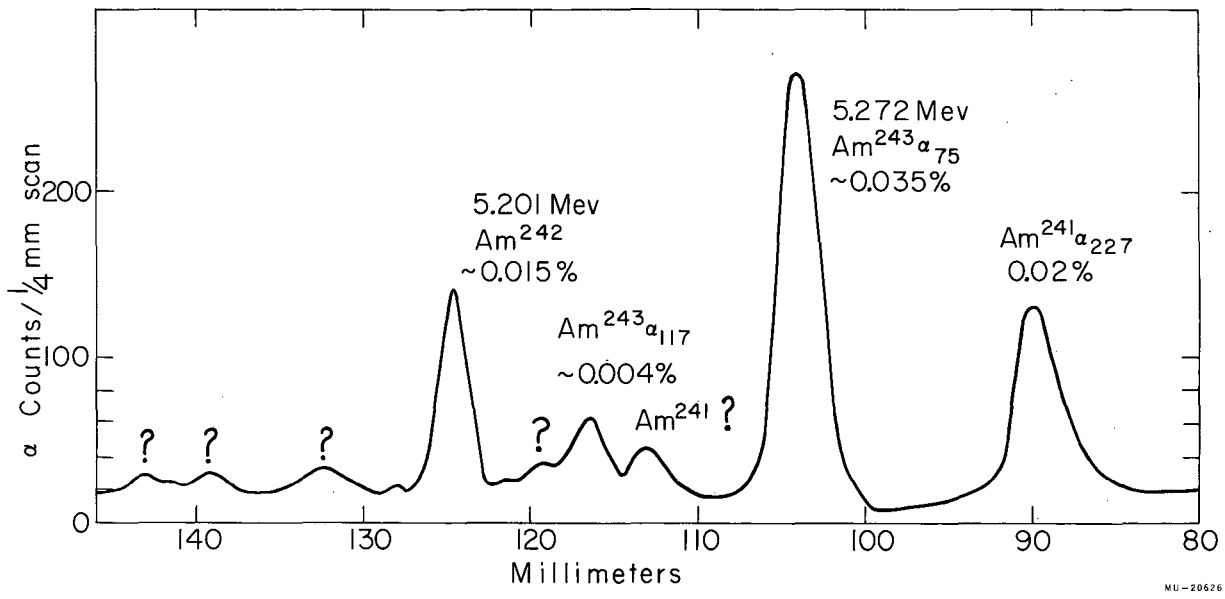

Fig. A. 8-1. Partial $Am^{241, 242, 243}$ alpha spectrum.

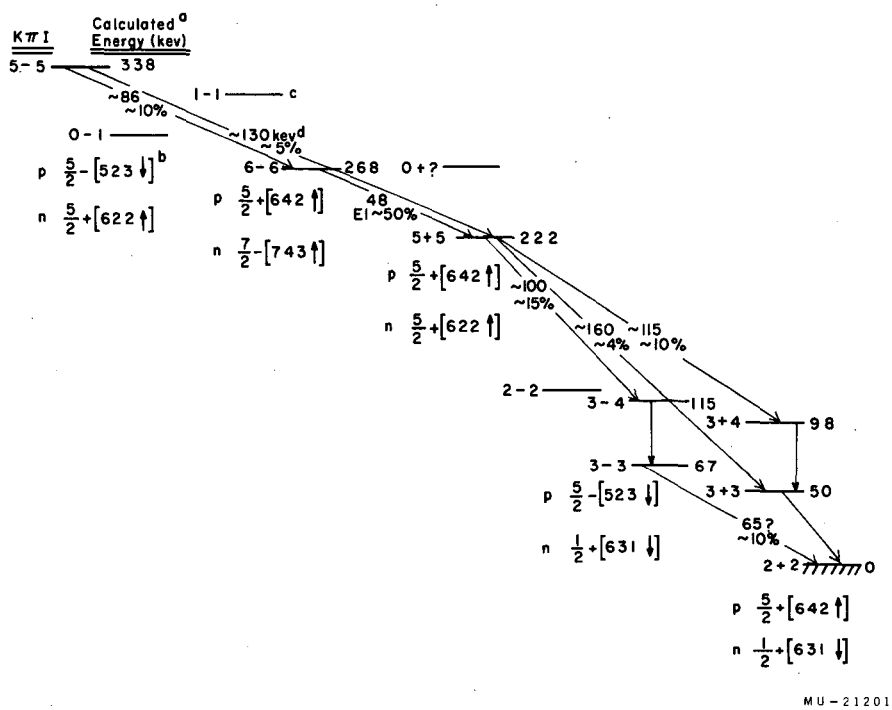

Fig. A. 8-2. Hypothetical energy levels of Np^{238}.

a. Calculated energy----------from the summing of the energies of the odd-proton and odd-neutron states.

b. p-proton state, n-neutron state, $\Omega\,\pi\,[Nn_z\Lambda\,\Sigma]$--Nilsson quantum numbers.

c. If the Σ values are antiparallel, 49 kev is added to the energy.

d. Experimental γ-ray energies (kev) and intensities.

in this fashion, we have added 49 kev to the higher state determined from the selection rule of Gallagher and Moszkowski.[5] Where pertinent to the decay scheme, we have included rotational levels, using a rotational constant of 6 kev.

The γ-ray intensities in the hypothetical decay scheme are consistent with reasonable multipolarity assignments. In addition the intensity of L x rays in coincidence with the 5.201-Mev group was 9±1% for our experimental setup, in good agreement with the corresponding value from the decay scheme in Fig. A.8-2, 9.2%. After the necessary corrections, the experimental value corresponds to 4.3±.5 electron vacancies per Am^{242} α particle. Together with the photon intensities, there are then about five transitions following each decay.

9. DECAY SCHEME OF EINSTEINIUM-253 (*)

Frank Asaro, Stanley G. Thompson, Frank S. Stephens Jr., and Isadore Perlman

The α and electron spectra of E^{253} were investigated with high-resolution magnetic spectrographs. Previous measurements were confirmed,[1-5] but in addition several new levels and transitions were observed leading to the identification of three rotational bands as shown in Fig. A.9-1. α-γ, α-e-, and L x ray–γ coincidence measurements reinforced these assignments.

As seen from Fig. A.9-1, the relative spacings of the assigned states in the 8.8-kev band are in excellent agreement with a spin of 3/2 for the base state. In addition the rotational constant for spin 3/2 is 6.1, in good agreement with the usual values for odd-mass nuclides in this region.

Although the parity of this band cannot be determined simply from the experimental data, inspection of a Nilsson diagram[6] readily shows that the most probable state is 3/2-[521]. These Nilsson quantum numbers[6] are partially defined in Fig. A.9-1.

---

*Paper given at International Conference on Nuclear Structure, Kingston, Ontario, 1960.

1. A. Ghiorso and B.G. Harvey, unpublished data (1954) reported in Ref.2.

2. Frank S. Stephens, Jr., Decay Schemes and Nuclear Spectroscopic States in the Heavy-Element Region, (Ph.D. Thesis), UCRL-2970, June 1955.

3. J.P. Hummel, G. Choppin, F. Asaro, and I. Perlman, unpublished data (1955) reported in Ref. 2.

4. Jones, Schuman, Butler, Cowper, and Eastwood, Phys. Rev. 102, 203 (1956).

5. John P. Hummel, Alpha-Decay Studies in the Heavy-Element Region (Ph. D. Thesis). UCRL-3456, July 1956.

6. S.G. Nilsson, Kgl. Danske Videnskab. Selskab Mat.-fys. Medd 29, No. 16 (1955); B.R. Mottelson and S.G. Nilsson, Kgl. Danske Videnskab. Selskab Mat.-fys. Skr. 1, No. 8 (1959).

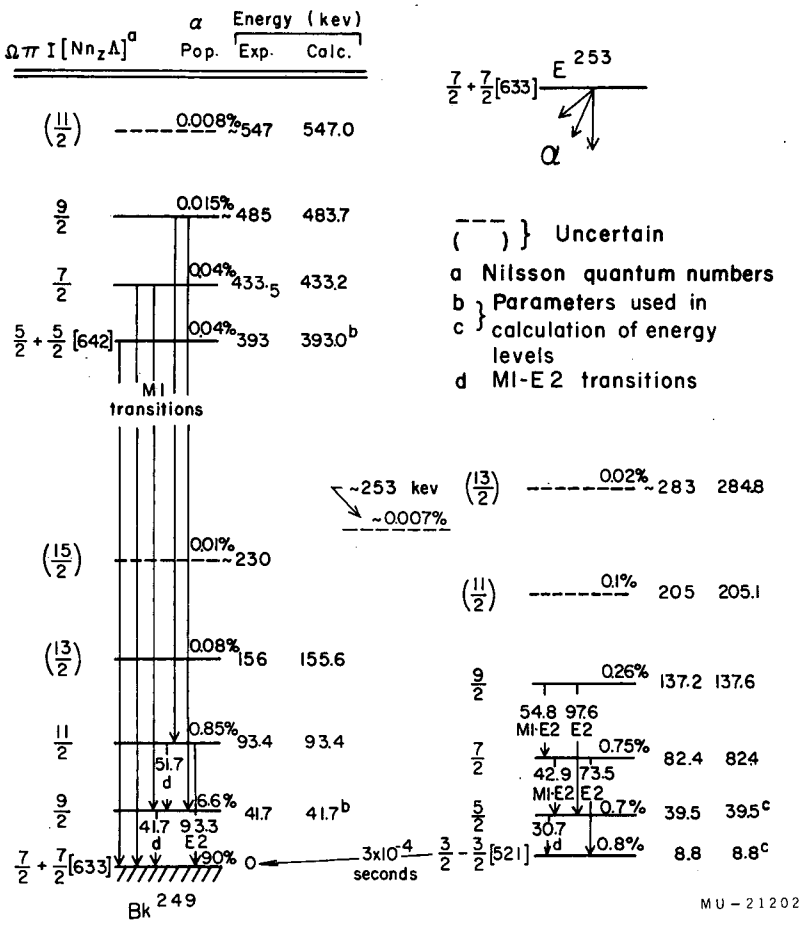

Fig. A. 9-1. Decay scheme of E^{253}--all dashed levels or quantities in parentheses are uncertain.

a. The Nilsson quantum numbers, $\Omega\pi[Nn_z\Lambda]$.

b. These energies were arbitrary parameters in the calculation of the level energies for the 5/2+ and 7/2+ bands.

c. These energies were arbitrary parameters in the calculation of the level energies for the 3/2- band.

It will be shown later that the ground-state spin of Bk^{249} is 7/2+. Thus an M2 transition might be expected between the 3/2- and 7/2+ states. α-e-delayed-coincidence measurements showed a half life of 0.3 msec for about 2% of the E^{253} α transitions, in good agreement with the total α population to the 3/2- band. This lifetime is retarded by a factor of about 50 over the single-proton M2 value.[7]

The ground-state and 393-kev bands are discussed together, as it will be shown that they are closely related. From the level spacing of this ground-state band, the spin of the ground state is calculated to be 3.16±.01. This value is closer to 7/2 than any other spin, but the agreement is not very good. Also, the rotational constant for this band has a value of 4.63 kev, which is unusually low. We have calculated the properties of this band, however, considering the Coriolis interaction[8] as modified by the pairing correlations,[9] and will show that these quantities are both well explained provided the assignment 7/2+ [633] is made for this band. This is consistent with what one would expect from the Nilsson diagram. The decay characteristics and spacing of the 393-kev band are also well accounted for if the 5/2+[642] assignment is made, which, again, is not unexpected considering the Nilsson diagram. This case is a particularly favorable one for detailed Coriolis calculations because

(a) within the entire 82-to-126-proton shell the only positive parity levels (a requirement for the interaction is no change of parity) are those originating from the $i_{13/2}$ shell-model level, and these can all be taken into account explicitly;

(b) the Coriolis matrix elements are large and do not depend on details of the Nilsson wave functions; and

(c) the positions and moments of inertia of two bands from the $i_{13/2}$ orbital are known. We have used two parameters in the calculation, which seem to fix the positions of the 393- and 41.7-kev levels. The other calculated energies are given in Fig. A.9-1, and agree well with the experimental values. It is interesting to note that the mixing causes positive deviations from the I(I+1) formula in the ground (K = 7/2) band and irregular deviations from the I(I+1) formula in the 393-kev (K = 5/2) band. The experimental data confirm the former trend but are not sufficiently accurate to test the latter. The transitions between the two bands are M1, as would be expected from calculations using the mixed Nilsson wave functions.

The theroetical α populations to various members in a rotational band are readily calculated for an α wave of a given angular momentum.[9] In addition, if the parent and daughter states have the same configuration, the α transition to the base state of the band is essentially unhindered, and the relative α populations to the various band members are explicitly determined. As seen from Table I, the above conditions are well met by the ground-state band, resulting in the same assignment for the E^{253} ground state, 7/2+[633], as found for Bk^{249}.

---

7. S.A. Moszkowski, Beta- and Gamma-Ray Spectroscopy, Kai Siegbahn, Ed. (Interscience Publishers Inc., New York 1955), p 390.

8. A. Kerman, Kgl. Danske Videnskab. Selskab Mat.-fys. Medd. 30, No. 15.

9. S.T. Belyaev, Kgl. Danske Videnskab. Selskab Mat.-fys. Medd. 31, No. 11 (1959).

Table I. Alpha decay of E^{253} to the 7/2+ band in Bk^{249}

Excited-state energy (kev)	I	Calculated abundances[a] (%) L=0	L=2	L=4	$\sum_L$	Experimental values (%)	Hindrance factors[b]
0	7/2	79.6	10.0	0.1	89.7	90	1.9
41.7	9/2	---	5.9	0.3	6.2	6.6	17
93.4	11/2	---	0.9	0.3	1.2	0.85	7.7
156	13/2	---	---	0.11	0.11	0.08	430
230	15/2	---	---	0.009	0.009	0.01	~1500

[a] The abundances are calculated from the expression

$$P_E = P_{0E} \sum_L C_L \begin{pmatrix} I_i & L & I_f \\ K_i & K_f-K_i & K_f \end{pmatrix}; \quad \sum_E P_E \text{ is the total population to the}$$

rotational band, P_{0E} is the unhindered population to a state E calculated from simple spin-independent α-decay theory, C_L is the reciprocal of the hindrance factors for the various L waves in the adjacent even-even nuclides ($C_0:C_2:C_4$= 1:0.27:0.023 from Fm^{254} and Cf^{252})(Ref. 10), and the last factor is a Clebsch-Gordan coefficient.

[b] The hindrance factors as used here are the ratio of the experimental partial half life of a given α group to the value calculated from spin-independent α-decay theory (Ref. 11) by using the radii of adjacent even-even nuclides.

In the hindered α decays to the other bands, the relative α populations are also in good agreement with the calculated values, consistent with the spin and parity assignments.

10. Helen V. Michel, Hindrance Factors for Alpha Decay, UCRL-9229, May 1960.

11. M. A. Preston, Phys. Rev. 71, 865 (1947).

10. ALPHA-PARTICLE AND GAMMA-RAY STUDIES, AND HALF-LIFE DETERMINATIONS OF MEMBERS OF THE URANIUM-229 AND URANIUM-228

Carl Ruiz, Frank Asaro, and I. Perlman

An investigation of the α-particle and γ-ray spectra and the half lives of various members of the U^{228} and U^{229} families has been completed. The most recent results are discussed below, and most of these data, along with our previous results,[1] are summarized in the decay schemes in Figs. A.10-1 and A.10-2.

U^{229}

Three new groups were observed, having the following energies and abundances: 6.255 Mev (1%), 6.218 Mev (3%), and 6.180 Mev (1%). The group

1. Ruiz, Asaro, and Perlman, in Chemistry Division Semiannual Report, UCRL-9093, Feb. 1960, p. 47.

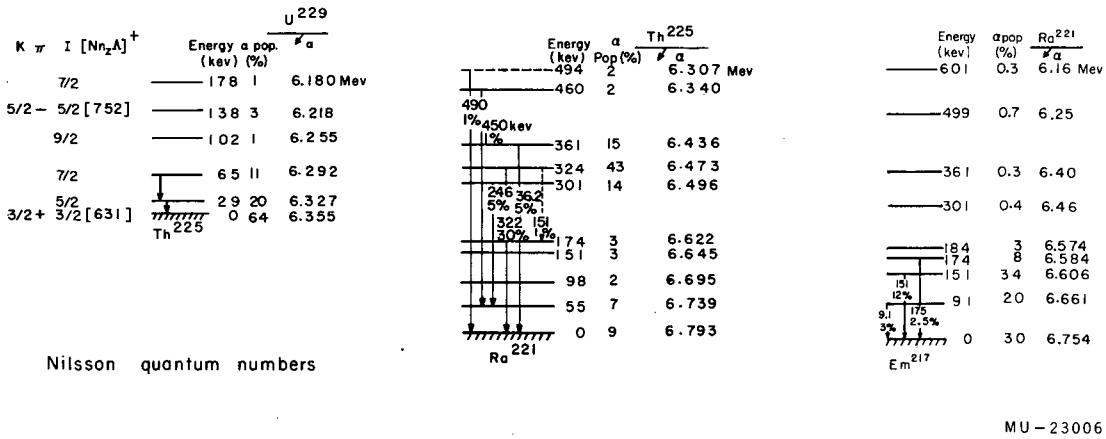

Fig. A.10-1. U^{229} family decay schemes. Alpha-particle energies are expressed relative to $Th^{226}\alpha_0$ (taken as 6.330 Mev) and $Ra^{222}\alpha$ (6.552 Mev).

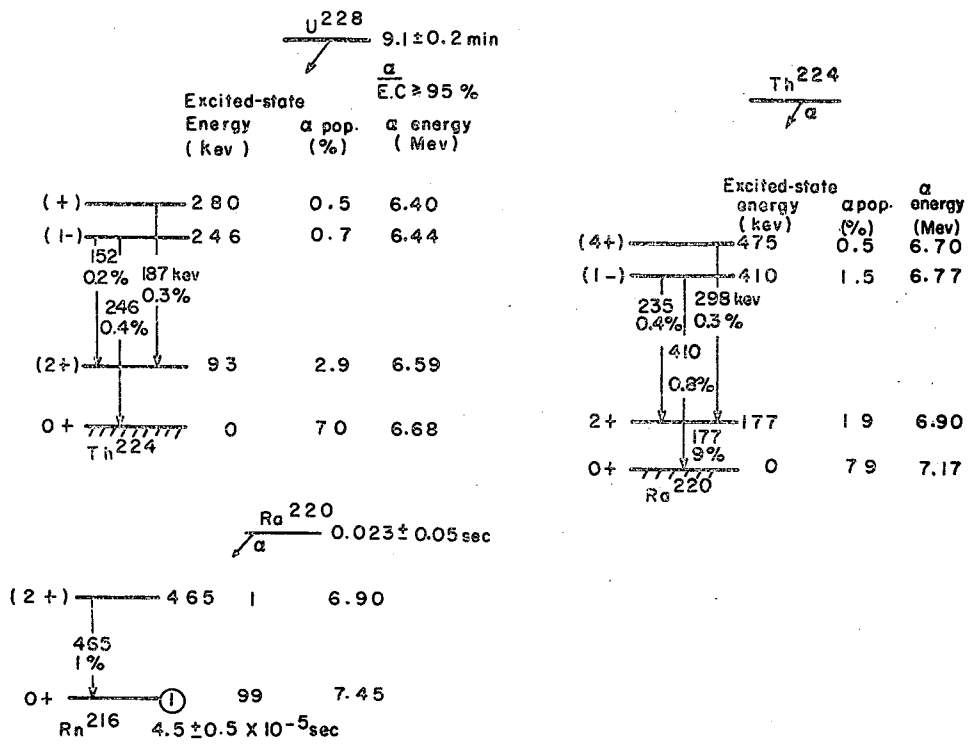

Fig. A. 10-2. U^{228} family decay schemes.

at 6.255 Mev is interpreted as the fourth member of the K = 3/2 rotational band having spin I = 9/2.

Th^{225}

One new α group was found at an energy of 6.340 Mev, in an abundance of 2%. Gamma rays of 450 kev (1%) and 490 kev (1%) were also seen.

Ra^{221}

Five new α groups were observed, with energies and abundances of 6.574 Mev (3%), 6.46 Mev (0.4%), 6.40 Mev (0.3%), 6.25 Mev (0.7%) and 616 Mev (0.3%). The last four groups were detected with an α-particle grid chamber. The existence of the 0.3% and 0.4% groups is not completely certain because of their low intensity. Gamma rays were also seen with the following energies and abundances per α disintegration: 219 kev (0.1%), 293 kev (0.6%), 320 kev (0.7%), and 415 kev (0.5%).

U^{228} Family

By means of α-particle γ-ray coincidence techniques, three γ rays were seen in the α decay of U^{228}: 152 kev (0.2%), 187 kev (0.3%), and 246 kev (0.4%). The 152- and 246-kev γ rays were interpreted as originating from the de-excitation of a 1- state 246 kev above the ground state. The 187-kev γ radiation was interpreted as that from a state at 280 kev above the ground state. The spin and parity of this state were assigned as 4+.

Half-Life Determination

By means of delayed-coincidence techniques, the half life of the 7.680-Mev α groups of Rn^{217} was measured as $5.4 \pm .5 \times 10^{-4}$ sec, which is to be compared with the previously determined value of 10^{-3} sec[2]. The half life of Rn^{216} was observed to be $4.5 \pm .5 \times 10^{-5}$ sec.

The half life of U^{228} was remeasured and found to be 9.1±.2 min, in good agreement with the previous value of 9.3±0.5 min.[2]

A moving metal tape was used to collect recoil atoms from a U^{228} source for the measurement of the Ra^{220} half life. The value obtained was 0.023±0.005 sec.

---

2. Meinke, Ghiorso, and Seaborg, Phys. Rev. 81, 782 (1951).

11. SEARCH FOR ELECTRIC MONOPOLE TRANSITION FOLLOWING ALPHA DECAY OF PLUTONIUM-239

S. Bjørnholm and Frank Asaro

Electric monopole, E0, transitions of energies 0.6 to 1 Mev have been observed in a number of heavy even-even nuclei. These transitions are thought to establish the existence of a collective quadrupole vibration (β vibration) of the deformed nucleus. In a few cases E0 transitions have been found in even-even α emitters in which the α decay to the β-vibrational band is only slightly hindered relative to the ground-state transition.

In order to get information about the existence of β vibrations in odd-A nuclei we have looked for highly K-converted transitions in the α decay $Pu^{239} \rightarrow U^{235}$.

Three mg of Pu^{239} was precipitated as the fluoride on a 1-mil platinum disc. The precipitate was spread over an area 0.8 cm in diameter. Aluminum and mylar foils of total thickness 11 mg/cm^2 covered the source. The source was sandwiched between a beryllium-window 1.5×0.5-in. sodium iodide scintillation counter, sensitive to U K x rays, and a 5/8×1/8-in. anthracene scintillator, sensitive to high-energy electrons but not to γ rays. Coincidences between γ pulses (corresponding to K x rays) and electron pulses (corresponding to a 1.0±0.05-Mev transition) were observed. The abundance of the transition was found to be $(1.5\pm0.8)\times10^{-7}$. No γ-ray peaks were observed in the region 900 to 1100 Mev, the upper limit for the intensity being 10^{-8}. The K-conversion coefficient thus seems to be >15±8, which is strong indication of an E0 transition. The experiment also indicates that any competing E2 γ radiation is weaker than the monopole transition by a factor of 15±8. Finally the α-decay hindrance factor is calculated to be between 0.1 and 1.2.

There thus seems to be evidence for the existence of collective excitations of the β-vibrational type in the odd-A nucleus U^{235}. Further investigations would be desirable in order to substantiate the preliminary findings here described.

12. ALPHA-DECAY STUDIES IN THE RARE EARTH REGION

Ronald D. Macfarlane

1. Long-Lived Dysprosium-154

Evidence was obtained by Toth that Dy^{154} may be stable, or at least possess a long β half life.[1] This evidence was based on the absence of the β-decay daughter Tb^{154} in a sample known to contain Dy^{154}.

From the trend of α-decay energies for Dy^{150-3} and the isotopes of neighboring elements,[2] it was expected that Dy^{154} should have a measurable alpha half life.

---

1. K.S. Toth, Nuclear Studies in the Rare Earth Region (Thesis), UCRL-8192, March 1958.

2. K.S. Toth and J.O. Rasmussen, Nuclear Phys. 16, 474 (1960).

Gadolinium oxide enriched in Gd^{154} to 33% was bombarded with α particles to form dysprosium isotopes. Alpha pulse analysis of the chemically separated dysprosium resulted in the observation of a new weak α activity of 2.85±.05 Mev. This activity was assigned to Dy^{154} on the basis of a rough excitation function and a consideration of the α-decay systematics of the neighboring dysprosium isotopes.

The α half life was calculated as approximately 1×10^6 years by estimating the amount of Dy^{154} produced and comparing it with the observed α intensity. A lower limit of 10 years for the β-decay half life was established on the basis of the absence of the prominent γ radiations of Tb^{154} in the photon spectrum.

This work has been submitted for publication.[3]

2. The Natural Occurrence of Samarium-146

Sm^{146} was discovered in 1953 by Seaborg and Dunlavey, who produced the nuclide by an intense bombardment of neodymium with α particles.[4] They reported that it emits α particles of 2.55 Mev energy and decays with an α half life of approximately 5×10^7 years.

Macfarlane and Kohman, in 1959, made a search of Sm^{146} α activity in natural samarium, employing a large internal-sample cylindrical ionization chamber.[5,6] They obtained a negative result and set an upper limit of 0.01 dis/g/sec for the specific activity in natural samarium.

A report has recently been made by Vorob'ev, Komar, Korolev, and Solgakin of an indication for the existence of Sm^{146} α particles in the natural samarium α spectrum, although the level observed was not considered by them to be statistically significant.[8] They established an upper limit of 0.03 dis/g/sec for the specific activity.

The purpose of this study was to increase the sensitivity over previous measurements for the detection of a natural Sm^{146} α activity by counting a sample "enriched in Sm^{146}". This sample was obtained from the mass-146

---

3. R.D. Macfarlane, Dysprosium-154, A Long-Lived Alpha Emitter (UCRL-9335), submitted to J. Nuclear Inorg. Chem.

4. D.C. Dunlavey and G.T. Seaborg, Phys. Rev. 92, 206 (1953).

5. R.D. Macfarlane, Natural Alpha Radioactivity in Medium-Heavy Elements, Department of Chemistry, Carnegie Institute of Technology, NYO-7687, 1959.

6. R.D. Macfarlane and T.P. Kohman, Natural Radioactivity in Medium-Heavy Elements, submitted to Phys. Rev.

7. A.A. Vorob'ev, A.P. Komar, V.A. Korobev, and G.E. Solgaken, J. Exptl. Zhur. Eksptl. i Teoret. Fiz. (USSR) 37, 546 (1959); Soviet Physics-JETP 37 386 (1960).

8. R.D. Macfarlane, Concerning the Natural Occurrence of Sm^{146} (UCRL-9352) submitted to Nature.

position of a calutron collection plate which had been used in the separation of macro amounts of samarium isotopes from natural samarium.

An 89-mg portion of this sample was counted in an internal-sample cylindrical ionization chamber providing an active sample area of 2000 cm^2. Over a period of 67 hr only the prominent Sm^{147} peak appeared in the α spectrum.

Estimating a possible factor-of-10 enrichment of Sm^{146} in the sample, an upper limit of 0.003 dis/g/sec was calculated for the specific activity of Sm^{146} in natural samarium. This corresponds to an upper limit of 2×10^{-7}% for the natural isotopic abundance of Sm^{146}, using the Dunlavey and Seaborg value for the half life.[4]

This work has been submitted for publication.[8]

3. Measurement of Alpha Branching Ratios

The majority of known α emitters in the rare earth region decay prominently by electron capture or positron emission or both. In order, therefore, to obtain α half lives for these nuclides (which are needed for calculations of reduced widths and hindrance factors[9]), the alpha-to-total branching ratio must be known.

Alpha branching ratios for several of the rare earth α emitters are known only to within a factor of three, and for a few are not known at all.[2] The purpose of this investigation was to obtain more precise values of known α-branching ratios and to measure previously unknown values. Samples of the isotopes to be measured were prepared by α-particle or heavy-ion bombardment of rare earth targets. When half lives permitted, chemical separations were performed. Two aliquots of the samples were prepared, one for 2π-geometry α counting and the other for 4π-geometry photon counting. The absolute disintegration rates were obtained by resolution of α and photon decay curves and correction for counting efficiencies. Results are shown in Table I.

Table I. Alpha branching ratios

Nuclide	$T_{1/2}$	Old value[3]	New value	Alpha half life
Tb^{151}	18 hr	$\approx 3\times10^{-6}$	$(4.7\pm.2)\times10^{-6}$	$(4.4\pm.2)\times10^{2}$ yr
Dy^{150}	9 min	--	0.179+.005	50 ± 2 min
Dy^{151}		--	0.062± 0.003	5.4± 0.2 hr
Dy^{153}	6.0 hr	$\approx 4\times10^{-5}$	$(3.3\pm.15)\times10^{-5}$	(20± 1) yr

Measurements of α branching ratios of other α-emitting rare earth nuclides are planned.

[9] J.O. Rasmussen, Phys. Rev. 113, 1593 (1959).

4. New Alpha-Emitting Rare Earth Nuclides (with R. D. Griffioen)

a. Holmium Isotopes

Bombardment of enriched Nd^{142} and Nd^{148} targets with N^{14} ions (65 to 130 Mev) using the Berkeley heavy-ion linear accelerator (Hilac) has led to the discovery of five new α-emitting isotopes of holmium produced by $Nd(N^{14}, xn)Ho$ reaction. Alpha spectra were obtained with a Frisch-grid ionization chamber, and half lives were measured by following the decay of α radioactivity. Mass assignments were obtained by identification of daughter activities and were supported by information obtained by rough excitation functions. For Ho^{151} and Ho^{152}, the parent-daughter relationship was established by electrostatically collecting in helium the β-decay daughter, Dy^{151} and Dy^{152}, recoiling from an extremely thin Ho^{151} and Ho^{152} source. Collection of samples at different time intervals identified the daughter with the appropriate parent half life.[10] A similar technique was employed for Ho^{153} except that the α-decay daughter (Tb^{149}) was used. The α-decay properites of these daughters were utilized for their identification.

Positive confirmation of the mass assignments of Ho^{154} and Ho^{155} has yet to be made. Neither the α- nor β-decay daughter possesses a significant α branch, so that identification must be made from β- and γ-decay properties of the daughters, which are not as unique as for α decay.

The α-decay properties of these nuclides are listed in Table II.

Table II. Alpha-decay properties of new holmium alpha emitters

Isotope	E_α (Mev)	$t_{1/2}$ (total)	Mass assignment
Ho^{151}	4.48 ± .03	31 ± 3 sec	daughter Dy^{151}
Ho^{152}	4.40 ± .03	64 ± 4 sec	daughter Dy^{152}
Ho^{153}	4.34 ± .03	187 ± 10 sec	daughter Tb^{149}
Ho^{154}	4.12 ± .03	5.6 ± 0.2 min	excitation function
Ho^{155}	3.96 ± .03	16.5 ± 0.5 min	excitation function

b. Erbium Isotopes

Bombardment of enriched samarium isotopes with C^{12} ions (65 to 110 Mev) has led to the discovery of five new α-emitting isotopes of erbium, ranging in α energy from 4.7 to 5.1 Mev and in half life from ≈1 sec to 30 sec. Evidence has also been obtained for the existence of an α-emitting isomer of Ho^{151} (4.58 Mev) presumably produced by the β decay of Er^{151}. The 4.48-Mev Ho^{151} was also seen in the α spectrum.

Detection and identification of these α activities were made by using a new system which allows for sample collection and α pulse analysis within milliseconds from the end of bombardment. The method involves the electrostatic collection of reaction recoils knocked from the target into a helium atmosphere.[10] The collector is a thin Zapon foil made conducting by an evaporated

silver deposit. Some α particles produced by radioactive decay of recoils collected on the foil (approx 50 μg/cm^2) pass through the foil and are detected by a diffuse barrier diode detector. It was found that the reaction recoils could be collected with fourfold greater efficiency as negative ions than as positive ions. The mechanism for the formation of negatively charged recoils in this system is being investigated.

[10] A Ghiorso, T. Sikkeland, J.R. Walton, and G.T. Seaborg, Phys. Rev. Letters 1, (1958).

13. ALPHA DECAY TO BETA VIBRATIONAL STATES IN EVEN-EVEN NUCLEI (*)

Frank Asaro and I. Perlman

Abstract

In the strong-coupling region, both Cm^{242} and Pu^{238} decay to excited 0+ states by nearly unhindered α emission (hindrance factors are 3 and 4 respectively). U^{234}, however, α-decays to an excited 0+ state in Th^{230} at 630 kev with a hindrance factor of about 70. Possible correlations between the α- and γ-ray transition probabilities are discussed.

This paper deals with highly converted (presumably completely converted) transitions from levels in Pu^{238}, U^{234}, and Th^{230} which are populated by α decay. As seen from Table I, the effective conversion coefficients are so large the only reasonable multipolarity assignments are E0. Also, with the observed γ-ray patterns the only reasonable spin and parity assignment for the states de-exciting by the E0 transitions is 0+.

Pu^{238} E0 Transition[1]

Electron and γ-ray spectra of several Cm^{242} sources were measured with anthracene and NaI spectrometers. The pertinent results are tabulated in Table I and show a 950-kev E0 transition as well as γ rays of 980 and 1010 kev. A more precise measurement of the K line with a permanent-magnet electron spectrograph yielded a value of 941.4±2 kev for the E0 transition. The data then correspond to a 0+ state at 941 kev which de-excites by an E0 transition to the ground state and 890-kev γ ray to the first excited state.

The 1010-kev γ ray may represent the de-excitation of the 2+ member of a Pu^{238} γ vibrational band observed[2] from the decay of Np^{238}, but this is not certain.

(*) Paper given at International Conference on Nuclear Structure, Kingston, Ontario, 1960.

[1] Perlman, Asaro, Harvey, and Stephens, Bull. Am. Phys. Soc. 2, 394 (1957).

[2] Rasmussen, Stephens, Strominger, and Åström, Phys. Rev. 99, 47 (1955).

Table I. High-energy radiations of Pu^{238}, U^{234}, and Th^{230}

	γ rays			Electrons					Alpha particles	
Nuclide	Energy	Intensity	L-γ coinc.(a)	Energy	Intensity	K-e coinc.(b)	Shell	γ energy	Intensity	Hindrance factor(c)
Pu^{238}	890±10	8×10^{-7}	Yes	830±30	4×10^{-7}	Yes	K	950±30	1.3×10^{-6}	3.3±1
				819.6±2	---	---	---	941.4±2		
				930±30	1×10^{-7}	No	L+M+..	950±30		
	1010±20	$\approx4\times10^{-8}$	?							
U^{234}	763±10	5×10^{-7}	Yes	690±20	6×10^{-7}	Yes	K	810±20	1.2×10^{-6}	4.2±1
				790±20	1×10^{-7}	No	L+M+..	810±20		
Th^{230}	580±10[d]	9×10^{-8}[d]	?	525±20	6×10^{-8}	Yes	K	630±20	1.6×10^{-7}	70±20

(a) L x ray-γ ray coincidences.

(b) K x ray-conversion electron coincidences.

(c) The hindrance factor for a given α group as defined here is the ratio of the experimental half life to the theoretical value. The theoretical half life is calculated according to Preston's equations (Ref. 3) for L = 0 transitions using the nuclear radius determined from the ground-state transition (Ref. 4).

(d) See Ref. 8.

[3] M. A. Preston, Phys. Rev. 71, 865 (1947).

[4] Helen V. Michel, Hindrance Factors for Alpha Decay, UCRL-9229, May 1960.

U^{234} E0 Transition

The measurements of Pu^{238} α decay were very similar to those of Cm^{242}. As seen in Table I, an 810-kev transition was observed as well as a γ ray of about 760 kev. The data correspond to a 0+ state at 810 kev which de-excites by an E0 transition to the ground state and a 760-kev γ ray to the first excited state. This E0 transition has been observed from the β decay of $Pa^{234}(UX_{11})$,[5] and the electron capture of Np^{234}.[6]

Other states and transitions have been observed from the beta decay of $Po^{234}(U_Z)$.[7]

Th^{230} E0 Transition

These measurements are similar to those previously described. In our measurements a K line of a 630-kev transition was observed in coincidence with K x rays. F. S. Stephens[8] measured the high-energy γ-ray spectrum of U^{234} and found radiations of 455, 503, and 580 kev. The two lower-energy γ rays were assigned to the de-excitation of a 1- state at 503 kev.[8,9] The data are interpreted as a 0+ state at 630 kev which de-excites by an E0 transition to the ground state and by a 580-kev γ ray to the first excited state. The 0+ and 1- states have also been identified[10] from the electron capture of Pa^{230}.

Discussion

Excited states of spin and parity 0+ are predicted from the Bohr-Mottelson theory, and it has been shown that the ratio of E0 to E2 transitions de-exciting the 0+ state in both Pu^{238} and U^{234} is in good agreement with the theoretical expectations for the strong-coupling region.[11-13] It has also been shown that a much lower value for the reduced ratio in Gd^{152} is in good agreement with the expectations for the "transition region."[14] As seen in Table II, however, both Sm^{152} and Th^{230} have intermediate ratios, although both nuclei are in the strong-coupling region. Th^{230} demonstrates additional unusual behavior in that the α decay to its 0+ state is hindered by a factor of > 10 more

[5] D. Strominger, J. M. Hollander, and G. T. Seaborg, Revs. Modern Phys. 30, 585 (1958).

[6] C. J. Gallagher, Jr., and T. D. Thomas, Nuclear Phys. 14, 1 (1959).

[7] Reported by G. T. Wood, Phys. Rev. (in press).

[8] F. S. Stephens, unpublished data (1954).

[9] F. S. Stephens, F. Asaro, and I. Perlman, Phys. Rev. 119, 796 (1960).

[10] E. Arbman and O. B. Nielsen, Nuclear Phys. (to be published)(private communication by S. Björnholm).

[11] D. C. Peaslee, Nuclear Monopole Matrix Elements, UCRL-3523, Sept. 1956.

[12] A. S. Reiner, Structure Effects in the Interaction between Nuclei and Atomic Electrons (Thesis), University of Amsterdam, 1958 (unpublished).

[13] J. O. Rasmussen, Theory of E0 Transitions of Spheroidal Nuclei, Nuclear Phys. 19, 85 (1960).

[14] I. Marklund, O. Nathan, and O. B. Nielsen, Nuclear Physics 15, 199 (1960).

than for the states in Pu^{238} or U^{234}. These effects may be related to a gradual change in the character of the β-vibrations as the transition region is approached.

Table II. Reduced ratios of competing E0 to E2 transition probabilities.

Nuclide	$\rho\,(F)^{1/2}$
Pu^{238}	0.20
U^{234}	0.21
Th^{230}	0.11
Sm^{152} (from Ref. 14)	0.063
Gd^{152} (from Ref. 14)	0.026

E0 transition probability $= \Omega\rho^2$ where Ω and ρ^2 represent the electronic and nuclear matrix elements respectively, as given by Church and Weneser. (Ref. 15).

E2 transition probability $= \frac{1}{F} \times$ (single-particle E2 transition probability) (Ref. 16).

[15] E. L. Church and J. Weneser, Phys. Rev. 103, 1035 (1956).

[16] S. A. Moszkowski in Beta- and Gamma-Ray Spectroscopy Kai Siegbahn, Ed. (Interscience Publishers Inc., New York, 1955), p.373.

14. HIGH-ENERGY GAMMA RAYS IN THE DECAY OF 27-HOUR HOLMIUM-166 (*)

Daniel J. Horen and Linda Chiao

Sources of Ho^{166} have been prepared by neutron irradiation of holmium oxide, and the high-energy singles γ-ray spectrum has been studied with a 3-in.-diameter by 3-in.-long NaI(Tl) crystal. Precautions were taken to reduce bremsstrahlung and low-energy γ rays. Figure A. 14-1 shows the high-energy singles spectrum so obtained. Analysis revealed the presence of γ rays with energies of 1747 ± 5 and 1825 ± 5 kev in addition to the previously known γ rays of 1380, 1582, and 1663 kev.

The two highest-energy γ rays suggest the existence of a 1826-kev level in Er^{166} decaying to the ground state and first excited state. This assumption was confirmed by experiments in which coincidences were searched for between high-energy photons and the 80-kev γ ray or K x rays or both. The coincidence spectra obtained by gating on the 80-kev γ ray and K x rays were identical. A typical coincidence spectrum is shown in Fig. A.14-2.

(*) To be published in Nuclear Physics jointly with P. Gregors-Hansen and K. Wilsky, Chemistry Department, Research Establishment, Risø, Denmark.

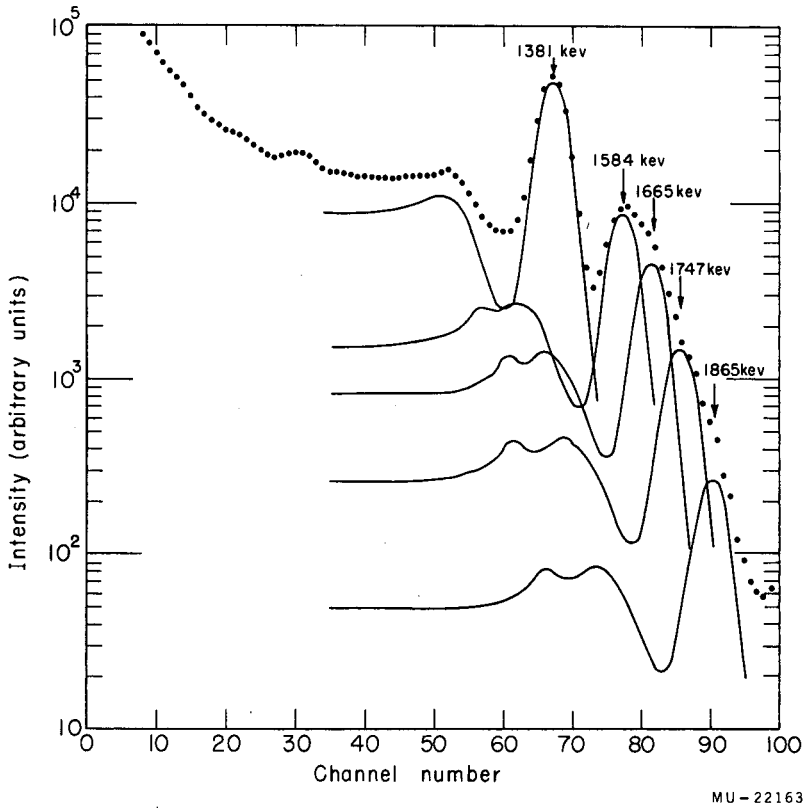

Fig. A. 14-1. Singles γ-ray spectrum of 27-hr Ho^{166} taken with a 3×3-in. NaI(Tl) crystal.

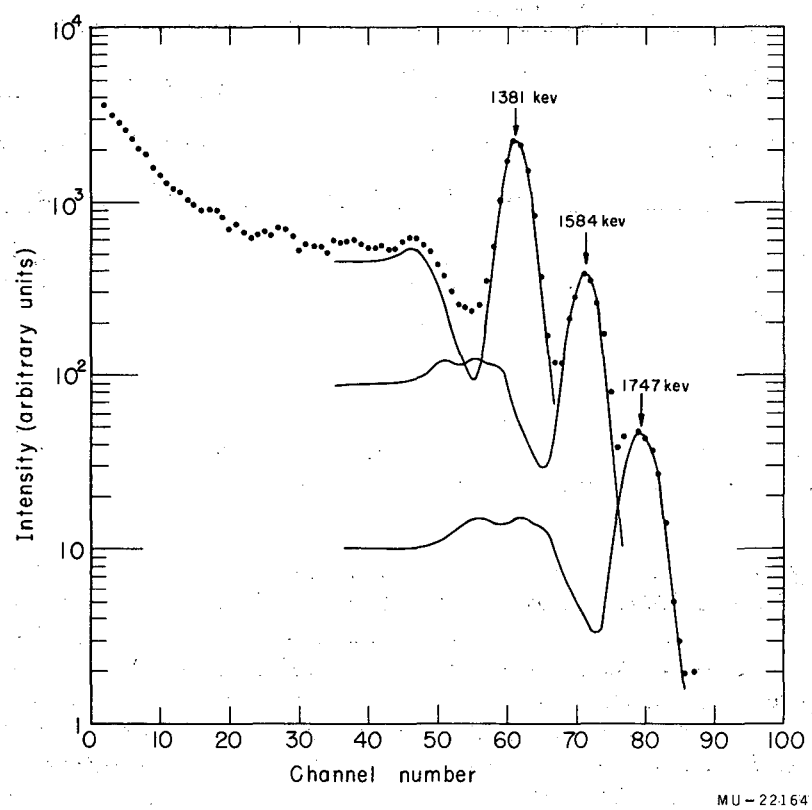

Fig. A. 14-2. High-energy γ-ray spectrum in coincidence with 80-kev γ rays and K x rays.

The relative intensities obtained from these measurements are given in Table I.

Table I. Energies and intensities of high-energy gamma rays from 27-hour Ho^{166}

Marklund et al. (Ref. 1)		This investigation	
E_γ (kev)	Intensity (%)	3×3-in. NaI relative intensity	Coincidence with 80-kev relative intensity
1379.8±.4	0.90	(0.90)[a]	(0.90)[a]
1582.4±.4	0.21	0.198	0.187
1663.0±.5	0.11	0.101	
		0.037	0.029
		0.007	

(a) This value has been used for normalization with the data in column 2.

The β-decay energy for the ground-state decay of Ho^{166} has been determined to be 1854±5 kev,[2] and 1839±5 kev.[3] The value obtained by Graham et al.[2] is presumably the most accurate, especially since a consistent value for the end point of the β group feeding the 80-kev state was determined independently in a coincidence experiment. Using this value, one obtains an energy for β decay to the 1826-kev state of 28±7 kev. Assuming that this state de-excites solely by the 1747- and 1825-kev transitions, one finds a log ft value of $5.2^{+0.3}_{-0.4}$ for this weak (0.033%) branch.

The most likely classification of this β group is: allowed, unhindered. In terms of the unified model[4] this requires $\Delta K = 0, 1$ and no change in the asymptotic quantum numbers. The odd-odd nucleus Ho^{166} has been assigned zero spin and odd parity.[3,5] This corresponds to the single particle configuration p : 7/2- [523], n : 7/2+ [633]. From available orbitals in this region[4] it is seen that the allowed, unhindered β decay can proceed only to a two-neutron state characterized by the quantum numbers 5/2- [523], 7/2+ [633], which give the required spin and parity, 1-.

[1] I. Marklund, B. van Nooijen, and Z. Gradowski, Nucl. Phys. 15, 533 (1960).

[2] R. I. Graham, J. L. Wolfson, and M. A. Clark, Phys. Rev. 98, 1173A (1955).

[3] Cork, Brice, Helmer, and Woods, Phys. Rev. 110, 526 (1958).

[4] B. R. Mottelson and S. G. Nilsson, Kgl. Danske Videnskab. Selskab Mat.-fys. Skr. 1, No. 8 (1959).

[5] L. S. Goodman, W. J. Childs, R. Marrus, I. P. K. Lindgren, and Y. A. Cabezas, Bull. Am. Phys. Soc. 5, 344 (1960).

15. ANOMALOUS ELECTRIC DIPOLE CONVERSION COEFFICIENTS IN ODD-MASS ISOTOPES OF THE HEAVY ELEMENTS (*)

Frank Asaro, Frank S. Stephens, Jr., J. M. Hollander, and I. Perlman

ABSTRACT

A detailed review is given in Table I of experimental data on the anomalous L- and M-shell conversion coefficients of low-energy electric dipole transitions observed in the decays of odd-A nuclei of high atomic number.

The data are consistent in every case with the interpretation that the E1 conversion coefficients in the L_{III} shell agree with the theoretical, model-independent coefficients calculated by Sliv and Band and by Rose. It is definitely established in several well-measured cases (see Table I) that the L_I and L_{II} coefficients are substantially larger than the theoretical values. The most striking anomaly occurs in the 84.2-kev transition in Pa^{231}, where the L_I and L_{II} coefficients are 21 and 15 times the theoretical values, respectively.

The experimental L_I and I_{II} coefficients are correlated with the lifetimes of the transitions, and it is shown in Fig. A. 15-1 that the magnitude of the anomaly (L_I plus L_{II}) is proportional to the retardation in gamma-ray lifetime over that calculated from the single-proton formulas. No systematic trend has been observed in the deviations of the L_I and L_{II} coefficients individually.

*Brief version of published paper, Phys. Rev. 117, 492 (1960).

16. ABSOLUTE MEASUREMENTS OF INTERNAL-CONVERSION COEFFICIENTS PARTICULARLY OF E2 CHARACTER, BY THE METHOD OF INTERNAL-EXTERNAL CONVERSION

J. M. Hollander, Daniel J. Horen, and Sölve Hultberg

The understanding of the internal conversion mechanism has been much improved by the recent calculations by Sliv and Band[1] and by Rose.[2] By making certain reasonable assumptions, these authors showed that the dependence of the internal-conversion coefficients on effects connected with the finite size of the nucleus can, in general, be fairly well understood. However, evidence has been obtained in the case of certain E2 conversion coefficients that experiment and theory may nevertheless still differ by as

[1] Sliv and Band, Table of γ-Ray Conversion Coefficients-Translation: Report 7ICCK Physics Dept., University of Illinois.

[2] M. E. Rose, Internal Conversion Coefficients (North Holland Publishing Co. Amsterdam, 1958).

Table I

Summary of L-shell E1 conversion coefficient data.

Nucleus	Transition Energy (kev)	Experimental Conversion Coefficients $\alpha(L_I)$	$\alpha(L_{II})$	$\alpha(L_{III})$	$\alpha(T)$	Theoretical Conversion Coefficients (Sliv and Band/Rose) $\alpha(L_I)$	$\alpha(L_{II})$	$\alpha(L_{III})$	Conversion Anomaly Factor*	Photon Retardation Factor ($t_{exp}/t_{s.\ proton}$)
Np^{237}	59.6	0.22 ± 0.02	0.46 ± 0.05	0.12 ± 0.03	1.0 ± 0.1	0.13 /0.11	0.12 /0.10	0.13 /0.13	1.1 ± 0.2	3.1×10^5
Np^{237}	26.4	2.0	3.9	1.2	10 ± 2	0.55 /0.22	1.1 /0.55	1.4 /1.3	1.3 ± 0.5	3.8×10^5
Np^{239}	74.6	0.08 ± 0.02	0.06 ± 0.02	0.06 ± 0.02	0.31	0.084/0.072	0.066/0.055	0.063/0.061	$0.04\ ^{+0.15}_{-0.04}$***	$\sim 5 \times 10^3$
Am^{243}	83.9	0.047 ± 0.011	0.057 ± 0.013	0.041 ± 0.009	0.20 ± 0.04	0.068/0.054	0.052/0.042	0.046/0.045	0.17 ± 0.10***	1.3×10^4
Pu^{239}	106.1	0.062 ± 0.007	0.071 ± 0.007	------	------	0.041/0.035	0.026/0.021	0.021/0.021	0.75 ± 0.11	2.4×10^6
Pu^{239}	61.4	0.4	------	------	------	0.13//0.10	------	------	------	----
Pa^{231}	84.2	1.3 ± 0.2	0.65 ± 0.15	0.046 ± 0.014	2.8 ± 0.4	0.064/0.055	0.042/0.037	0.039/0.039	12.8 ± 2.1	2.8×10^6
Pa^{231}	25.7	------	------	------	4.8 ± 1.0	------	------	------	0.18 ± 0.07**	4.5×10^4
Pa^{233}	86.3	0.35 ± 0.15	0.57 ± 0.26	0.08 ± 0.08	1.9 ± 0.7	0.060/0.052	0.039/0.034	0.036/0.036	6.4 ± 3.0	1.4×10^6
Pa^{233}	29.3	------	------	------	3.0 ± 0.8	------	------	------	$0.076\ ^{+0.18}_{-0.076}$**	7.2×10^4
Ra^{223}	50.0	------	------	------	0.7 ± 0.2	------	------	------	$0.045\ ^{+0.09}_{-0.045}$***	1.1×10^3
Ac^{227}	27.5	------	------	------	$\alpha(L)$ 2.8 ± 0.3	0.55 /0.28	1.2 /0.53	0.84 /1.1	0.24 ± 0.11**	3.3×10^4
Ac^{225}	40.0	0.23 ± 0.07	0.26 ± 0.09	0.41 ± 0.13	------	0.29 /0.21	0.32 /0.25	0.40 /0.37	0.13 ± 0.08***	$\leq 4.7 \times 10^3$

* Compared with theoretical conversion coefficients of Sliv and Band.
** From M-subshell ratios
*** From L-subshell ratios

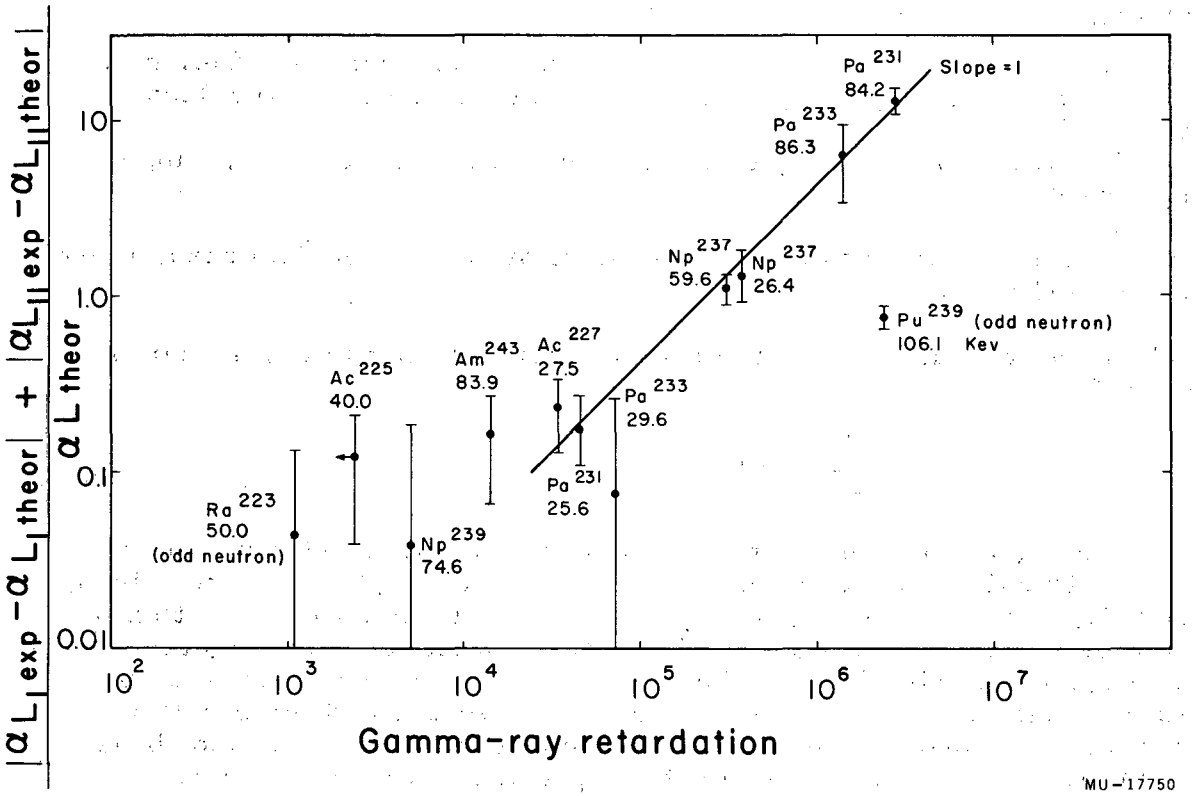

Fig. A. 15-1. E1 conversion coefficient anomaly vs γ-ray retardation. Retardation = (experimental partial photon half life) ÷ (theoretical single proton half life).

much as 20%. This work was undertaken to investigate, over a wide range of Z values, how theory and experiment compare for pure E2 transitions. The method used is that of internal-external conversion, first quantitatively applied by Hultberg.[3] To demonstrate the general use of this method we also include, in the table below, results from measurements of transitions of other multipolarities.

The most attractive features of the internal-external conversion method are:

1. It gives absolute values of the internal conversion coefficients.
2. It is completely independent of any knowledge about the decay scheme.
3. It utilizes only a very small fraction of the total energy range of the instrument.

The main limitation is the requirement of very strong sources, most often in the mC range.

The absolute value of the internal-conversion coefficient ϵ can be calculated from

$$\epsilon = \frac{A_\beta}{A_\gamma} \tau f d b,$$

where A_β and A_γ are the intensities, per unit momentum interval, of the β-spectrometrically recorded conversion electron and photoelectron lines, respectively; τ is the absolute value of the photoelectric cross section of a specific atomic shell; f is a correction factor which depends upon the photoelectric angular distribution and the particular values of the parameters that describe the sizes of the source and the converter and their relative distance; d is the absolute thickness of the converter material; and b is a dimension factor which is a constant for a given converter material.

Table I summarizes the results from the cases in which the internal-conversion coefficient has now been measured accurately by the internal-external conversion method. Measurements made at Amsterdam, Stockholm, and Nashville are also included, for completeness.

The accumulated evidence of the table leaves no doubt that even unhindered E2 transitions may have "anomalous" conversion coefficients for high-Z elements. The case of Hg^{198} is particularly well studied, and here the deviation is about 23% from the theoretical values of Rose and Sliv. At low-Z elements, however, there is good agreement with theory, which (a) supports the view that the deviations for high-Z elements may depend on nuclear structure effects, and (b) shows that there is no systematic tendency in the experimental method toward a constant shift.

[3] S. Hultberg, Arkio Fysik 15, 307 (1959).

Table I. Internal-conversion coefficients

Isotope	Energy (kev)	Multipolarity	Experiment	Rose, Sliv	Reference
$_{82}Pb^{206}$	1720	E1	$(8.2\pm1.5)\times10^{-4}$	8.2×10^{-4}	Stockendal and Hultberg (Nobel Institute)
	343	M1	0.25±0.03	0.24	"
	398	M1	0.18±0.02	0.16	"
	537	M1	0.070±0.008	0.073	"
$_{38}Sr^{87}$	483	M1	$(2.55\pm0.15)\times10^{-3}$	2.57×10^{-3}	Hultberg, Horen, and Hollander (UCLRL)
$_{82}Pb^{205}$	703	E2	0.011±0.001	0.0105	Stockendal and Hultberg (Nobel Institute)
$_{82}Pb^{206}$	803	E2	$(8.6\pm0.9)\times10^{-3}$	8.1×10^{-3}	"
$_{64}Gd^{152}$	344	E2	0.0281	0.0310	Hamilton (Vanderbilt)
$_{78}Pt^{194}$	328	E2	0.0409±0.0022	0.049	de Vries (Amsterdam)
$_{78}Pt^{196}$	354	E2	0.0367±0.0024	0.041	"
$_{79}Hg^{198}$	412	E2	0.0252±0.0013	0.03	"
			0.0243±0.001		Frey, Hamilton, and Hultberg (Vanderbilt)
			0.0241±0.0006		Hultberg, Horen, and Hollander (UCLRL)
$_{22}Ti^{46}$	892	E2	$(1.72\pm0.1)\times10^{-4}$	1.66×10^{-4}	Frey, Hamilton, and Hultberg (Vanderbilt)
$_{26}Fe^{58}$	805	E2	$(3.05\pm0.21)\times10^{-4}$	3.05×10^{-4}	"
$_{78}Pt^{192}$	317	E2	0.0476±0.0028	0.0545	"
	613	E2	0.0109±0.0008	0.012	"
$_{56}Ba^{137}$	662	M4	0.093±0.006	0.093	Hultberg and Stockendal (Nobel Institute)
			0.093±0.005		deVries (Amsterdam)
			0.093±0.004		Hultberg, Horen, and Hollander (UCLRL)
$_{38}Sr^{87}$	388	M4	0.165±0.012	0.175	"

17. THEORY OF E0 TRANSITION PROBABILITIES OF DEFORMED NUCLEI

John O. Rasmussen

There are now numerous examples that radiationless E0 electron-conversion transitions are often fairly prominent from levels of the first excited β vibrational band of spheroidal nuclei, especially in the heaviest elements.[1,2] The interesting fundamental question that arises is "Can we learn something about compressional modes of nuclear vibration from these data?" It is necessary first of all to develop as carefully as possible theories from which oscillations of nuclear density are excluded. We have re-examined earlier treatments of the quadrupole shape oscillations of a uniformly charged spheroid about an equilibrium spheroidal shape and have suggested minor modifications. We have also developed formulas for E0/E2 transition-probability ratios from a model in which the shape oscillation is expressed in terms of a coherent superposition of single-nucleon excitation.

These formulations were applied to transitions in Pu^{238} and Sm^{152}. Fair agreement by both models was found in the case of Pu^{238}, and serious overestimates of the E0/E2 ratio were obtained for Sm^{152}. Further refinements of theory and more experimental data are clearly needed before a real understanding of the E0 rate question can be claimed.

The above-mentioned work was published in Nuclear Phys. 19, 85 (1960).

The formulation of nuclear excited states in terms of single-particle excitations is the more fundamental approach. Our published calculations approximated the nucleon wave functions and energy denominators by their large deformation asymptotic limiting forms and ignored the pairing-interaction effects of smearing of the Fermi surface. A more important assumption to be noted is that the single-proton excitations considered were only the high-energy ones across two major shells. If it turns out that excitations within the shell at the Fermi surface play an important role in the first excited 0+ states of some deformed nuclei, there may be important modifications of the E0/E2 ratios we first calculated. Vibration-rotation interaction effects can also have important effects, especially on the E2 transition probabilities.[3]

---

[1] Paper A. 13.

[2] Comprehensive theoretical treatments and review of experimental data are to be found in A. S. Reiner, Nuclear Phys. (to be published).

[3] L. W. Person and J. O. Rasmussen, Effect of Vibration-Rotation Interaction on E2 Transition Probabilities in Spheroidal Nuclei, UCRL-9230, Aug. 1960 (unpublished).

18. ODD-EVEN SHIFT IN THE K=0 BAND OF ODD-ODD DEFORMED NUCLEI

Neal D. Newby, Jr.

During the past year it has become apparent that an unusual situation exists in the spacing of energy levels of certain odd-odd deformed nuclei. The best-known case is Ho^{166}. Other examples are Am^{242} and perhaps Ta^{180}. In these nuclei one expects to find low-lying energy states obeying the usual rotational level ordering, $E(I) = \hbar^2/2\mathfrak{J}\, I(I+1)$. Instead one finds that superimposed on this expected level sequence there seems to be a displacement which, at least provisionally, can be interpreted as a shift of levels of odd spin relative to those of even spin. An explanation of this "odd-even shift" has recently been suggested.[1] This proposal is as follows. The wave function of an odd-odd deformed nucleus may be written as

$$\psi = \sqrt{\frac{2I+1}{16\pi^2}} \cdot \left[\chi_{K_1}(1)\chi_{K_2}(2) D^I_{M(K_1+K_2)} + (-1)^{I+P_1P_2+1} \chi_{-K_1}(1)\chi_{-K_2}(2) D^I_{M-(K_1+K_2)} \right],$$

where $\chi_{K_1}(1)$ and $\chi_{K_2}(2)$ are the single-particle wave functions of the odd nucleons and P_1 and P_2 are their respective parities. If one now turns on a two-body interaction 0 between the odd particles and evaluates the diagonal matrix element one finds a term proportional to $(-1)^I$. Calling this term ΔE, we have

$$\Delta E = (-1)^{I+P_1P_2+1} \cdot \left\langle \chi_{-K_1}(1)\chi_{-K_2}(2) \,|\, 0 \,|\, \chi_{K_1}(1)\chi_{K_2}(2) \right\rangle \cdot \delta_{(K_1+K_2),\,-(K_1+K_2)}.$$

Clearly this term can be nonzero only when $K_1 = -K_2$. We conclude then that a residual n-p interaction in an odd-odd deformed nucleus will produce a shift, $\Delta E \approx (-1)^I$, in the level spacing of a rotational band only if that band has $K = K_1 + K_2 = 0$. (The bands in which the shift has been observed all seem to have K=0.)

Thus a measurement of ΔE is effectively a measurement of a certain off-diagonal matrix element. In order to obtain a more physical feeling for the type of scatterings which are contributing to E it is convenient to go to the limit of large deformation. In this limit we have two asymptotic selection rules on the parts of the two-nucleon interaction which can contribute to the odd-even shift:

(a) Only spin-dependent forces can contribute to ΔE. Contributions from pure Wigner or pure Majorana interactions, for example, are forbidden.
(b) In cases where $\Sigma_1 + \Sigma_2 = 1$ the shift is due to the tensor interaction only. Contributions from all central forces are forbidden.

The above selection rules are rigorously true only in the asymptotic limit. Their approximate validity for strongly deformed nuclei will depend on how closely the odd-particle wave functions approach their asymptotic values.

---

[1] F. Asaro, I. Perlman, J. O. Rasmussen, and S. G. Thompson, Phys. Rev. 120, 934 (1960).

In addition to the above selection rules another, more general, selection rule has been found: The Wigner component of the neutron-proton interaction cannot contribute to the odd-even shift--independent of nuclear deformation.

In computing the off-diagonal matrix element involved in ΔE it is rather important to use finite range forces. Calculations for Ho^{166} have been completed. We merely summarize the results here. It is found that a two-body interaction which is very similar to n-p interactions used previously in other calculations reproduces the experimental odd-even shift in Ho^{166}. That such a fit would be possible was by no means obvious a priori. (It was not obvious, for example, that the matrix element would even be of the proper sign.) That such a "realistic" two-nucleon force can provide agreement in Ho^{166} is highly satisfying and lends support to the physical model under study here.

Calculations are under way on Am^{242}, where it is believed that the situation is such as to make asymptotic selection rule No. 2 applicable. In such a case we expect a damping out of the contributions of central forces, and a study of the role of the tensor force becomes imperative.

19. TENSOR-FORCE EFFECTS IN ODD-ODD SPHERICAL NUCLEI (*)

Neal D. Newby, Jr.

A recent article has surveyed our present experimental and theoretical understanding of the ground-state coupling rules in odd-odd nuclei.[1] As summarized there, studies with zero-range central forces have yielded a qualitative theoretical foundation for Nordheim's coupling rules (we use the form of these rules as given in Ref. 1). Such calculations support the prediction of Nordheim's "strong rule" ($j_1=\ell_1\pm 1/2,\ j_2=\ell_2\mp 1/2 \Rightarrow J_{G.S.}=|j_1-j_2|$). In the "weak rule" situation ($j_1=\ell_1\pm 1/2,\ j_2=\ell_2\pm 1/2, \Rightarrow J_{G.S.}=j_1+j_2$) the calculations using central forces predict a competition between $J=|j_1-j_2|$ and $J=j_1+j_2$ for the ground state. Recent experimental studies show that in a weak rule situation $J=|j_1-j_2|$ seems to be preferred over $J=j_1+j_2$.[2]

In an effort to understand the breakdown of Nordheim's weak rule we have made a survey of the experimental data on weak rule situations. A surprising fact is that out of a total of 23 cases in which the weak rule is applicable we find that 20 cases have $j_1=\ell_1+1/2$, $j_2=\ell_2+1/2$ rather than spin and orbital momentum antiparallel for both particles.

---

*Brief version of published paper, Phys. Rev. 119, 747 (1960).

[1] C. J. Gallagher, Jr., and S. A. Moszkowski, Phys. Rev. 111, 1282 (1958).

[2] M. H. Brennan and A. M. Bernstein, Bull. Am. Phys. Soc. 5, 20 (1960).

Since previous calculations had been confined to central forces only, an attempt was made to investigate the effect on the coupling rules of an n-p tensor force. Two methods were used. The first utilized a semi-classical model. This model views the n-p tensor force as simply a classical tensor force (dipole-dipole interaction) and visualizes the wave functions as probability clouds. Such a picture is useful only for certain quantum mechanical states. Surprisingly enough this model predicts that a tensor interaction of the "right sign" (as in the deuteron) will raise the energy of the state,

$$\left|\ell_1 1/2\ j_1=\ell_1+1/2,\ \ell_2 1/2\ j_2=\ell_2+1/2,\ J=j_1+j_2\right\rangle = {}^3(L=\ell_1+\ell_2)_J.$$

This will tend to make the ground state $J = |j_1-j_2|$ in a weak rule situation, in agreement with observation.

The second method employed a previously used approximation.[3] This approximation involves computing the exact diagonal matrix element for a tensor force which gives more weight to interactions at large rather than small distances. This method substantiated the prediction of the semi-classical model that a tensor force of the "right sign" would tend to break down Nordheim's weak rule.

[3] N. Newby, Jr., and E. J. Konopinski, Phys. Rev. 115, 434 (1959).

20. THEORETICAL CALCULATIONS OF MAGNETIC MOMENTS OF SPHEROIDAL NUCLEI

Lung-Wan Chiao and John O. Rasmussen

We have noted that by simply reducing the gyromagnetic ratios g_s in the calculation of magnetic moments of odd-mass spheroidal nuclei a great systematic improvement in agreement with experimental values is obtained.[1] Accordingly, to test whether a uniform reduction of g_s is applicable we have recalculated magnetic moments of many spheroidal nuclei of odd-A and odd-odd types, using for the odd proton $g_s = 4$ and for the odd neutron $g_s = -2.4$. For odd-proton nuclei the collective gyromagnetic ratio g_R is taken as Z/A; for odd-neutron nuclei g_R is taken as Z/2A; and for odd-odd g_R is assumed 3Z/4A. The assumptions on g_R improve the general agreement and are semiquantitatively justified by theory.[2] The appropriate nucleonic wave functions of Nilsson[3, 4] are taken.

[1] J. O. Rasmussen and L. W. Chiao, Concerning the Magnetic Moments of Deformed Nuclei, in Proceedings of the International Conference on Nuclear Structure, 1960, p. 646.

[2] S. G. Nilsson and O. Prior (to be published).

[3] S. G. Nilsson, Kgl. Danske Videnskab. Selskab Mat.-fys Medd. 29, No. 16 (1955).

[4] B. R. Mottelson and S. G. Nilsson, Kgl. Danske Videnskab. Selskab Mat.-fys. Skr. 1, No. 8 (1959).

We have also called attention[1] to the often important influence on the magnetic moment calculations brought about by admixture into the wave function of components with different K values (K being the projection of the total nuclear angular momentum on the nuclear symmetry axis). We have carried out these further corrections in a few cases where they were expected to be significant.

Tables I, II, and III summarize the results of these calculations.

It is most likely that the success of the substantially "quenched" g_s factors is not caused primarily by alterations of the virtual meson contribution to the nucleonic magnetic moment for nucleons in nuclear matter. Recent theoretical calculations by Drell and Walecka[5] show this effect to be ≈ 7%. Furthermore, the experimental magnetic moment of the spherical nucleus Pr^{141}, possessing a closed neutron shell, has a value very near the upper Schmidt limit appropriate to a $d_{5/2}$ proton. Gauvin has made shell-model calculations[6] on spheroidal Lu^{175} and Ta^{181} which show the effect on the magnetic moment of systems with three unpaired particles brought about by configuration mixing. Our relatively good success with empirically reduced and constant g_s factors suggests that the apparent moment quenching throughout the deformed region arises from small admixtures of many different configurations.[7] Thus, there is an averaging effect extending throughout the deformed region. The more important configurations for quenching are presumably those in which a nucleon pair is broken by promotion of a nucleon to an unoccupied orbital of its spin-orbit conjugate. The proton configuration in Pr^{141} does not offer such a possibility, as the $g_{1/2}$ orbital is just completed and there is a single odd proton in the $d_{5/2}$ orbital. Throughout the deformed region there are always many ways of forming the broken pairs just mentioned.

---

[5] S. D. Drell and J. D. Walecka, Phys. Rev. 120, 1069 (1960).

[6] J. N. L. Gauvin, Nuclear Phys. 8, 213 (1958).

[7] We are indebted principally to B. R. Mottelson for discussion with us of his ideas along these lines.

Table I. Magnetic moments of odd-proton nuclei.

Isotope	Energy of state	I_{exp}	Assigned orbital $\langle N\ n_z\ \Omega\ \Sigma \rangle$	Assigned δ	$\langle S \cdot l \rangle$	$g_R = Z/A$	$\mu_{theo.}$ [a]	$\mu_{theo.}$ [b]	$\mu_{exp.}$
$_{63}Eu^{153}$		5/2	413↓	0.29	-0.946	0.412	1.3		1.50
$_{65}Tb^{159}$		3/2	411↑	0.29	0.609	0.409	1.9		±1.94
$_{67}Ho^{165}$		7/2	523↑	0.28	1.405	0.406	4.0	4.1	4.18
$_{69}Tm^{169}$		1/2	411↓	0.27	-0.125	0.408	-0.2		-0.21
$_{69}Tm^{169}$	118	5/2	411↓	0.27	0.058	0.408	0.7		0.55 ± 0.15
$_{71}Lu^{175}$		7/2	404↓	0.26	-1.565	0.406	2.0		2.0 ± 0.2
$_{71}Lu^{175}$	114	9/2	404↓	0.26	-1.565	0.406	2.5		2.25
$_{73}Ta^{181}$		7/2	404↓	0.23	-1.552	0.403	2.0		2.34
$_{73}Ta^{181}$	482	5/2	402↑	0.23	-1.202	0.403	3.1		3.0 - 3.3
$_{75}Re^{185}$		5/2	402↑	0.19	1.198	0.405	3.1		3.14
$_{75}Re^{187}$		5/2	402↑	0.19	1.198	0.401	3.1		3.18
$_{77}Zr^{191}$		3/2	402↓	0.14	-0.622	0.403	0.4		0.2
$_{77}Zr^{193}$		3/2	402↓	0.12	-0.613	0.399	0.4		0.2
$_{89}Ac^{227}$		1/2	530↑	~0.2	0.904	0.392	1.1		1.1
$_{91}Pa^{231}$		3/2	530↑	~0.3	~1.000	0.394	2.1		2.1
$_{91}Pa^{233}$		3/2	530↑	~0.3	~1.000	0.391	2.1		2.1
$_{93}Np^{237}$		5/2	642↑	0.25	0.734	0.392	2.7	3.0	>2.7
$_{93}Np^{237}$	60	5/2	523↓	0.25	-0.805	0.392	1.35		2.0 ± 0.5
$_{95}Am^{241}$		5/2	523↓	0.27	-0.826	0.394	1.4		1.4
$_{95}Am^{243}$		5/2	523↓	0.27	-0.826	0.391	1.4		1.4

a. Assumes K a good quantum number.

b. Corrected for K-configuration mixing via the Coriolis interaction.

Table II. Magnetic moments of odd-neutron nuclei.

Isotope	Energy of State	I_{exp}	Assigned orbital $\langle N\ n_z\ \Omega\ \Sigma \rangle$	Assigned δ	$\langle S \cdot l \rangle$	$g_R = Z/2A$	$\mu_{theo.}$ (a)	$\mu_{theo.}$ (b)	$\mu_{exp.}$
$_{64}Gd^{155}$		3/2	521↑	0.27	0.483	0.206	-0.37		-0.28
$_{64}Gd^{157}$		3/2	521↑	0.27	0.483	0.204	-0.37		-0.37
$_{66}Dy^{161}$		5/2	642↑	0.28	0.777	0.205	-0.39	-0.48	-0.48
$_{66}Dy^{163}$		5/2	523↓	0.28	-0.757	0.202	0.67		0.67
$_{68}Er^{167}$		7/2	633↑	0.29	1.302	0.204	-0.54	-0.65	-0.59
$_{70}Yb^{171}$		1/2	521↓	0.28	-0.250	0.205	0.40		0.46
$_{70}Yb^{173}$		5/2	512↑	0.27	1.008	0.202	-0.55		-0.65
$_{72}Hf^{177}$		7/2	514↓	0.25	-1.162	0.203	0.80		0.61
$_{72}Hf^{177}$	114	9/2	514↑	0.25	-1.162	0.203	0.97		0.99 ±0.27
$_{72}Hf^{179}$		9/2	624↓	0.23	-1.812	0.201	-0.63	-0.70	-0.47
$_{74}W^{183}$		1/2	510↑	0.21	-0.250	0.202	0.48		0.12
$_{76}Os^{187}$		1/2	510↑	0.18	-0.250	0.203	0.48		0.12
$_{76}Os^{189}$		3/2	512↓	0.15	-0.423	0.201	0.50		0.65
$_{92}U^{233}$		5/2	633↓	0.23	-0.408	0.197	0.42		0.97
$_{92}U^{235}$		7/2	743↑	0.24	1.100	0.196	-0.43	-0.49	-0.66±0.07
$_{94}Pu^{239}$		1/2	631↓	0.26	0.119	0.197	-0.06		±0.02 a = -0.96
$_{94}Pu^{241}$		5/2	622↑	0.27	0.783	0.195	-0.40		> 10.11

a. Assumes K a good quantum number.

b. Corrected for K-configuration mixing via the Coriolis interaction.

Table III. Magnetic moments of odd-odd nuclei.

Nucleus	Spin	Configuration Proton	Neutron	$\langle s_z \rangle_p$	$\langle l_z \rangle_p$	$\langle s_z \rangle_n$	$g_R = \frac{3Z}{4A}$	$\mu^*_{theo.}$	$\mu_{theo.}$	$\mu_{asymp-totic}$	μ_{exp}
$_{63}Eu^{152}$	3-	[411↑ +	521↑]	0.400	1.100	0.296	0.311	1.88	1.73	1.58	1.9
$_{63}Eu^{154}$	3-	[411↑ +	521↑]	0.400	1.100	0.296	0.307	1.88	1.72	1.58	2.0
$_{65}Tb^{160}$	3-	[411↑ +	521↑]	0.400	1.100	0.296	0.305	1.88	1.72	1.58	1.60 ± 0.25
$_{67}Ho^{162}$	6-	[523↑ +	642↑]	0.398	3.102	0.304	0.310	3.57	3.66	3.52	
$_{67}Ho^{166}$	7-	[523↑ +	633↑]	0.398	3.102	0.366	0.303	3.70	3.60	3.59	3.3 ± 0.5
$_{69}Tm^{170}$	1-	[411↓ +	521↓]	-0.356	0.856	-0.263	0.304	0.09	0.13	0.25	0.24
$_{71}Lu^{176}$	7-	[404↓ +	514↓]	-0.449	3.949	-0.362	0.334	2.77	2.94	3.09	3.27
$_{71}Lu^{176m}$	1+	[404↓ -	624↑]	-0.449	3.949	-0.417	0.334	1.74	1.74	1.77	
$_{73}Ta^{180m}$	1+	[404↓ -	624↑]	-0.449	3.949	-0.417	0.304	1.72	1.73	1.75	
$_{93}Np^{236}$	1+	[523↓ -	743↑]	-0.312	2.812	-0.326	0.295	1.31	1.32	1.60	
$_{93}Np^{236}$	6+	[523↑ -	743↓]	-0.312	2.812	0.326	0.295	0.10	0.70	0.08	
$_{93}Np^{238}$	2+	[642↑ -	631↓]	0.283	2.217	0.150	0.293	2.18	2.05	2.06	
$_{95}Am^{242}$	1-	[523↓ -	622↑]	-0.312	2.812	-0.792	0.294	0.29	0.29	0.29	0.33
$_{95}Am^{242}$	5-	[523↓ +	622↑]	-0.312	2.812	0.792	0.296	-1.39	-0.04	0.08	

μ^* : free space g_s values calculation.

μ : quenched g_s values calculation.

21. NUCLEAR ORIENTATION OF IODINE BY ELECTRIC hfs ALIGNMENT (*)

D. A. Shirley, C. E. Johnson,† and J. F. Schooley

Although suggested by Pound in 1949,[1] the method of nuclear alignment by quadrupole coupling had seen very limited use,[2] and no successful experiments employing pure quadrupole coupling had been performed in the adiabatic demagnetization temperature region.[3] The failure of previous experiments to show nuclear ordering could be accounted for by a long spin-lattice relaxation time, but simple theoretical calculations predict a very short relaxation time in crystals containing paramagnetic ions.

In order to extend the electric hfs alignment method into the adiabatic demagnetization temperature range, we prepared a single crystal of copper p-iodobenzenesulfonate containing some labeled I^{131} atoms. On demagnetization to 0.03°K this crystal exhibited a slow warm-up rate, linear in reciprocal magnetic temperature (Fig. A. 21-1). This may be interpreted as showing that no collective behavior is taking place among the copper ions, and indicating that the cooling process is stopped by entropy transfer from the iodine nuclear spin system (i. e., quadrupole alignment). Anisotropic angular distributions of the 637-kev γ ray and the 364-kev γ ray were observed. The anisotropies were found to vary inversely with temperature, as expected for quadrupole alignment (Fig. A. 21-2).

A detailed interpretation of this experiment leads to a spin assignment of 5/2+ for the 637-kev state of Xe^{131}. Assuming the 637-kev transition is pure E2, the amplitude mixing ratio $\delta(E2/M1)$ for the 364-kev γ ray is -6.7 ± 0.5. The quadrupole coupling constant is found to be eq Q=-950±190 Mc, in good agreement with quadrupole resonance results in similar molecules.

---

*Brief version of published paper, Phys. Rev. 120, 1777 (1960).

†Present address: AERE, Harwell, England.

[1] R. V. Pound, Phys. Rev. 76, 1410 (1949).

[2] J. W. T. Dabbs, L. D. Roberts, and G. W. Parker, Physica 24, 569 (1958).

[3] J. M. Daniels, Can. J. Phys. 32, 662 (1954).

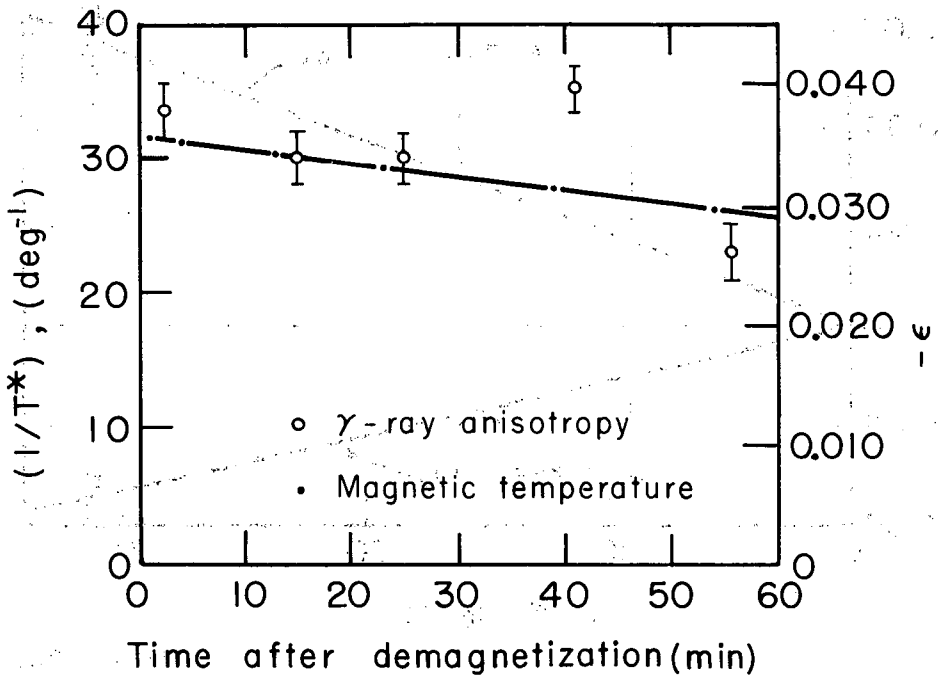

MU-20397

Fig. A.21-1. Magnetic temperature and anisotropy of the 364-kev γ ray of Xe^{131} vs time after demagnetization of copper p-iodobenzenesulfonate. The linear time dependence suggests that the cooling process is stopped by removal of entropy from the iodine nuclear spin system well above temperatures where the copper ions show appreciable collective behavior. No relaxation effects are evident.

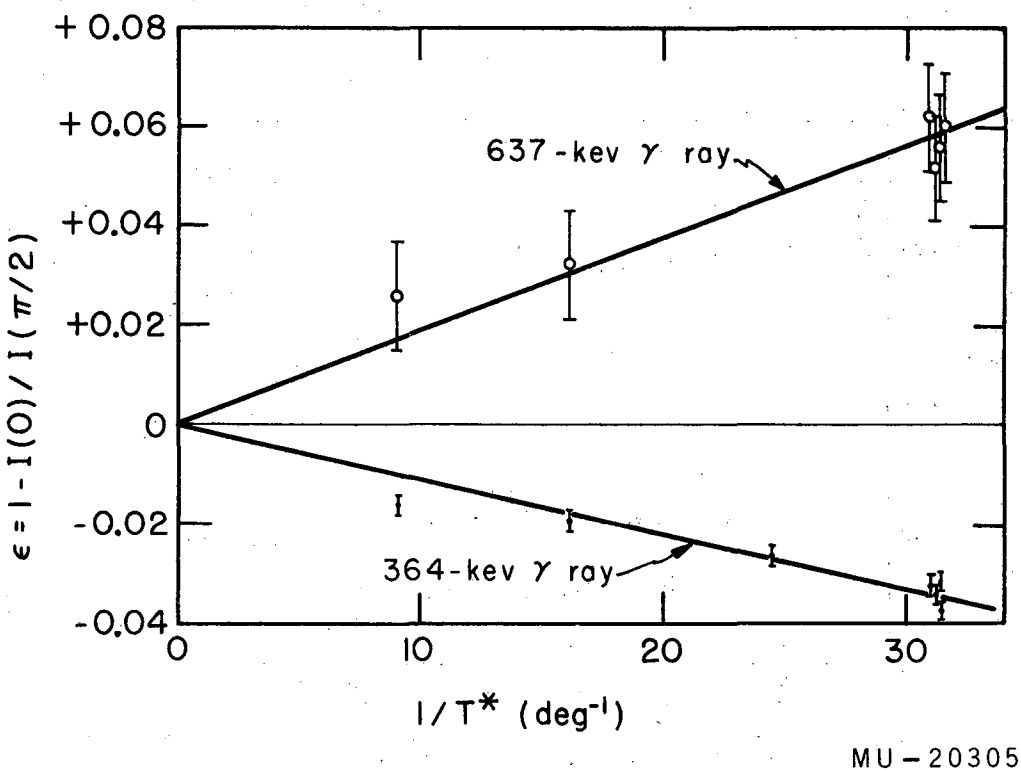

Fig. A.21-2. Anisotropies of the 364- and 637-kev γ rays of Xe^{131} vs reciprocal magnetic temperature. For quadrupole alignment the anisotropy would be expected to have a (1/T) dependence on temperature for low degrees of alignment.

22. NUCLEAR ORIENTATION OF TERBIUM-160 (*)

D. A. Shirley, C. E. Johnson,† and J. F. Schooley

Nuclear orientation of terbium isotopes offers an opportunity to study the effects of several terms in the spin Hamiltonian of Tb^{+3} in the ethyl-sulfate lattice,

$$\mathcal{H} = g_{||}\beta H_z S_z + A S_z I_z + \Delta_x S_x + \Delta_y S_y + P[I_z^2 - 1/3\, I(I+1)] + C S_z T_z, \qquad (1)$$

as well as nuclear properties.

Tripositive terbium is a non-Kramers ion (thus an electric field could split its energy levels into spin singlets), and the lowest doublet is split in this crystal by the term in Δ, which is due to the V_6^6 component of the crystal field potential.[1]

Terbium is unique among ions which have been used for nuclear alignment experiments, both in the cause of the term in Δ and in its magnitude. The effects of quadrupole coupling and the term in C had also not been observed previously in this lattice. These three interactions create an unusual dependence of the γ-ray anisotropy on temperature (Fig. A. 22-1).

The term in C is introduced to account for spin-spin interactions between the terbium ions and neighboring neodymium ions in the lattice. It is derived from a more general expression for spin-spin interactions,

$$\mathcal{H}_{ss} = -g_{Tb}\, g_{Nd}\, \beta^2 \sum_i \left[\frac{3(\vec{s}_j \cdot \vec{r}_{ij})(\vec{s}_i \cdot \vec{r}_{ij})}{|r_{ij}|^5} - \frac{(\vec{s}_i \cdot \vec{s}_j)}{|r_{ij}|^3} \right], \qquad (2)$$

by considering the magnitude of splittings caused by nearest neighbors, next neighbors, etc. When quantization along the C axis is introduced and the lattice parameters are considered, it turns out that only the contributions of the two nearest neighbors on the axis have an appreciable effect on the alignment of the terbium nuclei. Thus Eq. (2) becomes

$$\mathcal{H}_{ss} = \frac{-2 g_{\|Tb}\, g_{\|Nd}\, \beta^2}{d^3} S_z (S_{1z} + S_{2z}).$$

Defining the total spin operator for the nearest neighbors $\vec{T} = \vec{S}_1 + \vec{S}_2$, and gathering constants into C, the above becomes the last term in (1).

The theoretical curves in Fig. A. 22-1 were calculated with use of a Hamiltonian of the form (1). It was necessary to include all the terms to obtain agreement with the experimental data.

---

*Brief version of published paper, Phys. Rev. 120, 2108 (1960).

†Present address: AERE, Harwell.

[1] J. M. Baker and B. B. Bleaney, Proc. Roy. Soc. (London) A245, 150 (1958).

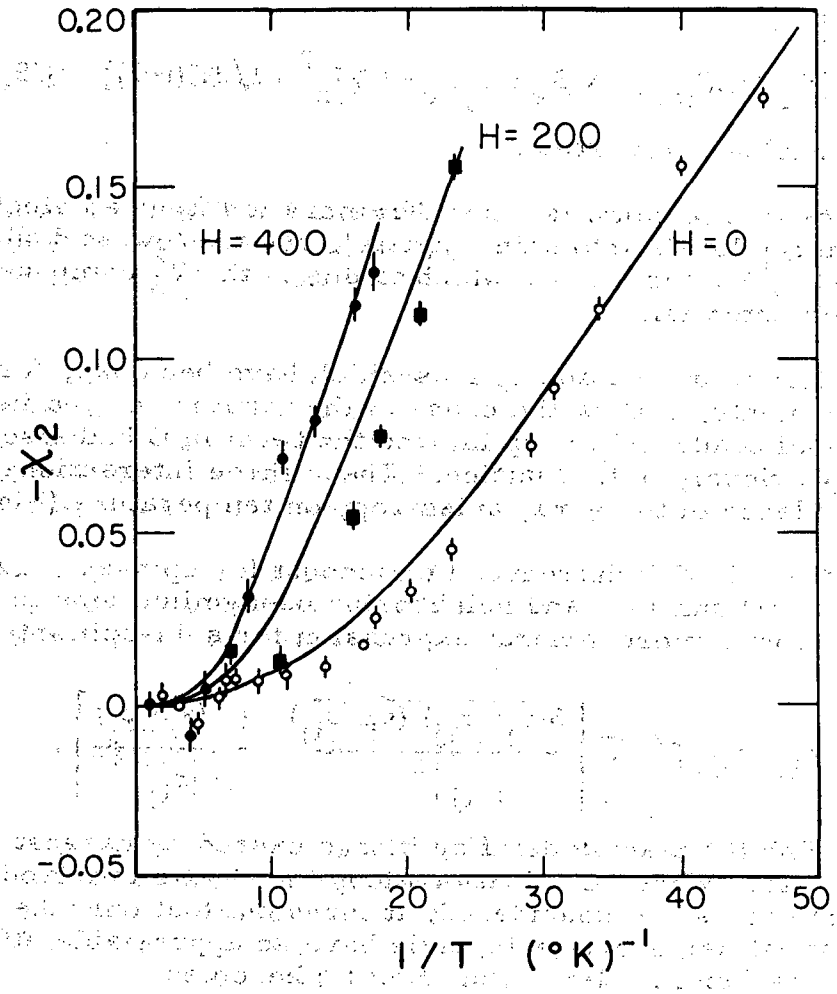

MU-20729

Fig. A.22-1. The coefficient X_2 of the 298-kev γ-ray of Dy^{160} vs reciprocal absolute temperature. Here O, □, and ● denote data taken in external magnetic fields of 0, 200, and 400 gauss, respectively.

From the temperature, magnetic field, and angular dependence of several γ rays following the decay of Tb^{160}, the following new information was obtained. The spin and parity of Tb^{160} are definitely 3-. The magnetic moment is $|\mu| = 1.60 \pm .25$ nm, and the quadrupole moment is $Q = +1.9 \pm .5$ b. The 1.36-Mev excited state of Dy^{160} has spin 2-. The 1178-kev γ ray is less than 0.7% quadrupole. The 962-kev γ ray is 94.7±3.5% E2, and the 880-kev γ ray is 97.0±1.5% E2.

23. NUCLEAR ALIGNMENT OF NEODYMIUM-147

Gene A. Westenbarger and D. A. Shirley

The isotope Nd^{147} has been aligned at low temperatures in a single crystal of neodymium ethylsulfate. The intensity of γ radiation was studied as a function of angle with respect to the crystalline c axis and of the temperature of the crystal. The anisotropy of each γ ray was found to follow a $P_2(\cos\theta)$ distribution pattern about the crystal axis.

The spin Hamiltonian for Nd^{147} in neodymium ethylsulfate is

$$\mathcal{H} = g_{||}\,\beta \mathcal{H}_z S_z + A S_z I_z + B\,(S_x I_x + S_y I_y) + C\,S_z\,(S_{1z} + S_{2z}),$$

where $A = (0.0289)\ cm^{-1}$ and $B = (0.0151)\ cm^{-1}$ as determined by paramagnetic resonance.[1] The spin-spin interaction term, C, is explained elsewhere.[2] The energy-level diagram for Nd^{147} calculated for different values of the magnetic field is shown in Fig. A. 23-1. This diagram shows the influence of the B term of the Hamiltonian in changing the energy levels and thus the alignment.

The dependence of the anisotropy of the 530-kev γ ray on temperature is shown in Fig. A. 23-2. The upper curves are obtained by increasing the orientation by the application of a small polarizing field along the c axis of the sample during the counting period. The curves are calculated theoretically and only a few experimental points are taken in order to show that one can accurately calculate the increase in anisotropy produced by a polarizing magnetic field. These data thus confirm the validity of the "saturation correction" for the susceptibility of this salt measured in a magnetic field.[2] Figure A. 23-3 shows a partial decay scheme[3] of Nd^{147}. The spins of the ground states of Nd^{147} and Pm^{147} have been measured,[1, 4] and the β transitions are all first-forbidden.[5] Thus the excited states of Pm^{147} which are populated by the β decay could have spins 3/2, 5/2, or 7/2, while the 412-kev state could be 3/2, 5/2, 7/2, or 9/2.

---

[1] R. W. Kedzie, M. Abraham, and C. D. Jeffries, Phys. Rev. 108, 54 (1957).

[2] C. E. Johnson, J. F. Schooley, and D. A. Shirley, Phys. Rev. (to be published).

[3] J. M. Cork, M. K. Brice, R. G. Helmer, and R. M. Woods, Phys. Rev. 110, 526 (1958).

[4] A. Cabezas, I. Lindgren, E. Lipworth, R. Marrus, and M. Rubinstein, Nuclear Phys. 20, 509 (1960).

[5] H. S. Hans, B. Saraf, and C. E. Mandeville, Phys. Rev. 97, 1267 (1955).

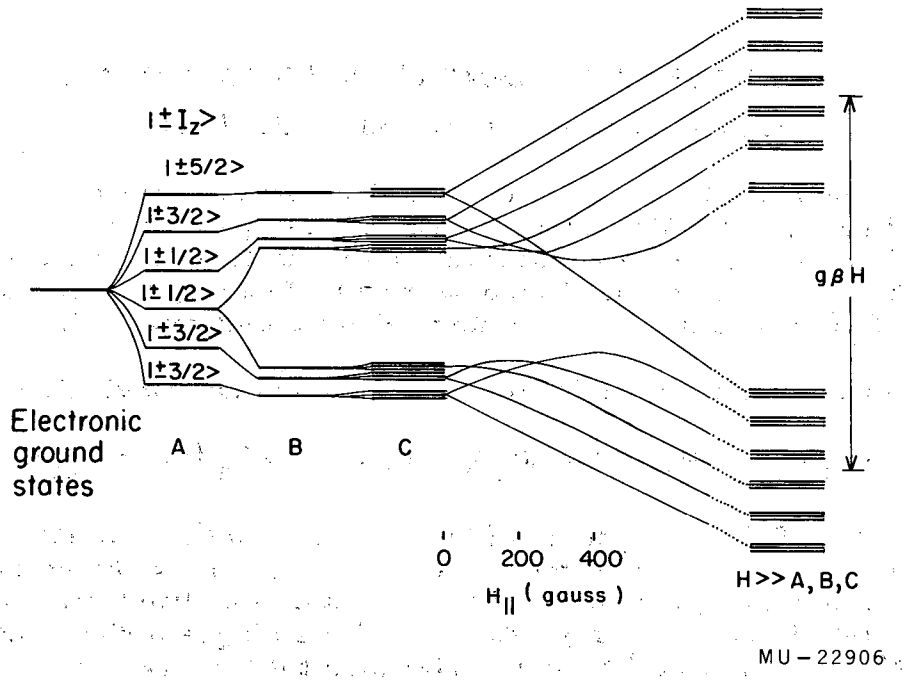

Fig. A. 23-1. Energy-level diagram for Nd^{147} in $Nd(C_2H_5SO_4)_3 \cdot 9\ H_2O$.

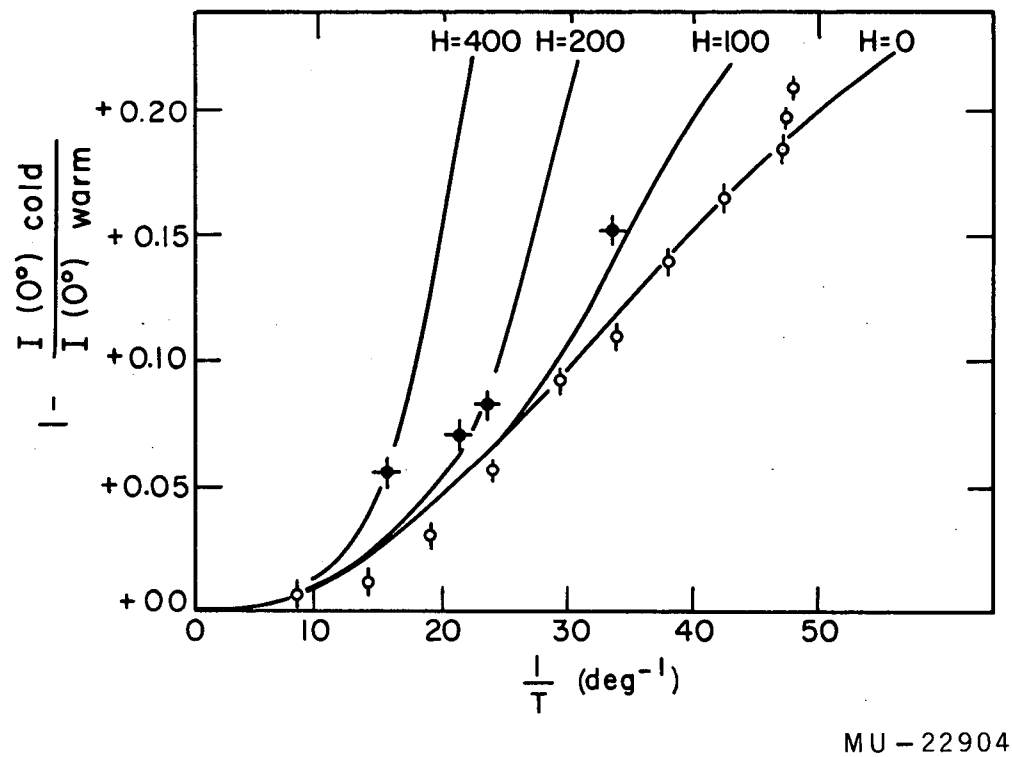

Fig. A. 23-2. Temperature dependence of the anisotropy of the 530-kev γ ray of Pm^{147}.

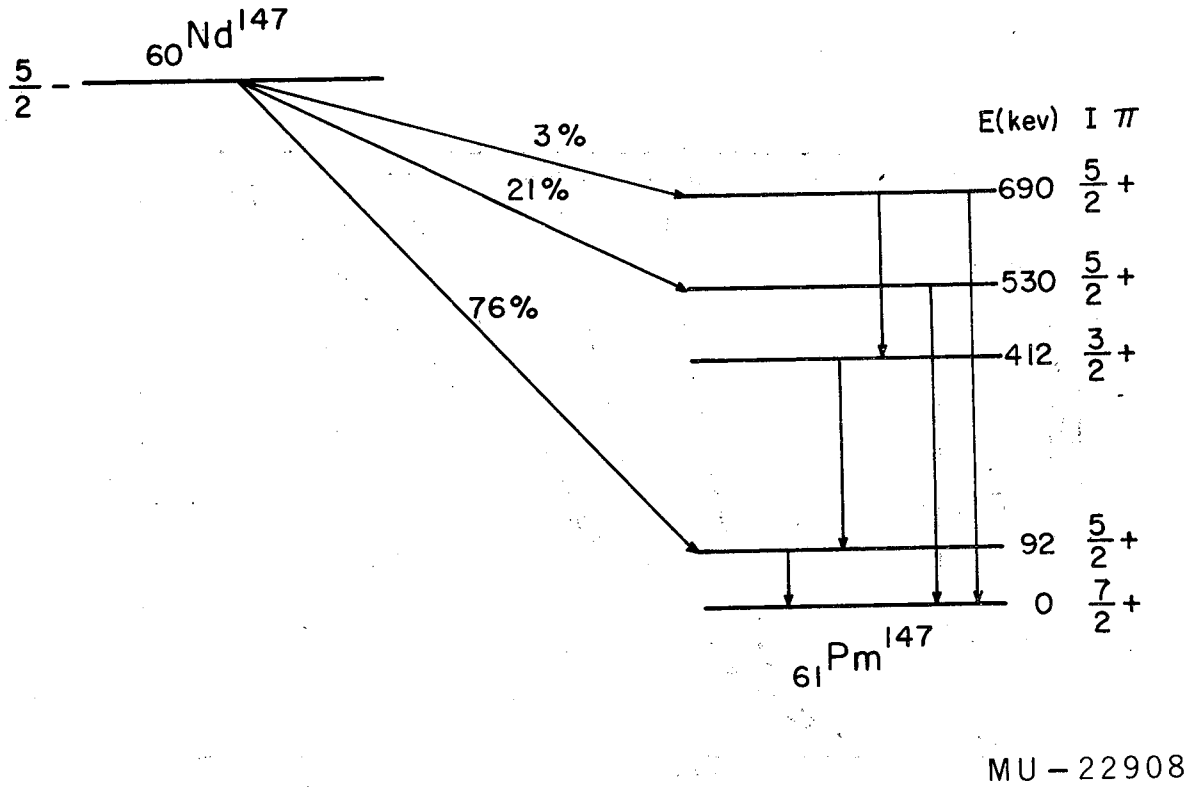

Fig. A. 23-3. Partial decay scheme for Nd^{147}. The spins of levels at 412, 530, and 690 kev were established by this investigation.

Shell-model systmatics indicate that the 92-kev level is 5/2+. Evidence for this given by polarization measurements of the 92-kev γ ray[6] and also by the internal-conversion coefficient. Both indicate an M1 character for the 92-kev γ ray. The 530-kev and 690-kev states cannot have spin 3/2, as this would require a pure E2 transition to the ground state and the measured anisotropies are too large for this to be true. Spin 7/2 is ruled out for the 530-kev state by measurements of the polarization of the 530-kev γ ray.[6] We have concluded therefore that the spin of the 530-kev level is 5/2+ and the E2/M1 mixing ratio is -0.95±.30.

The anisotropy of the 690-kev γ ray together with independent angular correlation measurements[7] eliminates the spin of 7/2 for the 690-kev level. Spin 5/2 is consistent with both experiments and so we have concluded that the 690-kev level has spin 5/2+. By the same type of reasoning we have determined that the 412-kev state has spin 3/2+. The final spin assignments are shown in the figure. All the γ rays indicated are mixed E2/M1 transitions with mixing ratios as follows:

Gamma-ray energy	δ(E2/M1)
92 kev	+0.13±.02
278 kev	+0.14±.02
320 kev	-0.36±.02
530 kev	-0.95±.30
690 kev	-0.95±.30

[6] G. R. Bishop, M. A. Grace, C. E. Johnson, H. R. Lemmer, and J. Perez y Jorba, Phil. Mag. 2, 534 (1957).

[7] E. Bodenstedt, private communication.

24. NUCLEAR ORIENTATION OF DYSPROSIUM-155 AND DYSPROSIUM-157

Quirino O. Navarro and D. A. Shirley

The isotopes Dy^{155} and Dy^{157} were aligned at low temperatures in a single crystal of neodymium ethylsulfate, by using the magnetic hfs method. The angular distribution of γ radiation following the decay of these isotopes was studied as a function of temperature in the region $0.02\,^{o}K < T < 1^{o}K$. From the multipolarities and the signs of the anisotropy of the observed γ rays, spin assignments of 5/2- were made to the states at 227 kev in Tb^{155} and at 327 kev in Tb^{157}, confirming the level assignments proposed earlier.[1, 2] Assuming I = 3/2 for both dysprosium isotopes as well as pure L = 1 β decay to the 5/2- states, nuclear moments of $|\mu_{155}| = 0.21 \pm .05$ nm and $|\mu_{157}| = .32 \pm .02$ were derived.

[1] K. S. Toth and J. O. Rasmussen, Phys. Rev. 115, 1950 (1959).

[2] K. S. Toth and O. B. Nielsen, private communication.

The observed values of the nuclear moment of Gd^{155}, the isotone of Dy^{157}, are -0.30 nm[3] and |0.30±.05| nm.[4, 5] The theoretical nuclear moments are based upon ground-state assignments similar to the isotonic gadolinium isotopes.[6] With use of the values of 0.28 and 0.32, respectively, for the deformation parameter δ and the gyromagnetic ratio of the core g_R given by Nilsson and Prior,[7] the theoretical moments of Dy^{155} and Dy^{157} are calculated to be -0.33 nm and -0.49 nm, respectively, which are in qualitative agreement with the present results.

---

[3] D. R. Speck, Phys. Rev. 101, 1725 (1956).

[4] W. Low, Phys. Rev. 103, 1309 (1956).

[5] Corrected for $\langle 1/\gamma^3 \rangle = 48.5\ A^{-3}$ (see Ref. 8).

[6] B. R. Mottelson and S. G. Nilsson, Kgl. Danske Videnskab. Selskab Mat. -fys. Skr. 1, No. 8 (1959).

[7] S. G. Nilsson and O. Prior, The Effect of Pair Correlation on the Moment of Inertia and the Collective Gyromagnetic Ratio of Deformed Nuclei, Kgl. Danske Videnskab. Selskab Mat. -fys. Medd. (to be published).

[8] B. R. Judd and I. P. K. Lindgren, "Theory of Zeeman Effects in the Ground Multiplets of Rare Earth Atoms," UCRL-9188, April 25, 1960 (submitted to Phys. Rev.).

25. NUCLEAR ORIENTATION OF PROMETHIUM-144 (*)

J. F. Schooley,† D. A. Shirley, and John O. Rasmussen

Tripositive promethium is a non-Kramers ion (i. e., it has an even number of electrons, and its energy levels can be split into singlets by an electric field) but calculations based upon the theory of Elliott and Stevens[1] with crystal-field parameters interpolated from other rare earth ethylsulfates[2] indicate that the ground electronic level of Pm^{+3} in the ethylsulfate lattice is a doublet composed of admixtures of the states $|J_z = \pm 4\rangle$ and $|J_z = \mp 2\rangle$. Further calculation yielded values of the spectroscopic splitting factor, $g_{\parallel}$, and the magnetic-hyperfine-structure constant A of 0.47±.04 and [(0.019±.002) (μ/I)] cm^{-1}, respectively. Thus an orientation experiment

---

*This work was reported at the seventh International Conference on Low-Temperature Physics, August 26-September 3, 1960, in Toronto, Canada. A detailed report is available in a report by J. F. Schooley, D. A. Shirley, and J. O. Rasmussen, Gamma-Ray Anisotropies from Oriented Pm^{144}, UCRL-9276, July 1960, scheduled for publication in Phys. Rev. in January 1961.

†Now at National Bureau of Standards, Washington, D. C.

[1] R. S. Elliott and K. W. H. Stevens, Proc. Roy. Soc. (London) A218, 553 (1953).

[2] B. R. Judd, Proc. Roy. Soc. (London) A251, 407 (1959).

on Pm^{144} in the ethylsulfate lattice could serve the twofold purpose of verifying the theory of Elliott and Stevens for promethium and of furnishing information on the magnetic moment of Pm^{144}. Accordingly, a crystal of $Nd(C_2H_5SO_5)_3 \cdot 9H_2O$ containing about 10 μC of Pm^{144} activity was prepared, and alignment and polarization data were obtained (Fig. A. 25-1).

From the signs and relative magnitudes of the anisotropies it is possible to confirm substantially the energy-level scheme of Nd^{144} proposed by Ofer[3] and by Toth and Nielsen.[4] The lower anisotropy of the 475-kev γ-ray suggests that the 1780-kev state has a lifetime in the millimicrosecond range, with consequent attenuation of the observed anisotropy, or that a substantial fraction of the electron-capture decay to the 1780-kev level involves two units of angular momentum.

The appropriate spin Hamiltonian for Pm^{+3} is[5]

$$\mathcal{H} = g_{\parallel}\beta H_z S_z + A S_z I_z + \Delta_x S_x + \Delta_y S_y + P\,[I_z^2 - 1/3\, I(I+1)] + cS_z(S_{1z}+S_{2z}),$$

where the last term represents dipole-dipole interaction with the nearest neighbor neodymium ions, and the other terms have their usual significance. For a quadrupole moment of approx 0.5 barn, estimated from nuclear systematics, P can be shown to be negligible by the theory of Elliott and Stevens. The value of c in the last term may be calculated from the equation

$$c = [-2\, g_{\parallel}\,(Pm^{+3})\, g_{\parallel}\,(Nd^{+3})\beta^2]/d^3.$$

The theoretical value of $g_{\parallel}(Pm^{+3})$, taken with the experimental quantities $g_{\parallel}(Nd^{+3}) = 3.54$ [6] and $d = 7.07$ A,[7] allows calculation of $c = 0.0039\ cm^{-1}$.

The energies of the $2^3(2I+1)$ hyperfine states of the lowest doublet can thus be calculated from the formula

$$E = \pm\, 1/2 \left\{ \Delta^2 + [\, g_{\parallel}\beta H_z + AI_z + c(S_{1z}+S_{2z})\,]^2 \right\}^{1/2},$$

where $\Delta[=(\Delta_x^{\ 2} + \Delta_y^{\ 2})^{1/2}]$, the Jahn-Teller splitting, and A are to be determined experimentally. The effects of the various terms on the level spacings are shown in Fig. A. 25-2. The solid and dashed curves in Fig. 25-1 were calculated for the alignment and polarization cases, respectively, for the Pm^{144} spin equal to 5 and to 6. It was not possible to decide between

---

[3] Shimon Ofer, Phys. Rev. 113, 895 (1959).

[4] K. S. Toth and O. Nielson, Phys. Rev. 115, 1004 (1959).

[5] J. M. Baker and B. Bleaney, Proc. Roy. Soc. (London) A245, 156 (1958).

[6] K. D. Bowers and J. Owen, Repts. Progr. in Phys. 18, 304 (1955).

[7] J. A. A. Ketelaar, Physica 4, 619 (1937).

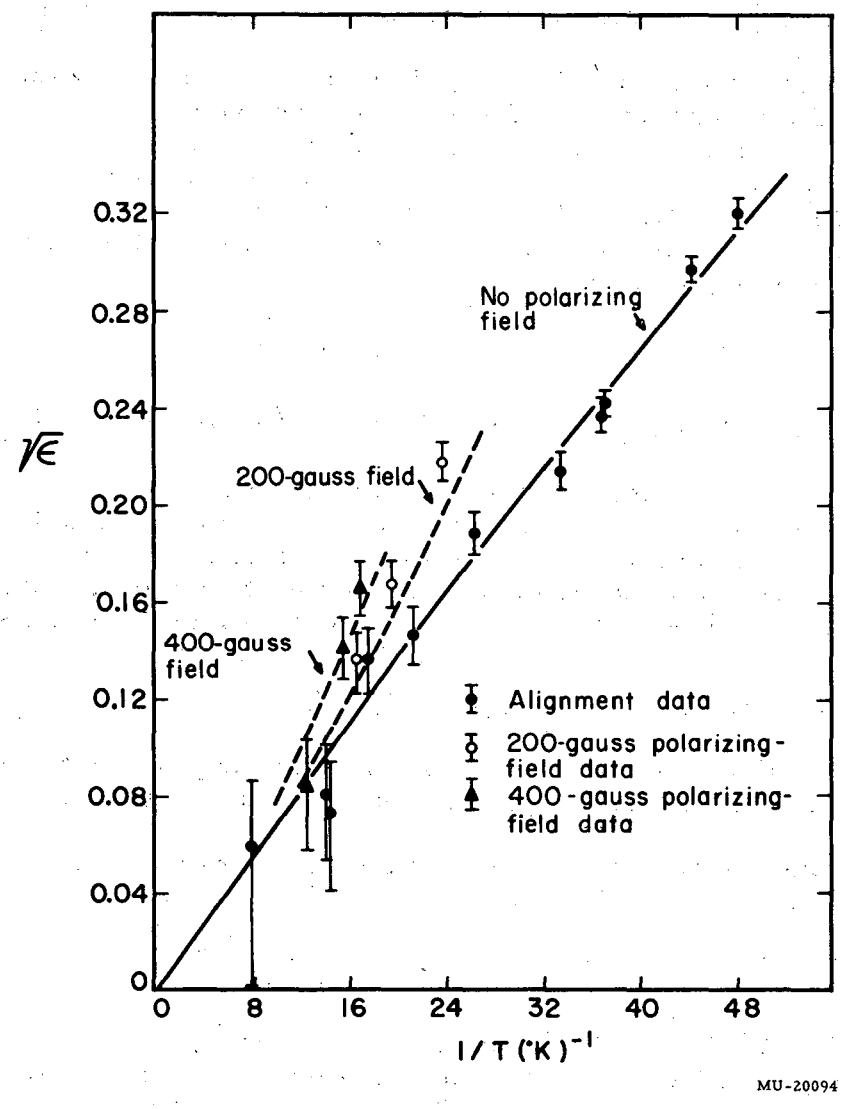

Fig. A.25-1. Experimental and calculated alignment and polarization data for 615- and 695-kev γ rays in Nd^{144}.

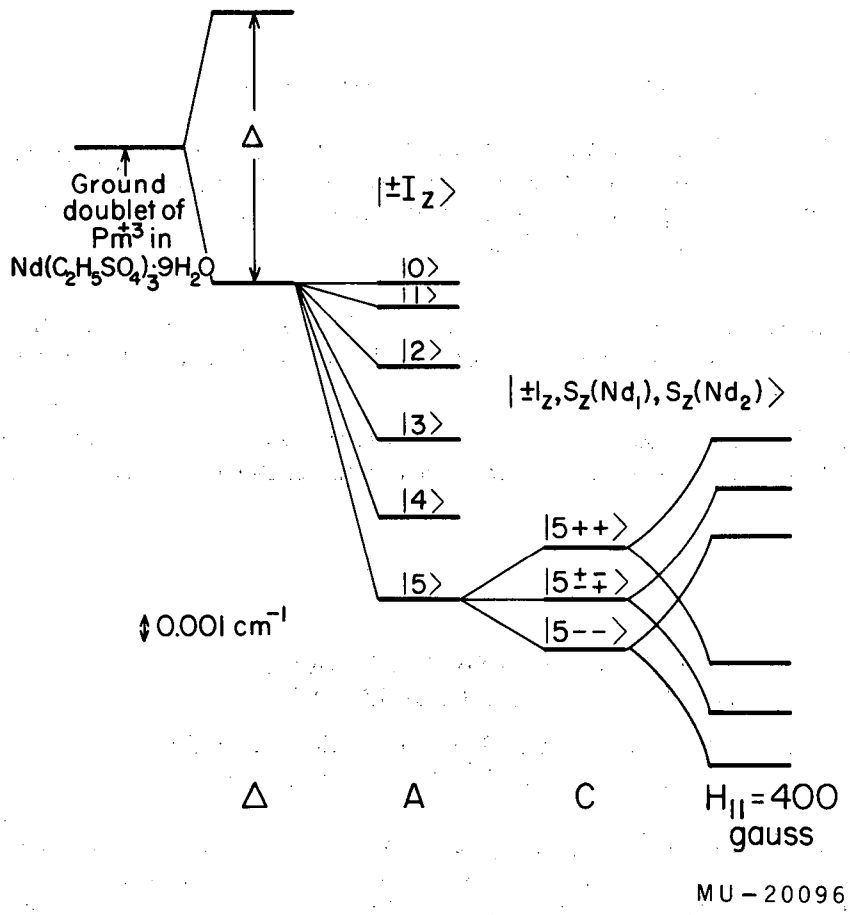

Fig. A.25-2. The energy levels of Pm^{144}.

these two spins, and the values of $|A|$ and of Δ which best fit the data are $|A|/k = 0.0091 \pm .0003^{o}K$ for I = 5, $|A|/k = 0.0079 \pm .0003^{o}K$ for I = 6, and $\Delta/k = 0.02 \pm .01^{o}K$. From the theory of Elliott and Stevens and the value[8] of $\langle r^{-3} \rangle = 36.8 \times 10^{-24}$ cm^{-3}, the nuclear magnetic moment of Pm^{144} can be calculated. These values for the two choices of spin are

$$|\mu| = 1.68 \pm .14 \text{ nm} \qquad \text{for } I = 5$$

and

$$|\mu| = 1.75 \pm .14 \text{ nm} \qquad \text{for } I = 6.$$

The possibility that the sixty-first proton might be in a $g_{7/2}$ state has been raised by the measurement of the ground-state spin of Pm^{147}.[9] However, the nuclear magnetic moment in this case would be ≈ -0.15 nm, so that the $d_{5/2}$ assignment is indicated.

[8] B. R. Judd and I. P. K. Lindgren, Theory of Zeeman Effects in the Ground Multiplets of Rare Earth Atoms, UCRL-9188, April 25, 1960 (submitted to Phys. Rev.).

[9] A. Cabezas, I. Lindgren, E. Lipworth, R. Marrus, and M. Rubinstein, Nuclear Spins of Neodymium-147 and Promethium-147, Nuclear Phys. 20, 509 (1960).

26. NUCLEAR MOMENT OF CERIUM-137 m BY NUCLEAR ALIGNMENT (*)

James N. Haag, C. E. Johnson, D. A. Shirley, and David H. Templeton

Cerium-137 is one of a large group of nuclides having an $h_{11/2}$ isomeric state ($t_{1/2}$ = 37 hr) that decays by emission of M4 radiation to a $d_{3/2}$ ground state.[1] We have measured the magnetic moment of Ce^{137m} by aligning Ce^{137m} nuclei and measuring the anisotropic distribution of the 255-kev γ radiation.

Cerium-137m was prepared by a (p, 3n) reaction of 21-Mev protons on natural lanthanum (99.911% La^{139}) in the Oak Ridge National Laboratory 86-inch cyclotron. Cerium was separated from the target material by oxidation to the +4 state, followed by solvent extraction, which yielded about 10^{12} atoms of Ce^{137m}. The cerium was then reduced to the +3 state and grown into a single crystal of $Nd(C_2H_5SO_4)_3 \cdot 9H_2O$ so that it occupied some of the Nd^{+3} lattice sites. The crystal was mounted in a demagnetization cryostat. Previous experiments on Ce^{139} and Ce^{141} had shown that nuclear alignment of the cerium isotopes was produced by cooling such a crystal to very low temperatures.

(*) Brief version of paper submitted to Phys. Rev.

[1] A. R. Brosi and B. H. Ketelle, Phys. Rev. 100, 169 (1955); Phys. Rev. 103, 917 (1956).

The crystal was cooled by adiabatic demagnetization from $1.1^{\circ}K$ and fields of up to 18,000 gauss. The intensity of the γ radiation was measured at several temperatures between 0.02 and $1.1^{\circ}K$ for a series of angles θ defined by the direction of propagation of the γ radiation with respect to the trigonal axis of the crystal. The γ rays were counted with 3×3-in. NaI(Tl) crystals and 100-channel pulse-height analyzers. The spectrum obtained is shown in Fig. A. 26-1. The peaks due to the 255-kev isomeric transition of Ce^{137m}, the 445-kev γ ray of La^{137}, and the 165-kev γ ray of La^{139} (from the decay of Ce^{139}, which was present as an impurity) are clearly resolved. The decay of these γ rays was followed over 10 half lives of the Ce^{137m}, and no other peaks were observed.

The time taken for the temperature to rise from the lowest temperatures reached to that of the helium bath ($1.1^{\circ}K$) was more than an hour, but in order to avoid errors due to inhomogeneous heating of the crystal, the γ-ray counting and the susceptibility measurements were continued for only 1 minute after the demagnetization. The crystal was then warmed to $1.1^{\circ}K$ by the introduction of helium exchange gas. A further 1-min γ-ray count at $1.1^{\circ}K$ was then taken for normalization. The γ radiation was isotropic within experimental error at this temperature. The γ-ray counting rates were corrected for background and finite counter size effects, and the anisotropies $\epsilon = 1-I(0\text{ deg})/I(90\text{ deg})$, were evaluated as a function of temperature.

The anisotropy of the 255-kev γ ray of Ce^{137m} plotted versus $1/T$ is shown in Fig. A. 26-2.

The intensity of the 255-kev γ ray at $0.018^{\circ}K$ was measured as a function of θ. This angular distribution, expressed in Legendre polynomials, was found to be

$$I(\theta) = 1 - (0.70\pm0.06)\, P_2(\cos\theta) + (0.05\pm0.01)\, P_4(\cos\theta). \qquad (1)$$

The angular distribution of γ radiation from aligned nuclei is given[2] by

$$I(\theta) = 1 + B_2U_2F_2P_2(\cos\theta) + B_4U_4F_4P_4(\cos\theta) + \cdots. \qquad (2)$$

The B_k's are a measure of the degree of orientation of the parent nucleus. The U_k's describe the amount of nuclear reorientation that takes place during any unobserved β or γ transitions preceding the observed γ ray. The F_k's are constants determined by the multipolarity and the initial and final spins of the observed γ transition.

The crystal field theory of Ce^{+3} in the ethylsulfate lattice has been worked out in detail by Elliott and Stevens,[3] and only a brief account is given here.

---

[2] T. P. Gray and G. R. Satchler, Proc. Phys. Soc. (London) A68, 349 (1955).

[3] R. J. Elliott and K. W. H. Stevens, Proc. Roy. Soc. (London) A215, 437 (1952).

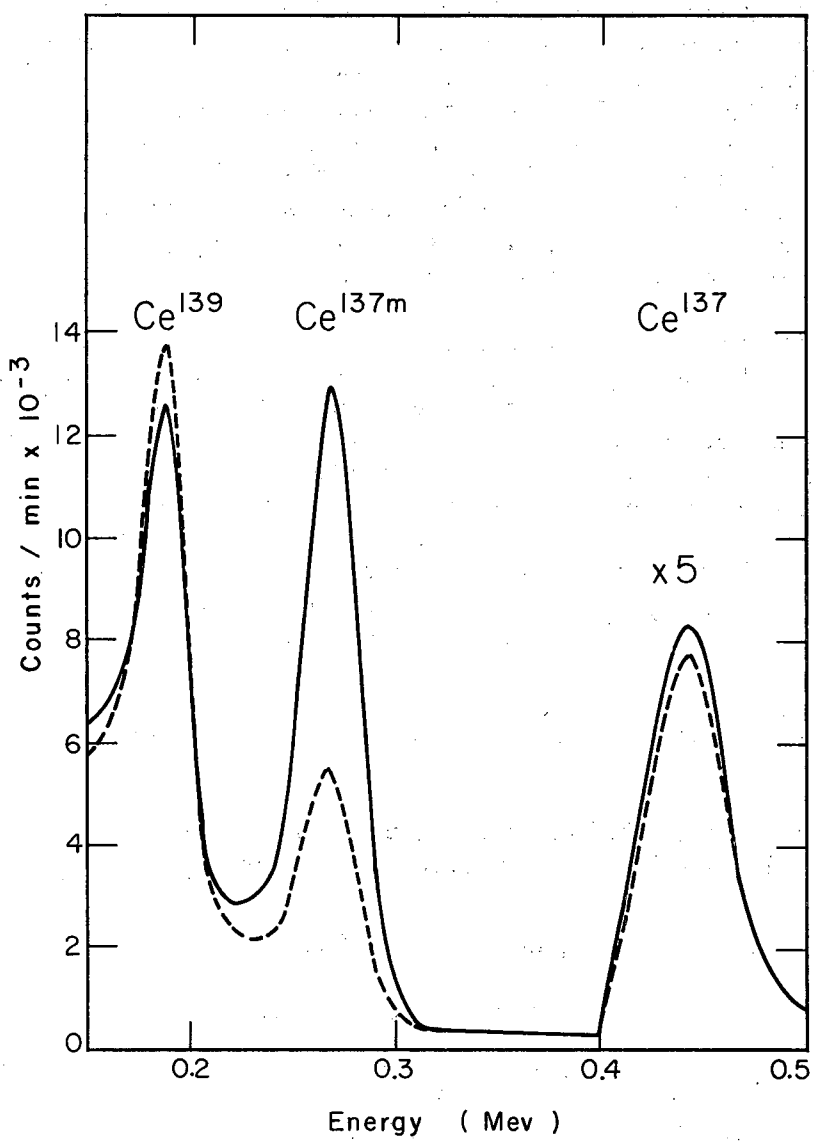

MU-20988

Fig. A. 26-1. Gamma-ray pulse-height spectrum at 1.1°K (solid line) and at 0.02°K (dashed line).

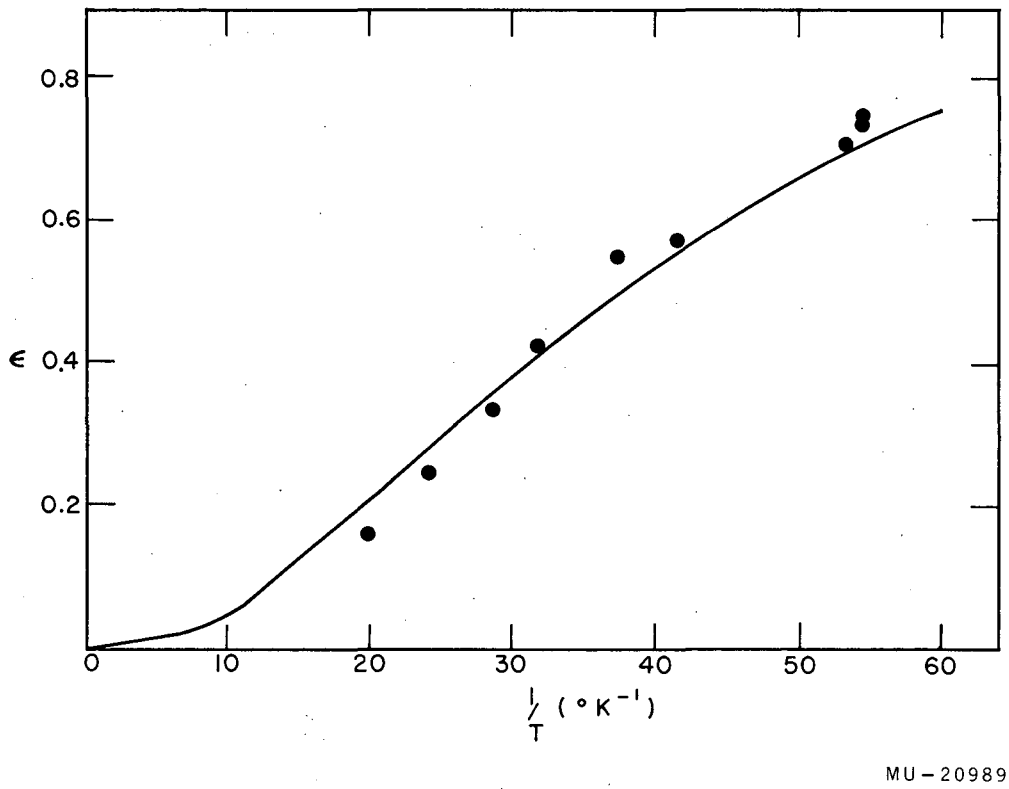

Fig. A. 26-2. Experimental values and corresponding theoretical fit for $|\mu_N| = 0.96$ nm.

The free ion Ce^{+3} has the configuration $4f^1$, and the ground term is $^2F_{5/2}$. In a trigonal crystalline field this term is split into doublets which may be characterized in the first approximation by $|\pm J_z\rangle$. In the ethylsulfate lattice, however, the lowest Kramers' doublet, which is made mostly of the state $|\pm 5/2\rangle$, contains in addition admixtures of other states from the $^2F_{5/2}$ ground term as well as from the next term $^2F_{7/2}$. It is essential that these admixtures be taken into account in calculating the nuclear magnetic moment from hyperfine-structure constants.

The effective spin Hamiltonian for the lowest Kramers' doublet of Ce^{137m} in the ethylsulfate is

$$\mathcal{H} = AS_zI_z + B(S_xI_x + S_yI_y) + P\left[I_z^2 - \frac{1}{3}I(I+1)\right].$$

The last term can be shown to have a negligible effect on nuclear alignment in this case, by using the theory of Elliott and Stevens[4] to calculate P and by using Q = 0.3 barn for an $(h_{11/2})^9$ neutron configuration.[5] The terms in B alter the energy levels of the hyperfine-structure multiplet slightly, and this has been taken into account. The energy levels of this multiplet are then given approximately by twelve doublets $|\pm I_z\rangle$, separated by A/2. In going from 1.1 to 0.02°K the percentage of the Ce^{137m} nuclei occupying the lowest doublet changes from 8.3% to 37%.

For the 255-kev isomeric transition in Ce^{137m} there are no unobserved preceding transitions, and $U_2 = U_4 = 1$. Thus, Eq. (2) becomes

$$I(\theta) = 1 - 0.8890\, B_2 P_2(\cos\theta) + 0.4434\, B_4 P_4(\cos\theta),$$

for the spin sequence $11/2 \xrightarrow{M4} 3/2$, or

$$I(\theta) = 1 - 0.7444\, B_2 P_2(\cos\theta) + 0.1693\, B_4 P_4(\cos\theta)$$

for the spin sequence $9/2 \xrightarrow{M4} 3/2$. The functions B_2 and B_4 depend on the single parameter $\beta = A/2kT$, and by varying A it is possible to fit the temperature dependence of the anisotropy for either spin sequence. Using the values of A which best fit the temperature dependence, we have calculated the angular distribution of the 255-kev γ ray at 0.018°K from each of the above expressions. The results are

$$I(\theta) = 1 - 0.65\, P_2(\cos\theta) + 0.04\, P_4(\cos\theta), \text{ for } I = 11/2, \quad (3)$$

$$I(\theta) = 1 - 0.60\, P_2(\cos\theta) + 0.02\, P_4(\cos\theta), \text{ for } I = 9/2. \quad (4)$$

---

[4] R. J. Elliott and K. W. H. Stevens, Proc. Roy. Soc. (London) A218, 553 (1953).

[5] Calculated by using the method of H. Kopfermann, in Nuclear Moments (English ed., Academic Press Inc., New York, 1958), p. 398.

Comparison with Eq. (1) shows that (4) is in disagreement with it. Thus the spin possibility of 9/2 is eliminated for Ce^{137m}. We are not aware of any direct measurements of the spin of 11/2 for the $h_{11/2} - d_{3/2}$ isomers, therefore this measurement offers the most direct evidence available for this spin assignment.

The value for A obtained in (3) above is $|A| = 0.0129\ cm^{-1}$. By use of the theory of Elliott and Stevens for the ground doublet, together with the value of $\langle r^{-3} \rangle$ obtained by Judd and Lindgren,[6] we calculate

$$A = 0.074\ \mu_N/I\ cm^{-1},\ B = 0.002\ \mu_N/I\ cm^{-1}.$$

Comparison with our value for A yields

$$|\mu_N| = 0.96 \pm .09\ nm.$$

The limits of error were obtained from the scatter of the experimental points.

This is the first nucleus with I = 11/2 for which the magnetic moment has been measured. We note that Ce^{137m} follows the trend of other even-odd nuclei in that the magnetic moment is about half way between the Schmidt limit and the Dirac limit.

[6] B. R. Judd and I. P. K. Lindgren, Theory of Zeeman Effects in the Ground Multiplets of Rare Earth Atoms, UCRL-9188, April 25, 1960 (submitted to Phys. Rev.)

27. THE MÖSSBAUER EFFECT IN GOLD-197

D. A. Shirley, P. Axel,* and M. Kaplan

A series of experiments was carried out in which the recoil-free resonant absorption of the 77-kev γ ray in Au^{197} was observed. Radioactive sources of Pt^{197} and Hg^{197} were incorporated into lattices of iron, cobalt, nickel, stainless steel, platinum, and gold, and measurements were made of the γ-ray intensity transmitted through a gold absorber, with both source and absorber at liquid helium temperature. The results of these measurements are shown in Table I and Figs. A. 27-1 and A. 27-2, where we have plotted the transmitted γ-ray intensity as a function of the relative velocity between source and absorber.

The velocity spectra of Au^{197} in platinum and gold each show a single resonance line. No hyperfine structure is to be expected, since platinum and gold are nonmagnetic and have cubic lattices (no electric quadrupole splitting is possible, since $\nabla^2 V = 0$ for a cubic lattice).

* Summer visitor from the Department of Physics, University of Illinois, Urbana, Illinois.

Table I. Gamma-ray intensities in resonant-absorption experiments

	I	II	III	IV	V	VI	VII	VIII	IX	X	XI
	Parent	Production reaction	Host	Au absorb. thick (mils)	$\frac{\Gamma_e}{\Gamma}$ [a]	Absorption area × 100 (cm/sec)	100f	$100f_D$	θ_D	θ_{eff}	Chem. shift [a, b] $\Delta E/\Gamma$
A. Sources produced in situ											
1	Hg^{197}	$Au^{197}(p, n)$	Au	10	6.7±0.8	2.34±0.70	5.8±0.9	18	185	98	0±.54
2	Pt^{197}	$Pt(n, \gamma)$	Pt	5	4.4±0.2	6.0 ±0.4	29±5	30	233	218	
3	Pt^{197}	$Pt(n, \gamma)$	Pt	10	6.6±0.3	13.4 ±3.0	34±8	30	233	248	1.07±.21
4	Hg^{197}	Pt(α, 3n(	Pt	10	4.8±0.2	5.6 ±0.4	14.3±1.1	30	233	137	
B. Alloys											
5	Pt^{197}	$Pt^{196}(n, \gamma)$	S. S. [c]	10	8.0 [d]	8.9 ±3.0	24±9				5.53±.54
6	Pt^{197}	$Pt^{196}(n, \gamma)$	Fe	10	6.5±1.0 [e]	12.4 ±3.0	32±8	55	467	243	5.91±.37
7	Pt^{197}	$Pt^{196}(n, \gamma)$	Co	10	7.0±0.8 [e]	10.5 ± 2.5	27±7	53	445	205	5.12±.33
8	Pt^{197}	$Pt^{196}(n, \gamma)$	Ni	10	6.5±0.6	13.8 ±2.5	35±7	53	441	255	4.62±.33

(a) Γ is natural width $= 2.4 \times 10^{-7}$ ev = 0.93 mm/sec

(b) All shifts imply emitted γ ray has higher energy than needed for resonant absorption.

(c) Stainless steel

(d) Non-Lorentzian; full width at half maximum

(e) Estimate of one component of a structured line

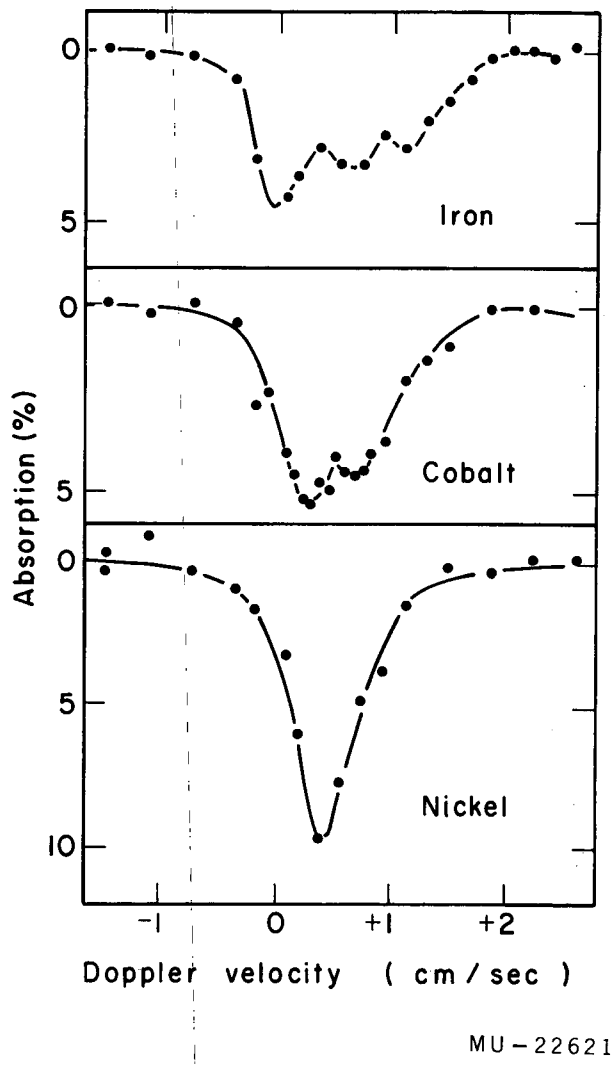

Fig. A.27-1. Doppler resonant absorption spectrum of the 77-kev γ ray of Au^{197} in a 10-mil gold absorber, for sources of Au^{197} in iron, cobalt, and nickel.

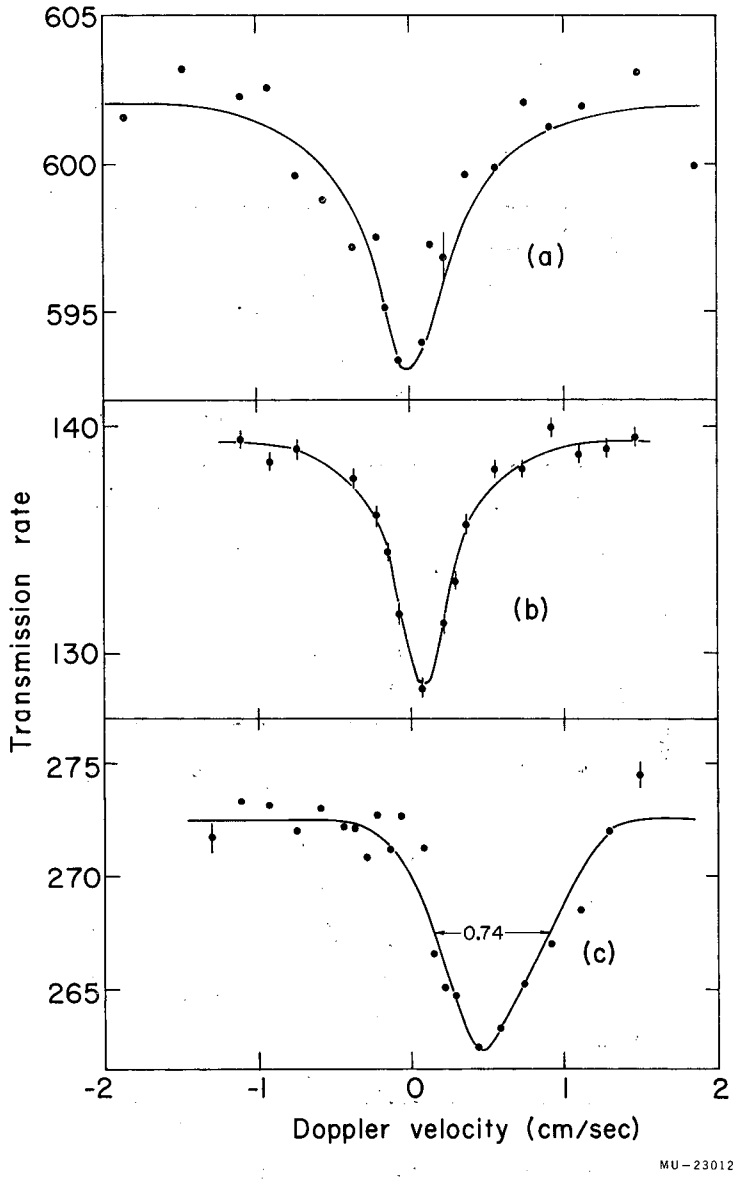

Fig. A. 27-2. Doppler velocity resonant absorption spectrum of the Au^{197} 77-kev γ ray for sources of Au^{197} in (a), gold, (b) platinum, and (c) stainless steel. Absorber was a 10-mil gold foil.

The observed resonance in stainless steel is unusually wide. This may be due to the presence of several crystalline phases, as the phase diagram for stainless steel indicates that the composition ranges of commercial stainless steels include a number of phases. No magnetic hyperfine structure is expected, as the time average of the internal magnetic field should be zero.

In iron, cobalt, and nickel, hyperfine structure is expected in the resonance, owing to the ferromagnetic character of these metals. We have observed the splitting of the resonance line in iron and cobalt. In nickel, an upper limit of 0.10 cm/sec can be set on the magnitude of the splitting.

The expected Zeeman splitting pattern for Au^{197} nuclei in a magnetic field is shown in Fig. A. 27-3. The ground-state magnetic moment, μ_g, is known to be 0.14 nm.[1] In interpreting our experimental results, we have assumed the excited-state (77-kev) moment, μ_e, to be 1.6 nm, by analogy with Tl^{203} and Tl^{205}.[2] From Fig. A. 27-3 and these magnetic moments, one would expect the dominant feature of the Zeeman pattern to be the splitting of the excited state, and this is what we observe in iron and cobalt. From the relationship $\Delta E = 2\,\mu_{ex}\,H_n$, where H_n is the magnetic field at the nucleus, and the Doppler formula $\Delta E/E = \Delta v/c$, we obtain $H_n = 282 \pm 10$ koe for gold in iron and $H_n = 122 \pm 10$ koe for gold in cobalt. From our upper limit of the splitting in nickel, we may set $H_n < 30$ koe for gold in nickel.

Our value of H_n for gold in iron is considerably lower than the values $H_n \geqslant 10^3$ koe or $H_n \geqslant 2 \times 10^3$ koe reported by Samoiliv,[3,4] obtained from nuclear polarization experiments. We attribute this discrepancy to the large uncertainty in the estimation of the absolute temperature in Sampilov's experiments. It is interesting that Samoilov's experiments with indium in nickel showed no nuclear polarization, consistent with our result of the absence of large internal fields at the impurity sites in nickel.

The half life of the 77-kev state in Au^{197}, as obtained from our measurements of the resonance line width, is 1.55±.20 nsec. This value is in fair agreement with the value 1.90±.20 nsec obtained from delayed-coincidence measurements by Sunyar,[5] but differs considerably from the value obtained in an earlier experiment reported by the Los Alamos group.[6]

---

[1] F. M. Kelly, Proc. Phys. Soc. (London) 65A, 250 (1952).

[2] H. E. Walchli, Table of Nuclear Moment Data, ORNL-1469, April 1953 and Supplement II, Feb., 1955.

[3] B. N. Samoilov, V. V. Sklyarevskii, and E. P. Stepanov, Soviet Physics-JETP 11, 261 (1960) (English translation).

[4] B. N. Samoilov, private communication, reporting results obtained at Leningrad, 1960.

[5] A. W. Sunyar, Phys. Rev. 98, 652 (1955).

[6] D. Nagle, P. P. Craig, J. G. Dash, and R. R. Reiswig, Phys. Rev. Letters 4, 237 (1960).

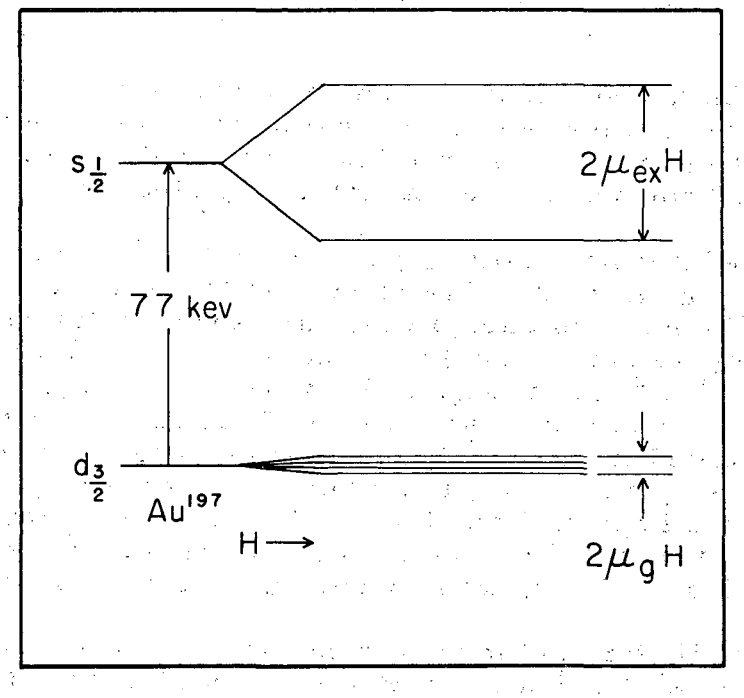

MU-22620

Fig. A. 27-3. Expected nuclear Zeeman splitting of Au^{197}.

Of special significance are the large chemical shifts of the resonance line observed in our experiments. These shifts are about 30 times as large as any observed in previous Mössbauer experiments. We attribute this effect to the presence of an odd proton in Au^{197}, since the shifts are due to the different charge overlap of the proton in the $s_{1/2}$ and $d_{3/2}$ states with different electron densities at the nucleus when the lattice environment is changed. In the free gold atom, the s electronic wave functions should be good eigenfunctions which, however, are delocalized and admixed in the lattice when the atom is bound. Thus the electron density should decrease and the nuclear level spacing should increase as the gold atom becomes more tightly bound. We have observed this as a large positive shift in iron, cobalt, and nickel, where the binding is tightest, and as a smaller but still positive shift in platinum.

It should be noted that this chemical shift is qualitatively different from the ordinary isotope shift, in that it is proportional to the difference in the average radius of a proton in two single-particle states, rather than an overall nuclear volume difference. On the basis of these arguments, we would predict large chemical shifts in all odd-Z Mössbauer nuclei in which the difference in average radius in the two isomeric states is appreciable.

28. THE NEUTRON-DEFICIENT CHAIN STRONTIUM-80–RUBIDIUM-80 (*)

Richard W. Hoff, J. M. Hollander, and Maynard C. Michel

The neutron-deficient pair Sr^{80}-Rb^{80} has been synthesized and identified by means of radiochemical studies, following irradiation of gallium targets with high-energy nitrogen ions from the Berkeley heavy-ion linear accelerator. The half life of Sr^{80} was found to be 100±6 min, and that of its daughter is 34±4 sec. The genetic relationship between these two activities was verified by rapid chemical separations ("milkings") of rubidium from the parent strontium fraction. The definite assignment to mass 80 was made by use of a time-of-flight isotope separator.[1]

By studies of the photon and particle spectra in scintillation spectrometers, the following information has been learned about Rb^{80} decay: Rb^{80} decays approx 60% to the ground state of Kr^{80} by the emission of a positron spectrum of E_{max} 4.1±.5 Mev, and approx 40% to the first excited state of Kr^{80} at 620 kev. The Rb^{80}-Kr^{80} mass difference is 5.1±.6 Mev, as compared with 5.5 Mev calculated from the Levy mass equation.[2] The log ft value of the positron decay to both the ground state (0+) and first excited state (2+) of Kr^{80} is 4.6, which is in the "allowed" category. Thus the ground-state spin of Rb^{80} is unambiguously 1 with even parity. If this spin and parity are considered in

*Brief version of a paper submitted to J. Nuclear Inorg. Chem.

[1] Maynard C. Michel, Separation and Assignment of Radioactive Isotopes (Thesis), UCRL-2267, July 1953.

[2] H. B. Levy, Phys. Rev. 106, 1265 (1957).

terms of single-particle orbitals, the choices would probably be a $p_{1/2}$ neutron state (as in Kr^{79}) and a $p_{3/2}$ proton state (as in Rb^{81}), which would couple, according to Nordheim's "strong rule," to the resultant 1+.

The only photon observed from Sr^{80} decay has the energy 580 kev.

29. NEW NEUTRON-DEFICIENT IRIDIUM ISOTOPES: IRIDIUM-182, -183, AND -184

Richard M. Diamond, J. M. Hollander, Daniel J. Horen, and Robert A. Naumann*

Several new neutron-deficient iridium isotopes have been synthesized by the $Tm^{169}(O^{16}, xn)$ and $Lu^{175}(C^{12}, xn)$ reactions in the heavy-ion linear accelerator (Hilac). After chemical purification of the iridium fractions, their decay was followed with end-window flowing-methane proportional counters. Photon spectra were examined with 1.5×1-in. and 3×3-in. NaI(Tl) scintillation spectrometers. Some γ-γ coincidence measurements were made with a conventional fast-slow coincidence circuit and with a two-dimensional analyzer.[1] Where possible, half lives and genetic relationships to known osmium and rhenium isotopes have also been ascertained by means of timed chemical separations of daughter osmium and granddaughter rhenium activities.

Following an irradiation of lutetium with carbon ions, the genetic relationship of Ir^{182} to its descendants, Os^{182} and Re^{182}, was established by a series of timed chemical separations ("milkings") in which OsO_4 was volatilized out of the iridium fraction every 15 minutes. In the early milkings, Os^{182} was clearly recognizable by its prominent 510-kev γ ray,[2] which showed the characteristic 21-hr half life of Os^{182}. From a plot of the yield of the 510-kev photon in each milking as a function of the time of the milking, the half life of Ir^{182} was found to be approx 17 minutes. Rhenium, chemically separated from the osmium fractions, exhibited spectra known[3] to occur in the decay of 13-hr Re^{182}. The decay curve obtained from the iridium fraction from a $Tm(O^{16}, xn)$ reaction yielded a half life of 15±1 min for Ir^{182}. In addition to K x rays, γ rays of 133±5 kev and 278±5 kev occur in the decay of Ir^{182}. These are interpreted as transitions that de-excite the first and second rotational states of Os^{182}, respectively. The spectrum above 500 kev is extremely complex and extends higher in energy than 4 Mev.

Iridium-183 was identified principally from a series of "milking" experiments done at 20- and 40-min intervals, extending over a period of 6 hr. The presence of 13.5-hr Os^{183}, and of 9.9-hr Os^{183m},[2] in the osmium

*On leave from Princeton University, Princeton, N. J.

[1] J. O. Rasmussen and M. Nakamura, in Chemistry Division Semiannual Report, UCRL-8867, July 1959, p. 56.

[2] J. O. Newton, Phys. Rev. 117, 1510 (1960); Phys. Rev. 117, 1520 (1960).

[3] C. J. Gallagher, Jr., J. O. Newton, and Virginia S. Shirley, Phys. Rev. 113, 1298 (1959).

fractions was indicated by peaks at 382 kev and 1100 kev, respectively. The early osmium fractions also contained Os^{182}, but the later ones did not. The half life of Ir^{183} was obtained by plotting the yield of the 380-kev Os^{183} and 1100-kev Os^{183m} peaks as a function of the time of separation of osmium from the parent iridium fraction. From several experiments of this kind, our best value for the Ir^{183} half life is 55±7 min. We were unable to obtain a sample of Ir^{183} sufficiently free of Ir^{182} and Ir^{184} so that a distinct γ-ray spectrum could be observed. However, in the iridium fraction from a carbon bombardment of lutetium a peak at about 238 kev was found to decay with a 58-min half life.

A 3-hr activity was observed to occur in the decay curve of the iridium fraction obtained from a $Lu(C^{12}, xn)$ reaction. Subsequent repurification revealed that this 3-hr activity arose from the decay of an iridium isotope. For the study of this activity, the irradiated target was allowed to stand for about 9 hr before chemical purification, to eliminate the shorter-lived iridium isotopes. The decay curve obtained with the proportional counter then showed 3-hr and approx 15-hr components, both of which arose from the decay of iridium isotopes, since the osmium fractions separated from these sources were essentially inactive. The γ-ray spectra of the approx 15-hr component showed transitions known to occur[4] in the decay of Ir^{185} and Ir^{186}. We assign the 3.2±.2-hr activity to Ir^{184}. The scintillation spectra of Ir^{184} show prominent γ rays of 125±5, 267±5, and 392±5 kev, which are believed to be the cascade transitions arising from the decay of the 2+, 4+, and 6+ rotational levels in Os^{184}. This was borne out by γ-γ coincidence measurements. The γ-ray spectrum above 500 kev is quite complex (analogous to Ir^{182}) and extends beyond 4 Mev.

In Fig. A. 29-1 we plot the energies of the first 2+ and 4+ states of the even-even osmium isotopes versus their mass number. The minimum occurring at Os^{184} seems to indicate that a peak in the moment of inertia is reached at this mass number.

---

[4] R. M. Diamond and J. M. Hollander, Nuclear Phys. 8, 143 (1958).

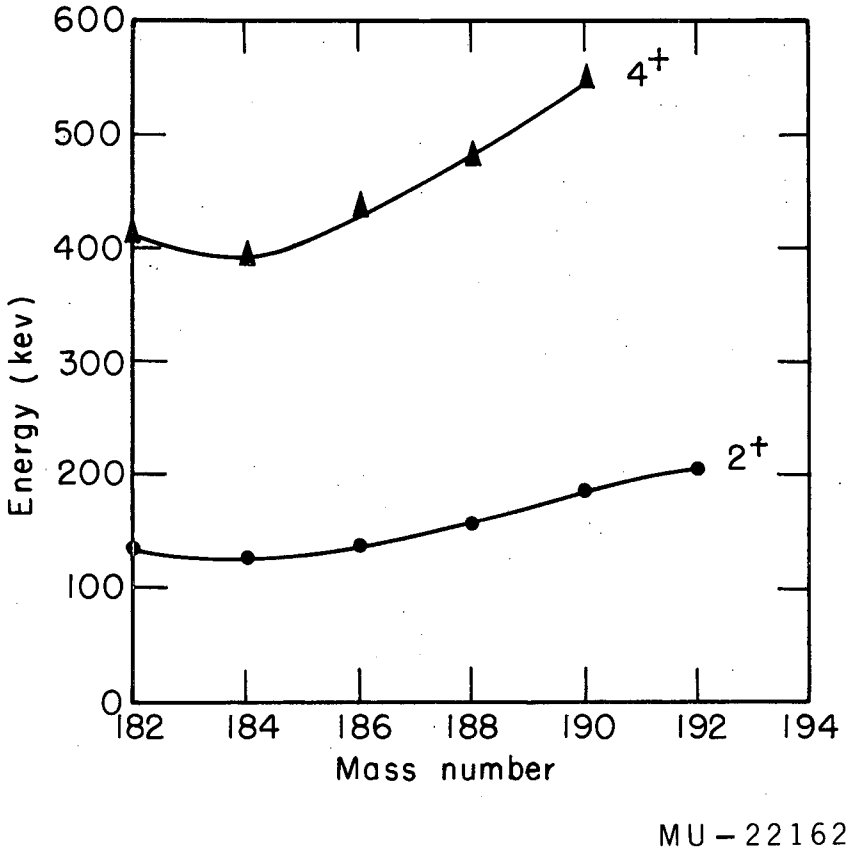

Fig. A. 29-1. Energies of first 2+ and 4+ states of even-even osmium isotopes.

B. FISSION

1. TERNARY SPONTANEOUS FISSION OF CALIFORNIUM-252

M. Brown, L.E. Gibson, J.A. Scheer, and S.G. Thompson

An earlier investigation of the spontaneous fission of Cf^{252} with photoplates[1] showed the emission of high-energy α particles associated with fission and also gave evidence of tripartition into fragments of roughly equal masses. Although the rate of occurrence and the energy distribution of the long-range α particles could be measured with some accuracy, this was not possible for fragments in the second mode of decay, owing to their very small number and the inherent limitations of the applied method.

In order to determine the energy and mass distribution of ternary fission fragments by measuring their energies and velocities separately, and also to get better information about the long-range α particles, the following experimental arrangement was constructed: Three diffused-junction Si detectors, arranged in a vacuum chamber at variable angles, look at a Cf^{252} source deposited on a 80-$\mu g/cm^2$ Ni foil. Pulses from these detectors are fed into

(a) Three slow linear channels to measure the energy of the fragments (resolution of 6.11-Mev α particles = 45 kev).

(b) Three channels of fast coincidence (coincidence interval $\leqslant 10^{-8}$ sec).

(c) Two time-of-flight channels. The time resolution for coincidences of two binary fission fragment pulses (two detectors at the source) was 2×10^{-10} sec full width at half maximum.

Preliminary results are as follows:

1. Long-range α-particle emission and ternary fission with comparable fragment masses were observed, the angles between the detected particles being 180, 90, and 90 deg and 120, 120, and 120 deg (± 5 deg each), respectively. The rates of occurrence at the above angles were approximately one apparent ternary fission giving comparable masses in 4×10^5 binary fissions.

2. The energy distribution of the long-range α particles was measured by using a 24.5-mg/cm^2 Au absorber foil to discriminate against heavy fission fragments and the 6.11-Mev α particles of Cf^{252} (Fig. B. 1-1). After correction for energy loss in the absorber, the distribution was found to extend up to 27.5 Mev, having a broad maximum around 15 Mev. The difference between this result and the work of Muga et al., who found a maximum at 19 Mev and a tail up to 34 Mev, remains to be explained.

A response of the Si detectors to fast neutrons (PoBe) due to the reaction Si^{28} was found by measuring the energy distribution of the protons stopped in the depletion layer and also by observing the subsequent β^- activity of Al^{28}.

[1] M.L. Muga, H.R. Bowman, and S.G. Thompson, Tripartition in the Spontaneous Fission Decay of Cf^{252} (UCRL-9044, Aug. 1960), submitted to Phys. Rev.

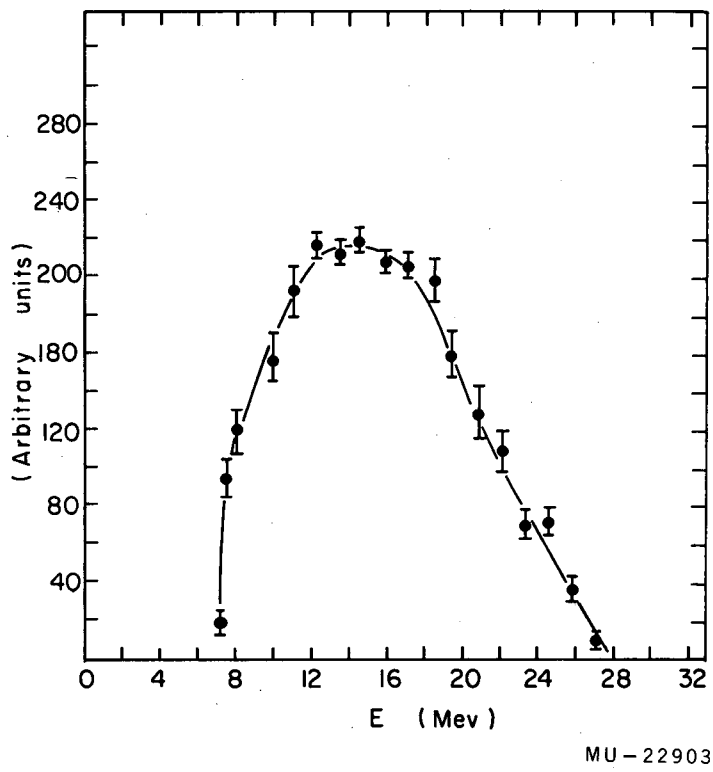

Fig. B. 1-1. Energy distribution of long-range α particles of Cf^{252} behind 24.5 mg/cm^2 Au foil; energies corrected for absorption.

2. FISSION OF GOLD BY CARBON IONS (*)

G. E. Gordon, A. E. Larsh, and T. Sikkeland

Angular distribution and kinetic-energy spectra of fragments and cross sections for fission of gold with 68- to 124-Mev C^{12} ions have been obtained by observation of the fragments in two types of detectors--gas scintillation chambers and silicon p-n junctions. Carbon ion beams were obtained from the Hilac (which accelerates heavy ions to 10.4Mev per nucleon). The experiments were performed in a vacuum tank, which has been described in some detail.[1]

The targets, previously consisting of approximately 200 $\mu g/cm^2$ of gold vaporized onto 0.1-mil aluminum backing foil, were oriented at 45 degrees to the beam with the gold facing toward the detector. The experiments were performed in a way similar to that described for the carbon-induced fission in uranium (this report, Paper B.6) where only silicon detectors were used. In the gold experiments, a gas scintillation counter was also used. The angular distributions and kinetic energies were determined with 72.3-, 93.3-, and 123.3-Mev C^{12}.

The most probable kinetic energy was determined as a function of the laboratory-system angle. We assumed then that this represents the energy per fragment when symmetric division occurs. From the change in energy of the peak with lab angle, we were able to obtain a value for the ratio X, given by:

$$X = \frac{\text{velocity of the fissioning nucleus along the beam axis}}{\text{velocity of the fission fragment in the center-of-mass system}} .$$

The values for X obtained this way are listed in Table I. These values were used in transforming the laboratory-system angular distribution into the system of the fissioning nucleus. Within the limits of error, this gave distributions that were symmetric about 90 deg in the new system. We also then obtained the most probable fission-fragment kinetic energy in the coordinate system of the fissioning nucleus. This quantity was found to be 73 ± 3 Mev over the entire range of bombarding energies. With the assumption of symmetric binary fission, this result gives a total kinetic energy release of 146±6 Mev. This value agrees well with Terrell's correlation of energy release with $Z^2 A^{1/3}$ of the fissioning nucleus[2] if we assume the fissioning nuclei to be astatine isotopes.

The values of the most probable fragment kinetic energy have been used to calculate the values of X corresponding to full linear momentum transfer by the bombarding particle to the fissioning nucleus. The results of these

*Brief version of published paper, Phys. Rev. 120, 1341 (1960).

[1] G. E. Gordon, A. E. Larsh, T. Sikkeland, and G. T. Seaborg, Phys. Rev. 113, 527 (1959).

[2] James Terrell, Phys. Rev. 113, 527 (1959).

calculations, given in Table I, indicate that the X values derived from the dependence of fragment kinetic energies on laboratory-system angle are consistent with full momentum transfer at all three bombarding energies.

Table I. Values of the quantity X

Laboratory energy of carbon ion (Mev)	X	
	From lab energy vs lab angle	For full momentum transfer
123.3	0.223 ± 0.01	0.218
93.3	0.188 ± 0.01	0.191
72.4	0.164 ± 0.01	0.169

The fragment angular distribution in the system of the fissioning nucleus was compared with theoretical curves calculated according to treatment by Halpern and Strutinski.[3] In Fig. B. 2-1 we have shown, as an example, the Halpern and Strutinski curve that best fits the experimental data at a bombarding energy of 93.3 Mev. A parameter p determines the angular distribution. The parameter p is equal to $I_m^2/4K_0^2$, where I_m is approximately the maximum angular momentum of the compound nuclei, and K_0 is the mean value of the projection of the angular momentum of the fissioning nucleus along the direction of the separating fission fragments (see Ref. 1). We have estimated I_m^2 from the compound-nucleus formation calculations of Thomas, assuming the square-well potential with a radius parameter of 1.5×10^{-13}cm.[4] In accord with Halpern and Strutinski, we assume that there is no change in the angular momentum of the compound nucleus if small particles are evaporated prior to fission. From the resulting value of K_0^2 and curve of Ref. 1 (Fig. B.2-2), we determine the value of the quantity $(E_{ex}-E_f)$, where E_{ex} is the excitation energy of the fissioning nucleus, and E_f is the height of the fission barrier. The fission-barrier heights have been estimated by using the equations of Pik-Pichak[5] and Hiskes[6] for fission of rotating nuclei. In this framework, the fission-barrier height is equal to the energy difference between the stable rotating nucleus and the fissioning nucleus at the saddle point.

[3] I. Halpern and V. Strutinski, in Proceedings of the Second United Nations International Conference on the Peaceful Uses of Atomic Energy, Geneva, 1958 (United Nations, New York, 1958), Vol. 15, p. 408.

[4] T.D. Thomas, Phys. Rev. 116, 703 (1959).

[5] G.A. Pik-Pichak, Soviet Physics-JETP 7, 238 (1958).

[6] John R. Hiskes (Lawrence Radiation Laboratory), private communication, 1960.

The calculated fission barriers are of the order of 10 to 15 Mev and seem reasonable when compared to those calculated according to Swiatecki's method, which involves the difference between actual ground-state masses and a smooth mass surface.[7] The results of this analysis of the angular-distribution data are given in Table II.

Table II. Quantities obtained from the angular-distribution data for fission of gold with carbon ions (From Sikkeland, Fission of Gold by Carbon Ions).

E_c^{12} (Mev)	E_{ex} of initial comp. nucl. (Mev)	p	I_m^2	K_0^2	$E_{ex}-E_f$ (Mev)	Calc. E_f (Mev)	E_{ex} (Mev)
123.3	98.6	10	4600	115	13.5	8-13	21.5-26.5
93.3	71.4	7.2	2530	87.8	12	10-16	22-28
72.4	51.6	6	1118	46.6	9	11-14	20-23

From the results presented in Table II, it would appear that fission occurs at about the same average excitation energy regardless of the excitation energy of the original compound nucleus. This observation implies the evaporation of a higher average number of particles prior to fission with increasing bombarding energy. For example, at the highest bombarding energy, this treatment of the angular-distribution data indicates that the following sequences of particles could be emitted before reaching the average fissioning nucleus: 7n; p6n; α5n; pα4n; 2α3n. Thesis results are consistent with Blann's radiochemical mass-yield data for fission of gold with carbon ions.[8]

Two types of experiments were done to obtain the fission cross sections as a function of bombarding energy. All fragment angular distributions were obtained at the energies indicated above. At closely spaced intervening energies, fragments were observed only at 90 deg to the beam. It is assumed that the integration factor from the angular-distribution experiments varies smoothly with bombarding energy. The absolute fission cross sections were obtained by relating the number of fragment counts to the number of elastically scattered carbon particles observed at small angles to the beam (approx 30 to 60 deg). At these angles it is assumed that, for 72.4-Mev C^{12} particles on gold, the scattering cross sections are equal to those calculated according to the Rutherford formula. The fission cross sections obtained by this procedure are shown in Fig. B.2-2 in units of the cross section for compound-nucleus formation calculated for a square-well model and radius parameter $r_0=1.5\times10^{-13}$ cm.[4]

[7] W. J. Swiatecki (Lawrence Radiation Laboratory), Private communication. The fission-barrier calculations are similar to those used in the systematics of spontaneous-fission half lives, W. J. Swiatecki, Phys. Rev. 100, 937 (1955).

[8] H. Marshall Blann, Fission of Gold with 112-Mev C^{12} ions: A Yield-Mass and Charge-Distribution Study (thesis), UCRL-9190, May 1960 (unpublished).

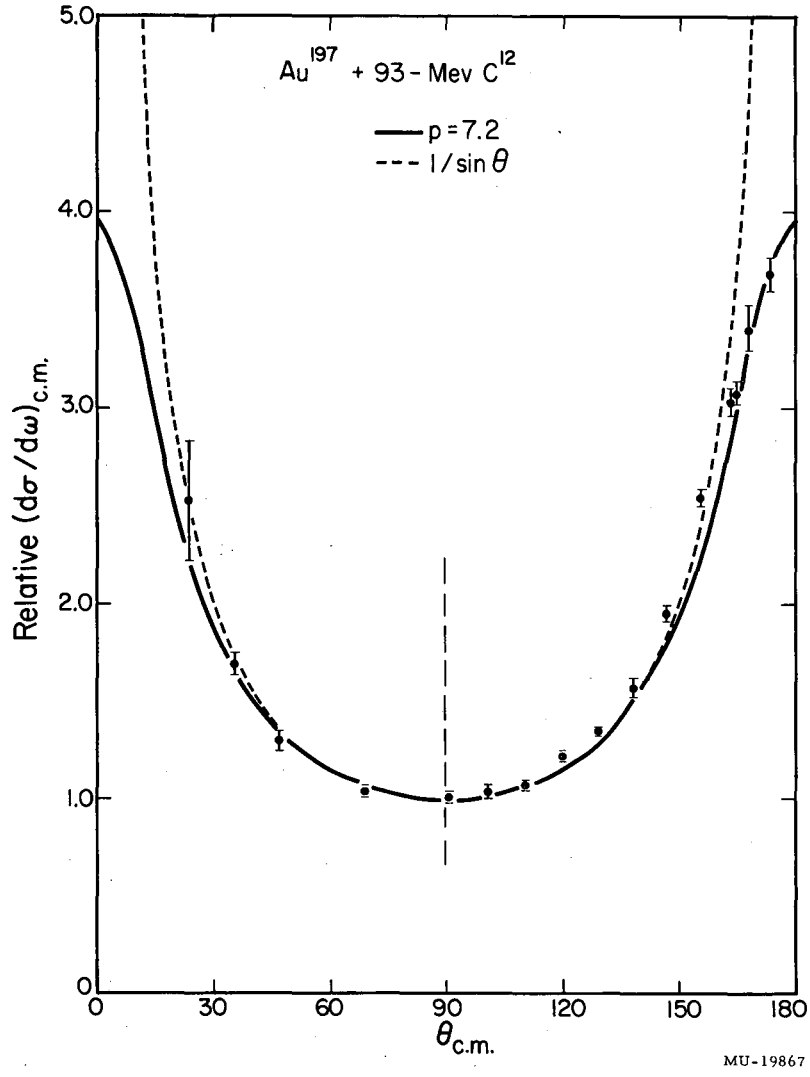

Fig. B. 2-1. Center-of-mass angular distribution of fragments from fission of Au^{197} induced by 93.3-Mev C^{12} ions. The solid curve represents Halpern and Strutinski's theoretical angular distribution with p = 7.2. (See text.)

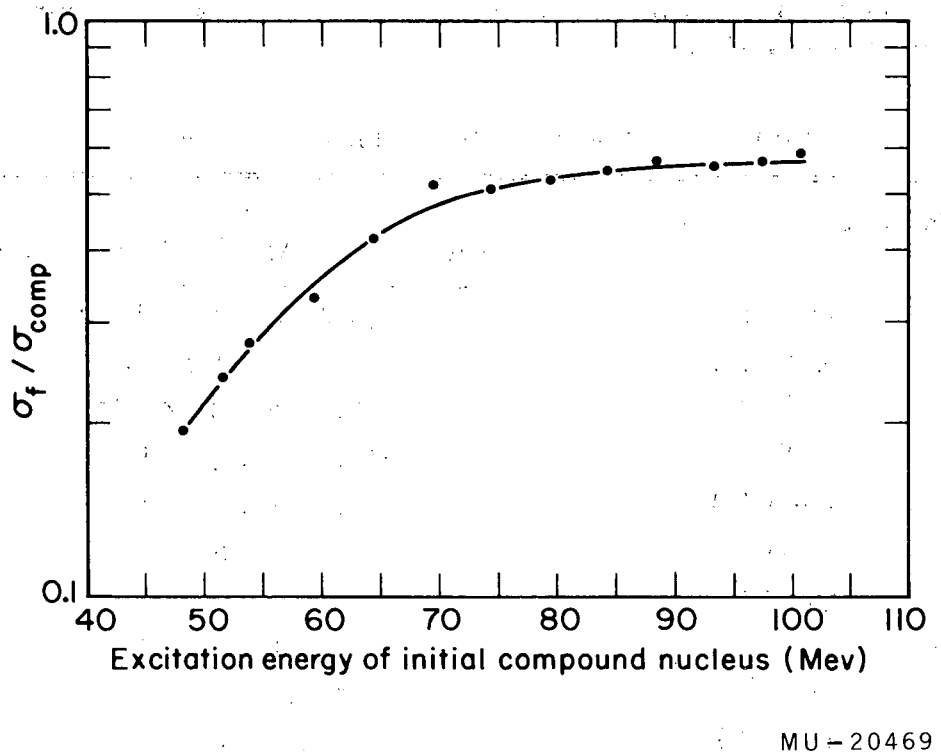

Fig. B. 2-2. Reduced fission cross section (σ_f/σ_{comp}) for Au^{197} bombarded with C^{12} ions as a function of excitation energy of the initial compound nucleus.

3. MASS-YIELD CURVE FOR FISSION IN THE REACTION C^{12}(112 Mev) + U^{238} → fission

Eldon Haines

A partial mass-yield curve for the reaction

$$C^{12}(112\ \text{Mev}) + U^{238} \rightarrow \text{fission}$$

has been obtained by radiochemistry. The representative yields are listed in Table I. Except for the region of the rare earth elements they represent yields from mass 56 to mass 188.

Table I. Mass yields from U^{238} fission induced by C^{12} at 112 Mev.

Isotope measured	Yield (relative to Mo^{99} taken as 1.00)
Mn^{56}(a)	$(2.25 \pm .30) \times 10^{-3}$
Ni^{66} (a)	$(1.39 \pm .06) \times 10^{-2}$
Br^{82} (b)	$(3.8 \pm .4) \times 10^{-2}$
Br^{83}	$(2.2 \pm .2) \times 10^{-1}$
Sr^{89} (a)	$(5.35 \pm .10) \times 10^{-1}$
Pd^{109}	$1.37 \pm .09$
Pd^{112}	$.75 \pm .04$
Ag^{111}	$1.31 \pm .01$
I^{126} (b)	≤ 0.1
I^{128} (b)	$0.52 \pm .04$
I^{130} (b)	$0.81 \pm .01$
I^{132} (b)	$0.32 \pm .09$
I^{134}	≤ 0.05
Ba^{140}	0.48 ± 0.03
Ce^{141}	$1.08 \pm .10$
Ce^{143}	$0.53 \pm .07$
Re^{186} (b)	$(6.4 \pm 4.0) \times 10^{-4}$
Re^{188} (b)	$(4.4 \pm 1.8) \times 10^{-3}$

(a) Total yield of that mass.

(b) Shielded isotopes. Unmarked yields represent only part of the total yield of that mass.

The iodine independent yields were especially important because they gave a directly measurable dispersion of charge at mass 130. This was done by using the approximate slope of the mass-yield curve at mass 130 to adjust each iodine isotope to represent an isobar of mass 130. By plotting Z as abscissa versus the sum of the yields of the isobars up to Z on probability paper it was observed that the form of the dispersion was Gaussian:

$$\phi(Z - Z_p) = \frac{1}{\sqrt{\pi\sigma}} \exp\left[-(Z - Z_p)/2\sigma^2)\right],$$

where

σ = rms dispersion = 0.85,
Z is the charge of the measured isobar,
Z_p is the most probable charge, or center of the dispersion, not necessarily integral.

With this information it is possible to calculate total yields by using partial yields. Let us assume (a) that the Gaussian form of the charge dispersion holds throughout the region from mass 80 to 160, and (b) that $\sigma = 0.85$ for this region. Then, choosing two measured partial yields y' and y'' not more than a few mass units apart, one may write

$$\frac{y'}{y''} = \frac{y_0'}{y_0''} \cdot \frac{\int_{-\infty}^{x'} \phi(x)\,dx}{\int_{-\infty}^{x''} \phi(x)\,dx},$$

where $x = Z - Z_p$
y_0 = total yield.

If the approximate slope of the mass-yield curve in the region of interest is known the ratio y_0'/y_0'' may be determined. Also, using one of the prescriptions for the change of Z_p with mass, one may find a relationship between x' and x''. Then the values of y_0' and y_0'' are determined. One must be careful in the use of these results, however, since a change of 10% to 15% in the total yield may result from a change in the prescription for $Z_p(A)$.

The mass-yield curve appears in Fig. B.3-1. The curve for 112-Mev carbon-ion bombardments is not Gaussian in form, being too broad near the top and narrow at the bottom. It appears to reach a maximum at mass 120± 2, implying that 10±4 neutrons are emitted with the more probable modes of fission.

For comparison the curve for U^{238} bombarded with 45.4-Mev α particles[1] is shown with the curve for carbon ion bombardments. It is apparent that moderately asymmetric fission relative to symmetric fission is more

[1] R. Vandenbosch, T.D. Thomas, S.E. Vandenbosch, R.A. Glass, and G.T. Seaborg, Phys. Rev. 111, 1358 (1958).

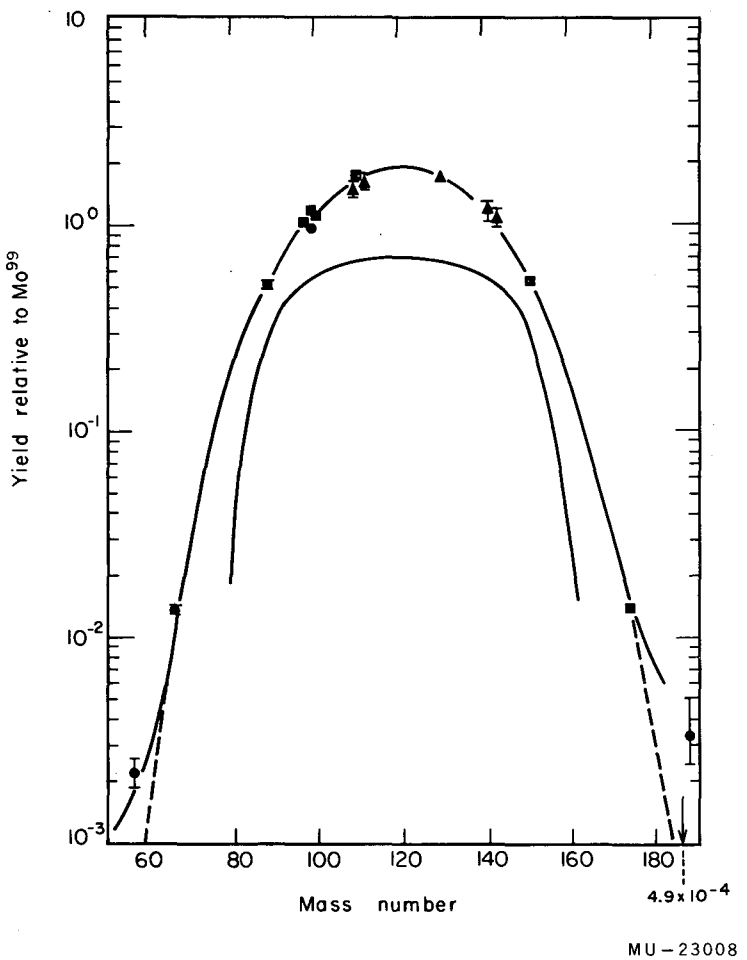

Fig. B. 3-1. Mass Yield, $C^{12} + U^{238}$
ϕ Total yields directly measured
● Total yields calculated from partial yields
□ Reflected points

probable for the 112-Mev carbon than for the 45-Mev α bombardments. An interesting feature of the curve is that the very asymmetric yields for mass 56 and the independent yields for Re^{186} and Re^{188} are much higher than expected from the trend in the moderately asymmetric yields. It is possible that this is the result of the entrance of a new mode of fission at high excitation, or perhaps a change of shape of the potential energy surface for very asymmetric fission.

4. ANGULAR DISTRIBUTIONS FROM HEAVY-ION-INDUCED FISSION REACTIONS

Victor Viola

The recoil collection technique is being used to determine the angular distributions of fragments from heavy-ion induced fission reactions at the Hilac. Target nuclei of Au^{197} and Bi^{209} have been studied with C^{12}, N^{14}, and O^{16} nuclei as a function of energy and with B^{11} at maximum energy.

Experimentally, differential range procedures are used to collect the gross fission products at regular angular intervals between 10 and 175 deg. The relative angular distributions are obtained from the ratios of the observed β activity. Within experimental error there is no deviation in the angular distributions as a function of decay time. To transform the laboratory-system data into the more meaningful center-of-mass system, it was assumed that all fission events were binary. Hence, the c.m. angular distributions were determined on the basis of maximum symmetry about 90 deg for angles θ and $\pi-\theta$. The values for the transformation parameters necessary to give such symmetry are consistent with full momentum transfer in reactions leading to fission. Above 140 Mev bombarding energy some deviation below this is indicated.

Halpern and Strutinski[1] and Griffin[2] have predicted fission fragment angular distributions from considerations of the spectrum of I and K quantum states in the compound nucleus: here I is the total spin of the compound nucleus and K is the projection of I on the nuclear symmetry axis. Qualitatively, I can be approximated by ℓ, the angular momentum transfer in the reaction, and K is related to the fissionability, which can be described by Z^2/A. The Halpern and Strutinski distributions are generated by the parameter $p = I_{max}^2/4K_0^2$, where K_0 is the mean value of K. Griffin's curves depend on the average parameter $r = \overline{I}/\overline{K}$. In general the former fit the data best between 0 and 20 deg, while the latter seems more appropriate from 20 to 50 deg. In Table I the experimentally determined anisotropy parameters, p and r, are summarized for the various systems. Also listed are

[1] I. Halper and V.M. Strutinski, in Proceedings of the Second International Conference on the Peaceful Uses of Atomic Energy, Geneva, 1958, Vol 15, p. 398.

[2] J. J. Griffin, Phys. Rev. 116, 107 (1959).

Table I. Summary of findings in heavy-ion-induced fission

Heavy ion	Heavy-ion energy (Mev)	Target: Au^{197}					Target: Bi^{209}				
		Z^2/A	E^*(Mev)	(K)	p	r	Z^2/A	E^*(Mev)	(K)	p	r
B^{11}	114	33.9	105	43.6	8.1	4.5	35.2	88.2	43.8	5.4	3.6
C^{12}	125	34.6	101	45.8	7.5	4.3	35.8	85.7	45.7	5.3	3.5
	112		89.0	41.3	7.2	4.1		73.4	41.3	5.0	3.4
	97.4							59.6	35.1	4.5	3.25
	81.0		59.7	27.3	5.9	3.75		44.3	26.4	3.6	2.9
	69.9		49.2	20.4	5.1	3.4					
N^{14}	145	35.1	118	53.6	7.0	4.1	36.3	102	53.5	5.0	3.4
	127		101	46.9	6.5	4.0		84.8	46.8	4.5	3.25
	107		82.9	38.3	5.4	3.7		65.9	37.8	3.5	2.9
	83.1		60.8	24.8	4.2	3.2		43.5	23.6	2.6	2.4
O^{16}	166	35.5	124	61.4	8.5	4.5	36.8	107	61.7	5.9	3.8
	143		103	52.8	7.7	4.3		86.0	52.7	5.7	3.7
	117		78.8	41.1	6.4	4.0		61.9	39.4	4.6	3.4
	84.3		49.8	20.0	3.6	2.9		31.7	14.2	1.7	2.0

corresponding values of Z^2/A, the excitation energy E^* calculated from Cameron,[3] and ℓ calculated by Thomas.[4]

The following conclusions can be drawn from the information in Table I: (a) For a given initial compound nucleus, the anisotropy is observed to increase regularly with increasing bombarding energy. This is consistent with the expectation that ℓ increases with increasing energy of the incident particle, and additionally, indicates that ℓ is increasing more rapidly than $\overline{K}$. (b) When the same heavy ion is involved, the angular distributions from gold are much more anisotropic than those from bismuth. This behavior is explained in terms of the greater fissionability of the compound nuclei formed with bismuth; i.e., $\overline{K}$ is larger and the anisotropy is therefore reduced. (c) Examination of different heavy ions and a single target at the same calculated values of E^* of ℓ shows that the anisotropy decreases in the order $B^{11} > C^{12} > O^{16} > N^{14}$. Because ℓ and Z^2/A of the initially formed compound nucleus both increase with increasing heavy-ion mass and charge, they produce opposite effects on the anisotropy. These results indicate that the fissionability is the more important of the two effects. The behavior of N^{14} is anomalous in this respect and is not yet explained.

[3] A. G. W. Cameron, A Revised Semi-Empirical Atomic Mass Formula, Chalk River, Ontario, CRP-690, AECL-433, Dec. 1958.

[4] T. D. Thomas, Phys. Rev. 116, 703 (1959).

5. THE EFFECT OF ANGULAR MOMENTUM ON FISSION PROBABILITY (*)

J. Gilmore, I. Perlman and S. G. Thompson

A series of experiments has been carried out to help elucidate the effect of angular momentum on fission probability. The liquid-drop-model calculations by Pik-Pichak[1] and Hiskes[2] have suggested that the nuclear deformation associated with large values of angular momentum should lead to a decreased barrier against fission. Halpern has considered the effect of large angular momentum on level widths for fission and neutron emission and also concluded that fission probability will be enhanced.[3]

The probability for fission of nuclei with large angular momenta may be conveniently studied by bombarding suitable target nuclei with heavy ions. Bombardment of Ta^{181} with O^{16} ions, for example, may give an angular momentum in the compound nucleus of $> 100\hbar$.

In this series of experiments it was found possible to select pairs of isotopes that could be bombarded with two different heavy ions to give the same compound nucleus. The excitation energies in the two compound nuclei

(*) Brief version of John Gilmore's Ph. D. Thesis (same title), UCRL-9304, July 1960.

[1] G. A. Pik-Pichak, Soviet Physics--JETP 7, 238 (1958).

[2] John R. Hiskes, The Liquid-Drop Model of Fission: Equilibrium Configurations and Energetics of Uniform Rotating Charged Drops (Ph. D. Thesis), UCRL-9275, June 1960.

[3] I. Halpern, Ann. Rev. Nuclear Sci. 9, 245 (1959).

could be made equal by adjustment of the bombarding energies, but the angular momentum brought in by the heavier ion was in general greater because of its larger mass and radius. It was then of interest to find whether, in bombardment by the heavier ion, the higher angular momentum might result in an increased fission probability. Here the fission probability was defined as the ratio of the fission cross section to that for compound-nucleus formation.

The experimental portion of this work involved determination of fission cross sections. In an evacuated fission chamber, nuclear emulsions recorded fission fragments recoiling from a thin target as the collimated heavy-ion beam passed through the target and into a Faraday cup. Microscopic examamination of selected portions of the emulsions and application of geometry correction factors then gave the fission-fragment angular distribution. Fission cross sections were obtained by integration of these angular distributions.

A major problem in developing the experimental methods was achievement of adequate discrimination between tracks of fission fragments and the densely ionizing heavy ions. In the procedure finally chosen, a relatively insensitive emulsion coupled with a weak development recorded fission fragments as continuous tracks but indicated neon and oxygen ions only by trails of individual grains, and did not record lighter ions.

Values of compound-nucleus-formation cross sections (σ_c) and angular momenta were taken from the calculations of Thomas.[4] The use of these cross sections represents one of the major uncertainties in this work, since their calculation does not take into account any deformation or polarization of the target or any interaction between target and bombarding particle other than complete merger.

Determination of fission probabilities and correlations with calculated angular momenta were performed for the following systems: ($C^{12} + Tm^{169}$; $O^{16} + Ho^{165}$), ($O^{16} + Tm^{169}$; $Ne^{20} + Ho^{165}$), ($C^{12} + Re^{185}$; $O^{16} + Ta^{181}$), ($O^{16} + Re^{185}$; $Ne^{20} + Ta^{181}$).

An example of the results may be seen in Figs. B.5-1 and B.5-2. At high excitation energies, the larger angular momentum in the heavier-ion bombardment correlates with a higher fission probability for that case, supporting the conclusions of Pik-Pichak and Halpern. At these energies well above the Coulomb barrier, the distribution of ℓ values begins to resemble the distribution for zero barrier, i.e., $\sigma_\ell \propto 2\ell + 1$, and a correlation of σ_f/σ_c with ℓ_{max} should be justified. At lower excitation energies, σ_f/σ_c in the O^{16} bombardment remains larger than σ_f/σ_c for the C^{12} bombardment, and here one would have to know the distribution in ℓ values to properly interpret the results. Similar correlations were found in the other pairs of bombardments. However, values of σ_f/σ_c in the bombardments with full-energy Ne^{20} ions were unexpectedly low. This leads to consideration of the possibility, suggested by liquid-drop calculations, that compound-nucleus formation would be forbidden for very large angular momenta.

[4] T. D. Thomas, Phys. Rev. 116, 703 (1959).

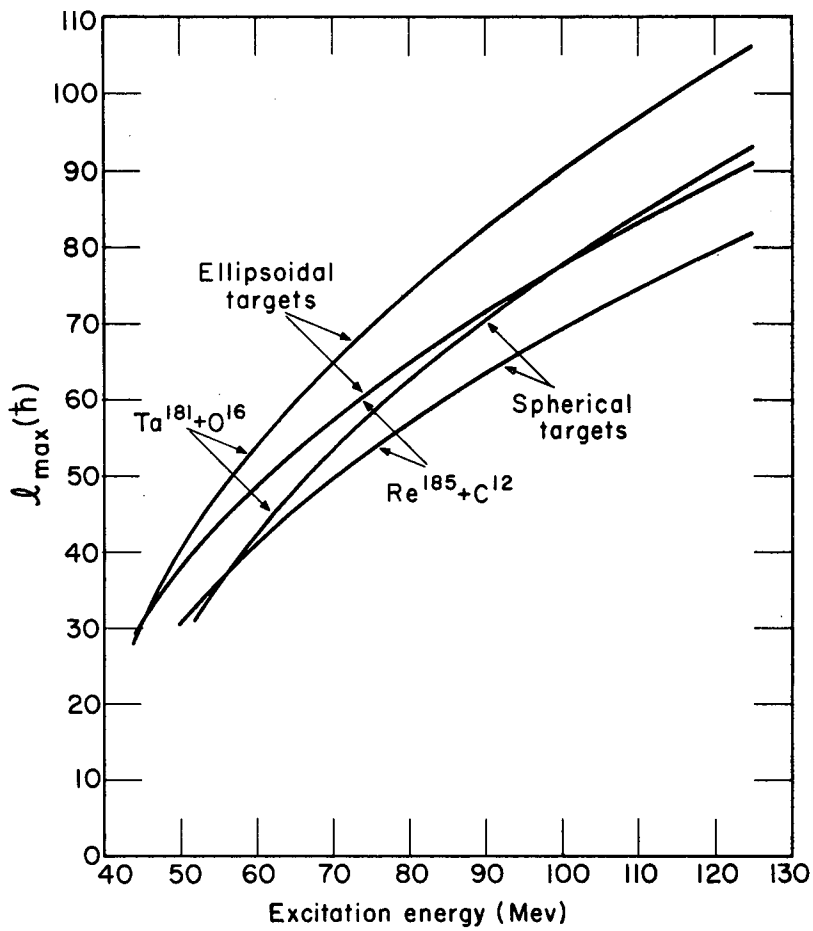

Fig. B. 5-1. Maximum angular momentum (classical) as a function of excitation energy in the compound nucleus for $Ta^{181} + O^{16}$ and $Re^{185} + C^{12}$.

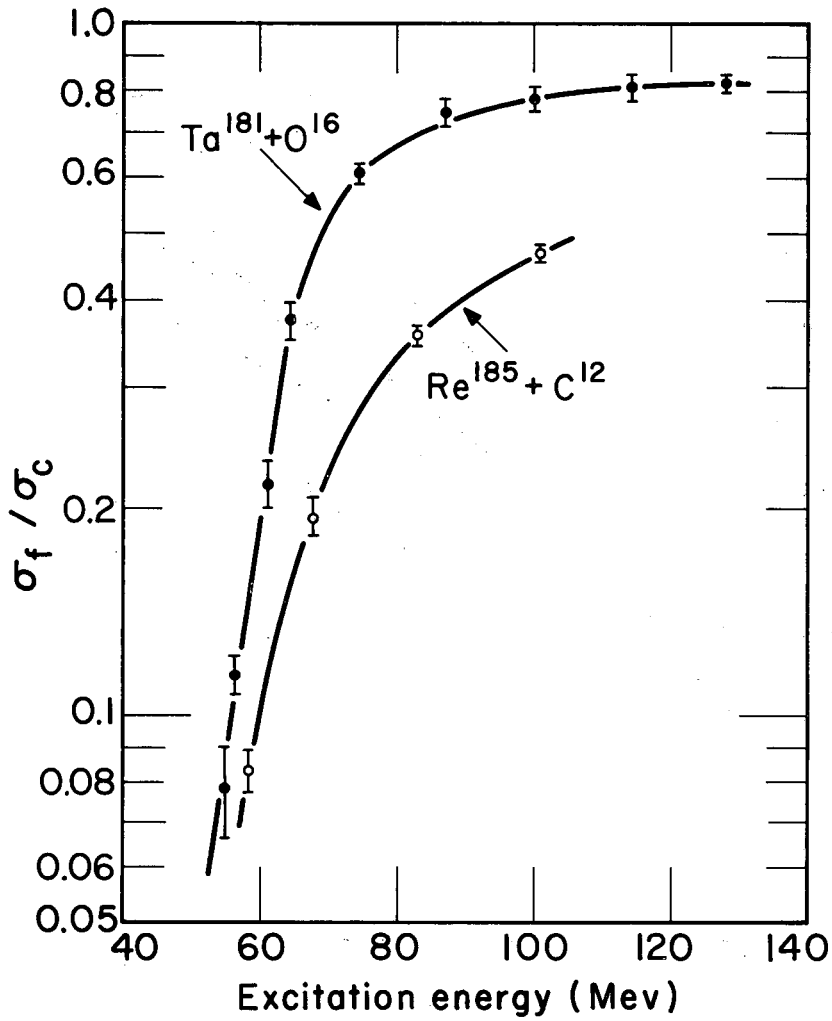

MU-21044

Fig. B.5-2. Probability for fission in the bombardments $Ta^{181} + O^{16}$ and $Re^{185} + C^{12}$ (square-well σ_c).

6. FISSION OF URANIUM-238 BY CARBON IONS (*)

T. Sikkeland, A. E. Larsh, and G. E. Gordon

With the use of a solid-state detector, the following quantities have been measured: (a) the differential cross section for fission and elastically scattered C^{12}, (b) the most probable kinetic energy of the fission fragments as a function of laboratory-system-angle, and (c) the total cross section for fission as a function of the energy of C^{12}.

A beam of 125-Mev C^{12} ions from the Hilac was passed through a bending magnet before the fission chamber. Lower energies were obtained by inserting weighed aluminum foils in the beam.[1] An uncertainty of 1 Mev was estimated for the energy. Targets were made by vaporizing UF_4 onto 800-$\mu g/cm^2$-thick nickel. The target most frequently used had 250 μg U^{238} per cm^2.

The target was oriented 45 deg to the beam with the uranium layer facing the detector. The detectors, chamber, and electronic system used have been described elsewhere.[2] The detector was calibrated with a Cf^{252} spontaneous fission source. It was found that electrons, knocked out of the target to the detector, had the effect of worsening the resolution of the peak of scattered C^{12}, but not a pulse-generator peak included in the system. This was overcome by introducing a 1000-gauss magnetic field in front of the detector, which removed most of the electrons over a distance of 1 cm.

Experimental Results

1. The angular distributions of the fission fragments in the laboratory system were transferred to the coordinate system of the fissioning nucleus by trial until a symmetric distribution about 90 deg in the new system was obtained.

An attempt was made to fit the distributions to the theory developed by Halpern and Strutinski.[3] The shape of the curve is, according to their formalism, determined by a parameter P, defined by $P = I_m^2/4K_0^2$, where K_0^2 is the mean value of K^2 in the $\overline{K}$ distribution, and I_m is approximately the maximum angular momentum of the fissioning nucleus. Curves corresponding to different values of P have been calculated.[4] With the high level width for fission, practically all the nuclei formed with an excitation energy above the fission barrier (≈ 5 Mev) will undergo fission. It is therefore to be expected that fission will occur from nuclei formed through a variety of reactions.

---

*Brief version of a paper (UCRL-9540) to be submitted to Phys. Rev.

[1] John R. Walton, (Lawrence Radiation Laboratory), unpublished data for range-energy-relations of C^{12} in Al 1959.

[2] G. E. Gordon, A. E. Larsh, T. Sikkeland, and G. T. Seaborg, Phys. Rev. 120, 1341 (1960).

[3] I. Halpern and V. Strutinski, in Proceedings of the Second United Nations International Conference on the Peaceful Uses of Atomic Energy, Geneva, 1958 (United Nations, New York 1958) Vol. 15, p. 408.

[4] J. R. Huizenga and R. Vandenbosch, Nuclear Fission, Argonne National Laboratory, Argonne, Illinois, 1960 (to be published).

We will try to compare the distributions with those predicted in the case in which compound nuclei are formed followed by evaporations of nucleons in competition with fission.

Monte Carlo calculations by Dostrovisky[5] predict that charged-particle evaporation is negligible in comparison with neutron evaporation.

The mean spin of the compound nucleus formed in the bombardment of U^{238} with C^{12} has been calculated by Thomas.[6] A neutron will classically reduce the spin by 1% for a nucleus with mass around 250. The excitation energy along an evaporation chain can be estimated from tabulated neutron-binding energies,[7] and by assuming the mean kinetic energy carried off by a neutron to be 2T. T is the nuclear temperature and is around 1.5 Mev in the region we are considering.

The over-all angular distribution can now be obtained by adding up the contribution from the different nuclei in the chain. In that case one has to know the percent fission at each step.

A formula for the ratio between level widths for neutron emission and for fission has been developed by Huizenga and Vandenbosch[4] which takes into account also the effect of rotation. The result of the calculations using their formula are given in Table I.

A typical over-all angular distribution calculated at 124 Mev C^{12} is shown in Fig. B.6-1 together with the experimental data. Similar distributions have been obtained at 73 Mev and 95.4 Mev. As is seen, the experimental distribution is more isotropic than predicted. The discrepancy can be explained by assuming a contribution from a non-compound-nucleus type of reaction by which particles are emitted with high orbital angular momenta prior to fission. In such reactions the nuclei will be left with low spin and subsequently give a more isotropic distribution of the fission fragments than estimated for an evaporation process.

2. The most probable kinetic energy in the laboratory system, E_L, is related to the kinetic energy in the system of the fissioning nucleus, E_C, through the equations

$$E_L = E_C(1 + X_{mp}^2 + 2X_{mp} \cos \theta_C), \tag{2}$$

$$\operatorname{tg} \theta_L = \frac{\sin \theta_C}{X_{mp} + \cos \theta_C}, \tag{3}$$

where X_{mp} is the most probable value of X, defined as

$$X = \frac{\text{velocity of the fissioning nucleus along the beam axis}}{\text{velocity of the fission fragment in the system of the fissioning nucleus}},$$

[5] Communication from Dostrovsky to Edward L. Hubbard (as reported by E. L. Hubbard, R. M. Main, and R. V. Pyle, Phys. Rev. 118, 507 (1960)

[6] T. D. Thomas, Phys. Rev. 116, 703 (1959).

[7] R. A. Glass, S. G. Thompson, and G. T. Seaborg, J. Inorg. and Nuclear Chem. 1, 3 (1955).

Table I. Result of calculations by Huizenga-Vandenbosch formula

$E_{C^{12}}$	A_{fN}	E	$\bar{T}$	fission (%)	$\bar{\nu}$	$\overline{A_{ff}}$	$\overline{X_{CN}^2}$	X_m^2	X_{mp}^2	K_0^2	P
	Cf^{250}	45.7	19.4	26	9.1	120.5				202	1.1
	Cf^{249}	36.0	19.2	20	7.7	120.7				175	1.2
73	Cf^{248}	27.4	19.0	30	6.5	120.8	0.018	0.018	0.016	150	1.4
	Cf^{247}	17.4	18.8	12	5.2	120.9		(+0.004)	(+.004)	100	2.0
	Cf^{246}	8.5	18.6	12	4.0	121.0				10	5.6
	Cf^{250}	67.0	33.5	28	11.6	119.2				249	2.5
	Cf^{249}	57.3	33.2	25	10.3	119.4				227	2.7
95.4	Cf^{248}	48.7	32.9	22	9.0	119.5	0.024	0.018	0.023	209	2.9
	Cf^{247}	38.7	32.6	16	7.7	119.7		(+.004)	(+.005)	183	3.3
	Cf^{246}	29.8	32.3	8	6.6	119.7				158	3.7
	Cf^{250}	94.2	45.9	33	14.9	117.6				298	4.0
	Cf^{249}	83.4	45.4	27	13.4	117.8				279	4.2
124	Cf^{248}	75.9	45.0	20	12.5	117.8	0.030	0.022	0.023	266	4.3
	Cf^{247}	65.9	44.5	12	11.0	118.0		(+0.004)	(+.005)	246	4.5
	Cf^{246}	57.0	44.1	6	9.8	118.1				228	4.8

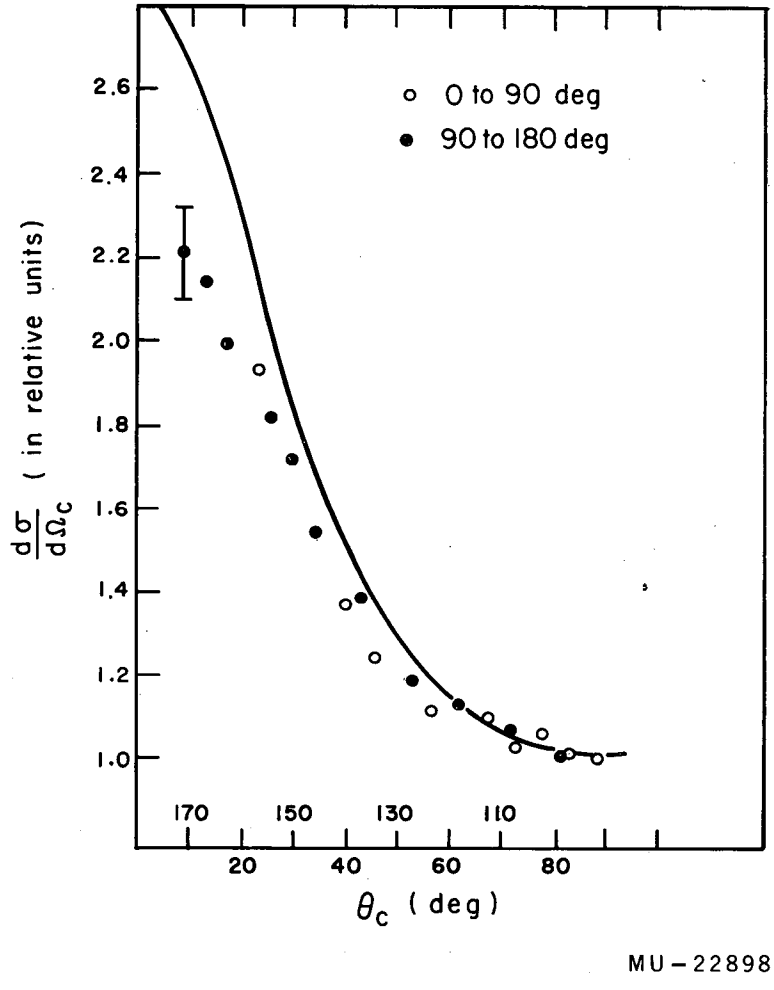

Fig. B.6-1. Differential cross section of fission fragments from the reaction between U^{238} and 124-Mev C^{12} ions. The transformation to the system of the fissioning nucleus was performed with $X_m^2 = 0.022$. The curve is a theoretical curve.

θ_L and θ_C are the angles in the laboratory system and in the coordinate system of the fissioning nucleus, and E_C and X_{mp} were adjusted to fit the experimental data. For E_C we obtained the value 93±3 Mev at all three bombarding energies. This is to be compared with 185 Mev as the most probable total kinetic energy release in the fission of Cf^{252},[8] and seems to indicate that the most probable fissioning nuclei are Cf isotopes. Independence of bombarding energy for the kinetic energy release in fission has been observed in the bombardment of Au with C^{12}.[2]

The va ues of X_{mp}, together with mean values of X, X_m, obtained from the transformations of the angular distributions, are given in Table I. These we will now compare with X_{CN} values which can be estimated for compound-nucleus reactions. In that case the mean moment of the fissioning nucleus is equal to that of the heavy ion, and we have

$$X_{CN}^2 = \frac{A_i E_i A_{ff}}{A_{fN}^2 \cdot E_C} \quad . \tag{4}$$

Here A_i and E_i are the mass and lab energy of the heavy ion, A_{ff} is mass of the fission fragment, and A_{fN} the mass of the fissioning nucleus; E_C is defined as before.

When neutrons are evaporated the mean excitation energy, E, of the fissioning nuclei can be estimated. The number of neutrons emitted from the fission fragments in the fission process, $\bar{\nu}$, is then, according to Leachman's empirical relationship;[9]

$$\bar{\nu} = \bar{\nu}_0 + 0.12\ E,$$

where $\bar{\nu}_0$ is the number emitted from a nucleus in the ground state as observed in spontaneous fission. For high-energy fission the mass-yield curve is symmetric and the mean mass of the fission fragments A_{ff} can thus be evaluated. The estimated values for A_{ff}, E, and X_{CN}^2 are given in Table I.

We see that, as a general rule, $X_{CN}^2 > X_{mp}^2 > X_m^2$. Apparently we have contribution from reactions in which the linear momentum of the fissioning nucleus is less than that of the heavy ion. Particles are emitted preferentially in the forward direction prior to the fission process.

High frequency of α particles has been observed emitted in the forward direction in the bombardment of Au^{197} with 160-Mev O^{16}.[10] A similar

[8] J.S. Fraser and J.C.D. Milton, in Proceedings of the Second United Nations International Conference on the Peaceful Uses of Atomic Energy, Geneva, 1958 (United Nations, New York, 1958) Vol. 15, p. 216.

[9] R.B. Leachman, op. cit., p. 299.

[10] W.J. Knox, C.E. Anderson, A.R. Quinton, and H.W. Brock, in Proceedings of the Second Conference on Reactions between Complex Nuclei, Gatlinburg, May 2-4 1960 (John Wiley and Sons Inc., New York, 1960), p. 263.

type of reaction could account for the apparent low mean spin and linear momentum of the fissioning nuclei in the case of $U^{238} + C^{12}$.

3. The total cross section for fission was determined by a direct comparison, using the same detector, target, and geometry, of the counting rate of carbon ions in the region of pure Coulomb scattering, with the fission counting rate, and allowing for the presence of two fragments in the latter case. The contribution to the scattering from the nickel backing was determined experimentally. The fission cross section was found to be 0.47 barn at 73 Mev, 1.4 barns at 95.4 Mev, and 2.3 barns at 124 Mev. For all three values we assign a standard deviation of 10%.

At other bombarding energies, the differential cross section at 90 deg to the beam was measured and the total cross section estimated from the known efficiency and by assuming a smooth variation in the angular distribution with bombarding energy. The error introduced by this method should be negligible because of the small changes in the distribution from 73 Mev to 124 Mev.

The results are given in Fig. B.6-2 together with the theoretical curve for compound-nucleus formation as calculated by Thomas[6] from the square-well model and $\nu_0 = 1.5 \times 10^{-13}$ cm. We see the agreement is satisfactory, and this cross section represents, then, the total cross section for reactions which produce nuclei with more than 5 Mev excitation energy.

7. COMPOSITION-DEPENDENT SURFACE ENERGY OF HEAVY NUCLIDES AND SPONTANEOUS FISSION

Reinhard Brandt and Stanley G. Thompson

This report is a summary of a preliminary investigation of the influence of a composition dependence of the nuclear surface tension on some phenomena of fission such as fission barrier height, spontaneous fission rates, and asymmetry.

The liquid-drop model is employed in the semiempirical mass formula and in the theory of fission. The attractive nuclear forces are idealized in a surface energy, which has in the standard semiempirical mass formula (for example, Green[1]) the form

$$E(\text{surface}) = (\text{constant}) \cdot A^{2/3} \qquad (1)$$

There is some evidence that for a given A the nuclear attractive forces may be composition-dependent, i.e., may depend on the neutron-to-proton ratio. Kolesnikov - Larkin-Mottelson[2] (K-L-M) proposed the composition-dependent surface energy term

[1] A. E. S. Green, Phys. Rev. 95, 1006 (1954).

[2] R. Brandt, F. Werner, M. Wakano, R. Fuller, and J. A. Wheeler, in Conference on Nuclidic Masses, edited by H. E. Duckworth (University of Toronto Press, Toronto, 1961).

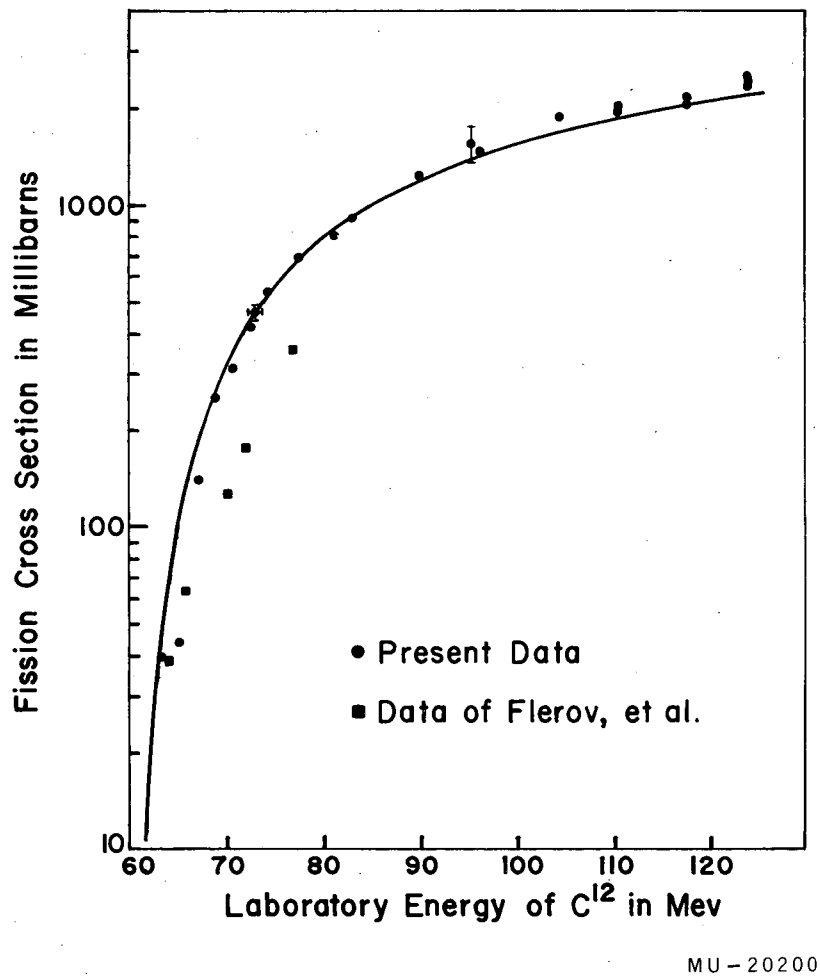

Fig. B.6-2. Total fission cross section for fission of U^{238} by C^{12} ions. Calculated compound-nucleus formation cross section, square-well model, with $r_0 = 1.5 \times 10^{-13}$ cm.

$$E(\text{surface}) = (\text{constant}) \cdot A^{2/3} \left[1 - C_1 \left(\frac{N-Z}{A} \right)^2 \right] . \qquad (2)$$

It has been shown[2] that one cannot get a better or worse semiempirical mass formula by using $C_1 = 0$ of $C_1 = 2.5$. Also, the plot of the spontaneous fission half lives vs the fissionability parameter $X = E(\text{Coulomb})/2\,E(\text{surface})$ could not be smoothed out with these two values of C_1. Concerning the question of the stability of heavy nuclei (with half lives $> 10^{-4}$ sec), Werner and Wheeler[3] showed that for $C_1 = 0$, nuclei up to $Z = 147$ and $A = 500$ might be expected. For $C_1 = 2.7$ it was shown[2] that the stability region would be confined to ($A \leq 274$; $Z \leq 96$ for $A = 250$). Thus there exists no evidence for or against the K-L-M term so far as the semiempirical mass formula or the spontaneous fission half-lives are concerned.

But a value of the term C_1 between 0 and 2.7 might be obtained that would permit a better prediction. Some insight into the magnitude of this term is obtained in the following discussion.

Swiatecki[5] has shown, for the uniformly charged liquid drop, that the threshold energy is related to X in the following way, assuming that for $X < X_C$ the nucleus is asymmetrically deformed at the threshold:

$$E(\text{threshold}) = \text{"function"}\,(1 - X) - C_2\,(X_C - X)^2 , \qquad (3)$$

where C_2, X_C are constants.
By using a classical liquid drop, it is shown[6] that

$$\frac{\text{"function"}\,(1-X)}{E(\text{surface})} = 0.73\,(1-X)^3 - 0.33\,(1-X)^4 + 1.9\,(1-X)^5 - 0.21\,(1-X)^6 . \qquad (4)$$

The constant X_C appears also in the relation of the asymmetry of mass-yield curves vs X,[4]

$$\left(\frac{M_H - M_L}{A} \right)^2 = (\text{constant}) \cdot (X_C - X), \qquad (5)$$

where M_H = the mass of the most probable heavy fragment,
M_L = the mass of the most probable light fragment.

The constants C_2 and X_C in Eq. (3) can be determined by fitting Eq. (3) to two observed fission-activation energies[7] (for example, Cm^{242} and Th^{234}). Then this X_C is compared with the X_C from the plot of observed asymmetry data vs X. For $C_1 = 0$ (this affects X and Eqs. (4) and (5)) the two independently determined values of X_C do not agree, nor do they agree for $C_1 = 1.2$. But for $C_1 = 0.8$ the X_C from the threshold calculation agrees with the asymmetry curve (see Fig. B.7-1). If then the other activation energies for even-even nuclei are calculated from Eq. (3), it is found that they agree within 0.15 Mev with those computed by Vandenbosch and Seaborg.[7] The question

[3] F. G. Werner and J. A. Wheeler, Phys. Rev. 109, 126 (1958).

[4] W. J. Swiatecki, Phys. Rev. 100, 936 (1955).

[5] W. J. Swiatecki, Phys. Rev. 101, 651 (1956).

[6] Earl K. Hyde, A Review of Nuclear Fission. Part I. Fission Phenomena at Low Energy, UCRL-9036, Jan. 1960, p. 28.

[7] R. Vandenbosch and G. T. Seaborg, Phys. Rev. 110, 507 (1958).

[8] S. A. E. Yohansson, Nucl. Phys. 12, 449 (1959).

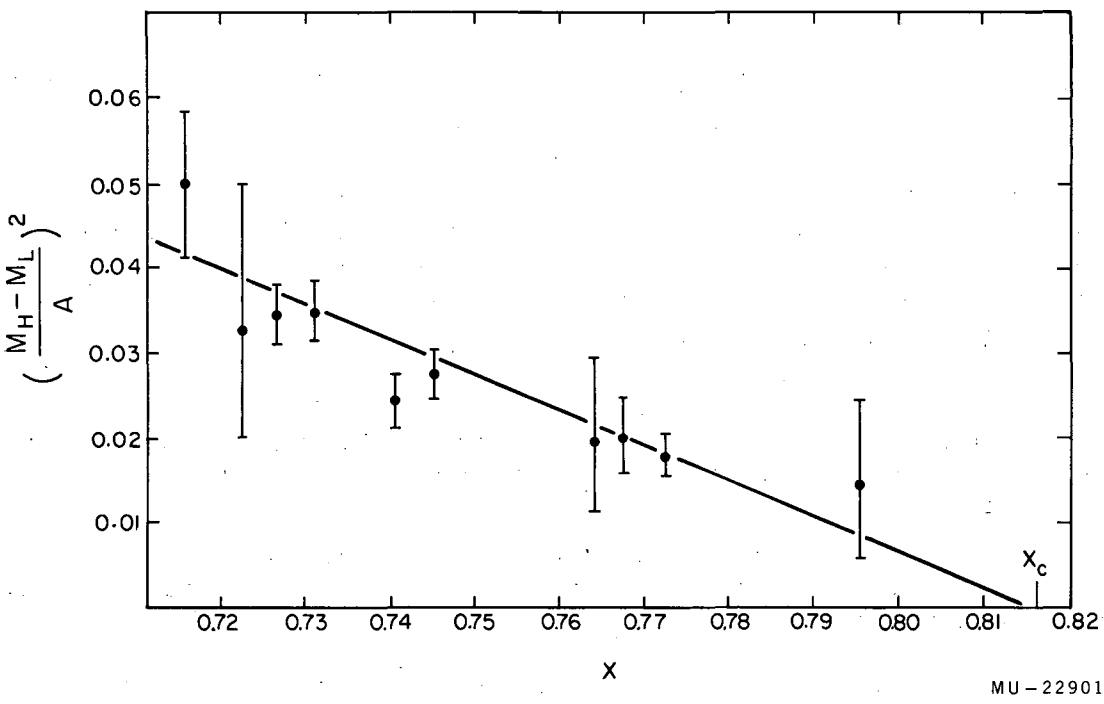

Fig. B.7-1. The observed fission asymmetry $\left(\frac{M_H - M_L}{A}\right)$ plotted against the improved x value.

$x = Z^2/51.350 \cdot A \left\{1-0.8[(N-Z)/A]^2\right\}$

X_C (from threshold calculations) = 0.08165;

M_H and M_L = masses of most probable heavy and light fragments.

remains now as to how large C_1 must be to give similar agreement when the fission barriers are used instead of fission-activation energy.[7]

Johansson employed single-particle effects to improve the correlation of spontaneous fission half lives with X.[8] However, the variations in curve can be smoothed out considerably by using $C_1 = 1.0 \pm .3$.

The influence of $C_1 = 1.0 \pm .3$ on the expected half lives of higher elements is also being considered.

8. FISSION BARRIER HEIGHTS IN ELEMENTS LIGHTER THAN RADIUM

D.S. Burnett and S.G. Thompson

A program has been initiated to study the fission barrier heights in elements lighter than radium. At present there are no directly measured values for barrier heights in this region; however, these values are of considerable significance for the following reasons.

(a) Fission has been observed to be symmetric for all nuclides studied in this region, even at energies close to the barrier; thus it might be expected that in this region the (conventional) liquid-drop model would be a better approximation to the actual situation than for heavy elements where the liquid drop in its original form did not predict the observed trends in barrier heights and did not explain the asymmetry in fission.

(b) Fission barrier heights are important in the study of the nuclear reactions in this region at moderate excitation, since fission can compete effectively as a nuclear reaction mode under these conditions.

One purpose of the present program is to attempt direct measurement of fission-barrier heights for these nuclides. In order to guide experimental work and provide preliminary estimates for comparison with experimental data, approximate calculations of barrier heights have been carried out[1] in two ways.

A. Following an approach similar to one suggested by Halpern[2] we can write, as a very rough approximation,

$$\Gamma_f/\Gamma_n \approx N(Z,A) \exp\left[(B_n - B_f)/ c \sqrt{E_x}\right] ,$$

where B_f is barrier height, B_n is the neutron binding energy, c is a constant, and E_x is excitation energy. Γ_f/Γ_n, the probability for fission relative to neutron emission, is equal to the ratio of the observed fission cross section to the formation cross section of the compound nucleus, since neutron emission is the most probable reaction at these energies, making the total

[1] Donald S. Burnett and Stanley G. Thompson, Fission Thresholds for Elements Lighter than Radium, UCRL-9321, July 1950.

[2] I. Halpern, Ann. Rev. Nuclear Sci. 9, (1959).

reaction width very close to Γ_n. Values for B_f can be obtained from the slope of a log plot of Γ_f/Γ_n vs $1/\sqrt{E_x}$ provided c is known. A value for c was estimated from a plot of Γ_f/Γ_n vs $(B_n - B_f)$ for heavy elements at constant excitation which had been made by Vandenbosch and Huizenga.[3] Thus estimates of B_f could be obtained.

B. Let us define ξ as a dimensionless measure of the fission barrier, B_f, by $\xi = B_f/E_s^0$, where E_s^0 is the initial surface energy of the undeformed nucleus, and define x, the fissionablitity parameter, as $(Z^2/A)/(Z^2/A)_0$, where $(Z^2/A)_0$ is a limiting value at which the nucleus will fission spontaneously without deformation. Previous work had suggested that in the region from $x = 0$ (uncharged drop) to $x = 0.7$ the values of ξ based on the liquid-drop model could be well represented by a parabolic expression, $\xi = c + bx + ax^2$, where c and b are respectively the value and first derivative of ξ at $x = 0$ and had been previously calculated by Bohr and Wheeler.[4] The value a was obtained by estimating a threshold for the Ra^{226} (nf) data of Nobles and Leachman.[5] This equation was used to calculate fission-barrier heights for elements in this region.

Some sample results are given in Table I. A more complete tabulation may be found in Ref. 1.

Table I. Comparison of results from two methods for calculating fission-barrier heights.

Compound nucleus	Barrier height (Mev)	
	Method A	Method B
At^{213}	16	15.6
Po^{212}	17	21.1
Po^{210}	22	21.3
Tl^{201}	26	25.6
Ta^{179}	—	35.4

The approximations made in obtaining the expression used in Method A are not very good for the cases considered, consequently the values so obtained must be taken merely as order-of-magnitude estimates. The values obtained from Method B would be more appropriately used to compare with any experimental values if direct measurement of these fission barriers turned out to be feasible.

[3] R. Vandenbosch and J.R. Hiuzenga, in Proceedings of the Second International Conference on Peaceful Uses of Atomic Energy, Geneva, 1958, (United Nations, Geneva, 1958) Vol. 15, Paper 688.

[4] N. Bohr and J.A. Wheeler, Phys. Rev. 56, 426 (1939).

[5] R.A. Nobles and R.B. Leachman, Nuclear Phys. 5, 211 (1958).

C. NUCLEAR REACTIONS

1. TOTAL REACTION CROSS SECTIONS

Bruce D. Wilkins and George Igo

Recently elastic scattering data of various ions have been fitted with several nuclear models.[1] In particular, work has been done using an optical-model potential[2]

$$\frac{V + iW}{1+\exp\left(\frac{r-R}{a}\right)} .$$

The parameters V, W, R, and a represent respectively the depths of the real and imaginary potentials, the radius, and the diffuseness parameters of the potential. In addition the optical model also predicts total reaction cross sections σ_R. Measurements of σ_R help resolve the ambiguity in determining the shape of the optical-model potentials for various ions. With this in mind we have begun a program at the heavy-ion linear accelerator and at the 60-inch cyclotron to measure σ_R for O^{16} ions and protons.

We have used the method of beam attenuation.[3] The beam particles pass through two thin ΔE plastic scintillators and an attenuator of the material under investigation, and finally into a stopping plastic scintillator. A nuclear reaction in the attenuator causes an anticoincidence between the two ΔE counters and the stopping counter. Attenuator-in and attenuator-out measurements are necessary to see the effect of the attenuator. With the use of nanosecond electronic techniques we have been able to count at a rate of 4×10^5 counts per second.

Corrections which must be made are (a) subtraction of elastic scattering through angles greater than that subtended by the stopping counter, (b) addition of inelastic or reaction events in which the product cannot be distinguished from the beam particle in the stopping counter, (c) transfer reactions. The discrimination against inelastic or reaction events in the stopping counter is accomplished by placing an absorber between target and plastic scintillator. The solid angle subtended by the stopping counter is determined by measuring the anticoincidence rate as a function of the distance of the stopping counter from the attenuator (see Fig. C. 1-1). The flat portion

[1] J. S. Blair, Phys. Rev. 95, 1218 (1954); F. Bjorklund, in Proceedings of the International Conference on the Nuclear Optical Model, Tallahassee, 1959; K. W. Ford and J. A. Wheeler, Annals of Physics 7, 287 (1959); C. E. Porter, Phys. Rev. 99, 1400 (1955); G. Igo and R. M. Thaler, Phys. Rev. 106, 126 (1957).

[2] R. D. Woods and D. S. Saxon, Phys. Rev. 95, 577 (1954).

[3] R. M. Eisberg, in Proceedings of the International Conference on the Nuclear Optical Model, Tallahassee, 1959.

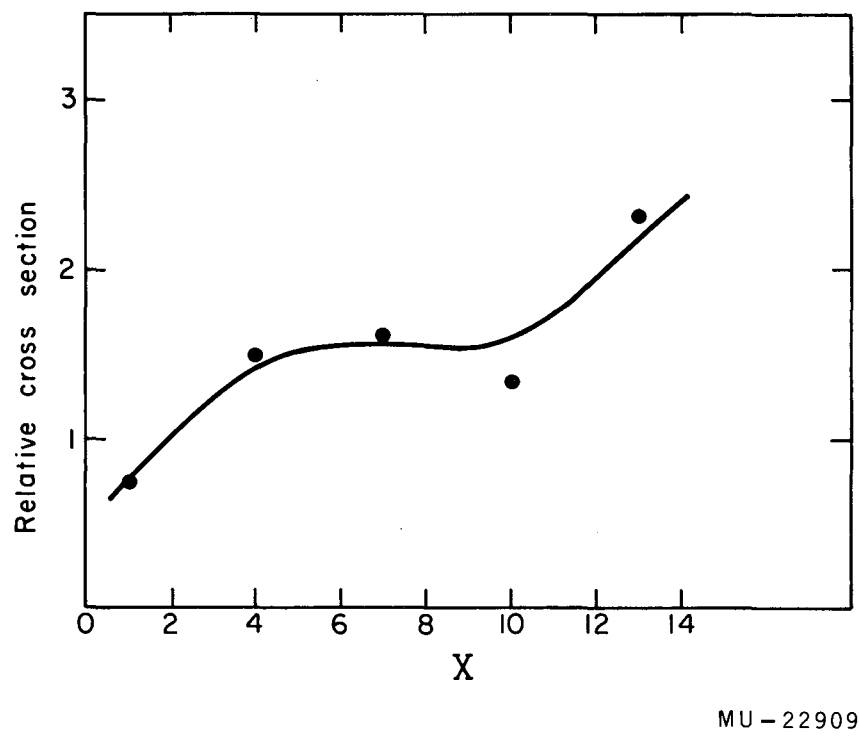

Fig. C. 1-1. The dependence of the measured cross section on the distance X of the stopping counter from the attenuator. The points ⊙ are the measurements for 152±8-Mev O^{16} ions on Cu. A smooth curve has been drawn through the points.

of the curve in Fig. C. 1-1 is where the elastic scattering correction is approximately equal and opposite to the inelastic and reaction scattering correction. The statistics on the individual points in Fig. C. 1-1 are of the order of 6%.

Preliminary results on the total reaction cross sections for 152±8-Mev O^{16} ions are listed in Table I. Further corrections (to be determined later) due to elastic, inelastic, and reaction scattering effects may change these results by as much as 10%. If the cross section is written as $\sigma_R = \pi R_0^2 (A_1^{1/3} + A_2^{1/3})^2$, where A_1 and A_2 are the atomic numbers of ion and target respectively, then the values of R_0 obtained from this analysis are also listed in Table I.

Table I. Reaction cross sections for 152±8-Mev O^{16} ions

	σ_t(barns)	R_0(fermis)
Al	2.09±0.08	1.48
Cu	3.35±0.14	1.59
Ag	4.18±0.16	1.59
Au	5.82±0.22	1.63

These values of R_0 are consistent with those found in elastic scattering analyses by using the Blair model.[4]

[4] J. S. Blair, Phys. Rev. 95, 1218 (1954).

2. THEORETICAL REACTION CROSS SECTIONS FOR ALPHA PARTICLES WITH THE OPTICAL MODEL

John R. Huizenga* and George Igo

Shapiro[1] and Blatt and Weisskopf[2] have calculated total reaction cross sections for α particles with a square-well potential. The total reaction cross section is given by

$$\sigma_R = \pi \lambda\!\!\!^{-2} \sum_{\ell=0}^{\ell=\ell'} (2\ell+1)\, T_\ell\, (\epsilon), \qquad (1)$$

*Summer visitor from Argonne National Laboratory, Argonne, Illinois.

[1] M. M. Shapiro, Phys. Rev. 90, 171 (1953).

[2] J. M. Blatt and V. F. Weisskopf, Theoretical Nuclear Physics (John Wiley and Sons, Inc., New York, 1952), p. 352.

where $\lambda\!\!\!^{-}$ is the de Broglie wave length, ℓ is the angular momentum of the incident particle in units of $\hbar$, $T_\ell(\epsilon)$ is the transmission coefficient of the incident particle of energy ϵ. The transmission coefficients (actually $4/T_\ell$ are tabulated) for α particles derived from the square-well potential are available for target nuclei with $Z < 40$.[3] Igo has calculated total reaction cross sections with a complex nuclear potential for six target nuclei with α-particle projectiles of several energies.[4] Transmission coefficients calculated with the complex nuclear potential are not available.

Since α-particle transmission coefficients for high-Z targets are not available, we have calculated this quantity for a large variety of targets at a number of α energies with a complex nuclear potential.

The optical-model potential employed in these calculations is written as

$$V_\ell(r)=V_c+\frac{\ell(\ell+1)\hbar^2}{2M_\alpha r^2}-1100\exp\left[-\left(\frac{r-1.17A^{1/3}}{0.574}\right)\right]-45.7\,i\exp\left[-\left(\frac{r-1.40\,A^{1/3}}{0.578}\right)\right], \tag{2}$$

where V_c is the Coulomb potential, M_α the reduced mass of the α particle, and the third and fourth terms, in units of Mev, are the real and imaginary parts, respectively, of the α-nucleus potential[4] exclusive of the Coulomb and centrifugal potentials. The Coulomb potential of the Hill-Ford[5] charge distribution was employed in Eq. (2). This is given by

$$V_c=\frac{2Ze^2}{r_c}\left[\frac{1}{n^2}+\frac{1}{2}-\frac{x^2}{6}+\frac{e^{-n}}{n^2}\left(\frac{1-e^{nx}}{nx}+\frac{e^{nx}}{2}\right)\right]\Big/\left(\frac{1}{3}+\frac{2}{n^2}+\frac{e^{-n}}{n^3}\right)\quad\text{for } X<1 \tag{3}$$

and

$$V_c=\frac{2Ze^2}{r_c}\left\{\frac{1}{x}-\left[\frac{\left(\frac{1}{x}+\frac{n}{2}\right)e^{n-nx}}{e^{-n}+2n+\frac{1}{3}n^3}\right]\right\}\quad\text{for } X>1, \tag{4}$$

where $x = r/r_c$ and where n is 10 for heavy elements and is proportional to $A^{1/3}$. The quantity r_c is the distance out to the half-value point of the charge distribution. The value $1.17A^{1/3}\times10^{-13}$ cm for r_c was chosen larger than the value obtained from the electron scattering experiments[6]

[3] H. Feshbach, M. M. Shapiro, and V. F. Weisskopf, NYO-3077, June, 1953 (unpublished).

[4] G. Igo, Phys. Rev. 115, 1665 (1959).

[5] K. W. Ford and D. L. Hill, Phys. Rev. 94, 1617 (1954).

[6] R. Hofstadter, Ann. Rev. Nuclear Sci., 7, 231 (1957).

to take roughly into account the effect of the finite size of the α-particle charge distribution.

In order to use an existing calculational program, it was necessary to choose the parameters V, W, r_0, and d for the Wood-Saxon potential,[7]

$$(V + i\,W) \Big/ \left[1 + \exp\left(\frac{r - r_0}{d}\right)\right],$$

to reproduce the nuclear potential of Eq. (2) for values of r such that the real part of the nuclear potential is greater than -10 Mev. These parameters are given in Table I. The depth of the potential for small values of r is also fixed when the parameters of Table I are used, although it has been shown that α-particle scattering is not sensitive to the potential depth.

The total reaction cross sections, σ_R, and the transmission coefficients, T_ℓ, have been calculated with the parameters of Table I. Figures C. 2-1 and C. 2-2 show the energy variation of the total reaction cross sections for V^{51} and for U^{235}. For comparison the same quantity is calculated by Shapiro[1] and by Feshbach, Shapiro, and Weisskopf.[3]

Table I. Woods-Saxon potential parameters

Nuclide	V (Mev)	W (Mev)	r_0 (fermis)	d (fermis)	r_c (fermis)	n
$_{19}K^{41}$	-50	-8.70	$1.17A^{1/3} + 1.77$	0.576	$1.17A^{1/3}$	5.60
$_{22}Ti^{48}$	-50	-9.51				5.91
$_{23}V^{51}$	-50	-10.00				6.04
$_{24}Cr^{52}$	-50	-9.90				6.07
$_{25}Mn^{53}$	-50	-9.98				6.11
$_{25}Mn^{55}$	-50	-10.25				6.19
$_{26}Fe^{56}$	-50	-10.26				6.23
$_{27}Co^{55}$	-50	-10.17				6.19
$_{32}Ge^{72}$	-50	-11.85				6.77
$_{37}Rb^{85}$	-50	-13.30				7.16
$_{41}Nb^{93}$	-50	-13.74				7.37
$_{45}Rh^{103}$	-50	-14.30				7.62
$_{50}Sn^{119}$	-50	-16.20				8.00
$_{60}Nd^{144}$	-50	-18.23				8.53
$_{70}Yb^{173}$	-50	-20.79				9.07
$_{78}Pt^{195}$	-50	-22.10				9.44
$_{82}Pb^{206}$	-50	-23.00				9.61
$_{90}Th^{232}$	-50	-26.11				10.00
$_{92}U^{235}$	-50	-27.00				10.04

[7] R. D. Woods and D. S. Saxon, Phys. Rev. 95, 577 (1954).

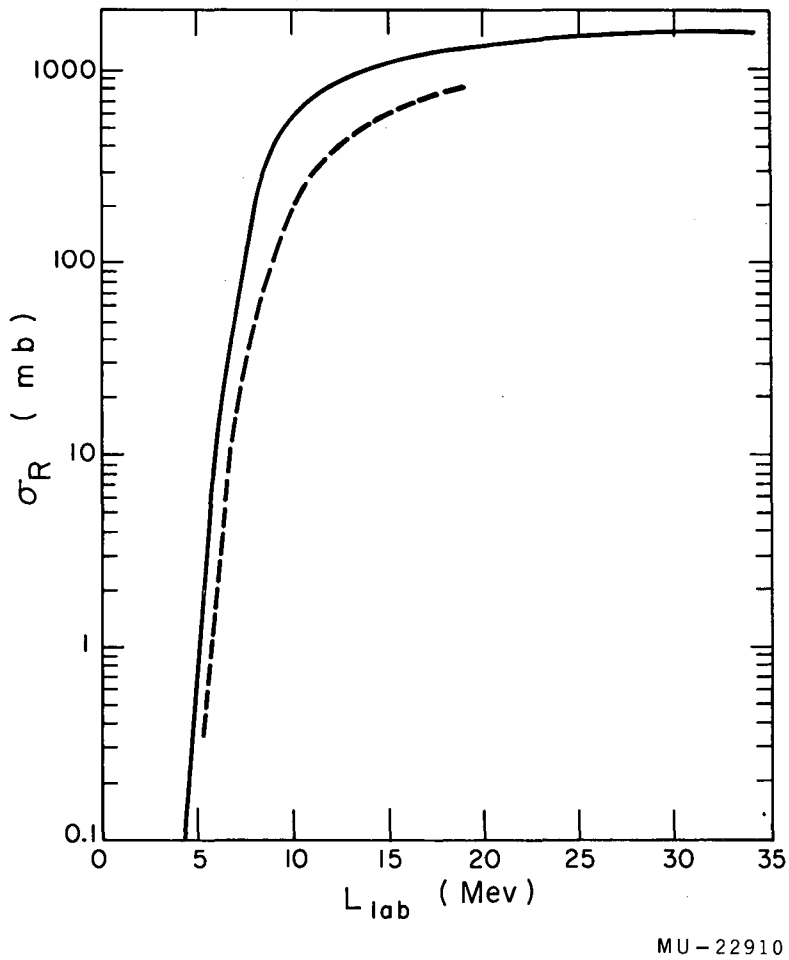

Fig. C. 2-1. The total reaction cross section versus laboratory energy for alpha particles incident on V^{51}. The solid curve has been calculated by using the surface nuclear potential discussed in the text. The dashed line is the same quantity calculated by Shapiro (Ref. 1).

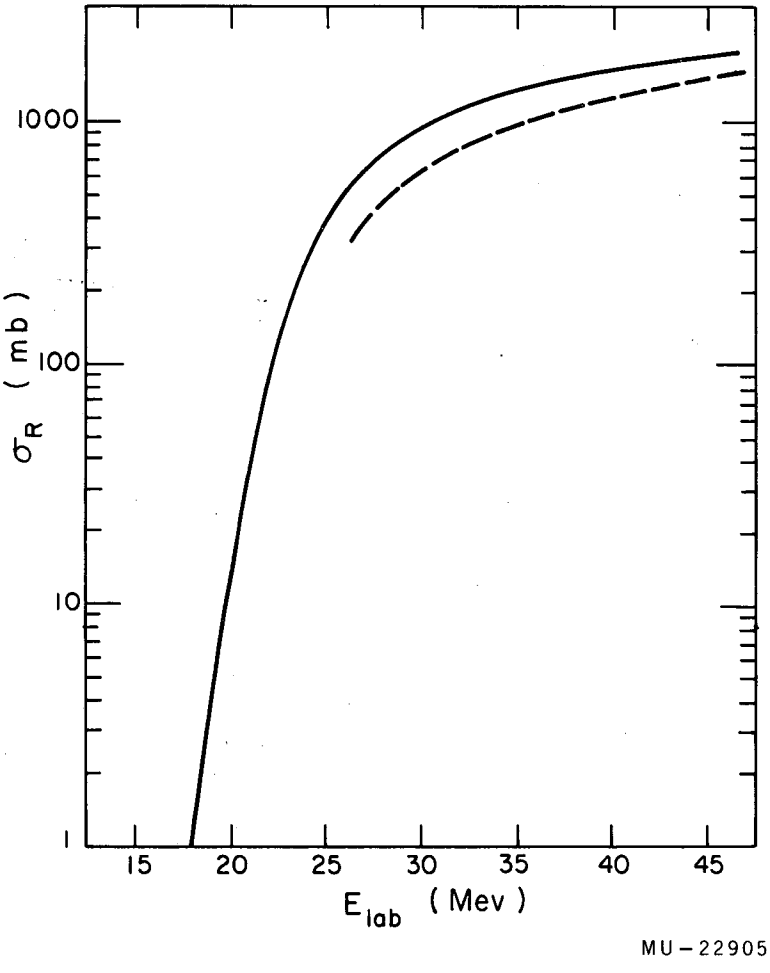

Fig. C. 2-2. The total reaction cross section versus laboratory energy for alpha particles incident on U^{235}. The solid curve has been calculated by using the surface nuclear potential discussed in the text. The dashed line is the same quantity from the paper of Feshbach, Shapiro, and Weisskopf (Ref. 3).

3. THE REACTION $C^{12}(\alpha, d)N^{14}$ (*)

Joseph Cerny, III, and Bernard G. Harvey

The reaction $C^{12}(\alpha, d)N^{14}$ was studied in almost the same way as the reactions described in the previous report. Angular distributions were obtained for the deuteron groups leading to the ground state and 3.95-Mev state of N^{14}.

The 2.31-Mev 0+, T=1 state of N^{14} was not observed: it was excited less than 3% as strongly as the ground state. This observation, however, is not strong evidence for the isotopic spin purity of the level, because formation of a 0+ level from a 0+ target is also forbidden by angular momentum and parity conservation in an (α, d) or (d, α) reaction. Furthermore, several well-known T=0 levels of N^{14} were not observably excited: the (α, d) reaction is somewhat specific.

The angular distribution of deuterons corresponding to formation of the ground state of N^{14} is shown in Fig. C. 3-1. Good agreement was obtained with the Butler stripping theory by using $\ell=2$ and r=6.3 f. However, an equally good fit was obtained for l=0 and r=6.45 f. Figure C. 3-2 shows the best fit obtained with the two-nucleon stripping theory of Glendenning for capture of the proton and neutron into the $p_{1/2}$ shell, with r=4.70 f. Equally good fits (but with slightly larger values of r) were obtained for several other configurations. The cross section for formation of the N^{14} ground state (integrated between 10 and 133 deg) is 1.8 mb.

Figure C. 3-3 shows the angular distribution of deuterons corresponding to formation of the 3.95-Mev 1+, T=0 level of N^{14}. Good agreement was obtained on Butler theory for $\ell=2$, r=5.5 f, or $\ell=0$, r=5.7 f. Figure C. 3-4 shows the fit obtained with the Glendenning theory, assuming that the captured nucleons enter the $p_{1/2}$ shell, with r=4.33 f. Again, equally good fits were obtained for other configurations.

The multiple fitting is characteristic of stripping reactions that involve a large momentum transfer. The arguments of the spherical Bessel functions are then large enough for the functions to approach their asymptotic forms, which are sine and cosine functions for even and odd ℓ values respectively. It is quite impossible to distinguish between $\ell=0$ and $\ell=2$, and, in some cases at least, $\ell=1$ or $\ell=3$ would give angular distributions that would be experimentally indistinguishable from the even-ℓ values, since the required interaction radius may change by an amount too small to permit rejection of any of the ℓ values.

---

*Brief version of published paper, Phys. Rev. 120, 2162 (1960).

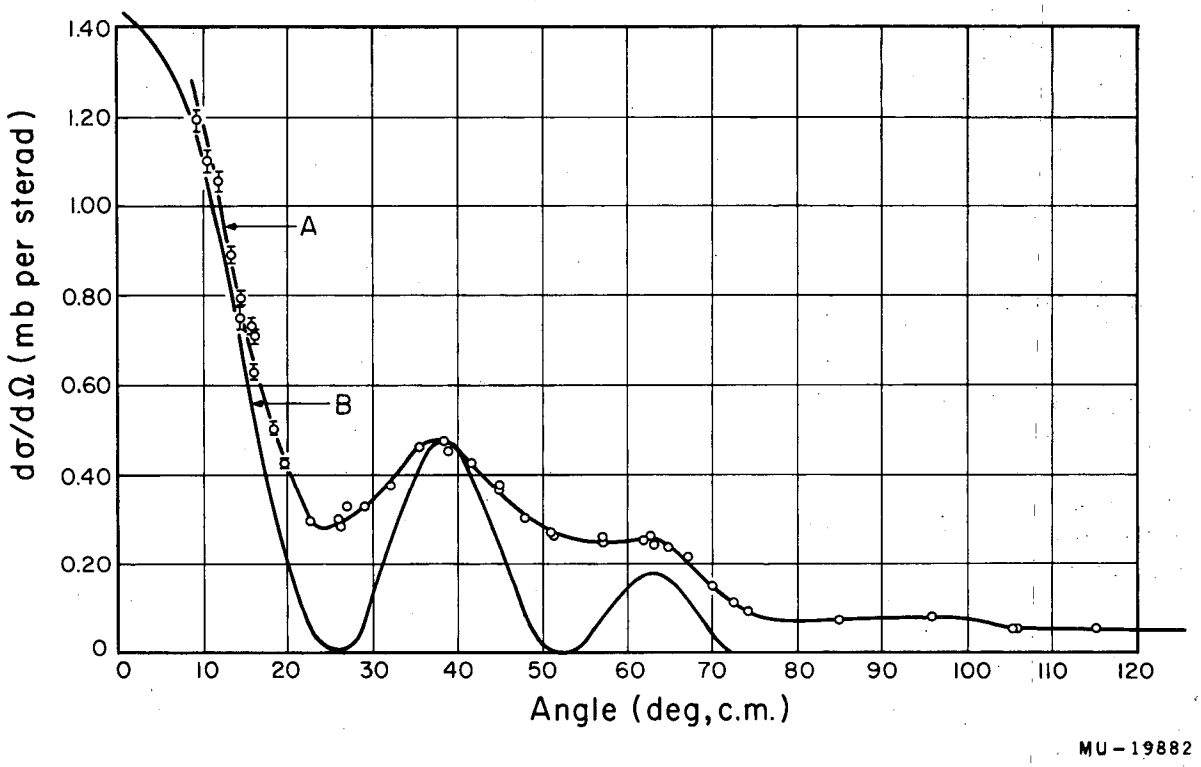

Fig. C. 3-1. Angular distribution of deuterons from formation of the ground state of N^{14} in the reaction $C^{12}(\alpha, d)N^{14}$. Curve A presents the experimental results; Curve B, results calculated from the Butler equation by using $\ell = 2$, $r = 6.3$ fermis.

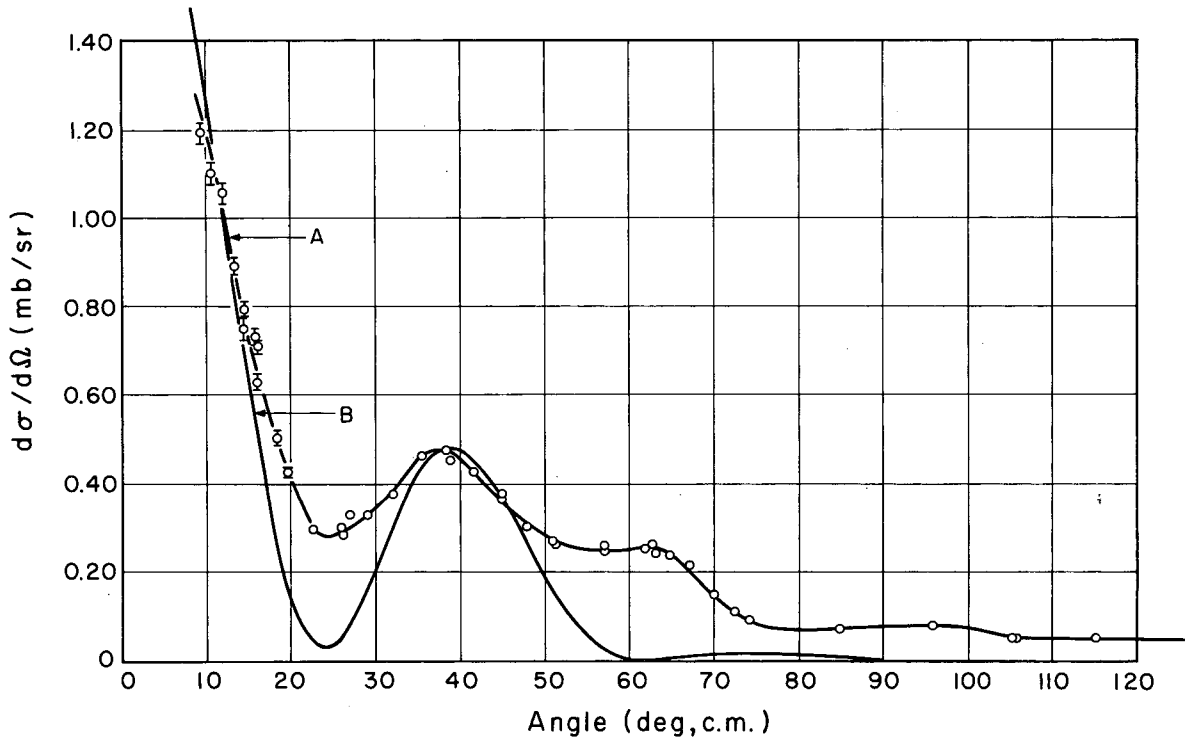

MU-21995

Fig. C. 3-2. Angular distribution of deuterons from formation of the ground state of N^{14} in the reaction $C^{12}(\alpha, d)N^{14}$. Curve A presents the experimental results calculated from Glendenning's theory assuming capture of both nucleons into the $p_{1/2}$ shell, and r = 4.70 fermis.

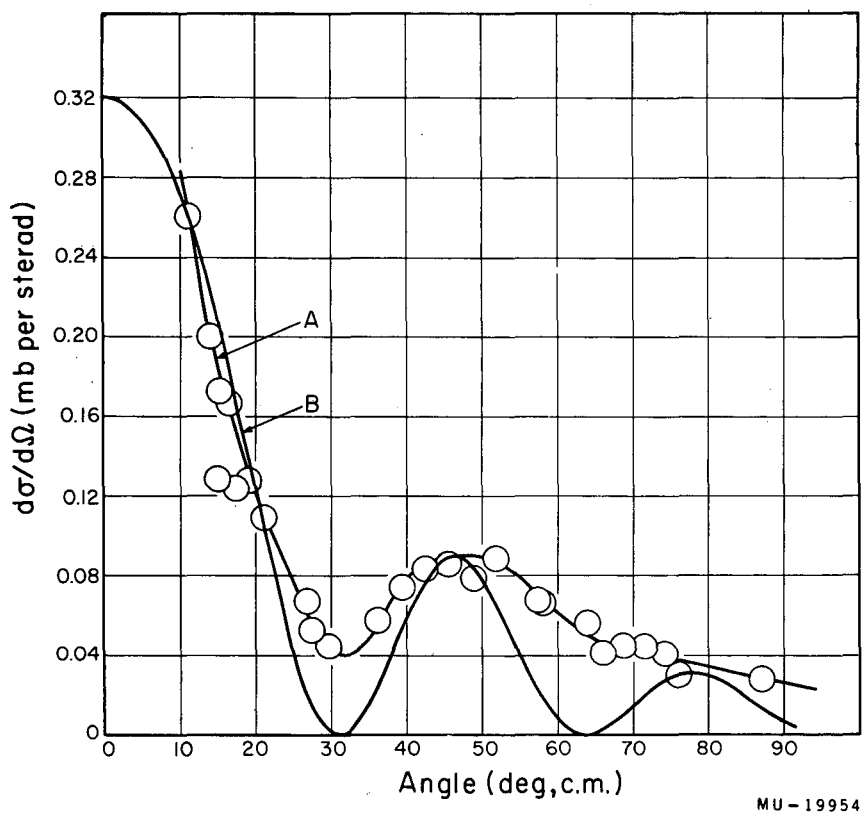

Fig. C. 3-3. Angular distribution of deuterons from formation of the 3.95-Mev state of N^{14} in the reaction $C^{12}(\alpha, d)N^{14}$. Curve A presents the experimental results; Curve B, results calculated from the Butler equation by using $\ell = 2$, $r = 5.5$ fermis.

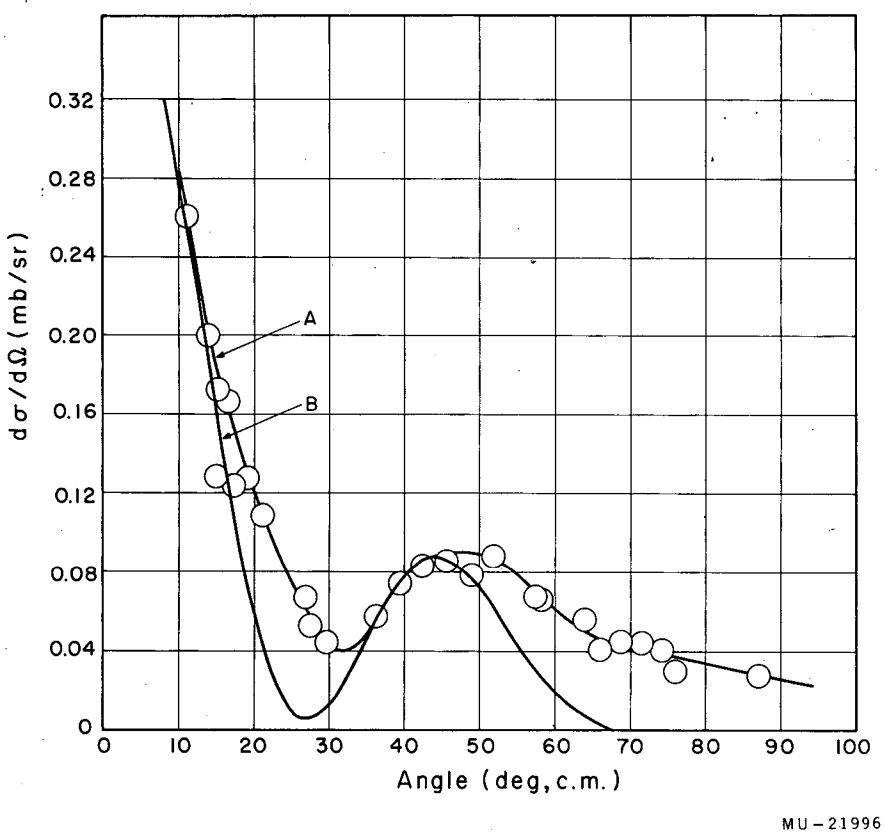

Fig. C. 3-4. Angular distribution of deuterons from formation of the 3.95-Mev state of N^{14} in the reaction $C^{12}(\alpha, d)N^{14}$. Curve A presents the experimental results; Curve B, results calculated from Glendenning's theory assuming capture of both nucleons into the $p_{1/2}$ shell, and r=4.33 fermis.

4. THE REACTIONS $Li^6(\alpha, d)Be^8$ AND $N^{14}(\alpha, d)O^{16}$

Joseph Cerny, III, Bernard G. Harvey, and Richard H. Pehl

The reactions $Li^6(\alpha, d)Be^8$ and $N^{14}(\alpha, d)O^{16}$ were induced by 48-Mev helium ions from the Crocker Laboratory 60-inch cyclotron. The deuterons were detected and identified by means of an E-dE/dx counter telescope system in which the dE/dx counter was a diffused-junction silicon detector. The particle energy (E) was measured with a conventional NaI(Tl) crystal and photomultiplier. The complete separation of deuterons from protons and tritons obtained in this way is illustrated in Fig. C. 4-1. Angular distributions were measured for several of the deuteron groups which correspond to the formation of previously known energy levels of Be^8 and O^{16}. They were compared with angular distributions calculated from the two-nucleon stripping theory of N. K. Glendenning, (Paper A. 5). In most cases, a very satisfactory fit was obtained, although the value of the interaction radius was not always entirely satisfactory. For example, Fig. C. 4-2 shows the theoretical fit obtained for the reaction $Li^6(\alpha, d)Be^8$(2.90-Mev state). It was assumed that the configuration of this Be^8 state is $(p_{3/2}{}^4)_{J=2+}$. No fit could be obtained for the unlikely configuration $(p_{3/2}{}^3 p_{1/2})_{J=2+}$. The theoretical line shown in Fig. C. 4-2 was obtained with an interaction radius of 2.1 f, which is certainly a very small value. However, it is very satisfactory that the theory is able to reproduce so accurately an experimental angular distribution which shows no diffraction structure.

Figure C. 4-3 shows the experimental and theoretical angular distributions for the reaction $N^{14}(\alpha, d)O^{16}$ (ground state). With the assumption that the configuration of this level in O^{16} is $(p_{1/2}{}^4)_{J=0+}$, an interaction radius of 5.35 f was obtained. Figure C. 4-3 shows that the theoretical angular distribution is too strongly damped at large angles. This difficulty can be partly removed only by assuming a radius for the incident helium ion that is smaller than the value obtained from the Stanford electron scattering.

In terms of the cluster model, the states of O^{16} at 9.58, 10.36, 11.26, and 11.62 Mev consist of an α particle and a C^{12} core in its ground state,[1] and there are no others below 12.43 Mev for which this description is well established. These states were not observably excited in the $N^{14}(\alpha, d)O^{16}$ reaction. If the reaction takes place by a knockout mechanism in which the incident helium ion knocks out a deuteron cluster and is then itself captured, the $(\alpha + C^{12})$ states should be strongly excited. Since they are not, it seems that a stripping mechanism is more likely than knockout.

In the $Li^6(\alpha, d)Be^8$ reaction, the integrated cross sections for formation of the Be^8 ground-state, 2.90- and 11.7-Mev levels increase with increasing α-particle reduced width of the level, as shown in Table I.

---

[1] B. Roth and K. Wildermuth, Reduced Widths in O^{16} and Gamma Transition Probabilities in F^{19}, Florida State University Report, to be published.

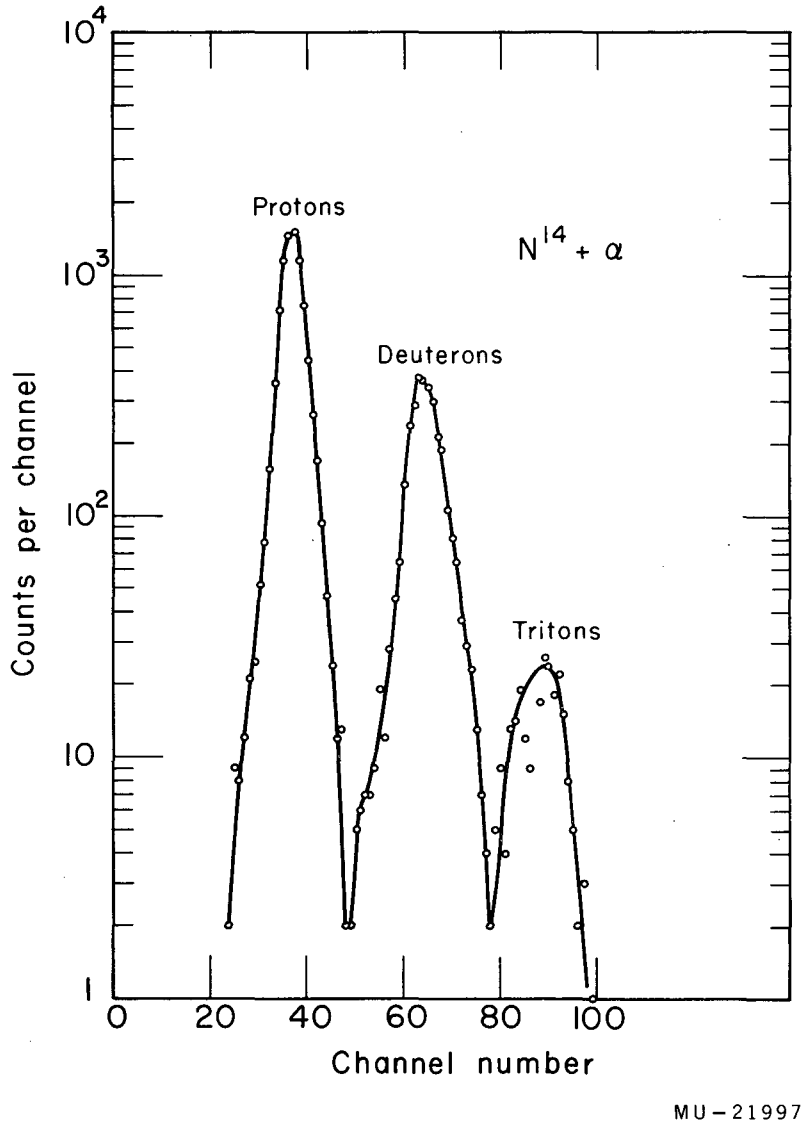

Fig. C.4-1. Spectrum of pulse heights obtained from E-dE/dx particle identifier, for the reactions between N^{14} and 48-Mev helium ions.

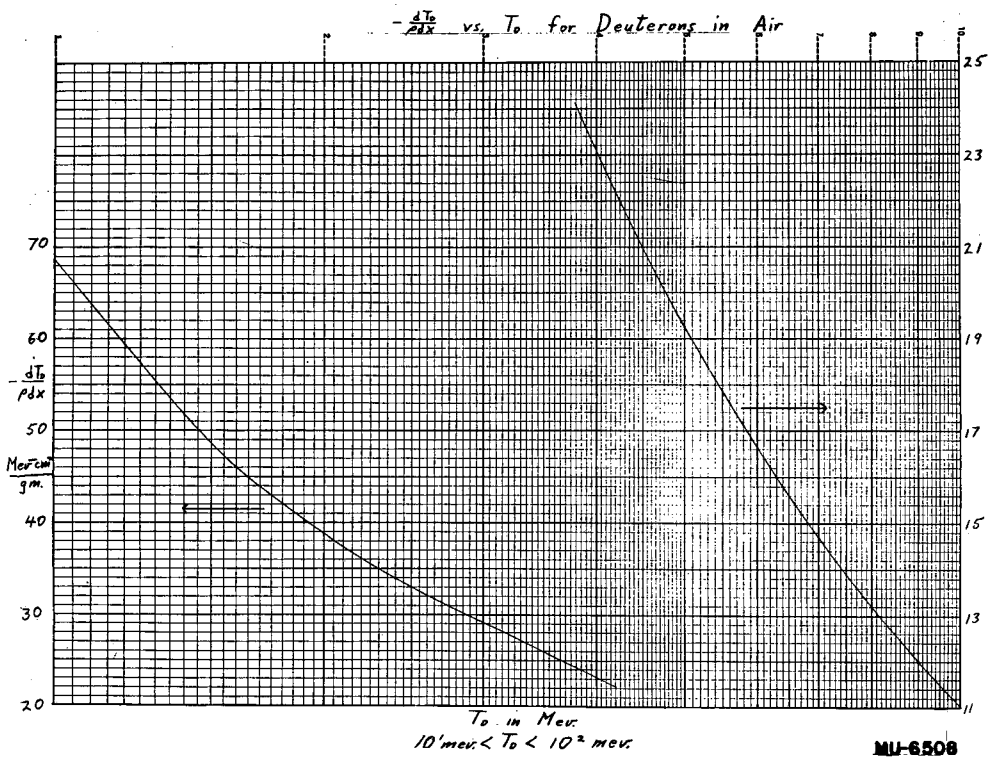

Fig. C.4-2. Angular distribution of deuterons from the reaction $Li^6(\alpha, d)Be^8$ (2.90 Mev). The line is calculated, the points are experimental.

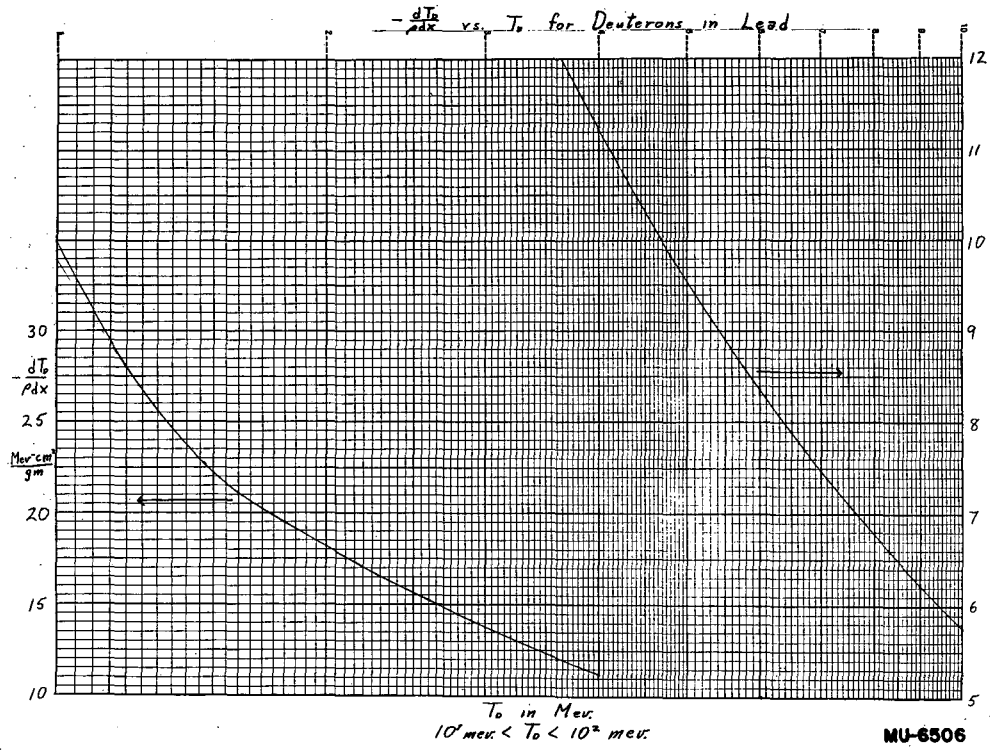

Fig. C.4-3. Angular distribution of deuterons from the reaction $N^{14}(\alpha, d)O^{16}$ (ground state). The line is calculated, the points are experimental.

Table I. Correlation between α-particle reduced width ($\theta^2_{\alpha+\alpha}$) and cross section for formation of level, in the reaction $Li^6(\alpha, d)Be^8$.

Level energy (Mev)	$J\theta$, T	$\theta^2_{\alpha+\alpha}$	$\langle 0_f \rangle / (2J+1)$ (mb)
0	0+, 0	0.15	1.02
2.90	2+, 0	0.7	1.42
11.7	4+, 0	0.95	2.67

It is not clear why formation of states with large α-particle widths is preferred in the Li^6 reaction but not in the N^{14} reaction. A natural (but not unique) explanation is possible in terms of the cluster model if it is assumed that (He^4+d) gives a good description of Li^6, but (C^{12}+d) does not adequately represent N^{14}. Capture of a proton and neutron in a relative ^3S_i state could lead to formation of (α+α) states of Be^8. If the coupling of the odd particles to the core is strong in N^{14}, then the O^{16} states formed by capture of the ^3S_i pair would perhaps be ($\alpha+C^{12*}$) states or states of cluster configurations other than ($\alpha+C^{12}$) ground state.

In formation of the O^{16} ground state, the captured nucleons are both added to the $p_{1/2}$ shell. In forming the 8.88-Mev 2- state, they are not, since--according to the analysis by Elliott and Flowers,[2] this level is 75% $[(p_{1/2})(d_{5/2})]_{2-}$ + approx 7% $[(p_{1/2})(d_{3/2})]_{2-}$. The cross-section ratio $\left[\langle\sigma_{gs}\rangle/(2J+1)\right]/\left[\langle\sigma_{8.88}\rangle/(2J+1)\right]$ was found experimentally to be about 4. Ball and Goodman found that pickup of two neutrons from the $1g_{9/2}$ shell was at least about three times as probable as pickup of one neutron from the $2d_{5/2}$ shell and one from the $1g_{9/2}$ shell.[3] Calculations show that the preference for capture into, or pickup from, the same shell is partly due to the greater probability that the two nucleons are in a relative ^3S_i state when they are in the same shell.[4] Owing to this effect alone, the cross section for formation of the O^{16} ground state in the reaction $N^{14}(\alpha, d)O^{16}$ should be 2.6 times the cross section for formation of the 8.88-Mev state.

[2] J. P. Elliott and B. H. Flowers, Proc. Roy. Soc. A242, 57 (1957).

[3] J. B. Ball and C. D. Goodman, Phys. Rev. 120, 488 (1960).

[4] Norman K. Glendenning (Lawrence Radiation Laboratory), private communication, Dec. 1960.

θ_L and θ_C are the angles in the laboratory system and in the coordinate system of the fissioning nucleus, and E_C and X_{mp} were adjusted to fit the experimental data. For E_C we obtained the value 93±3 Mev at all three bombarding energies. This is to be compared with 185 Mev as the most probable total kinetic energy release in the fission of Cf^{252},[8] and seems to indicate that the most probable fissioning nuclei are Cf isotopes. Independence of bombarding energy for the kinetic energy release in fission has been observed in the bombardment of Au with C^{12}.[2]

The va ues of X_{mp}, together with mean values of X, X_m, obtained from the transformations of the angular distributions, are given in Table I. These we will now compare with X_{CN} values which can be estimated for compound-nucleus reactions. In that case the mean moment of the fissioning nucleus is equal to that of the heavy ion, and we have

$$X_{CN}^2 = \frac{A_i E_i A_{ff}}{A_{fN}^2 \cdot E_C} \quad . \tag{4}$$

Here A_i and E_i are the mass and lab energy of the heavy ion, A_{ff} is mass of the fission fragment, and A_{fN} the mass of the fissioning nucleus; E_C is defined as before.

When neutrons are evaporated the mean excitation energy, E, of the fissioning nuclei can be estimated. The number of neutrons emitted from the fission fragments in the fission process, $\bar{\nu}$, is then, according to Leachman's empirical relationship;[9]

$$\bar{\nu} = \bar{\nu}_0 + 0.12\ E,$$

where $\bar{\nu}_0$ is the number emitted from a nucleus in the ground state as observed in spontaneous fission. For high-energy fission the mass-yield curve is symmetric and the mean mass of the fission fragments A_{ff} can thus be evaluated. The estimated values for A_{ff}, E, and X_{CN}^2 are given in Table I.

We see that, as a general rule, $X_{CN}^2 > X_{mp}^2 > X_m^2$. Apparently we have contribution from reactions in which the linear momentum of the fissioning nucleus is less than that of the heavy ion. Particles are emitted preferentially in the forward direction prior to the fission process.

High frequency of α particles has been observed emitted in the forward direction in the bombardment of Au^{197} with 160-Mev O^{16}.[10] A similar

[8] J.S. Fraser and J.C.D. Milton, in Proceedings of the Second United Nations International Conference on the Peaceful Uses of Atomic Energy, Geneva, 1958 (United Nations, New York, 1958) Vol. 15, p. 216.

[9] R.B. Leachman, op. cit., p. 299.

[10] W.J. Knox, C.E. Anderson, A.R. Quinton, and H.W. Brock, in Proceedings of the Second Conference on Reactions between Complex Nuclei, Gatlinburg, May 2-4 1960 (John Wiley and Sons Inc., New York, 1960), p. 263.

type of reaction could account for the apparent low mean spin and linear momentum of the fissioning nuclei in the case of $U^{238} + C^{12}$.

3. The total cross section for fission was determined by a direct comparison, using the same detector, target, and geometry, of the counting rate of carbon ions in the region of pure Coulomb scattering, with the fission counting rate, and allowing for the presence of two fragments in the latter case. The contribution to the scattering from the nickel backing was determined experimentally. The fission cross section was found to be 0.47 barn at 73 Mev, 1.4 barns at 95.4 Mev, and 2.3 barns at 124 Mev. For all three values we assign a standard deviation of 10%.

At other bombarding energies, the differential cross section at 90 deg to the beam was measured and the total cross section estimated from the known efficiency and by assuming a smooth variation in the angular distribution with bombarding energy. The error introduced by this method should be negligible because of the small changes in the distribution from 73 Mev to 124 Mev.

The results are given in Fig. B.6-2 together with the theoretical curve for compound-nucleus formation as calculated by Thomas[6] from the square-well model and $\nu_0 = 1.5 \times 10^{-13}$ cm. We see the agreement is satisfactory, and this cross section represents, then, the total cross section for reactions which produce nuclei with more than 5 Mev excitation energy.

7. COMPOSITION-DEPENDENT SURFACE ENERGY OF HEAVY NUCLIDES AND SPONTANEOUS FISSION

Reinhard Brandt and Stanley G. Thompson

This report is a summary of a preliminary investigation of the influence of a composition dependence of the nuclear surface tension on some phenomena of fission such as fission barrier height, spontaneous fission rates, and asymmetry.

The liquid-drop model is employed in the semiempirical mass formula and in the theory of fission. The attractive nuclear forces are idealized in a surface energy, which has in the standard semiempirical mass formula (for example, Green[1]) the form

$$E(\text{surface}) = (\text{constant}) \cdot A^{2/3} \qquad (1)$$

There is some evidence that for a given A the nuclear attractive forces may be composition-dependent, i.e., may depend on the neutron-to-proton ratio. Kolesnikov - Larkin-Mottelson[2] (K-L-M) proposed the composition-dependent surface energy term

[1] A. E. S. Green, Phys. Rev. 95, 1006 (1954).

[2] R. Brandt, F. Werner, M. Wakano, R. Fuller, and J. A. Wheeler, in Conference on Nuclidic Masses, edited by H. E. Duckworth (University of Toronto Press, Toronto, 1961).

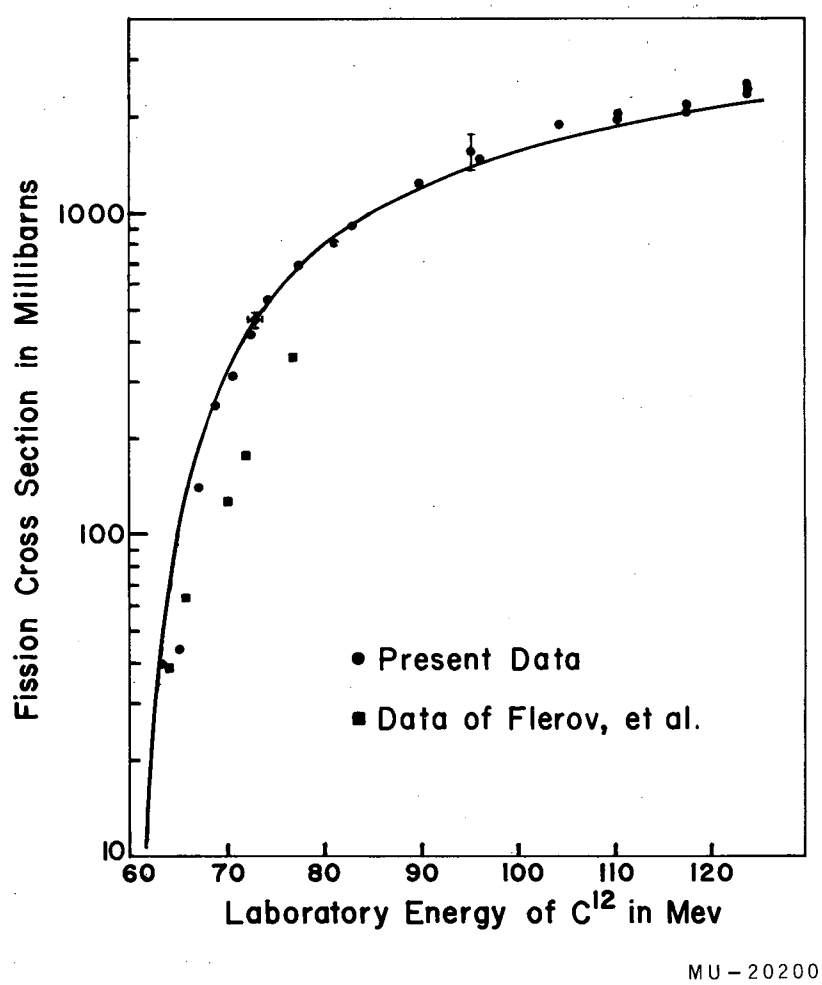

Fig. B.6-2. Total fission cross section for fission of U^{238} by C^{12} ions. Calculated compound-nucleus formation cross section, square-well model, with $r_0 = 1.5 \times 10^{-13}$ cm.

$$E(\text{surface}) = (\text{constant}) \cdot A^{2/3} \left[1 - C_1 \left(\frac{N-Z}{A} \right)^2 \right] . \qquad (2)$$

It has been shown[2] that one cannot get a better or worse semiempirical mass formula by using $C_1 = 0$ of $C_1 = 2.5$. Also, the plot of the spontaneous fission half lives vs the fissionability parameter $X = E(\text{Coulomb})/2\,E(\text{surface})$ could not be smoothed out with these two values of C_1. Concerning the question of the stability of heavy nuclei (with half lives $> 10^{-4}$ sec), Werner and Wheeler[3] showed that for $C_1 = 0$, nuclei up to $Z = 147$ and $A = 500$ might be expected. For $C_1 = 2.7$ it was shown[2] that the stability region would be confined to ($A \leqslant 274$; $Z \leqslant 96$ for $A = 250$). Thus there exists no evidence for or against the K-L-M term so far as the semiempirical mass formula or the spontaneous fission half-lives are concerned.

But a value of the term C_1 between 0 and 2.7 might be obtained that would permit a better prediction. Some insight into the magnitude of this term is obtained in the following discussion.

Swiatecki[5] has shown, for the uniformly charged liquid drop, that the threshold energy is related to X in the following way, assuming that for $X < X_C$ the nucleus is asymmetrically deformed at the threshold:

$$E(\text{threshold}) = \text{"function"}\,(1 - X) - C_2\,(X_C - X)^2 , \qquad (3)$$

where C_2, X_C are constants.
By using a classical liquid drop, it is shown[6] that

$$\frac{\text{"function"}\,(1-X)}{E(\text{surface})} = 0.73\,(1-X)^3 - 0.33\,(1-X)^4 + 1.9\,(1-X)^5 - 0.21\,(1-X)^6 . \qquad (4)$$

The constant X_C appears also in the relation of the asymmetry of mass-yield curves vs X,[4]

$$\left(\frac{M_H - M_L}{A} \right)^2 = (\text{constant}) \cdot (X_C - X), \qquad (5)$$

where M_H = the mass of the most probable heavy fragment,
M_L = the mass of the most probable light fragment.

The constants C_2 and X_C in Eq. (3) can be determined by fitting Eq. (3) to two observed fission-activation energies[7] (for example, Cm^{242} and Th^{234}). Then this X_C is compared with the X_C from the plot of observed asymmetry data vs X. For $C_1 = 0$ (this affects X and Eqs. (4) and (5)) the two independently determined values of X_C do not agree, nor do they agree for $C_1 = 1.2$. But for $C_1 = 0.8$ the X_C from the threshold calculation agrees with the asymmetry curve (see Fig. B.7-1). If then the other activation energies for even-even nuclei are calculated from Eq. (3), it is found that they agree within 0.15 Mev with those computed by Vandenbosch and Seaborg.[7] The question

[3] F. G. Werner and J. A. Wheeler, Phys. Rev. 109, 126 (1958).

[4] W. J. Swiatecki, Phys. Rev. 100, 936 (1955).

[5] W. J. Swiatecki, Phys. Rev. 101, 651 (1956).

[6] Earl K. Hyde, A Review of Nuclear Fission. Part I. Fission Phenomena at Low Energy, UCRL-9036, Jan. 1960, p. 28.

[7] R. Vandenbosch and G. T. Seaborg, Phys. Rev. 110, 507 (1958).

[8] S. A. E. Yohansson, Nucl. Phys. 12, 449 (1959).

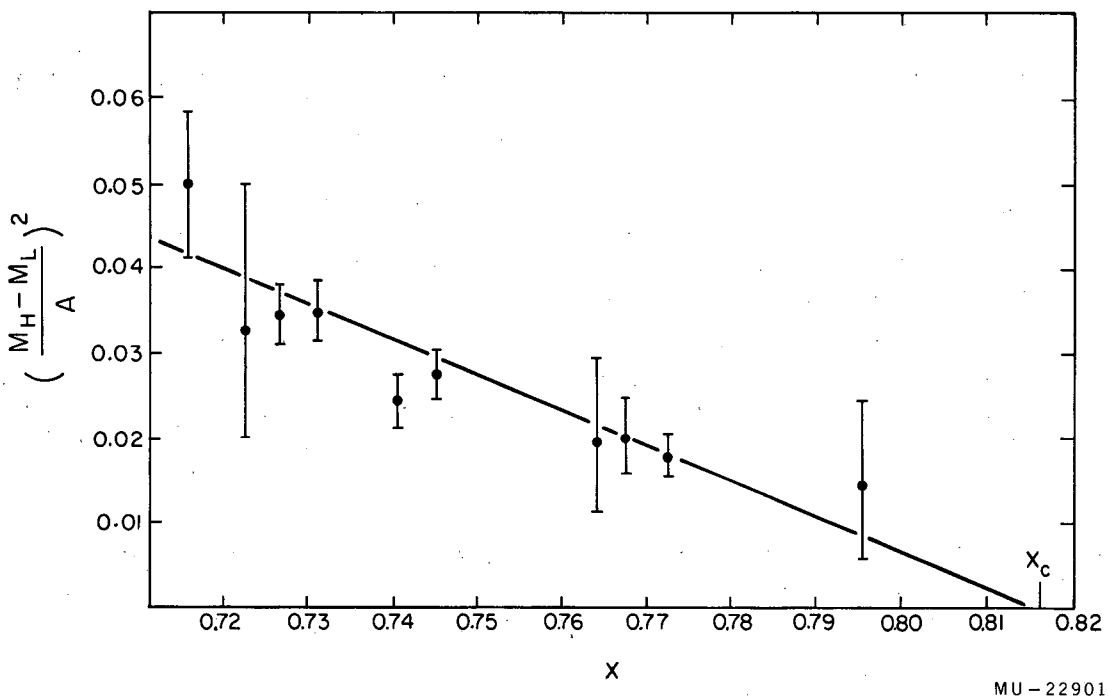

Fig. B.7-1. The observed fission asymmetry $\left(\frac{M_H - M_L}{A}\right)$ plotted against the improved x value.

$x = Z^2/51.350 \cdot A \left\{1-0.8[(N-Z)/A]^2\right\}$

X_C (from threshold calculations) = 0.08165;

M_H and M_L = masses of most probable heavy and light fragments.

remains now as to how large C_1 must be to give similar agreement when the fission barriers are used instead of fission-activation energy.[7]

Johansson employed single-particle effects to improve the correlation of spontaneous fission half lives with X.[8] However, the variations in curve can be smoothed out considerably by using $C_1 = 1.0 \pm .3$.

The influence of $C_1 = 1.0 \pm .3$ on the expected half lives of higher elements is also being considered.

8. FISSION BARRIER HEIGHTS IN ELEMENTS LIGHTER THAN RADIUM

D.S. Burnett and S.G. Thompson

A program has been initiated to study the fission barrier heights in elements lighter than radium. At present there are no directly measured values for barrier heights in this region; however, these values are of considerable significance for the following reasons.

(a) Fission has been observed to be symmetric for all nuclides studied in this region, even at energies close to the barrier; thus it might be expected that in this region the (conventional) liquid-drop model would be a better approximation to the actual situation than for heavy elements where the liquid drop in its original form did not predict the observed trends in barrier heights and did not explain the asymmetry in fission.

(b) Fission barrier heights are important in the study of the nuclear reactions in this region at moderate excitation, since fission can compete effectively as a nuclear reaction mode under these conditions.

One purpose of the present program is to attempt direct measurement of fission-barrier heights for these nuclides. In order to guide experimental work and provide preliminary estimates for comparison with experimental data, approximate calculations of barrier heights have been carried out[1] in two ways.

A. Following an approach similar to one suggested by Halpern[2] we can write, as a very rough approximation,

$$\Gamma_f/\Gamma_n \approx N(Z,A) \exp\left[(B_n - B_f)/c\sqrt{E_x}\right],$$

where B_f is barrier height, B_n is the neutron binding energy, c is a constant, and E_x is excitation energy. Γ_f/Γ_n, the probability for fission relative to neutron emission, is equal to the ratio of the observed fission cross section to the formation cross section of the compound nucleus, since neutron emission is the most probable reaction at these energies, making the total

[1] Donald S. Burnett and Stanley G. Thompson, Fission Thresholds for Elements Lighter than Radium, UCRL-9321, July 1950.

[2] I. Halpern, Ann. Rev. Nuclear Sci. 9, (1959).

reaction width very close to Γ_n. Values for B_f can be obtained from the slope of a log plot of Γ_f/Γ_n vs $1/\sqrt{E_x}$ provided c is known. A value for c was estimated from a plot of Γ_f/Γ_n vs $(B_n - B_f)$ for heavy elements at constant excitation which had been made by Vandenbosch and Huizenga.[3] Thus estimates of B_f could be obtained.

B. Let us define ξ as a dimensionless measure of the fission barrier, B_f, by $\xi = B_f/E_s^0$, where E_s^0 is the initial surface energy of the undeformed nucleus, and define x, the fissionablitity parameter, as $(Z^2/A)/(Z^2/A)_0$, where $(Z^2/A)_0$ is a limiting value at which the nucleus will fission spontaneously without deformation. Previous work had suggested that in the region from $x = 0$ (uncharged drop) to $x = 0.7$ the values of ξ based on the liquid-drop model could be well represented by a parabolic expression, $\xi = c + bx + ax^2$, where c and b are respectively the value and first derivative of ξ at $x = 0$ and had been previously calculated by Bohr and Wheeler.[4] The value a was obtained by estimating a threshold for the Ra^{226} (nf) data of Nobles and Leachman.[5] This equation was used to calculate fission-barrier heights for elements in this region.

Some sample results are given in Table I. A more complete tabulation may be found in Ref. 1.

Table I. Comparison of results from two methods for calculating fission-barrier heights.

Compound nucleus	Barrier height (Mev)	
	Method A	Method B
At^{213}	16	15.6
Po^{212}	17	21.1
Po^{210}	22	21.3
Tl^{201}	26	25.6
Ta^{179}	—	35.4

The approximations made in obtaining the expression used in Method A are not very good for the cases considered, consequently the values so obtained must be taken merely as order-of-magnitude estimates. The values obtained from Method B would be more appropriately used to compare with any experimental values if direct measurement of these fission barriers turned out to be feasible.

[3] R. Vandenbosch and J.R. Hiuzenga, in Proceedings of the Second International Conference on Peaceful Uses of Atomic Energy, Geneva, 1958, (United Nations, Geneva, 1958) Vol. 15, Paper 688.

[4] N. Bohr and J.A. Wheeler, Phys. Rev. 56, 426 (1939).

[5] R.A. Nobles and R.B. Leachman, Nuclear Phys. 5, 211 (1958).

C. NUCLEAR REACTIONS

1. TOTAL REACTION CROSS SECTIONS

Bruce D. Wilkins and George Igo

Recently elastic scattering data of various ions have been fitted with several nuclear models.[1] In particular, work has been done using an optical-model potential[2]

$$\frac{V + iW}{1+\exp\left(\frac{r-R}{a}\right)} .$$

The parameters V, W, R, and a represent respectively the depths of the real and imaginary potentials, the radius, and the diffuseness parameters of the potential. In addition the optical model also predicts total reaction cross sections σ_R. Measurements of σ_R help resolve the ambiguity in determining the shape of the optical-model potentials for various ions. With this in mind we have begun a program at the heavy-ion linear accelerator and at the 60-inch cyclotron to measure σ_R for O^{16} ions and protons.

We have used the method of beam attenuation.[3] The beam particles pass through two thin ΔE plastic scintillators and an attenuator of the material under investigation, and finally into a stopping plastic scintillator. A nuclear reaction in the attenuator causes an anticoincidence between the two ΔE counters and the stopping counter. Attenuator-in and attenuator-out measurements are necessary to see the effect of the attenuator. With the use of nanosecond electronic techniques we have been able to count at a rate of 4×10^5 counts per second.

Corrections which must be made are (a) subtraction of elastic scattering through angles greater than that subtended by the stopping counter, (b) addition of inelastic or reaction events in which the product cannot be distinguished from the beam particle in the stopping counter, (c) transfer reactions. The discrimination against inelastic or reaction events in the stopping counter is accomplished by placing an absorber between target and plastic scintillator. The solid angle subtended by the stopping counter is determined by measuring the anticoincidence rate as a function of the distance of the stopping counter from the attenuator (see Fig. C. 1-1). The flat portion

[1] J. S. Blair, Phys. Rev. 95, 1218 (1954); F. Bjorklund, in Proceedings of the International Conference on the Nuclear Optical Model, Tallahassee, 1959; K. W. Ford and J. A. Wheeler, Annals of Physics 7, 287 (1959); C. E. Porter, Phys. Rev. 99, 1400 (1955); G. Igo and R. M. Thaler, Phys. Rev. 106, 126 (1957).

[2] R. D. Woods and D. S. Saxon, Phys. Rev. 95, 577 (1954).

[3] R. M. Eisberg, in Proceedings of the International Conference on the Nuclear Optical Model, Tallahassee, 1959.

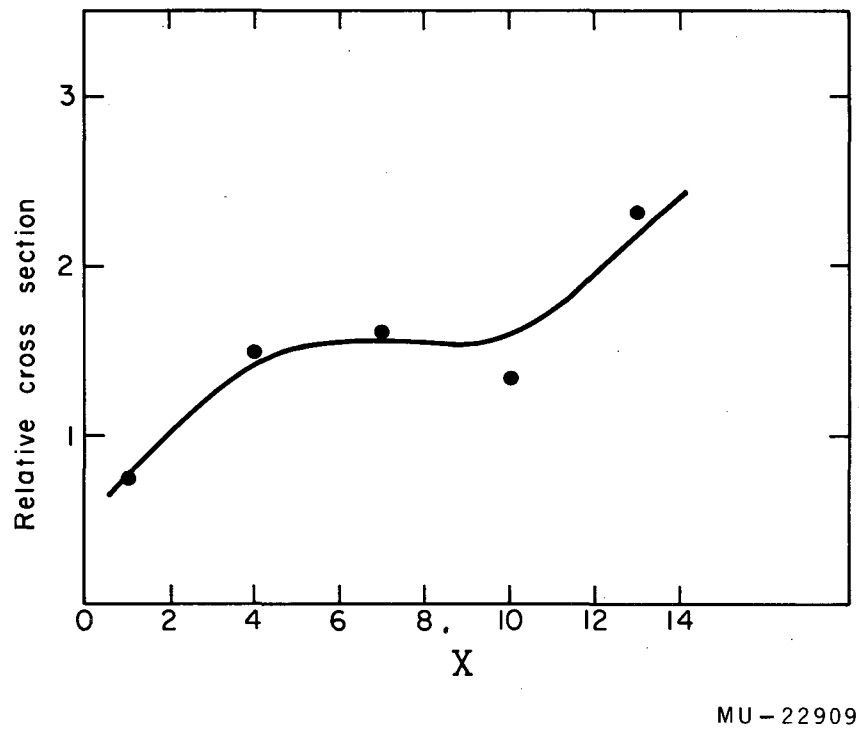

Fig. C. 1-1. The dependence of the measured cross section on the distance X of the stopping counter from the attenuator. The points ⊙ are the measurements for 152±8-Mev O^{16} ions on Cu. A smooth curve has been drawn through the points.

of the curve in Fig. C. 1-1 is where the elastic scattering correction is approximately equal and opposite to the inelastic and reaction scattering correction. The statistics on the individual points in Fig. C. 1-1 are of the order of 6%.

Preliminary results on the total reaction cross sections for 152±8-Mev O^{16} ions are listed in Table I. Further corrections (to be determined later) due to elastic, inelastic, and reaction scattering effects may change these results by as much as 10%. If the cross section is written as $\sigma_R = \pi R_0^2 (A_1^{1/3} + A_2^{1/3})^2$, where A_1 and A_2 are the atomic numbers of ion and target respectively, then the values of R_0 obtained from this analysis are also listed in Table I.

Table I. Reaction cross sections for 152±8-Mev O^{16} ions

	σ_t(barns)	R_0(fermis)
Al	2.09±0.08	1.48
Cu	3.35±0.14	1.59
Ag	4.18±0.16	1.59
Au	5.82±0.22	1.63

These values of R_0 are consistent with those found in elastic scattering analyses by using the Blair model.[4]

[4] J. S. Blair, Phys. Rev. 95, 1218 (1954).

2. THEORETICAL REACTION CROSS SECTIONS FOR ALPHA PARTICLES WITH THE OPTICAL MODEL

John R. Huizenga* and George Igo

Shapiro[1] and Blatt and Weisskopf[2] have calculated total reaction cross sections for α particles with a square-well potential. The total reaction cross section is given by

$$\sigma_R = \pi \lambda\!\!\!^{-2} \sum_{\ell=0}^{\ell=\ell'} (2\ell+1)\, T_\ell\, (\epsilon), \qquad (1)$$

*Summer visitor from Argonne National Laboratory, Argonne, Illinois.

[1] M. M. Shapiro, Phys. Rev. 90, 171 (1953).

[2] J. M. Blatt and V. F. Weisskopf, Theoretical Nuclear Physics (John Wiley and Sons, Inc., New York, 1952), p. 352.

where $\lambda\!\!\!^{-}$ is the de Broglie wave length, ℓ is the angular momentum of the incident particle in units of $\hbar$, $T_\ell(\epsilon)$ is the transmission coefficient of the incident particle of energy ϵ. The transmission coefficients (actually $4/T_\ell$ are tabulated) for α particles derived from the square-well potential are available for target nuclei with $Z < 40$.[3] Igo has calculated total reaction cross sections with a complex nuclear potential for six target nuclei with α-particle projectiles of several energies.[4] Transmission coefficients calculated with the complex nuclear potential are not available.

Since α-particle transmission coefficients for high-Z targets are not available, we have calculated this quantity for a large variety of targets at a number of α energies with a complex nuclear potential.

The optical-model potential employed in these calculations is written as

$$V_\ell(r)=V_c+\frac{\ell(\ell+1)\hbar^2}{2M_\alpha r^2}-1100\exp\left[-\left(\frac{r-1.17A^{1/3}}{0.574}\right)\right]-45.7\,i\exp\left[-\left(\frac{r-1.40\,A^{1/3}}{0.578}\right)\right], \tag{2}$$

where V_c is the Coulomb potential, M_α the reduced mass of the α particle, and the third and fourth terms, in units of Mev, are the real and imaginary parts, respectively, of the α-nucleus potential[4] exclusive of the Coulomb and centrifugal potentials. The Coulomb potential of the Hill-Ford[5] charge distribution was employed in Eq. (2). This is given by

$$V_c=\frac{2Ze^2}{r_c}\left[\frac{1}{n^2}+\frac{1}{2}-\frac{x^2}{6}+\frac{e^{-n}}{n^2}\left(\frac{1-e^{nx}}{nx}+\frac{e^{nx}}{2}\right)\right]\Big/\left(\frac{1}{3}+\frac{2}{n^2}+\frac{e^{-n}}{n^3}\right)\quad\text{for } X<1 \tag{3}$$

and

$$V_c=\frac{2Ze^2}{r_c}\left\{\frac{1}{x}-\left[\frac{\left(\frac{1}{x}+\frac{n}{2}\right)e^{n-nx}}{e^{-n}+2n+\frac{1}{3}n^3}\right]\right\}\quad\text{for } X>1, \tag{4}$$

where $x = r/r_c$ and where n is 10 for heavy elements and is proportional to $A^{1/3}$. The quantity r_c is the distance out to the half-value point of the charge distribution. The value $1.17A^{1/3}\times10^{-13}$ cm for r_c was chosen larger than the value obtained from the electron scattering experiments[6]

[3] H. Feshbach, M. M. Shapiro, and V. F. Weisskopf, NYO-3077, June, 1953 (unpublished).

[4] G. Igo, Phys. Rev. 115, 1665 (1959).

[5] K. W. Ford and D. L. Hill, Phys. Rev. 94, 1617 (1954).

[6] R. Hofstadter, Ann. Rev. Nuclear Sci., 7, 231 (1957).

to take roughly into account the effect of the finite size of the α-particle charge distribution.

In order to use an existing calculational program, it was necessary to choose the parameters V, W, r_0, and d for the Wood-Saxon potential,[7]

$$(V + i\,W) \Big/ \left[1 + \exp\left(\frac{r - r_0}{d}\right)\right],$$

to reproduce the nuclear potential of Eq. (2) for values of r such that the real part of the nuclear potential is greater than -10 Mev. These parameters are given in Table I. The depth of the potential for small values of r is also fixed when the parameters of Table I are used, although it has been shown that α-particle scattering is not sensitive to the potential depth.

The total reaction cross sections, σ_R, and the transmission coefficients, T_ℓ, have been calculated with the parameters of Table I. Figures C. 2-1 and C. 2-2 show the energy variation of the total reaction cross sections for V^{51} and for U^{235}. For comparison the same quantity is calculated by Shapiro[1] and by Feshbach, Shapiro, and Weisskopf.[3]

Table I. Woods-Saxon potential parameters

Nuclide	V (Mev)	W (Mev)	r_0 (fermis)	d (fermis)	r_c (fermis)	n
$_{19}K^{41}$	-50	-8.70	$1.17A^{1/3} + 1.77$	0.576	$1.17A^{1/3}$	5.60
$_{22}Ti^{48}$	-50	-9.51				5.91
$_{23}V^{51}$	-50	-10.00				6.04
$_{24}Cr^{52}$	-50	-9.90				6.07
$_{25}Mn^{53}$	-50	-9.98				6.11
$_{25}Mn^{55}$	-50	-10.25				6.19
$_{26}Fe^{56}$	-50	-10.26				6.23
$_{27}Co^{55}$	-50	-10.17				6.19
$_{32}Ge^{72}$	-50	-11.85				6.77
$_{37}Rb^{85}$	-50	-13.30				7.16
$_{41}Nb^{93}$	-50	-13.74				7.37
$_{45}Rh^{103}$	-50	-14.30				7.62
$_{50}Sn^{119}$	-50	-16.20				8.00
$_{60}Nd^{144}$	-50	-18.23				8.53
$_{70}Yb^{173}$	-50	-20.79				9.07
$_{78}Pt^{195}$	-50	-22.10				9.44
$_{82}Pb^{206}$	-50	-23.00				9.61
$_{90}Th^{232}$	-50	-26.11				10.00
$_{92}U^{235}$	-50	-27.00				10.04

[7] R. D. Woods and D. S. Saxon, Phys. Rev. 95, 577 (1954).

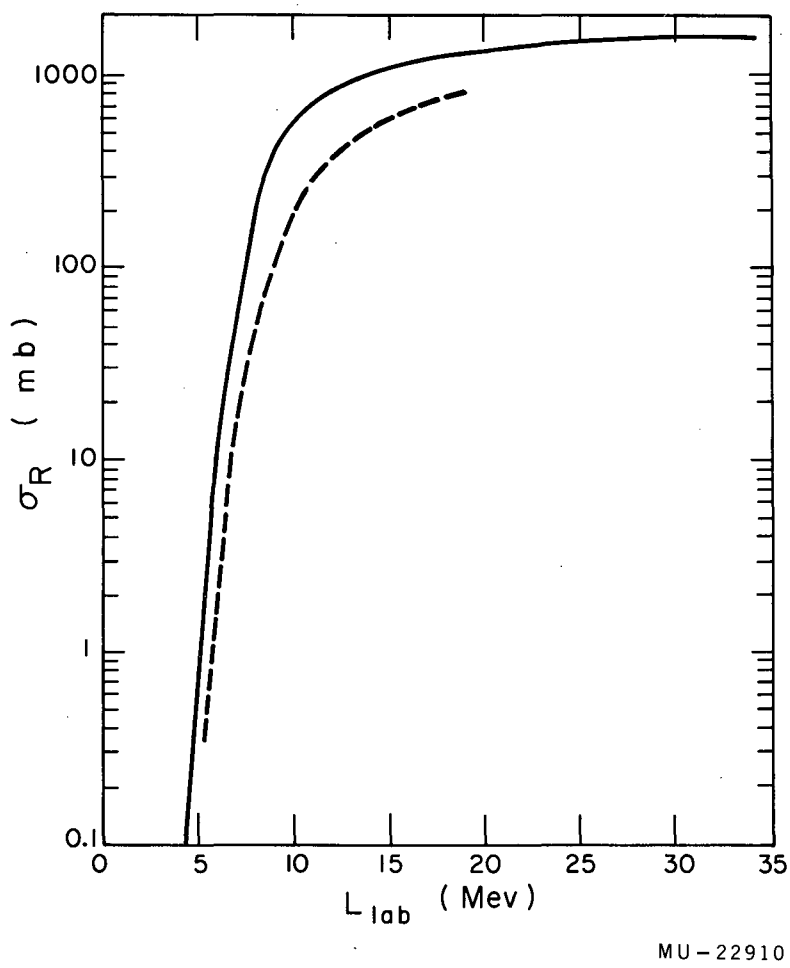

Fig. C. 2-1. The total reaction cross section versus laboratory energy for alpha particles incident on V^{51}. The solid curve has been calculated by using the surface nuclear potential discussed in the text. The dashed line is the same quantity calculated by Shapiro (Ref. 1).

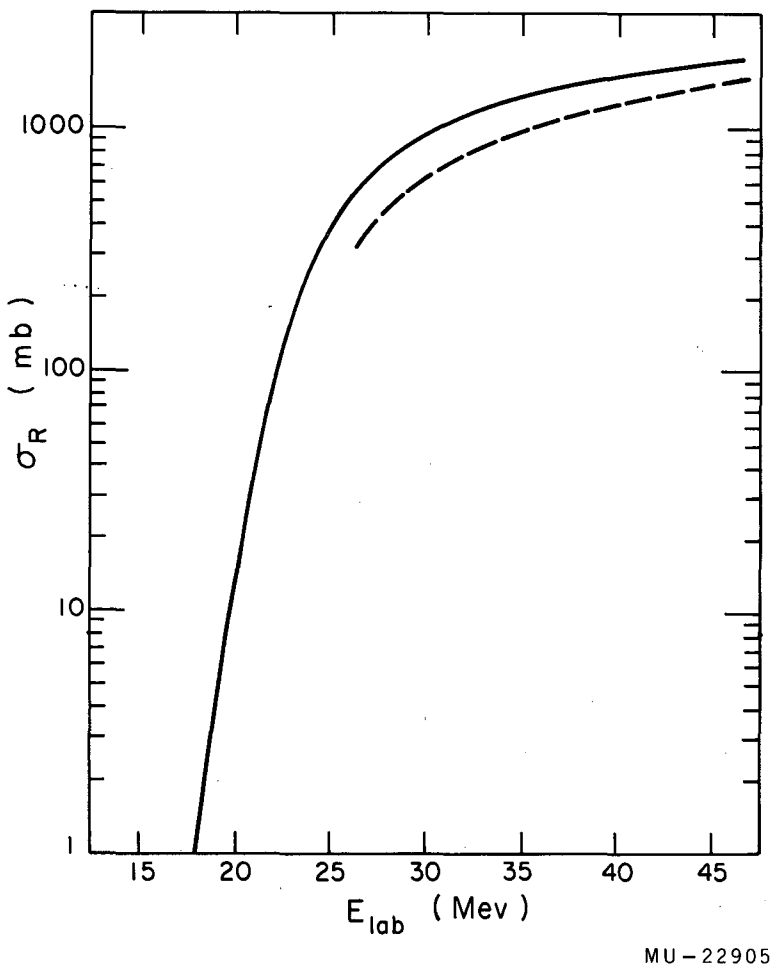

Fig. C. 2-2. The total reaction cross section versus laboratory energy for alpha particles incident on U^{235}. The solid curve has been calculated by using the surface nuclear potential discussed in the text. The dashed line is the same quantity from the paper of Feshbach, Shapiro, and Weisskopf (Ref. 3).

3. THE REACTION $C^{12}(\alpha, d)N^{14}$ (*)

Joseph Cerny, III, and Bernard G. Harvey

The reaction $C^{12}(\alpha, d)N^{14}$ was studied in almost the same way as the reactions described in the previous report. Angular distributions were obtained for the deuteron groups leading to the ground state and 3.95-Mev state of N^{14}.

The 2.31-Mev 0+, T=1 state of N^{14} was not observed: it was excited less than 3% as strongly as the ground state. This observation, however, is not strong evidence for the isotopic spin purity of the level, because formation of a 0+ level from a 0+ target is also forbidden by angular momentum and parity conservation in an (α, d) or (d, α) reaction. Furthermore, several well-known T=0 levels of N^{14} were not observably excited: the (α, d) reaction is somewhat specific.

The angular distribution of deuterons corresponding to formation of the ground state of N^{14} is shown in Fig. C. 3-1. Good agreement was obtained with the Butler stripping theory by using $\ell=2$ and r=6.3 f. However, an equally good fit was obtained for l=0 and r=6.45 f. Figure C. 3-2 shows the best fit obtained with the two-nucleon stripping theory of Glendenning for capture of the proton and neutron into the $p_{1/2}$ shell, with r=4.70 f. Equally good fits (but with slightly larger values of r) were obtained for several other configurations. The cross section for formation of the N^{14} ground state (integrated between 10 and 133 deg) is 1.8 mb.

Figure C. 3-3 shows the angular distribution of deuterons corresponding to formation of the 3.95-Mev 1+, T=0 level of N^{14}. Good agreement was obtained on Butler theory for $\ell=2$, r=5.5 f, or $\ell=0$, r=5.7 f. Figure C. 3-4 shows the fit obtained with the Glendenning theory, assuming that the captured nucleons enter the $p_{1/2}$ shell, with r=4.33 f. Again, equally good fits were obtained for other configurations.

The multiple fitting is characteristic of stripping reactions that involve a large momentum transfer. The arguments of the spherical Bessel functions are then large enough for the functions to approach their asymptotic forms, which are sine and cosine functions for even and odd ℓ values respectively. It is quite impossible to distinguish between $\ell=0$ and $\ell=2$, and, in some cases at least, $\ell=1$ or $\ell=3$ would give angular distributions that would be experimentally indistinguishable from the even-ℓ values, since the required interaction radius may change by an amount too small to permit rejection of any of the ℓ values.

---

*Brief version of published paper, Phys. Rev. 120, 2162 (1960).

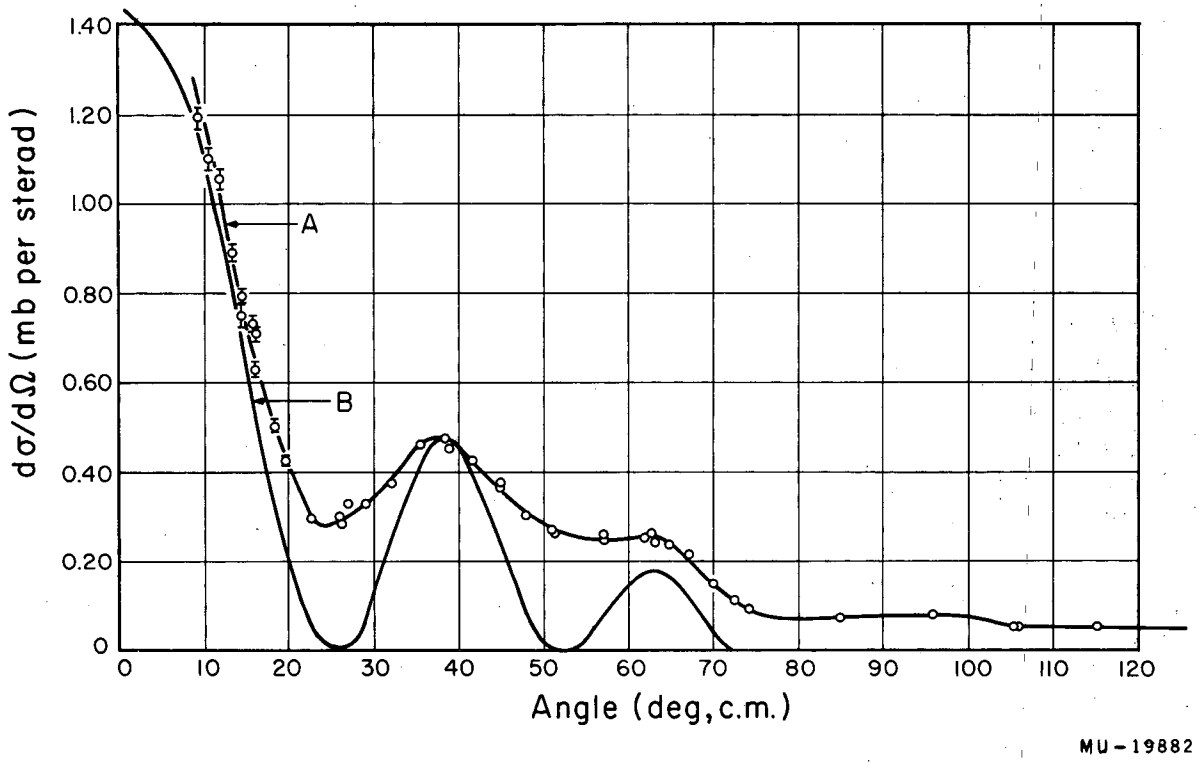

Fig. C. 3-1. Angular distribution of deuterons from formation of the ground state of N^{14} in the reaction $C^{12}(\alpha, d)N^{14}$. Curve A presents the experimental results; Curve B, results calculated from the Butler equation by using $\ell = 2$, $r = 6.3$ fermis.

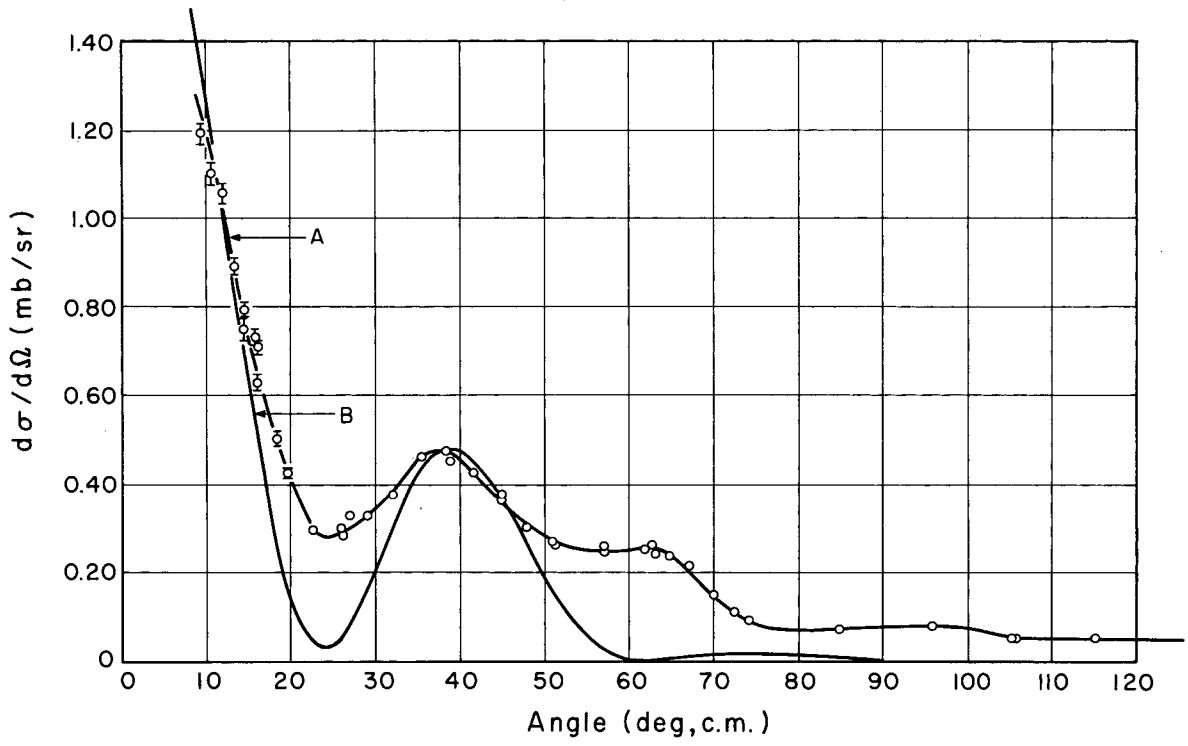

MU-21995

Fig. C. 3-2. Angular distribution of deuterons from formation of the ground state of N^{14} in the reaction $C^{12}(\alpha, d)N^{14}$. Curve A presents the experimental results calculated from Glendenning's theory assuming capture of both nucleons into the $p_{1/2}$ shell, and r = 4.70 fermis.

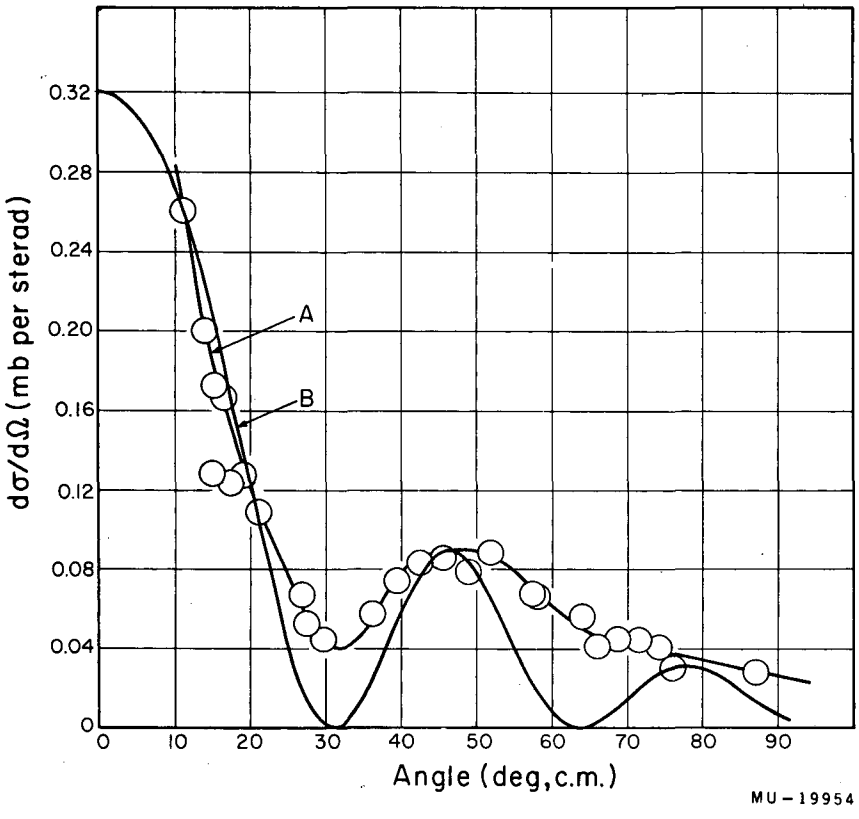

Fig. C. 3-3. Angular distribution of deuterons from formation of the 3.95-Mev state of N^{14} in the reaction $C^{12}(\alpha, d)N^{14}$. Curve A presents the experimental results; Curve B, results calculated from the Butler equation by using $\ell = 2$, $r = 5.5$ fermis.

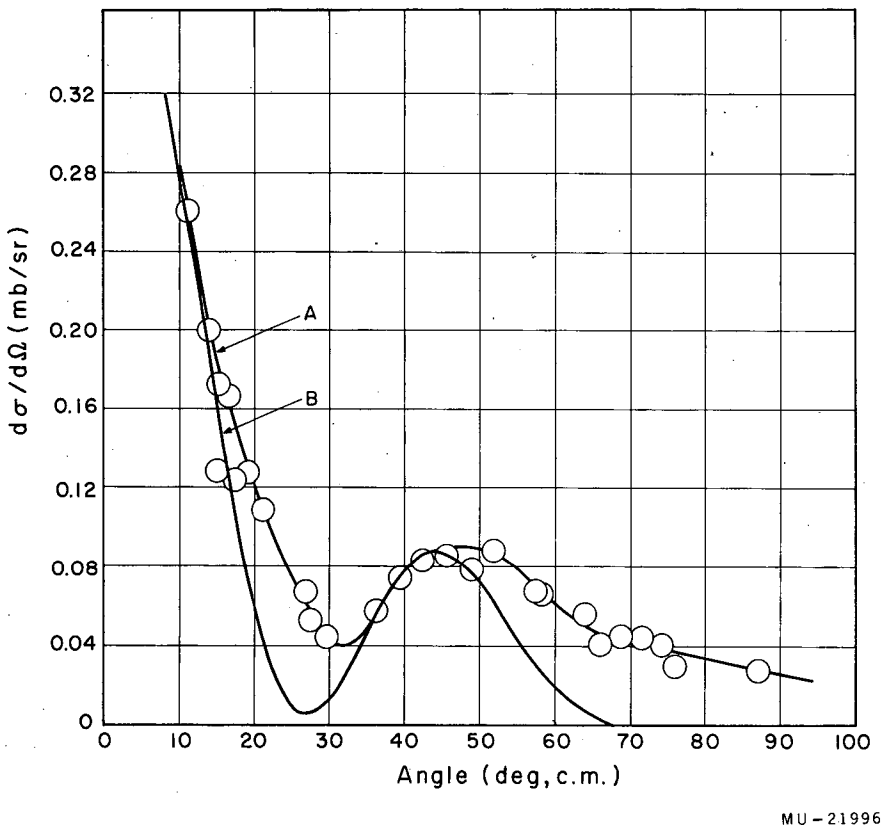

Fig. C. 3-4. Angular distribution of deuterons from formation of the 3.95-Mev state of N^{14} in the reaction $C^{12}(\alpha, d)N^{14}$. Curve A presents the experimental results; Curve B, results calculated from Glendenning's theory assuming capture of both nucleons into the $p_{1/2}$ shell, and r=4.33 fermis.

4. THE REACTIONS $Li^6(\alpha, d)Be^8$ AND $N^{14}(\alpha, d)O^{16}$

Joseph Cerny, III, Bernard G. Harvey, and Richard H. Pehl

The reactions $Li^6(\alpha, d)Be^8$ and $N^{14}(\alpha, d)O^{16}$ were induced by 48-Mev helium ions from the Crocker Laboratory 60-inch cyclotron. The deuterons were detected and identified by means of an E-dE/dx counter telescope system in which the dE/dx counter was a diffused-junction silicon detector. The particle energy (E) was measured with a conventional NaI(Tl) crystal and photomultiplier. The complete separation of deuterons from protons and tritons obtained in this way is illustrated in Fig. C. 4-1. Angular distributions were measured for several of the deuteron groups which correspond to the formation of previously known energy levels of Be^8 and O^{16}. They were compared with angular distributions calculated from the two-nucleon stripping theory of N. K. Glendenning, (Paper A. 5). In most cases, a very satisfactory fit was obtained, although the value of the interaction radius was not always entirely satisfactory. For example, Fig. C. 4-2 shows the theoretical fit obtained for the reaction $Li^6(\alpha, d)Be^8$(2.90-Mev state). It was assumed that the configuration of this Be^8 state is $(p_{3/2}{}^4)_{J=2+}$. No fit could be obtained for the unlikely configuration $(p_{3/2}{}^3 p_{1/2})_{J=2+}$. The theoretical line shown in Fig. C. 4-2 was obtained with an interaction radius of 2.1 f, which is certainly a very small value. However, it is very satisfactory that the theory is able to reproduce so accurately an experimental angular distribution which shows no diffraction structure.

Figure C. 4-3 shows the experimental and theoretical angular distributions for the reaction $N^{14}(\alpha, d)O^{16}$ (ground state). With the assumption that the configuration of this level in O^{16} is $(p_{1/2}{}^4)_{J=0+}$, an interaction radius of 5.35 f was obtained. Figure C. 4-3 shows that the theoretical angular distribution is too strongly damped at large angles. This difficulty can be partly removed only by assuming a radius for the incident helium ion that is smaller than the value obtained from the Stanford electron scattering.

In terms of the cluster model, the states of O^{16} at 9.58, 10.36, 11.26, and 11.62 Mev consist of an α particle and a C^{12} core in its ground state,[1] and there are no others below 12.43 Mev for which this description is well established. These states were not observably excited in the $N^{14}(\alpha, d)O^{16}$ reaction. If the reaction takes place by a knockout mechanism in which the incident helium ion knocks out a deuteron cluster and is then itself captured, the $(\alpha + C^{12})$ states should be strongly excited. Since they are not, it seems that a stripping mechanism is more likely than knockout.

In the $Li^6(\alpha, d)Be^8$ reaction, the integrated cross sections for formation of the Be^8 ground-state, 2.90- and 11.7-Mev levels increase with increasing α-particle reduced width of the level, as shown in Table I.

---

[1] B. Roth and K. Wildermuth, Reduced Widths in O^{16} and Gamma Transition Probabilities in F^{19}, Florida State University Report, to be published.

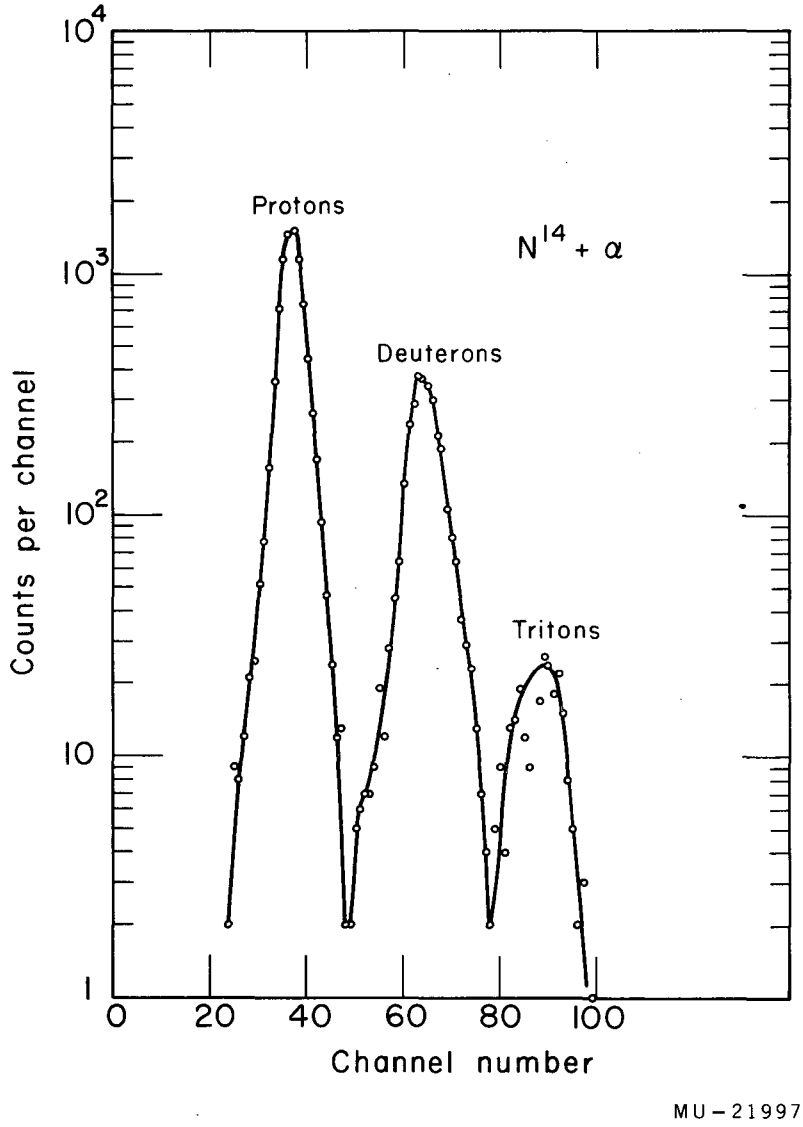

Fig. C. 4-1. Spectrum of pulse heights obtained from E-dE/dx particle identifier, for the reactions between N^{14} and 48-Mev helium ions.

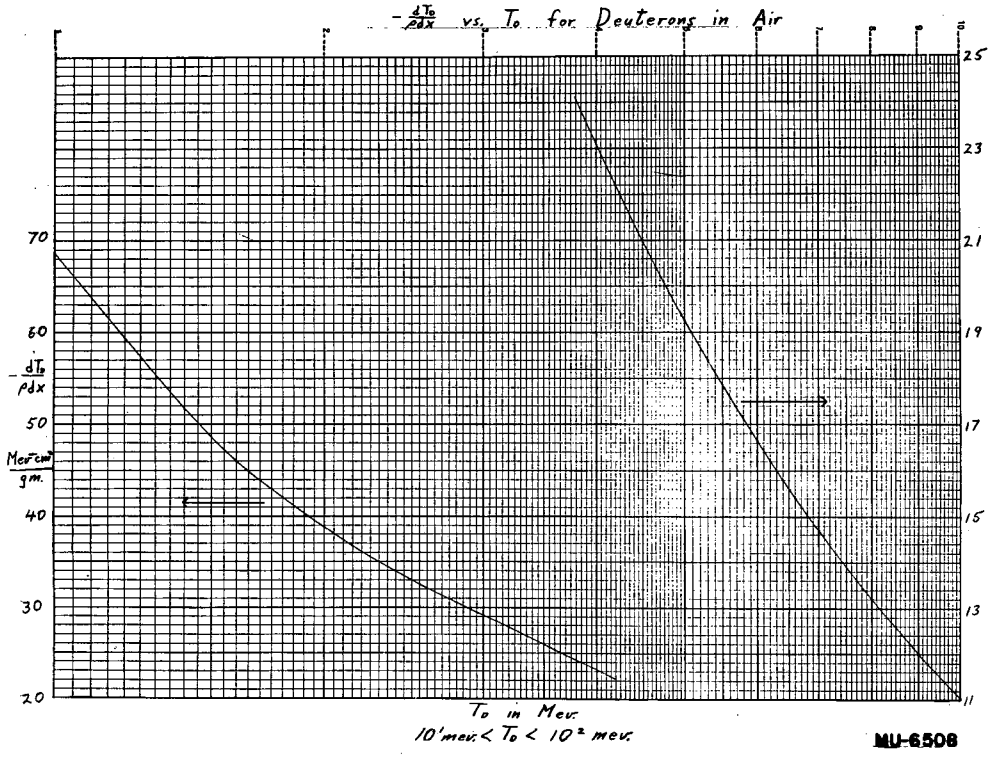

Fig. C.4-2. Angular distribution of deuterons from the reaction $Li^6(\alpha, d)Be^8$ (2.90 Mev). The line is calculated, the points are experimental.

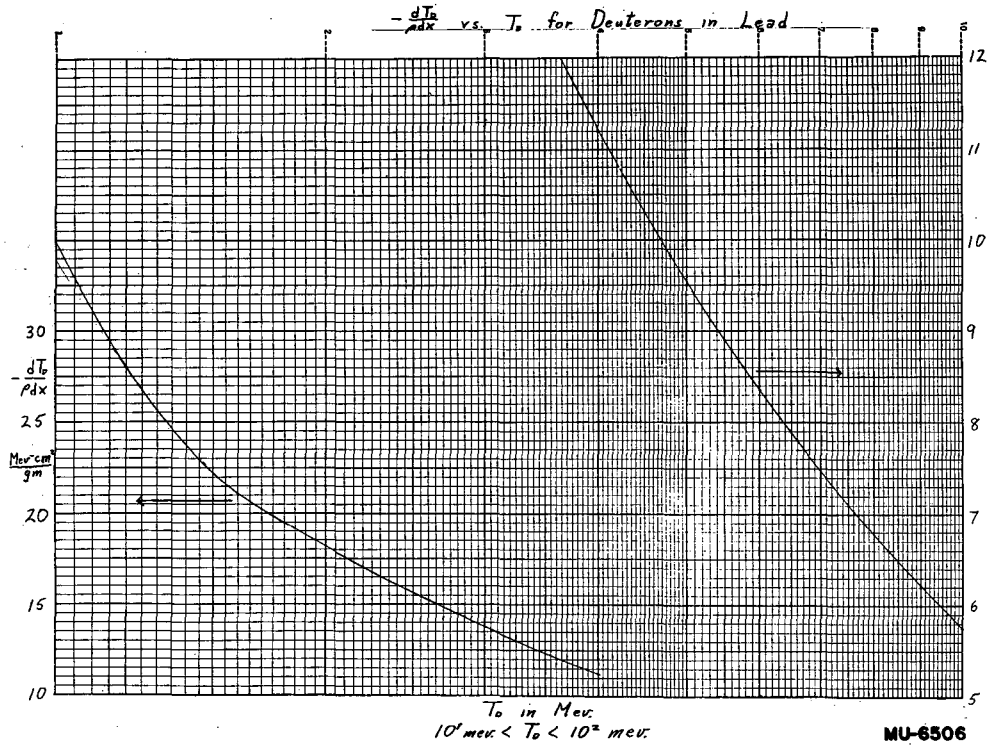

Fig. C.4-3. Angular distribution of deuterons from the reaction $N^{14}(\alpha, d)O^{16}$ (ground state). The line is calculated, the points are experimental.

Table I. Correlation between α-particle reduced width ($\theta^2_{\alpha+\alpha}$) and cross section for formation of level, in the reaction $Li^6(\alpha, d)Be^8$.

Level energy (Mev)	$J\theta$, T	$\theta^2_{\alpha+\alpha}$	$\langle 0_f \rangle / (2J+1)$ (mb)
0	0+, 0	0.15	1.02
2.90	2+, 0	0.7	1.42
11.7	4+, 0	0.95	2.67

It is not clear why formation of states with large α-particle widths is preferred in the Li^6 reaction but not in the N^{14} reaction. A natural (but not unique) explanation is possible in terms of the cluster model if it is assumed that (He^4+d) gives a good description of Li^6, but (C^{12}+d) does not adequately represent N^{14}. Capture of a proton and neutron in a relative ^3S_i state could lead to formation of (α+α) states of Be^8. If the coupling of the odd particles to the core is strong in N^{14}, then the O^{16} states formed by capture of the ^3S_i pair would perhaps be ($\alpha+C^{12*}$) states or states of cluster configurations other than ($\alpha+C^{12}$) ground state.

In formation of the O^{16} ground state, the captured nucleons are both added to the $p_{1/2}$ shell. In forming the 8.88-Mev 2- state, they are not, since--according to the analysis by Elliott and Flowers,[2] this level is 75% $[(p_{1/2})(d_{5/2})]_{2-}$ + approx 7% $[(p_{1/2})(d_{3/2})]_{2-}$. The cross-section ratio $\left[\langle\sigma_{gs}\rangle/(2J+1)\right]/\left[\langle\sigma_{8.88}\rangle/(2J+1)\right]$ was found experimentally to be about 4. Ball and Goodman found that pickup of two neutrons from the $1g_{9/2}$ shell was at least about three times as probable as pickup of one neutron from the $2d_{5/2}$ shell and one from the $1g_{9/2}$ shell.[3] Calculations show that the preference for capture into, or pickup from, the same shell is partly due to the greater probability that the two nucleons are in a relative ^3S_i state when they are in the same shell.[4] Owing to this effect alone, the cross section for formation of the O^{16} ground state in the reaction $N^{14}(\alpha, d)O^{16}$ should be 2.6 times the cross section for formation of the 8.88-Mev state.

[2] J. P. Elliott and B. H. Flowers, Proc. Roy. Soc. A242, 57 (1957).

[3] J. B. Ball and C. D. Goodman, Phys. Rev. 120, 488 (1960).

[4] Norman K. Glendenning (Lawrence Radiation Laboratory), private communication, Dec. 1960.

5. THE TWO-NUCLEON STRIPPING REACTION (*)

Norman K. Glendenning

A considerable body of experimental data is accumulating on the two-nucleon stripping reactions (α, d), (He^3, p). The simplest way of treating such a reaction from the theoretical point of view is to regard the incident particle as consisting of two structureless particles, one of which is stripped by the target. Such a treatment would make sense if the residual nucleus had a cluster configuration consisting of the target and the composite particle that is stripped. If, however, the residual nucleus is best described within the framework of the shell model, then the reaction should be specifically treated as the stripping of two nucleons into the appropriate shell-model states. Such reactions should yield information on the configurations of the residual states, some of which will be two-nucleon excitations.

This problem was first considered by El Nadi, and we shall take advantage of some of his work.[1] We consider separately the cases of even-even, even-odd, and odd-odd target nuclei with appropriate coupling schemes in the j-j limit.

The principal assumptions used to calculate the angular distribution are: (a) The center-of-mass motions of incident and outgoing particles are described by plane waves. (b) The target nucleus forms the core of the residual nucleus and is not excited by the reaction. (c) The neutron and proton are captured into spin-orbit states in the nucleus.

For the internal wave function of the α particle we use

$$\chi_0(\alpha) \propto X^0_0(n, n')X^0_0(p, p') \exp(-\gamma^2 \Sigma r_{ij}^2) \tag{1}$$

which is properly antisymmetric. X^0_0 denotes the singlet spin function for two nucleons. We note

$$X^0_0(n, n')\, X^0_0(p, p') = \frac{1}{2} \sum_{S=1,0} \sum_{M=-S}^{S} \sqrt{2S+1}\; C(SSO, M\text{-}MO)\, X^M_S(n, p) X^{-M}_S(n', p'). \tag{2}$$

We assume that the interaction responsible for the (α, d) reaction is between the captured pair and the target nucleus. The outgoing deuteron merely conserves energy and momentum. It is clear, therefore, that in the matrix element for the reaction in which $\chi_0(\alpha)$ appears in the initial state and the spin function $X^M_1(n', p')$ for the outgoing deuteron appears in the final state, only the triplet part of (b) survives. Hence only the triplet component of the wave function describing the captured pair in the final nucleus contributes to the reaction.

---

*Brief version of a paper (UCRL-9505, Jan. 1961), to be submitted to Nuclear Phys.

[1] M. El Nadi, Proc. Roy. Soc. (London) A70, 62 (1957).

The angular distribution for coupling schemes appropriate to even-even, odd-odd, and even-odd nuclei can all be expressed in the form

$$\frac{d\sigma}{d\Omega} \propto \sum \frac{C_L}{2L+1} \; |B(\ell_n \ell_p L; Q|^2,$$

where

$$B(\ell_n \ell_p L; Q) = \sum_{n=0}^{\infty} (-)^n (2n+1) I_{n+1/2}(4\gamma^2 R_0{}^2)$$

$$\times \sum_{\lambda_n \lambda_p} i^{\lambda_n + \lambda_p} \sqrt{(2\lambda_n+1)(2\lambda_p+1)}\, C(\ell_n n \lambda_n; 000) C(\ell_p n \lambda_p; 000)$$

$$\times \; C(\lambda_n \lambda_p L; 000) W(\ell_n \ell_p \lambda_n \lambda_p; Ln)\; j_{\lambda_n}(QR_0/2) . j_{\lambda_p}(QR_0/2).$$

In this expression R_0 is the radius at which the captured particles are assumed to be stripped, and

$$I_{n+1/2}(X) = i^{n+1/2}\, J_{n+1/2}\,(-iX).$$

The series on n converges rapidly, and the range of λ_n, λ_p is limited by the Clebsch-Gordan coefficients. The ℓ_n and ℓ_p are the orbital states into which the neutron and proton are captured. The information on the nuclear coupling scheme is contained in the coefficients C_L. For example, if the target is an even-even nucleus and the neutron and proton are captured into the spin-orbit states $j_n = \ell_n + 1/2$ and $j_p = \ell_p + 1/2$, then

$$C_L = \left\langle (\ell_n \ell_p) L, (1/2\ 1/2) 1;\quad J \,\middle|\, (\ell_n 1/2) j_n, (\ell_p 1/2) j_p; J \right\rangle ,$$

where J is the spin of the final nucleus. This is the transformation coefficient from LS to j-j coupling.

Details of the calculation for this case and for odd-odd and odd-even targets can be found in the full-length version of this paper.* Comparison of the theory with experimental results can be found in the work of Cerny, Harvey, and Pehl.[2]

---

[2] J. Cerny, B. G. Harvey, and R. H. Pehl, (a, d) Reactions on Odd-Odd Targets (UCRL-9525, Jan. 1961), to be submitted to Nuclear Phys.

6. RECOIL STUDIES OF NUCLEAR REACTIONS INDUCED BY HEAVY IONS (*)

John M. Alexander and Lester Winsberg

The mechanism of nuclear reactions induced by heavy ions (HI) was investigated by measuring the recoil ranges of Tb^{149}, At^{211}, and other α-particle-emitting isotopes of At and neighboring elements, and by determining the cross sections for the formation of Tb^{149} and At^{211}.

Recoil ranges were consistent with compound-nucleus formation at all energies studied for the reactions $Pr^{141}(C^{12}, 4n)Tb^{149}$, $Ce(N^{14}, xn)Tb^{149}$, $La^{139}(O^{16}, 6n)Tb^{149}$, $La^{139}(O^{18}, 8n)Tb^{149}$, and $Ba(Ne^{22}, pxn)Tb^{149}$. A similar result was obtained for the reaction $Pr^{141}(O^{16}, 2p6n)Tb^{149}$ at 138 and at 146 Mev and for the reactions $Au^{197}(O^{16}$, 2pxn and 3pxn)At, Po at energies below 100 Mev. The excitation functions of the $(HI, xn)Tb^{149}$ reactions seem to be characteristic of an evaporation process but have smaller peak cross sections than do the excitation functions of the reactions $Ba(Ne^{22}, pxn)Tb^{149}$ or $Pr^{141}(O^{16}, 2p6n)Tb^{149}$. We conclude that most reactions probably involve charged-particle emission. The reaction $Ba(Ne^{22}, pxn)Tb^{149}$ seems to occur with much greater probability than the reaction $Ba(Ne^{20}, pxn)Tb^{149}$.

In many cases the compound-nucleus mechanism cannot account for our results. Partial momentum transfer is observed in the reactions $Au^{197}(O^{16}$, 2pxn and 3pxn)At, Po at energies above 100 Mev. Partial momentum transfer also occurs when Bi is bombarded at energies 1.3 times the barrier energy or greater. Reactions of Bi with heavy ions (Ne^{20} is possible exception) at energies near the Coulomb barrier produce At^{211} with greater recoil energy than expected from a compound-nucleus mechanism. Apparently, particles are emitted in the backward direction. Near the barrier the cross section for the production of At^{211} by C^{12}, O^{16}, and Ne^{20} bombardment comprises about 1/4 the value calculated for compound-nucleus formation. Therefore, the cross section for all non-compound-nucleus reactions must comprise a large fraction of the total interaction cross section. The experiments with Pb as a target are also consistent with this conclusion.

*Abstract of a published paper, Phys. Rev. 121, 529 (1961).

7. RECOIL PROPERTIES OF FISSION PRODUCTS (*)

John M. Alexander and M. Frances Gazdik

A knowledge of the recoil properties of fission products is of value for understanding the fission process and the stopping of fission products in matter. Many studies of the fission process have been made by observing

*Introduction of a published paper, Phys. Rev. 120, 874 (1960).

the recoil properties of the fission products.[1-11] An adequate evaluation of the experimental results requires information about the relation of range to energy and the deviations from straight-line motion. This information is still fragmentary. In order to improve our knowledge of these matters, we have measured the range and relative energy loss in Al and Au of five products from the thermal neutron fission of U^{235}. We also report here information about the scattering of these fission products in Al and Au.

In previous work the recoil properties of fission products have been observed by several techniques. The range,[11] energy,[12] rate of energy loss,[13-14] and angular distribution[5-10] have been measured with well-collimated recoils. These experiments require intense fission sources or must be limited to work with gross fission products. Measurements with large angular acceptance have given information on the range,[1-4, 15, 16] the velocity of the fissile nucleus,[2-4] and certain features of the angular distribution.[3] Weaker sources may be used for the latter type of experiment. However, the interpretation of these experiments requires information about the form of the angular distribution and the nature of the stopping process.

---

[1] E. M. Douthett and D. H. Templeton, Phys. Rev. 94, 128 (1954).

[2] Nathan Sugarman, Milton Compos, and Karoline Wielgoz, Phys. Rev. 101, 388 (1956).

[3] Norbert T. Porile and Nathan Sugarman, Phys. Rev. 107, 1410 (1957); Norbert T. Porile, Phys. Rev. 108, 1526 (1957).

[4] Christiane Baltzinger, Yield and Range Studies of Selected Fission Products from Uranium Bombarded with Bev Protons, UCRL-8430, Aug. 1958.

[5] Cohen, Jones, McCormick, and Ferrell, Phys. Rev. 94, 625 (1954).

[6] Cohen, Ferrell-Bryan, Coombe, and Hullings, Phys. Rev. 98, 685 (1955).

[7] E. J. Winhold and I. Halpern, Phys. Rev. 103, 990 (1956).

[8] C. T. Coffin and I. Halpern, Phys. Rev. 112, 536 (1958).

[9] J. W. Meadows, Phys. Rev. 110, 1109 (1958).

[10] R. Wolke and J. Gutmann, Phys. Rev. 107, 850 (1957).

[11] Katcoff, Miskel, and Stanley, Phys. Rev. 74, 631 (1948).

[12] William E. Stein, Phys. Rev. 108, 94 (1957).

[13] R. B. Leachman and H. W. Schmitt, Phys. Rev. 96, 1366 (1954).

[14] Clyde B. Fulmer, Phys. Rev. 108, 1113 (1957); also Fission Fragment Studies by Magnetic Analysis, ORNL-2320, Aug. 1957.

[15] P. F. Suzor, Ann. Phys. 4, 269 (1949).

[16] Finkle, Hoagland, Katcoff, and Sugarman, in Radio-Chemical Studies: The Fission Products, National Nuclear Energy Series (McGraw-Hill Book Co., Inc., New York, 1951), Div. IV, Vol. 9, p. 471.

From the measurements reported here and elsewhere[15, 16] we have constructed curves of the range in Al and Au as a function of the mass number of the recoiling fission product. These curves define quite accurately the ranges of the median light and heavy products. (By "median product" is meant that fragment that is the median of all the light fission products or all the heavy fission products.) We normalize the available energy-loss data for median light and heavy products to the range values. This combination of information provides range-velocity curves for the median light and heavy products. Similar curves are proposed for all fission products. Finally, we estimate the kinetic energies of products of low yield from their range.

8. THE n, α REACTION INDUCED BY THERMAL NEUTRONS

Roger D. Griffioen

I. Calculation of Cross Sections

(with John O. Rasmussen)

The absorption of a thermal neutron by a nucleus, followed by the decay of the compound system, can be described very accurately as a two-step process. The first step, the absorption of a thermal neutron, has been the object of a large amount of research. The absorption cross sections used in this work are taken from the tabulations by Hughes and Schwartz.[1] In general, the primary decay mode of the compound system is by γ emission. The level widths for γ decay do not vary to a large extent, and the measured widths have been fitted to an empirical formula by Stolovy and Harvey,[2]

$$\Gamma_\alpha = 5.3\times10^{-4}\, A^{2/3}\, [D(U)]^{0.25}\, U^{4.3},$$

where U is the "effective" excitation energy corrected for odd-even effects, D(U) is the level spacing at U of levels of given spin and parity, and A is the mass number. This formula is used for obtaining the partial gamma widths.

A calculation is made here of the competition between α decay and the most probable mode, γ decay. The calculation of level widths for α decay is based on a single semiclassical treatment of α decay first given by von Laue.[3] The decay constant λ is taken as the product of a frequency factor W_0, giving the collisions per second with the barrier, and the barrier penetration factor P. The partial level width is then given by

$$\Gamma_\alpha = \hbar W_0 P.$$

[1] D. J. Hughes and R. B. Schwartz, Neutron Cross Sections, BNL-325 and Supplements, 2nd edition (1958).

[2] A. Stolovy and J. A. Harvey, Phys. Rev. 108, 353 (1957).

[3] M. von Laue, Z. Physik 52, 726 (1928).

The barrier-penetration factor P is calculated by using an exponential nuclear potential as discussed by Rasmussen.[4] The method involves a numerical integration with the IBM 650 computer of the JWKB integral, using the real part of an α-nuclear potential given by Igo to fit α elastic scattering data,[5]

$$V(r) = -1100 \exp \left\{ \frac{1.17\ A^{1/3} - r}{0.574} \right\} \text{Mev.}$$

The energies available for α decay are taken from available mass data or from Cameron's Semi-Empirical Atomic Mass Formula.[6] The centrifugal barrier due to angular momentum is included, and results are obtained for both the possible spin states formed by absorption of an S-wave neutron (only one state is possible for even-even targets). In some cases α decay to the ground state is forbidden, and the calculation is then made for decay to the first excited state. This may affect the barrier penetration greatly, depending on which spin state is formed.

The frequency factor W_0 can be related to the spacing of levels of given spin and parity, assuming a sequence of equally spaced levels,[7]

$$W_0 = D/2\pi\hbar,$$

where D is again the spin-dependent level spacing. Using this relationship gives

$$\Gamma_\alpha = (D/2\pi)P.$$

The spin-dependent level spacings are obtained from the formulas of Cameron[8] based on the Fermi gas model of the nucleus and utilizing empirical atomic masses. Computing the level spacing involves an iterative procedure, therefore a 650 computer program was written to facilitate this calculation.

In this manner n, α cross sections were obtained for the most neutron-deficient stable even-Z even-N isotopes, for most of the stable even-Z odd-N isotopes, for a few favorable cases of odd-Z even-N isotopes, and for all the stable odd-Z odd-N isotopes, a total of more than 100 different cases.

Table I shows the results for a few of the most favorable cases, some of which are now being investigated (see Section III).

---

[4] J. O. Rasmussen, Phys. Rev. 113, 1593 (1959).

[5] G. Igo, Phys. Rev. Letters 1, 72 (1958).

[6] A. G. W. Cameron, A Revised Semi-Empirical Atomic Mass Formula, CRP-690, March 1957 (AECL-433, July 1958).

[7] J. M. Blatt and V. F. Weisskopf, Theoretical Nuclear Physics (John Wiley and Sons, New York, 1952) p. 386.

Table I. Calculated n, α cross sections

Target nuclide	Spin and parity: Target	Spin and parity: Compound system	Spin and parity: Final state	Energy of final state (Mev)	P	D (ev)	n, α cross section (mb)
Nd^{143}	1/2-	3-	0+	0	3.60×10^{-6}	248	420
Nd^{143}	1/2-	4-	2+	1.60	9.13×10^{-9}	228	1.0
Ru^{96}	0+	1/2+	(5/2+)	0	3.17×10^{-6}	756	0.20
Pd^{102}	0+	1/2+	5/2+	0	2.17×10^{-8}	402	0.05
Te^{123}	1/2+	0+	0+	0	2.07×10^{-6}	140	98
Te^{123}	1/2+	1+	2+	1.18	5.75×10^{-9}	49	0.12
Sm^{147}	7/2-	3-	0+	0	2.48×10^{-6}	41	17
Sm^{147}	7/2-	4-	2+	0.69	2.41×10^{-7}	38	1.6
Sm^{149}	7/2-	3-	0+	0	4.65×10^{-7}	11	570
Sm^{149}	7/2-	4-	2+	0.46	8.93×10^{-8}	10	110
Gd^{155}	3/2-	1-	0+	0	2.24×10^{-7}	6.2	170
Gd^{155}	3/2-	2-	2+	1.22	1.37×10^{-9}	4.1	0.79
Gd^{157}	3/2-	1-	0+	0	1.48×10^{-9}	14	14
Gd^{157}	3/2-	2-	2+	0.08	1.05×10^{-9}	9.4	7.0

II. Comparison with Available Experimental Data

Although the assumptions involved in the cross-section calculations probably become worse as the light-mass region is approached, it seemed worth while to extend the calculations to the region where there are experimental data available for comparison.[1]

Table II summarizes the results of the measured and calculated cross sections. Where the thermal neutron absorption cross section is not known it is taken as 1 barn. One can comment as follows:

S^{32} -- the agreement is remarkable

S^{33} -- a 1+ state is most likely populated

Fe^{57} - the experimental α energy is high by a factor of two compared with mass data, and puts doubt on the experimental cross section

Zn^{64} - the agreement is fair

Zn^{67} - the agreement is good for a 2- state being formed

A^{36} -- the experimental cross section is extrapolated from data with 2- to 4-Mev neutrons

III. Experimental Work

(with Ronald D. MacFarlane)

The first apparatus used in this work made use of a Pu-Be neutron source immersed in a water tank to thermalize the neutrons. A small target sample was placed directly in front of a solid-state detector, and this system was placed in the water tank. The signal from the crystal was amplified and fed into a pulse-height analyzer.

The neutron flux was maintained by means of the $Li^6(n, \alpha)T^3$ reaction, and the energy calibration was determined by a source consisting of Ra^{224} and its daughters. Since the maximum neutron energy from the Pu-Be source is well above the α energy region we are interested in, there was considerable background, thus limiting the sensitivity of this setup.

In Sm^{149} (see Table I) the decay of a 3- state to the daughter ground state would give rise to a 9.23-Mev α particle. The counting rate observed at this energy indicates that if this spin state is formed the n, α cross section is lower than the calculated cross section by a factor of about five. If a 4- state is formed, decay can proceed only to an excited state, and the alpha energy to the first excited state would be 8.78 Mev. The counting rate observed at this energy sets an upper limit on the cross section of about twice the calculated one.

The equipment is now being redesigned for use in the thermal column of the Livermore reactor, where a much higher neutron flux will be available and the background due to very-high-energy neutrons will be eliminated. This should allow a study of many examples of these n, α reactions.

Table II. Comparison of experimental and calculated cross sections

Target nuclide	Spin and parity			Energy of final state (Mev)	Calculated cross section	Experimental cross section
	Target	Compound system	Final state			
S^{32}	0+	1/2+	1/2+	0	1.5 mb	1.8 ± 1.0 mb
S^{33}	3/2+	1+	(2+)	2.24	≈ 5 μb	< 8 mb
S^{33}	3/2+	2+	0+	0	≈ 1 b	< 8 mb
Fe^{57}	1/2-	1-	0+	0	1 μb	< 5 mb
Fe^{57}	1/2-	0-	?	?	<< 1 μb	< 5 mb
Zn^{64}	0+	1/2+	3/2-	0	200 μb	15 ± 10 μb
Zn^{67}	5/2-	3-	0+	0	6.5 mb	6 ± 4 μb
Zn^{67}	5/2-	2-	2+	1.34	15 μb	6 ± 4 μb
A^{36}	0+	1/2+	3/2+	0	11 mb	(8.5 mb)

9. STUDIES IN LOW-LEVEL LIQUID SCINTILLATION COUNTING

W. J. Kaufman,* Aharon Nir,† and G. Parks*

Investigation of the low-level liquid scintillation counting system described by Kaufman et al.,[1] was continued with the object of improving its sensitivity, stability, and accuracy. This system was designed primarily for hydrological tracing with tritium. Sensitivity improvement was achieved by use of high-gain quartz face photomultipliers in contact with the solution, use of teflon liquid cells, and operation in the violet part of the spectrum. Long-term stability data were determined on this system. Accuracy was improved by the introduction of a Co^{57} internal standard, which obviates the use of an internal tritium standard and consequent destruction of the original sample. The Co^{57} channel count ratio proved to be a reliable counting-efficiency monitor with up to 0.05% accuracy and 3 to 7% efficiency for short counting periods (days) or up to 0.1% for longer periods.

From indirect computational evidence, the contribution of the light interaction is limited to an insignificant part of the background. An experimental limit of this contribution was investigated with an anticoincidence cosmic shield.

---

*Department of Sanitary Engineering, University of California, Berkeley.

†On leave from Weizmann Institute of Science, Rehovoth, Israel.

[1] W. J. Kaufman and others, in Proceedings of the University of New Mexico Conference on Organic Scintillators, August 1960.

10. ON SOME APPLICATIONS OF THE α, n REACTIONS ON OXYGEN-18

Aharon Nir*

The information on thick-target yields of α, n reactions on heavy isotopes of oxygen is of value for the estimation of certain geochemical processes, in production of liquid and gaseous neutron sources, and in tracing the kinetics of oxygen reactions. Recent determinations give the α, n yield on O^{18} as 31 n/10^6α for Po^{210}α [1] and 650±90 n/10^6α for α's following Pb^{212}.[2] No measurements are available of the corresponding yield on O^{17}, because of lack of highly enriched targets, but it is shown that with present sensitivity of mass spectrometry and O^{17} enrichment, Ne^{20} measurements would give a good estimate of this yield.

---

*On leave from Weizmann Institute of Science, Rehovoth, Israel.

[1] I. A. Serkynkova, et al., Izvest. Akad. Nauk. SSSR(Fiz) 21, 1017 (1957).

[2] S. Amiel and A. Nir, to be published.

The above α, n yields on O^{18} are used to make a new evaluation of the Ne^{21} production in the lithosphere.[3] It is shown that the maximum effect on the atmospheric abundance would be 6 to 12%, depending on the actual depth of the crust and the variation of U and Th with depth. The actual contribution to atmospheric abundance could be found by comparison with the cosmic isotopic ratio of Ne. This value could be used then to estimate a lower limit for the escape from the earth crust.

The application of the above reaction as a liquid and gaseous neutron source offers new possibilities by combining high yield with greater flexibility of handling and transportation, reproducible preparation, and ability to change target thickness and thus the neutron spectrum.

Analytical and tracing applications include α-activity measurements in solutions[4] and tracing of oxygen reactions kinetics[2] between different phases, including surface reactions.

[3] G. W. Wetherill, Phys. Rev. 96, 679 (1954).

[4] V. V. Ivanova et al., Atomnaya Energ. 7, 166 (1959).

11. HEAVY-ION ELASTIC SCATTERING

Jonas Alster and Homer E. Conzett

The elastic scattering of C^{12} ions from several nuclei was studied.[1] The 124.5-Mev C^{12} beam of the heavy-ion linear accelerator was magnetically deflected and brought into a scattering chamber through two collimators, 1/8 in. each, 3 feet apart. The targets were placed in the center of the scattering chamber.

The angular distribution was measured by swinging two counters around the center of the chamber. The scattered particles left the chamber through a 0.002-in. -thick Mylar foil. The counters consisted of a thin CsI(Tl) crystal, mounted on a photomultiplier tube in an evacuated holder. The angular resolution of the system was 7 deg and the energy resolution 1.3%. In the latter part of the experiment the CsI crystals were replaced by solid-state radiation detectors, which gave us a resolution of 1%. The beam was monitored with a Faraday cup-electrometer system and with a monitor counter, mounted through the bottom of the scattering chamber, at a fixed angle.

The measured angular distributions for Ni, Ag^{107}, In, and Ta are shown in Fig. C. 11-1. The errors in the measurements are indicated by the sizes of the dots in the figure. Each point represents 10,000 counts except for the largest angles.

[1] Proceedings of the Second Conference on Reactions between Complex Nuclei (John Wiley and Sons, New York, 1960).

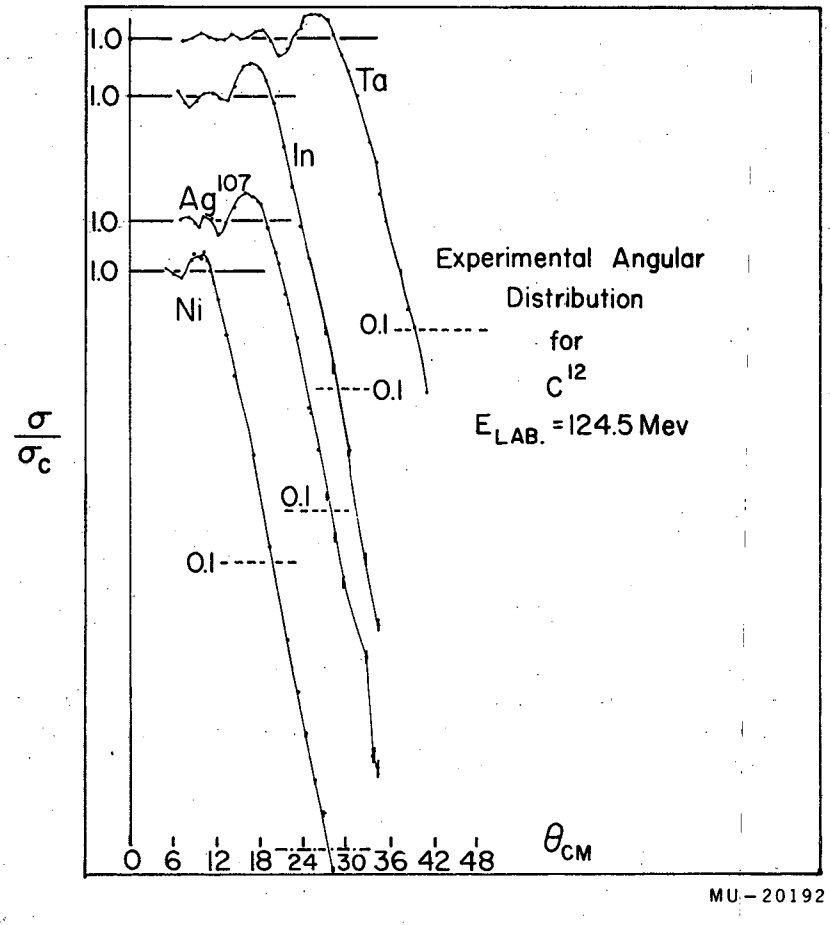

Fig. C.11-1. Experimental angular distributions for 124.5-Mev C^{12} ions scattered from Ni, Ag^{107}, In, and Ta. The cross section divided by the Rutherford cross section is plotted as a function of the center-of-mass angle. The curves are normalized to unity at small angles.

The analysis of the data is based on the Blair model.[2] The final analysis was a comparison of our data with the McIntyre model.[3] In their model the cross section divided by the Rutherford cross section has the form

$$\frac{\sigma(\theta)}{\sigma_R(\theta)} = \Bigg\{\cos\left(n \ln \sin^2 \frac{\theta}{2}\right) + \frac{\sin^2 \frac{\theta}{2}}{n} \sum_{\ell=0}^{\infty} (2\ell+1) \left[\sin 2\,(\sigma_\ell - \sigma_0) - A_\ell \sin 2\,(\sigma_\ell - \sigma_0 + \delta_\ell) P_\ell\,(\cos\theta)\right]\Bigg\}^2$$

$$+ \Bigg\{\sin\left(n\,\theta n \sin^2 \frac{\theta}{2}\right) + \frac{\sin^2 \frac{\theta}{2}}{n} \sum_{\ell=0}^{\infty} (2\ell+1) \cos 2(\sigma_\ell - \sigma_0) - A_\ell \cos 2(\sigma_\ell - \sigma_0 + \delta_\ell)\Big] P_\ell(\cos\theta)\Bigg\}^2 ,$$

where

$$\sigma_\ell = \sigma_0 + \sum_{k=1}^{\ell} \arctan \frac{n}{k}; \quad n = \frac{Z_1 Z_2 e^2}{\hbar v}; \quad A\ell = \frac{1}{1+\exp\left\{\frac{\ell_A - \ell}{\Delta \ell_A}\right\}};$$

$$\delta_\ell = \frac{\delta_0}{1+\exp\left\{\frac{\ell - \ell_\delta}{\Delta \ell_\delta}\right\}} .$$

A_ℓ is the amplitude of ℓth outgoing partial wave, δ_ℓ is the real nuclear phase shift that is added to the Coulomb phase shift. In this model five parameters are available, ℓ_A, $\Delta\ell_A$, δ, ℓ_δ, $\Delta\ell_\delta$. In the Blair sharp-cutoff model one has

$$\begin{cases} A_\ell = 0 \text{ for } \ell \leqslant \ell', \\ A_\ell = 1 \text{ for } \ell > \ell', \text{ and} \\ \delta = 0 \text{ for all } \ell. \end{cases}$$

[2] J. S. Blair, Phys. Rev. 95, 1218 (1954); 108, 827 (1957); D. D. Kerlee, J. S. Blair, and G. W. Farwell, Phys. Rev. 107, 1343 (1957).

[3] J. A. McIntyre, K. K. Way, and R. C. Becker, Phys. Rev. 117, 1337 (1960).

A computer program for the IBM 704 was written for the calculation of $\sigma(\theta)/\sigma_R(\theta)$ according to this formula.

Figure C. 11-2 gives an example of a fit with the McIntyre model. From this figure it becomes clear that it is very important to do these experiments with good statistics because we try to fit small oscillations around $\sigma(\theta)/\sigma_R(\theta) = 1$.

The results of these experiments show that the Blair sharp-cutoff model is not good enough to fit elastic scattering data for cross sections $\sigma(\theta)/\sigma_R(\theta) < 0.2$. For a given value of n, increasing $\ell_A = \ell_\delta$ moves the breakoff from Rutherford scattering to smaller angles. Increasing $\Delta\ell_A = \Delta\ell_\delta$ makes the falloff steeper and tends to wash out the oscillations around Rutherford scattering. In none of the cases was it possible to get agreement with experiment without making $\delta \neq 0$. Introducing δ steepens the falloff and increases the amplitudes of the oscillations around Rutherford scattering. It is clear that rounding of the cutoff is not sufficient to explain the data, but a real phase shift δ_ℓ has to be added.

The results are summarized in Table I. R_0 is the radius parameter of the formula $R = R_0(A_1^{1/3} + A_2^{1/3})$, and is calculated from the formula

$$E_{c.m.} = \frac{Z_1 Z_2 e^2}{R} + \frac{\hbar^2 l_A(l_A+1)}{2\mu R^2} .$$

Scattering data from Fe and argon have not yet been analyzed.

Table I. Summary of results

Target	SCO[a] ℓ'	McIntyre Model $\ell_A=\ell_\delta$	$\Delta\ell_A=\Delta\ell_\delta$	δ	$(R\times10^{13})$	R_0
Ni n=8.28	56	56	3	0.4	9.39±.21	1.52±.03
	57	57	3	0.4	9.53±.21	1.54±.03
Ag^{107} n=13.91	62, 63, 64	62	3	0.5	10.48±.23	1.49±.03
In n=14.49	62, 63	62	2	1.0	10.36±.23	1.45±.03
Ta n=21.59	65, 66	66	3	0.4	11.63±.26	1.46±.03

[a]SCO = Blair sharp-cutoff model.

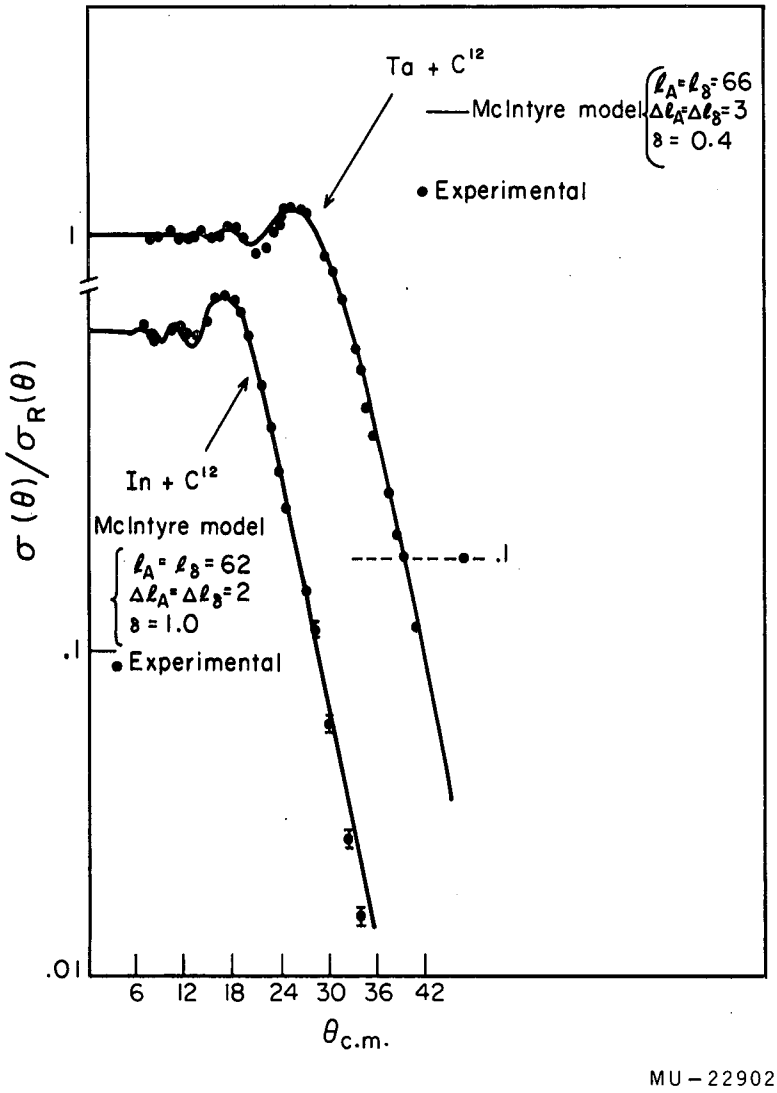

Fig. C.11-2. Angular distributions for C^{12} elastically scattered from In and Ta. The solid line is the calculation according to the McIntyre model.

12. ELASTIC SCATTERING OF 31-Mev He^3 IONS

Jose Gonzalez-Vidal, George Igo, and Samuel S. Markowitz

The absolute differential cross sections for elastic scattering of 31-Mev He^3 ions on Be, Al, Cu, $Sn^{(nat)}$, Sn^{120}, and Bi have been measured in the angular range of about 10 to 120 deg in the center-of-mass system. The purpose of these measurements is to compare the optical-model potential necessary to fit the He^3 data with that for He^4 scattering.[1-4] Presumably the He^3 results should reflect the effects of low binding energy and nonzero spin. The optical-model theoretical treatment is in progress and is to be reported later; the experimental part is completed.

The above target elements were selected because they cover a wide range of the parameter $A^{1/3}$ (A is the mass number), which is important in optical-model theory; also inelastic events from these targets could be separated from the elastic scattering, with our energy resolution. The He^3 was accelerated as He^3 (+1) ions in the heavy-ion linear accelerator. The ions were magnetically analyzed and allowed to impinge upon self-supporting targets of thicknesses in the range 1 to 4 mg/cm^2. The beam was collimated down to a 0.125-in. spot and was monitored with a calibrated Faraday cup. The Faraday cup was protected from scattered electrons by magnets, or by an electric potential applied to a brass plate. In addition a NaI scintillation counter held at a fixed angle was used to check the relative beam intensity by detecting scattered He^3 ions.

The elastically scattered He^3 particles were counted by stopping them in CsI scintillation crystals of thickness slightly greater than the range of the particles at 31 Mev. The pulse-height analysis energy resolution was approx 3%; the angular resolution, approx 1 deg. The background in the region of the elastic scattering peak in the pulse-height spectra obtained from the counters consisted of: (a) pulses due to α particles produced by the exoergic He^3, He^4 reactions, (b) inelastic He^3 scattering, and (c) scattering from the tantalum collimators. The background was subtracted in a consistent manner. The magnitude of the background varied with target and angle of observation. For Bi, between 10 and 98 deg, the background varied from 0.7 to 1.6% of the peak area; for Sn^{120}, between 20 and 120 deg, background was 0.5 to 13%; for Cu, between 10 and 64 deg, background was 1 to 5%; for Al, between 14 and 68 deg, background was 0.9 to 19%; and for Be, between 17 and 65 deg, background was 0.8 to 30% of peak area. The number of counts accumulated at most angles gave a standard deviation of about 1.5%. The reproducibility of a series of points taken at the same angle, which includes the effects of statistics, Faraday cup integrator readings, and graphical analysis, was about 2.3%.

---

[1] Seidlitz, Bleuler, and Tendam, Bull. Am. Phys. Soc., Ser. II, 1, 29 (1956).

[2] Igo, Wegner, and Eisberg, Phys. Rev. 101, 1508 (1956).

[3] R. Ellis and L. Schecter, Phys. Rev. 101, 636 (1956).

[4] G. Igo and R. M. Thaler, Phys. Rev. 106, 126 (1957).

The data in final form are summarized in Tables I through VI. Both the absolute differential cross sections and the ratio of the absolute differential cross section to the calculated Rutherford-scattering cross section in the center-of-mass system are presented. In Figs. C. 12-1 through C. 12-6 the absolute differential cross sections are presented for each element, and in Fig. C. 12-7 the ratios of the cross sections to the Rutherford cross sections for all the elements are displayed. The size of the symbol or flag on a plotted point indicates the standard deviation, which is the rms of the uncertainties mentioned above. The differential cross sections for Rutherford scattering[5] have been calculated with the aid of an IBM 704 computer program written for this purpose. The variables are: charge of target, charge of projectile, mass of target, mass of projectile, energy of incident particle, and angular interval. The output is the differential cross section in cm^2/sr versus angle in the center-of-mass system.

The results indicate strong diffraction effects in the light elements and a smooth decrease of the differential cross sections with increasing angle for the heavier elements.[6] Optical-model analyses are in progress.

A preliminary report of this research was presented at the Washington, D. C., meeting of the American Physical Society April 25, 1960.[7]

---

[5] $(d\sigma/d\Omega)_R = (Z Z' e^2/4T)^2 \sin^{-4}(\theta_{c.m.}/2)$, where Z and Z' are the atomic numbers of target and incident particle, T is the kinetic energy, and $\theta_{c.m.}$ is the scattering angle in the center-of-mass system.

[6] Scatterings of 29-Mev He^3 ions have been reported: Aguilar, Burcham, England, Garcia, Hodgson, March, McKee, Mosinger, and Toner, Proc. Roy. Soc. (London) A 257, 13 (1960); G. W. Greenlees and P. C. Rowe, Nuclear Phys. 15,687 (1960). We appreciate the communication of these and other results to us by Professor Burcham in advance of publication.

[7] Igo, Markowitz, and Gonzalez-Vidal, Bull. Am. Phys. Soc., Ser II, 5, 229 (1960).

C. 12

Table I. The differential cross section for elastic scattering of 31.2-Mev He^3 ions incident on beryllium and the ratio of the experimental cross section to the Rutherford cross section in the center-of-mass system.

$\theta_{c.m.}$ (deg)	$(d\sigma/d\Omega)$ (barns/sr)	$\frac{(d\sigma/d\Omega)}{(d\sigma/d\Omega)_R}$
17.1	5.85×10^{-1}	1.86×10^{0}
19.7	2.01×10^{-1}	1.14×10^{0}
22.4	6.38×10^{-2}	4.09×10^{-1}
25.0	7.04×10^{-3}	1.02×10^{-1}
27.1	5.49×10^{-3}	1.09×10^{-1}
27.6	8.88×10^{-3}	1.89×10^{-1}
28.9	1.49×10^{-2}	3.82×10^{-1}
31.6	3.00×10^{-2}	1.09×10^{0}
32.9	2.92×10^{-2}	1.24×10^{0}
35.5	2.81×10^{-2}	1.60×10^{0}
36.8	2.57×10^{-2}	1.68×10^{0}
38.1	2.43×10^{-2}	1.81×10^{0}
38.6	2.36×10^{-2}	1.86×10^{0}
39.1	2.02×10^{-2}	1.66×10^{0}
39.4	1.95×10^{-2}	1.66×10^{0}
39.9	1.93×10^{-2}	1.72×10^{0}
42.5	1.03×10^{-2}	1.18×10^{0}
43.0	6.84×10^{-3}	8.13×10^{-1}
43.8	6.72×10^{-3}	8.57×10^{-1}
44.0	5.40×10^{-3}	7.02×10^{-1}
46.2	2.74×10^{-3}	4.28×10^{-1}
46.8	2.12×10^{-3}	3.47×10^{-1}
47.6	1.82×10^{-3}	3.19×10^{-1}
47.9	1.31×10^{-3}	2.35×10^{-1}
49.4	1.07×10^{-3}	2.15×10^{-1}
50.1	1.36×10^{-3}	2.88×10^{-1}
50.4	1.01×10^{-3}	2.18×10^{-1}
51.4	1.67×10^{-3}	3.89×10^{-1}
56.9	2.20×10^{-3}	7.51×10^{-1}
57.9	2.46×10^{-3}	8.95×10^{-1}
59.7	2.59×10^{-3}	1.05×10^{0}
60.7	2.48×10^{-3}	1.06×10^{0}
61.7	3.21×10^{-3}	1.46×10^{0}
64.6	1.82×10^{-3}	9.59×10^{-1}

C. 12

Table II. The differential cross section for elastic scattering of 31.2-Mev He^3 ions incident on aluminum and the ratio of the experimental cross section to the Rutherford cross section in the center-of-mass system.

$\theta_{c.m.}$ (deg)	$(d\sigma/d\Omega)$ (barns/sr)	$\frac{(d\sigma/d\Omega)}{(d\sigma/d\Omega)_R}$
13.8	3.96×10^{0}	7.43×10^{-1}
14.9	2.45×10^{0}	6.22×10^{-1}
16.0	1.51×10^{0}	5.10×10^{-1}
18.2	5.32×10^{-1}	2.99×10^{-1}
19.3	3.51×10^{-1}	2.49×10^{-1}
20.4	2.54×10^{-1}	2.25×10^{-1}
20.6	2.37×10^{-1}	2.19×10^{-1}
21.5	2.36×10^{-1}	2.57×10^{-1}
21.7	2.29×10^{-1}	2.60×10^{-1}
22.9	2.34×10^{-1}	3.27×10^{-1}
23.9	2.39×10^{-1}	3.84×10^{-1}
24.0	2.17×10^{-1}	4.00×10^{-1}
26.2	2.03×10^{-1}	4.82×10^{-1}
27.2	1.58×10^{-1}	4.39×10^{-1}
28.3	1.26×10^{-1}	4.04×10^{-1}
29.5	9.60×10^{-2}	3.36×10^{-1}
30.6	6.97×10^{-2}	3.04×10^{-1}
31.7	4.00×10^{-2}	1.99×10^{-1}
32.3	3.53×10^{-2}	1.90×10^{-1}
32.6	2.67×10^{-2}	1.49×10^{-1}
32.8	2.59×10^{-2}	1.47×10^{-1}
34.8	8.70×10^{-3}	6.26×10^{-2}
34.9	8.92×10^{-3}	6.46×10^{-2}
35.8	7.77×10^{-3}	6.27×10^{-2}
37.0	7.71×10^{-3}	6.98×10^{-2}
37.2	9.90×10^{-3}	9.25×10^{-2}
38.2	1.36×10^{-2}	1.40×10^{-1}
39.1	1.20×10^{-2}	1.36×10^{-1}
40.2	1.43×10^{-2}	1.79×10^{-1}
40.4	1.63×10^{-2}	2.08×10^{-1}
42.4	1.51×10^{-2}	2.32×10^{-1}
43.5	1.36×10^{-2}	2.31×10^{-1}
43.7	1.37×10^{-2}	2.36×10^{-1}
44.6	1.18×10^{-2}	2.21×10^{-1}
45.9	9.33×10^{-3}	1.94×10^{-1}
46.9	7.89×10^{-3}	1.78×10^{-1}
48.0	5.24×10^{-3}	1.29×10^{-1}
48.9	3.67×10^{-3}	9.68×10^{-2}
51.2	1.19×10^{-3}	3.74×10^{-2}
52.2	1.02×10^{-3}	3.42×10^{-2}
53.4	9.68×10^{-4}	3.54×10^{-2}
54.5	1.29×10^{-3}	5.10×10^{-2}
55.4	1.29×10^{-3}	5.42×10^{-2}
57.7	2.12×10^{-3}	1.03×10^{-1}
58.6	1.80×10^{-3}	9.29×10^{-2}
60.9	1.93×10^{-3}	1.14×10^{-1}
61.8	1.41×10^{-3}	8.81×10^{-2}
64.0	1.05×10^{-3}	7.52×10^{-2}
65.0	8.18×10^{-4}	6.20×10^{-2}
67.2	3.94×10^{-4}	3.36×10^{-2}
68.1	3.73×10^{-4}	3.33×10^{-2}

C. 12

Table III. The differential cross section for elastic scattering of 31.2-Mev He^3 ions incident on copper and the ratio of the experimental cross section to the Rutherford cross section in the center-of-mass system.

$\theta_{c.m.}$ (deg)	$(d\sigma/d\Omega)$ (barns/sr)	$\frac{(d\sigma/d\Omega)}{(d\sigma/d\Omega)_R}$
10.9	5.22×10^{1}	0.863×10^{0}
11.6	4.86×10^{1}	1.02×10^{0}
11.9	3.90×10^{1}	0.915×10^{0}
12.0	4.30×10^{1}	1.05×10^{0}
13.0	2.87×10^{1}	0.959×10^{0}
14.0	1.93×10^{1}	0.864×10^{0}
14.1	2.02×10^{1}	0.933×10^{0}
15.1	1.24×10^{1}	0.748×10^{0}
16.1	8.65×10^{0}	0.676×10^{0}
16.2	1.06×10^{1}	0.846×10^{0}
17.1	6.26×10^{0}	0.620×10^{0}
18.2	4.50×10^{0}	0.572×10^{0}
18.3	4.84×10^{0}	0.630×10^{0}
19.2	3.33×10^{0}	0.524×10^{0}
20.4	2.59×10^{0}	0.519×10^{0}
21.7	1.59×10^{0}	0.408×10^{0}
22.3	1.54×10^{0}	0.438×10^{0}
23.2	1.17×10^{0}	0.387×10^{0}
23.8	1.00×10^{0}	0.369×10^{0}
25.9	6.18×10^{-1}	0.325×10^{0}
26.7	5.01×10^{-1}	0.294×10^{0}
27.9	3.57×10^{-1}	0.251×10^{0}
30.0	2.16×10^{-1}	0.198×10^{0}
30.3	1.71×10^{-1}	0.163×10^{0}
30.7	1.83×10^{-1}	0.184×10^{0}
32.1	1.40×10^{-1}	0.167×10^{0}
32.6	1.38×10^{-1}	0.174×10^{0}
34.2	1.11×10^{-1}	0.172×10^{0}
34.7	1.04×10^{-1}	0.169×10^{0}
35.0	1.20×10^{-1}	0.199×10^{0}
38.3	5.68×10^{-2}	0.134×10^{0}
38.9	4.99×10^{-2}	0.125×10^{0}
42.5	2.23×10^{-2}	0.784×10^{-1}
43.0	1.99×10^{-2}	0.733×10^{-1}
46.6	1.33×10^{-2}	0.665×10^{-1}
47.6	1.37×10^{-2}	0.741×10^{-1}
50.8	8.76×10^{-3}	0.604×10^{-1}
51.9	7.91×10^{-3}	0.590×10^{-1}
54.9	3.95×10^{-3}	0.365×10^{-1}
55.4	3.41×10^{-3}	0.325×10^{-1}
59.0	2.11×10^{-3}	0.253×10^{-1}
59.5	2.04×10^{-3}	0.252×10^{-1}
63.1	1.88×10^{-3}	0.288×10^{-1}
63.6	1.74×10^{-3}	0.273×10^{-1}

C. 12

Table IV. The differential cross section for elastic scattering of 31.2-Mev He^3 ions incident on tin of natural isotopic composition and the ratio of the experimental cross section to the Rutherford cross section in the c. m. system.

$\theta_{c.m.}$ (deg)	$(d\sigma/d\Omega)$ (barns/sr)	$\frac{(d\sigma/d\Omega)}{(d\sigma/d\Omega)_R}$
10.7	1.82×10^{2}	1.00×10^{0}
11.7	1.33×10^{2}	1.04×10^{0}
12.7	9.30×10^{1}	9.94×10^{-1}
13.7	7.13×10^{1}	1.03×10^{0}
14.7	5.58×10^{1}	1.07×10^{0}
15.8	4.32×10^{1}	1.10×10^{0}
16.8	3.31×10^{1}	1.08×10^{0}
17.8	2.80×10^{1}	1.15×10^{0}
18.9	2.25×10^{1}	1.17×10^{0}
19.2	2.20×10^{1}	1.22×10^{0}
20.2	1.62×10^{1}	1.09×10^{0}
21.2	1.30×10^{1}	1.06×10^{0}
22.2	1.06×10^{1}	1.04×10^{0}
23.3	9.04×10^{0}	1.07×10^{0}
24.3	7.12×10^{0}	9.99×10^{-1}
26.2	4.15×10^{0}	7.83×10^{-1}
26.3	4.70×10^{0}	9.01×10^{-1}
28.4	2.80×10^{0}	7.30×10^{-1}
29.7	2.29×10^{0}	7.07×10^{-1}
30.1	2.00×10^{0}	6.50×10^{-1}
30.4	1.88×10^{0}	6.35×10^{-1}
31.0	1.79×10^{0}	6.54×10^{-1}
32.1	1.49×10^{0}	6.22×10^{-1}
32.4	1.33×10^{0}	5.75×10^{-1}
33.1	1.13×10^{0}	5.32×10^{-1}
34.5	8.67×10^{-1}	4.79×10^{-1}
35.1	7.84×10^{-1}	4.64×10^{-1}
37.2	5.48×10^{-1}	4.03×10^{-1}
37.6	5.40×10^{-1}	4.15×10^{-1}
39.2	4.01×10^{-1}	3.62×10^{-1}
41.2	2.74×10^{-1}	3.00×10^{-1}
43.7	1.89×10^{-1}	2.60×10^{-1}
46.3	1.33×10^{-1}	2.27×10^{-1}
46.7	1.21×10^{-1}	2.18×10^{-1}
47.4	1.04×10^{-1}	1.94×10^{-1}
49.4	7.39×10^{-2}	1.61×10^{-1}
52.8	5.01×10^{-2}	1.40×10^{-1}
53.4	4.24×10^{-2}	1.23×10^{-1}
54.9	3.79×10^{-2}	1.22×10^{-1}
56.9	3.05×10^{-2}	1.12×10^{-1}
57.5	2.68×10^{-2}	1.03×10^{-1}
60.9	1.98×10^{-2}	9.33×10^{-2}
61.6	1.77×10^{-2}	8.68×10^{-2}

C. 12

Table V. The differential cross section for elastic scattering of 31.2-Mev He^3 ions incident on tin enriched to 85% in Sn^{120} and the ratio of the experimental cross section to the Rutherford cross section in the c.m. system.

$\theta_{c.m.}$ (deg)	$(d\sigma/d\Omega)$ (barns/sr)	$\frac{(d\sigma/d\Omega)}{(d\sigma/d\Omega)_R}$
20.8	9.85×10^{0}	7.46×10^{-1}
25.9	3.48×10^{0}	6.33×10^{-1}
30.4	1.41×10^{0}	4.76×10^{-1}
31.0	1.28×10^{0}	4.67×10^{-1}
35.5	5.90×10^{-1}	3.64×10^{-1}
36.1	5.67×10^{-1}	3.75×10^{-1}
40.6	2.38×10^{-1}	2.44×10^{-1}
41.2	2.39×10^{-1}	6.62×10^{-1}
46.3	1.19×10^{-1}	2.03×10^{-1}
50.8	5.58×10^{-2}	1.35×10^{-1}
51.4	5.80×10^{-2}	1.46×10^{-1}
56.5	2.93×10^{-2}	8.71×10^{-2}
60.9	1.80×10^{-2}	8.49×10^{-2}
61.6	1.73×10^{-2}	8.48×10^{-2}
66.6	7.90×10^{-3}	5.13×10^{-2}
69.0	5.90×10^{-3}	4.32×10^{-2}
71.7	4.84×10^{-3}	4.07×10^{-2}
75.1	3.33×10^{-3}	3.30×10^{-2}
77.7	2.50×10^{-3}	2.77×10^{-2}
81.1	1.76×10^{-3}	2.24×10^{-2}
83.7	1.23×10^{-3}	1.74×10^{-2}
86.1	1.11×10^{-3}	1.72×10^{-2}
92.1	6.31×10^{-4}	1.21×10^{-2}
95.7	4.25×10^{-4}	9.18×10^{-3}
98.1	3.84×10^{-4}	8.93×10^{-3}
101.7	2.48×10^{-4}	6.41×10^{-3}
104.1	2.04×10^{-4}	5.64×10^{-3}
107.7	1.45×10^{-4}	4.39×10^{-3}
112.0	1.07×10^{-4}	3.61×10^{-3}
113.6	1.03×10^{-4}	3.61×10^{-3}
116.0	1.01×10^{-4}	3.74×10^{-3}
119.6	7.06×10^{-5}	2.81×10^{-3}

C. 12

Table VI. The differential cross section for elastic scattering of 31.2-Mev He^3 ions incident on bismuth and the ratio of the experimental cross section to the Rutherford cross section in the center-of-mass system.

$\theta_{c.m.}$ (deg)	$(d\sigma/d\Omega)$ (barns/sr)	$\frac{(d\sigma/d\Omega)}{(d\sigma/d\Omega)_R}$
10.6	4.86×10^{2}	9.36×10^{-1}
11.2	3.66×10^{2}	8.78×10^{-1}
11.6	3.59×10^{2}	9.89×10^{-1}
12.6	2.39×10^{2}	9.16×10^{-1}
13.6	1.79×10^{2}	9.32×10^{-1}
14.6	1.31×10^{2}	9.04×10^{-1}
15.6	9.91×10^{1}	8.93×10^{-1}
16.6	8.09×10^{1}	9.30×10^{-1}
17.7	6.26×10^{1}	9.43×10^{-1}
18.7	5.16×10^{1}	9.43×10^{-1}
18.9	4.68×10^{1}	9.00×10^{-1}
19.9	3.91×10^{1}	9.24×10^{-1}
20.9	3.13×10^{1}	8.97×10^{-1}
21.2	2.96×10^{1}	8.97×10^{-1}
21.5	2.71×10^{1}	8.69×10^{-1}
22.1	2.41×10^{1}	8.61×10^{-1}
22.9	2.05×10^{1}	8.44×10^{-1}
23.0	2.14×10^{1}	8.95×10^{-1}
23.1	2.00×10^{1}	8.51×10^{-1}
24.1	1.63×10^{1}	8.19×10^{-1}
25.0	1.40×10^{1}	8.14×10^{-1}
25.1	1.47×10^{1}	8.70×10^{-1}
26.0	1.19×10^{1}	8.10×10^{-1}
26.1	1.13×10^{1}	7.79×10^{-1}
27.0	1.11×10^{1}	8.74×10^{-1}
27.2	1.02×10^{1}	8.23×10^{-1}
29.0	9.02×10^{0}	9.40×10^{-1}
29.2	8.74×10^{0}	9.35×10^{-1}
29.8	7.67×10^{0}	8.87×10^{-1}
30.2	6.97×10^{0}	8.51×10^{-1}
30.7	6.49×10^{0}	8.44×10^{-1}
30.8	6.94×10^{0}	9.15×10^{-1}
31.0	6.78×10^{0}	9.17×10^{-1}
31.2	6.52×10^{0}	9.03×10^{-1}
31.7	6.50×10^{0}	9.59×10^{-1}
31.8	6.37×10^{0}	9.50×10^{-1}
32.2	5.83×10^{0}	9.14×10^{-1}
32.9	5.63×10^{0}	9.59×10^{-1}
33.2	5.22×10^{0}	9.17×10^{-1}
33.9	5.43×10^{0}	1.04×10^{0}
34.2	4.64×10^{0}	9.19×10^{-1}
34.7	4.27×10^{0}	8.93×10^{-1}
34.9	4.77×10^{0}	1.03×10^{0}
35.1	4.58×10^{0}	1.00×10^{0}
35.2	4.05×10^{0}	8.96×10^{-1}
35.7	3.97×10^{0}	9.30×10^{-1}
36.8	3.52×10^{0}	9.26×10^{-1}
36.9	3.75×10^{0}	9.97×10^{-1}
37.1	3.51×10^{0}	9.54×10^{-1}
37.8	3.32×10^{0}	9.68×10^{-1}
37.9	3.27×10^{0}	9.62×10^{-1}
38.8	2.94×10^{0}	9.51×10^{-1}

C. 12

Table VI. Bi + 31.2-Mev He^3 (continued)

$\theta_{c.m.}$ (deg)	$(d\sigma/d\Omega)$ (barns/sr)	$(d\sigma/d\Omega)/(d\sigma/d\Omega)_R$
38.9	3.15×10^{0}	1.03×10^{0}
39.1	2.73×10^{0}	9.05×10^{-1}
39.8	2.50×10^{0}	8.87×10^{-1}
40.8	2.19×10^{0}	8.55×10^{-1}
40.9	2.37×10^{0}	9.37×10^{-1}
41.2	2.47×10^{0}	1.00×10^{0}
41.8	1.88×10^{0}	8.07×10^{-1}
43.0	1.94×10^{0}	9.28×10^{-1}
43.8	1.56×10^{0}	8.00×10^{-1}
45.0	1.49×10^{0}	8.47×10^{-1}
45.2	1.50×10^{0}	8.67×10^{-1}
47.0	1.29×10^{0}	8.66×10^{-1}
47.4	1.06×10^{0}	7.36×10^{-1}
47.9	9.63×10^{-1}	6.93×10^{-1}
49.2	9.46×10^{-1}	7.51×10^{-1}
51.3	8.24×10^{-1}	7.63×10^{-1}
51.4	6.97×10^{-1}	6.51×10^{-1}
51.9	6.33×10^{-1}	6.15×10^{-1}
52.1	6.31×10^{-1}	6.25×10^{-1}
54.3	5.43×10^{-1}	6.28×10^{-1}
55.3	5.78×10^{-1}	7.11×10^{-1}
55.5	4.47×10^{-1}	5.57×10^{-1}
55.9	4.00×10^{-1}	5.12×10^{-1}
56.1	4.70×10^{-1}	6.08×10^{-1}
58.1	3.61×10^{-1}	5.32×10^{-1}
59.3	3.01×10^{-1}	4.78×10^{-1}
59.5	2.78×10^{-1}	4.47×10^{-1}
60.1	3.29×10^{-1}	5.48×10^{-1}
61.5	2.19×10^{-1}	3.97×10^{-1}
62.0	1.92×10^{-1}	3.58×10^{-1}
63.3	2.29×10^{-1}	4.60×10^{-1}
64.2	2.01×10^{-1}	4.27×10^{-1}
65.5	1.68×10^{-1}	3.81×10^{-1}
66.0	1.40×10^{-1}	3.26×10^{-1}
66.4	1.55×10^{-1}	3.69×10^{-1}
67.4	1.57×10^{-1}	3.94×10^{-1}
68.2	1.33×10^{-1}	3.47×10^{-1}
70.2	9.35×10^{-2}	2.71×10^{-1}
72.2	9.91×10^{-2}	3.16×10^{-1}
75.4	7.67×10^{-2}	2.84×10^{-1}
76.2	6.32×10^{-2}	2.42×10^{-1}
79.4	5.31×10^{-2}	2.34×10^{-1}
80.2	4.79×10^{-2}	2.19×10^{-1}
81.5	3.72×10^{-2}	1.79×10^{-1}
83.4	3.70×10^{-2}	1.92×10^{-1}
84.2	3.38×10^{-2}	1.82×10^{-1}
88.2	2.31×10^{-2}	1.43×10^{-1}
90.4	2.03×10^{-2}	1.36×10^{-1}
92.2	1.55×10^{-2}	1.11×10^{-1}
94.4	1.45×10^{-2}	1.12×10^{-1}
98.4	9.69×10^{-3}	8.43×10^{-2}

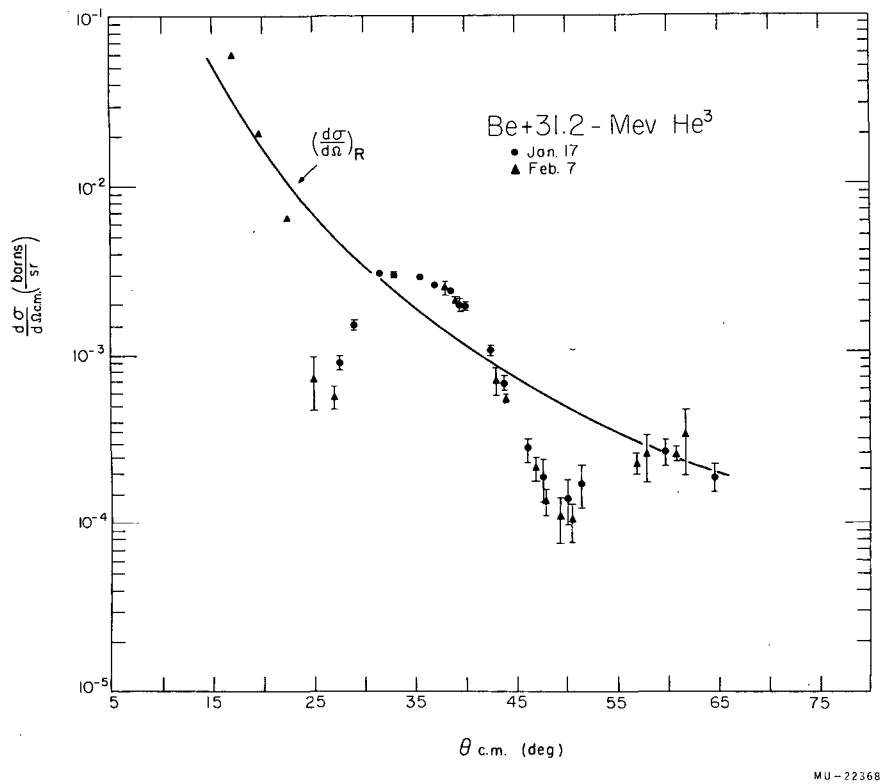

Fig. C. 12-1. Angular distribution for elastic scattering of 31.2-Mev He^3 ions from beryllium. The symbols indicate the experimental points and their standard deviations; the solid line is the calculated differential cross section for Rutherford scattering in the center-of-mass system.

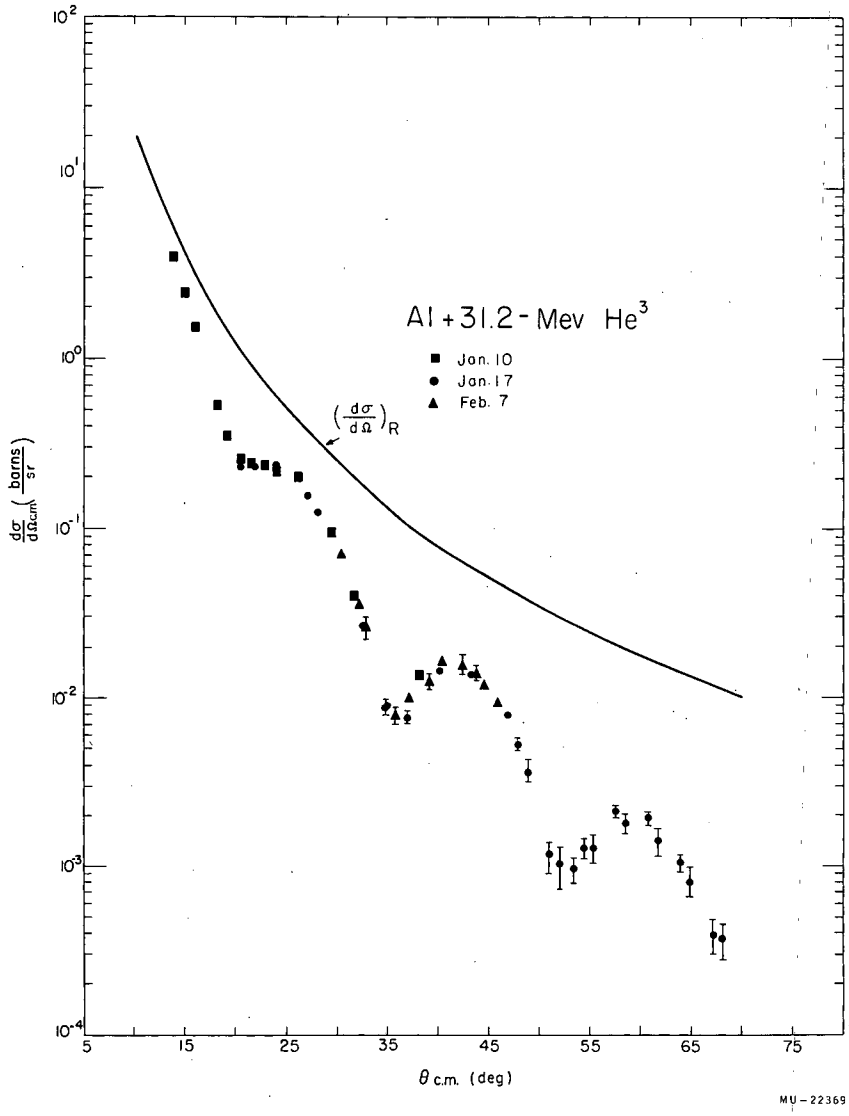

Fig. C.12-2. Angular distribution for elastic scattering of 31.2-Mev He^3 ions from aluminum. The symbols indicate the experimental points and their standard deviations; the solid line is the calculated differential cross section for Rutherford scattering in the c.m. system.

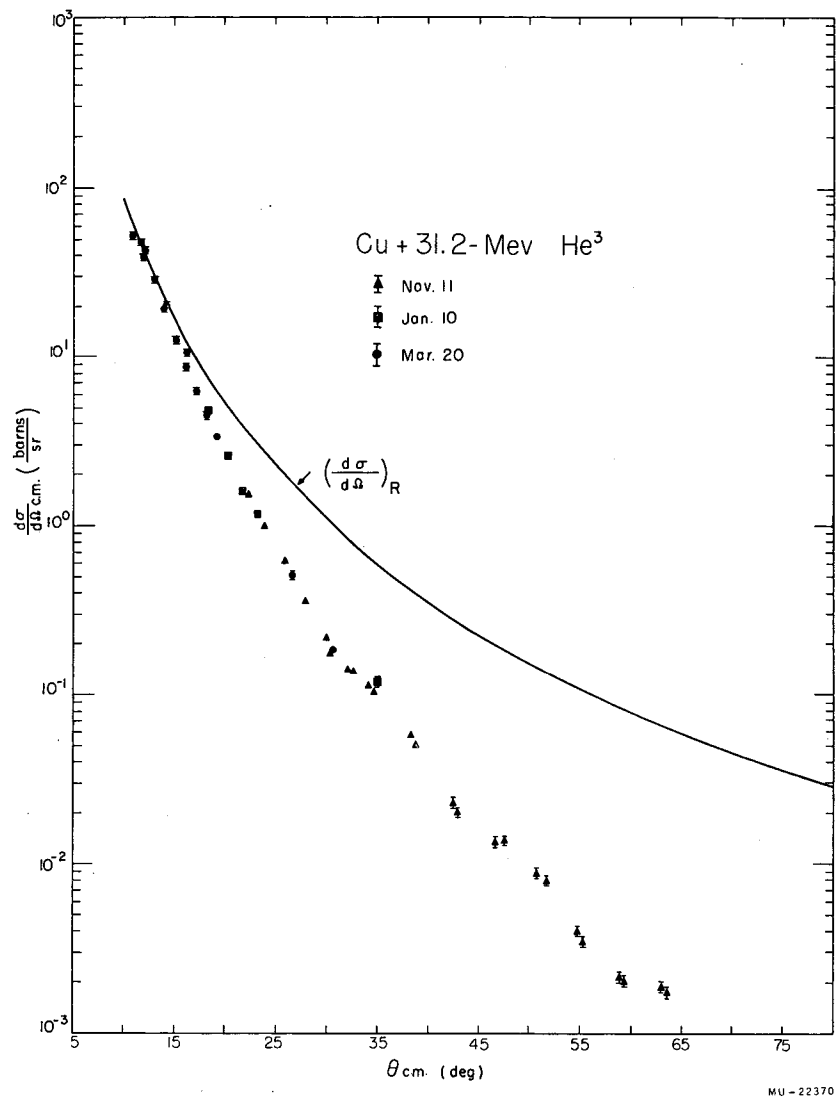

Fig. C.12-3. Angular distribution for elastic scattering of 31.2-Mev He^3 ions from copper. The symbols indicate the experimental points and their standard deviations; the solid line is the calculated differential cross section for Rutherford scattering in the c.m. system.

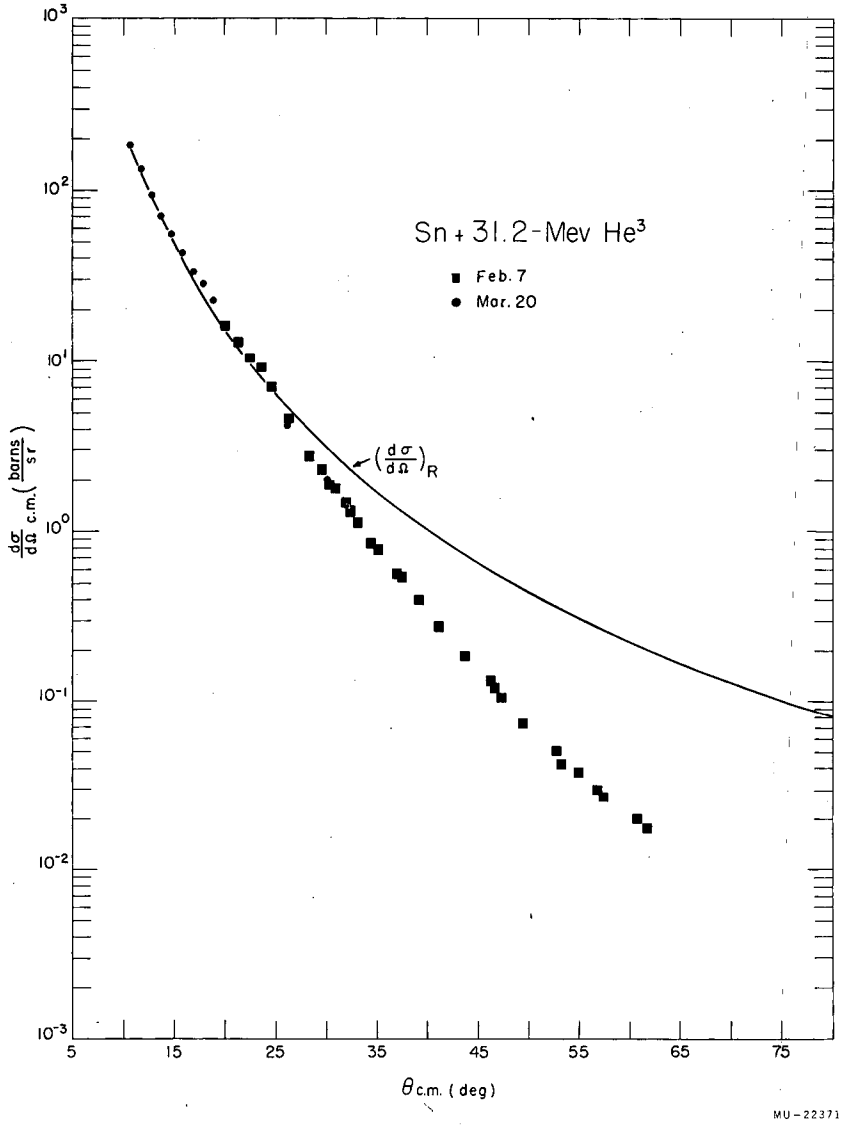

Fig. C.12-4. Angular distribution for elastic scattering of 31.2-Mev He^3 ions from tin of natural isotopic composition. The symbols indicate the experimental points and their standard deviations; the solid line is the calculated differential cross section for Rutherford scattering in the c.m. system.

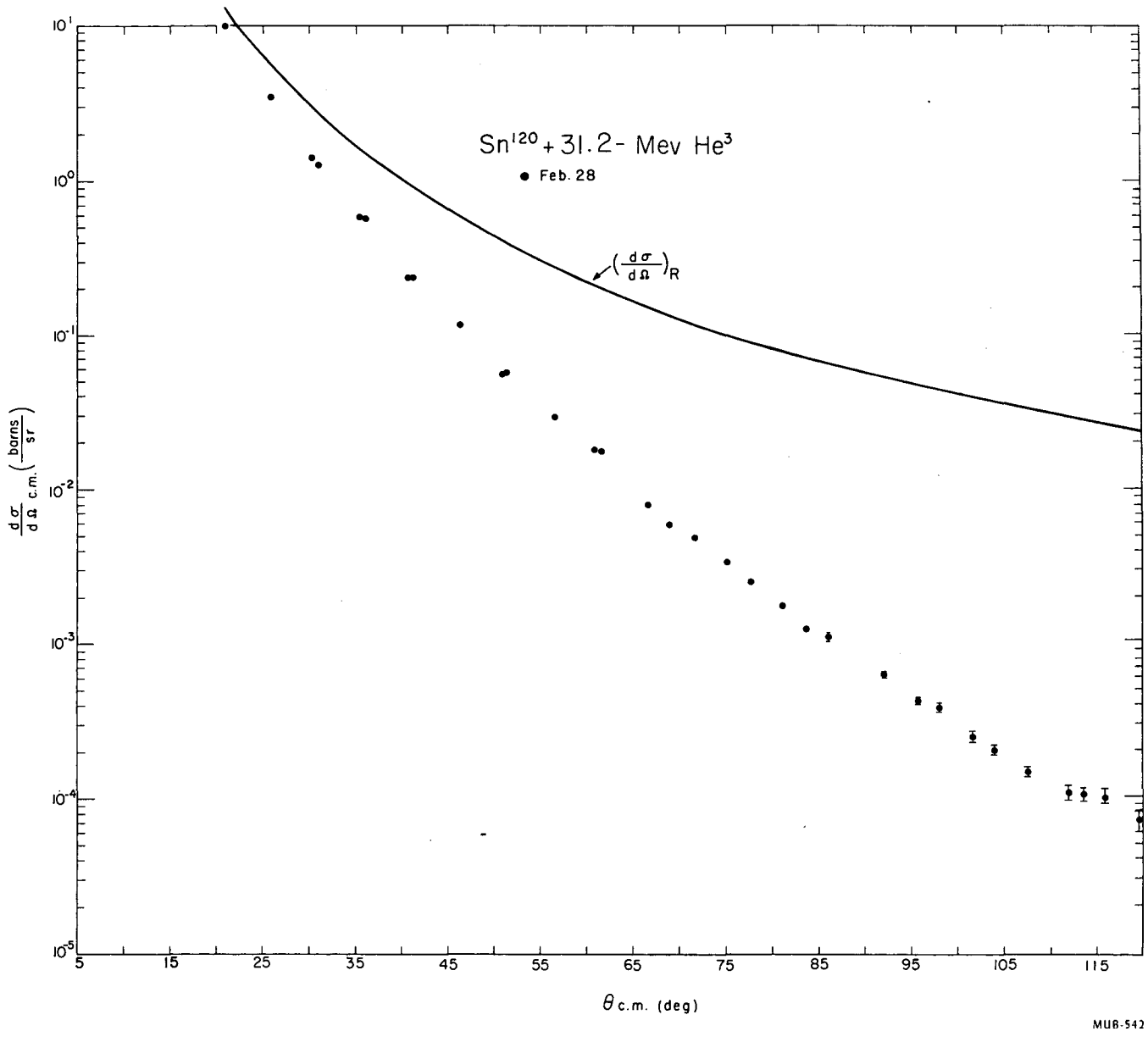

Fig. C.12-5. Angular distribution for elastic scattering of 31.2-Mev He^3 ions from tin enriched to 85% in Sn^{120}. The symbols indicate the experimental points and their standard deviations; the solid line is the calculated differential cross section for Rutherford scattering in the c.m. system.

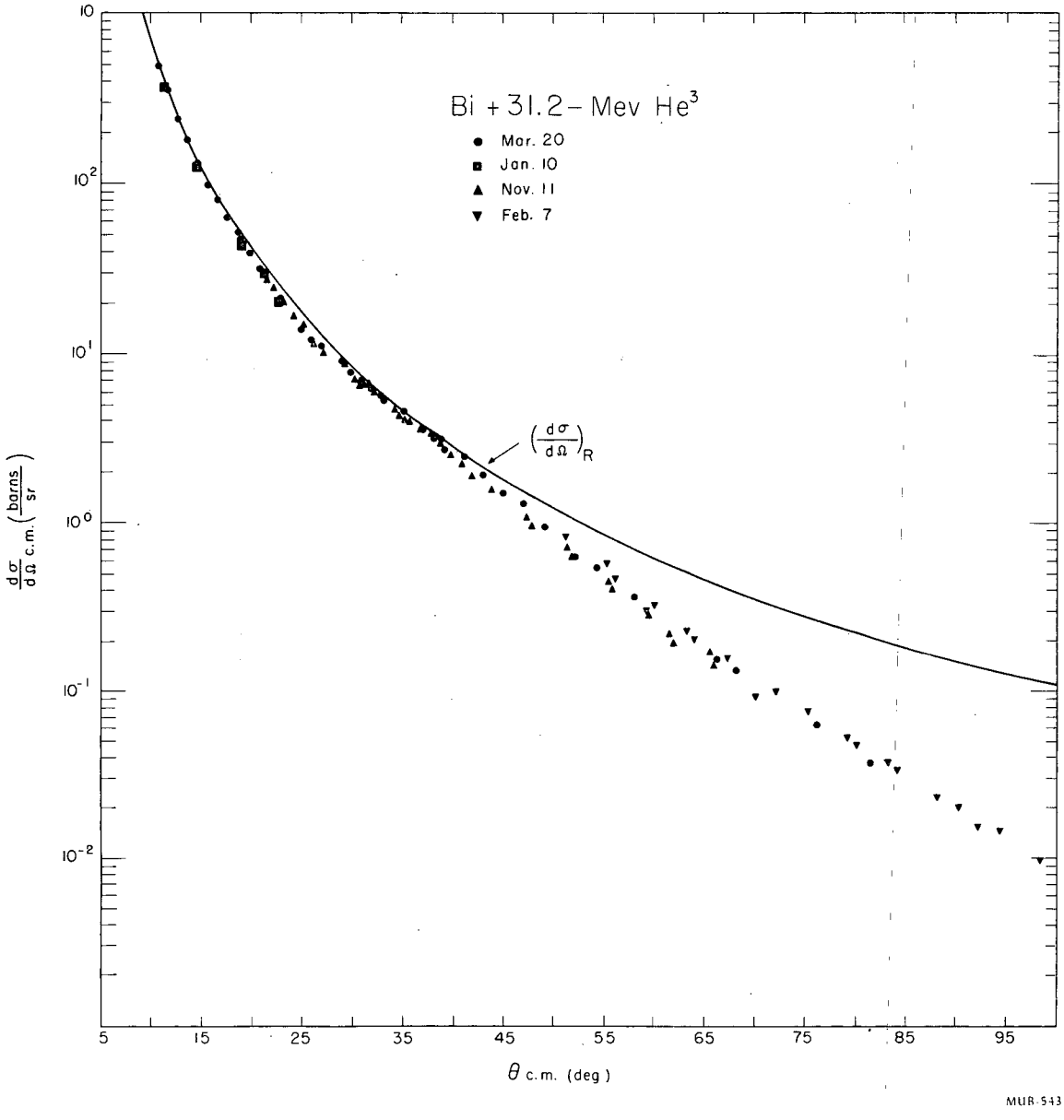

Fig. C. 12-6. Angular distribution for elastic scattering of 31.2-Mev He^3 ions from bismuth. The symbols indicate the experimental points and their standard deviations; the solid line is the calculated differential cross section for Rutherford scattering in the c. m. system.

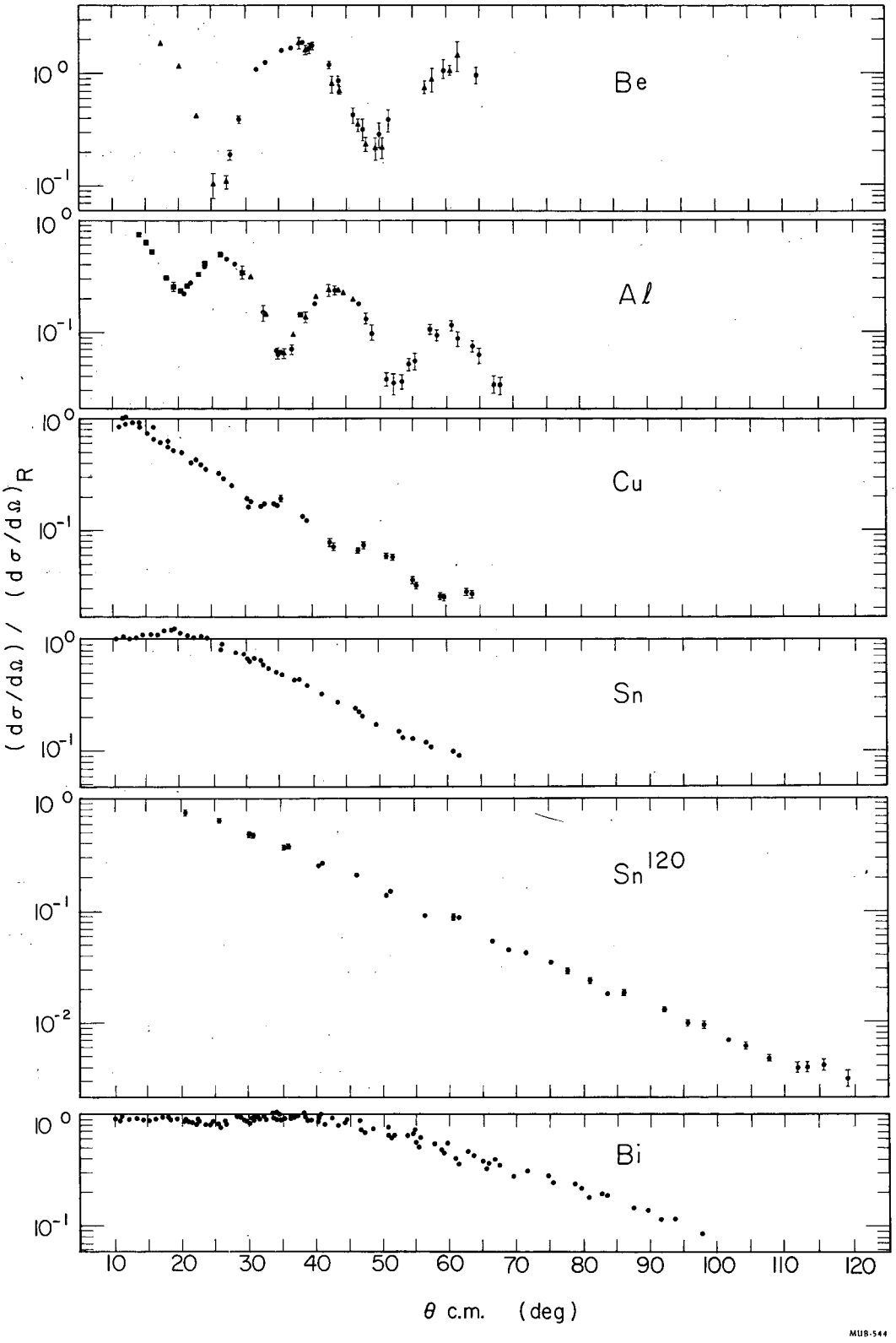

Fig. C. 12-7. The ratio of the experimental differential elastic scattering cross sections to the Rutherford scattering cross sections for 31.2-Mev He^3 ions incident on various elements. The scale of the ordinate is divided between the elements.

13. RANGES AND RANGE STRAGGLING OF TERBIUM-149, ASTATINE, AND POLONIUM

Lester Winsberg and John M. Alexander

Measurements of the kinetic energies of the heavy recoil atoms are very informative in the study of nuclear reactions. One of the best experimental means to this end is the measurement of recoil ranges. Therefore it is important in nuclear science as well as in atomic physics to have measurements of range and range straggling as a function of recoil energy.

We have studied the recoil properties of Tb^{149}, At, and Po produced in heavy-ion (HI) bombardments of various targets. Strong arguments are presented for the formation of a compound nucleus in HI, xn and HI, pxn reactions. By use of the compound-nucleus model for these reactions the recoil energy has been calculated, and ranges and range straggling have been measured. Targets of Cs, Ba, La, Ce, Pr, Ir, Pt, Au, and Re have been irradiated with beams of C^{12}, N^{14}, O^{16}, O^{18}, Ne^{20}, and Ne^{22} from the Berkeley heavy-ion linear accelerator.

The dependence on recoil energy of range and range straggling has been obtained for Tb^{149} in Al (recoil energies of 4 to 29 Mev), for At and Po in Al (4 to 15 Mev), and for At and Po in Au (4 to 9 Mev). This work is reported in detail by these authors, Phys. Rev. 121, 518 (1961).

14. POLARIZATION IN p-He^4 SCATTERING AT 22 Mev

Homer E. Conzett, George Igo, and Aharon Nir*

Following the method first used by Rosen and Brolley[1] three years ago, we have developed a beam of 22-Mev protons, using p-He^4 scattering as the polarizing mechanism. The availability of experimental information on p-He^4 scattering is summarized in Table I.

*On leave from the Weizmann Institute, Rehovoth, Israel.

[1] L. Rosen and J. E. Brolley, Jr., Phys. Rev. 107, 1454 (1957).

Table I. Availability of data on p-He^4 scattering

E_{lab} (Mev)	Data $\sigma(\theta)$	Data $P(\theta)$	Reference
0.95 to 18	X	-	2[a]
20.1	X	-	3
39.8	X	-	4
1.37	-	One angle	
2.02	-	One angle	5
3.58	-	One angle	
7.8	-	One angle	
11.4	-	One angle	6
14.4	-	One angle	
10	-	Ten angles	1
15.5	-	Two angles	2

[a]Reference 2 contains a list of authors whose work is referred to here.

Phase shifts derived from analyses of the very complete differential cross section data have been used to calculate the polarizations; and finally, description of the p-α interaction in terms of an effective two-body potential with a central and a spin-orbit term has resulted in interpolations and predictions of the phase shifts, and thus the polarizations, up to 40 Mev.[7] It should be noted (table) that the polarization measurements at these energies are sparse; and, since the polarizations are more sensitive than the angular distributions of the differential cross sections to uncertainties in the phase shifts, it is important to extend these measurements in order to provide further checks on the theory, and thus to enable experimenters to use the calculated values more confidently.

Figure C. 14-1 is a schematic drawing of our scattering geometry. Protons, knocked on at 25 deg by the α-particle beam incident on an H_2 gas target, are collimated into a second scattering chamber. Measured left-right asymmetries in the second scattering give us $P_2(\theta)$, the polarization that would be induced in the second scattering if the proton beam were unpolarized. The following conditions apply:

[2]K. W. Brockman, Jr., Phys. Rev. 108, 1000 (1957).

[3]J. W. Burkig, Phys. Rev. 116, 674 (1959).

[4]M. K. Russell and J. H. Williams, Phys. Rev. 106, 286 (1957).

[5]M. J. Scott, Phys. Rev. 110, 1398 (1958).

[6]J. Sanada et al., J. Phys. Soc. (Japan) 15, 754 (1960).

[7]J. L. Gammel and R. M. Thaler, Phys. Rev. 107, 2041 (1958).

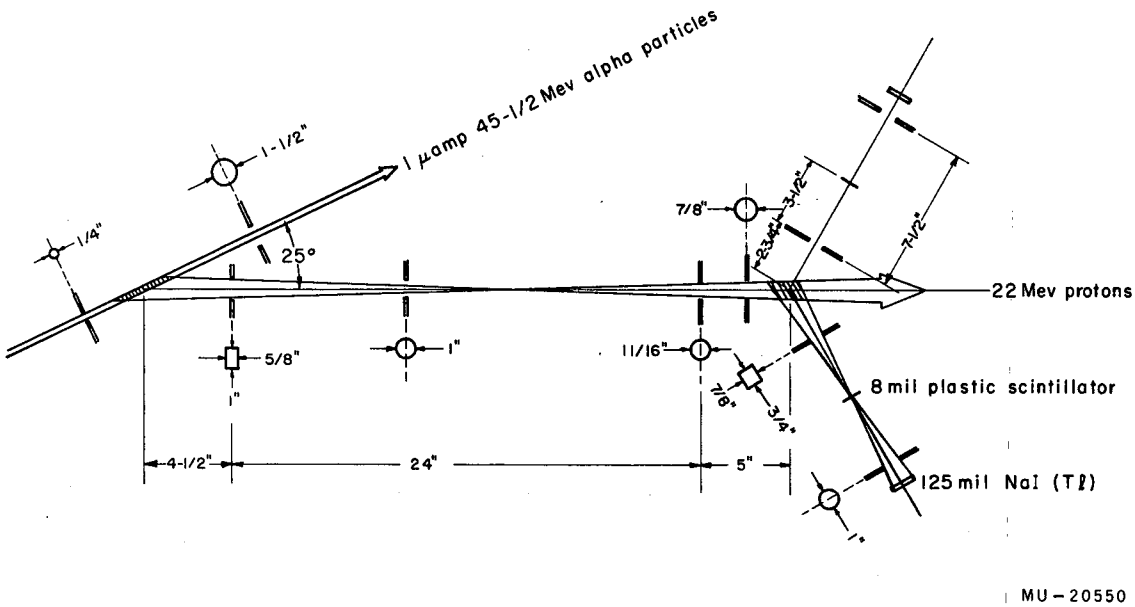

Fig. C. 14-1. Schematic drawing of scattering geometry.

1. First scattering: 8 atm of H_2, E_α = 43.1 Mev, Ep = 23 Mev.

2. Second scattering: 6 atm of He^4, Ep = 22 Mev, polarization of proton beam essentially 100%.[1]

3. This geometry gives us second-scattered counting rates in each counter of about 3000 per hour in p-He^4 scattering at an angle of 45 deg.

4. We use a simple coincidence counting arrangement to reduce the background.

A pulse from the plastic scintillator photomultiplier tube is used to gate on the pulse-height analyzer which records the pulses from the C_sI crystal counter.

A measurement of P_2 comes directly from the asymmetry measurement, because $E = (L-R)/(L+R) = P_1P_2$, and our P_1 is 100% within something like 2 or 3%. Figure C. 14-2 shows, then, our results to date on p-He^4 polarization at 22 Mev. The probable errors indicated are due only to counting statistics. The solid curve represents calculated values from Gammil and Thaler.[7]

15. SURVEY OF TRITIUM-PRODUCING NUCLEAR REACTIONS (*)

Jose Gonzalez-Vidal and William H. Wade†

Previously we have reported on the α, t, p, t, and d, t reactions in the heavy elements.[1] In the work reported here this investigation of the integrated cross sections of these reactions has been extended to light and intermediate elements.

The experimental procedure for these studies has already been discussed elsewhere.[1, 2, 3] It consisted essentially of the bombardment of thick metal foils with beams of the desired particles. The bombardment was followed by thermal extraction of the tritium produced in the target. The tritium activity was measured with a proportional counter. Only full-energy beams were used, since degrading foils would introduce an extraneous source of tritons.

Since, owing to their long range, tritons appearing in one foil may have originated in another, it was impossible to obtain true excitation functions. "Apparent" cross sections for each foil were calculated on the basis of thin-target approximations as if the beam were incident on each

*Brief presentation of work reported in Phys. Rev. 120, 1354 (1960).

†Now at the Chemistry Department, University of Texas, Austin 12, Texas.

[1] W. H. Wade, J. Gonzalez-Vidal, R. A. Glass, and G. T. Seaborg, Phys. Rev. 107, 1311 (1957).

[2] R. L. Wolfgang and W. Libby, Phys. Rev. 85, 437 (1952).

[3] L. A. Currie, W. F. Libby, and R. L. Wolfgang, Phys. Rev. 101, 1557 (1956).

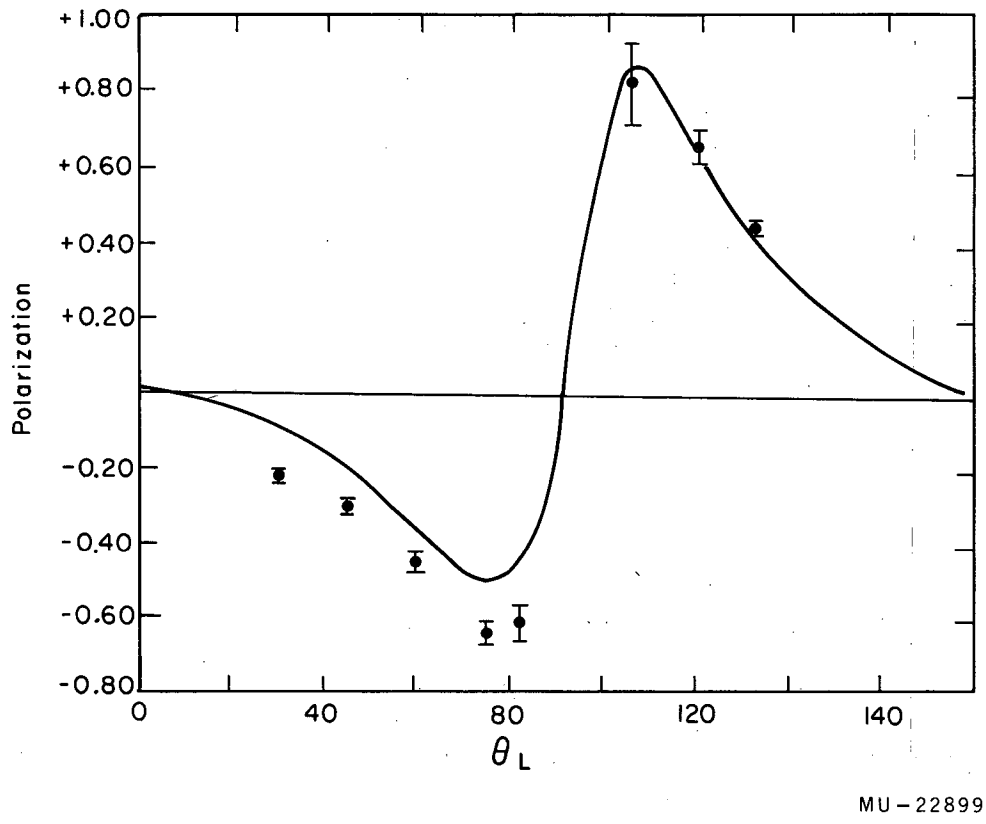

Fig. C. 14-2. p-He^4 polarization at 22 Mev.

foil in which tritons were detected. Summation of these apparent cross sections over total foil depth can be made to give the triton yield per incident bombarding particle.

α, t Cross Sections

Figure C.15-1 shows the apparent excitation functions for this reaction for three elements. From the shape of these curves the periodic table can be divided into three regions. First there is a light-element region (Fig. C. 15-1a) whose excitation functions are characterized by a peak occurring in foils in which the beam still has high energy and a long "tail" extending well beyond the point at which the beam has been completely degraded.

Second, there is a region of medium-weight elements (Fig. C. 15-1b), characterized by the presence of two peaks; a first peak similar to that of the preceding region and a second peak which appears in foils the beam has never reached.

Figure C. 15-1c represents a typical case of the third region for a heavy nonfissionable element. Only one peak is in evidence; it always appears at a target depth greater than the beam range.

The markings R, Q, and B in the figures indicate the end of the range of the incident beam, the position at which the beam has been degraded to its classical Coulomb-barrier energy, and an energy corresponding to the reaction threshold, respectively.

p, t and d, t Cross Sections

Here the excitation functions show broad maxima throughout the periodic table. Most of the tritium appears in foils where the beam energy is high enough to surmount the Coulomb barrier and to satisfy the threshold requirements of the reaction.

Integrated Cross Sections

Figures C. 15-2 and C. 15-3 show the integrated cross sections vs Z, for p, t and d, t reactions. Figure C. 15-4 shows the same type of curve for d, t reactions. For this case, the apparent excitation functions can be roughly analyzed into two components, one component corresponding to low-energy tritons and a component given by high-energy tritons.

Discussion

p, t and d, t Reactions

Previous work[2, 3, 4] has shown that both compound-nucleus and direct-interaction processes play an important role in these reactions. The curve for integrated cross section vs Z can be interpreted as a strong compound-nucleus contribution at low Z (decreasing rapidly as Z increases) and a direct-interaction contribution which increases with nuclear size. These effects combine to give the observed curve shape.

[4] B. L. Cohen and T. H. Handley, Phys. Rev. 93, 514 (1954).

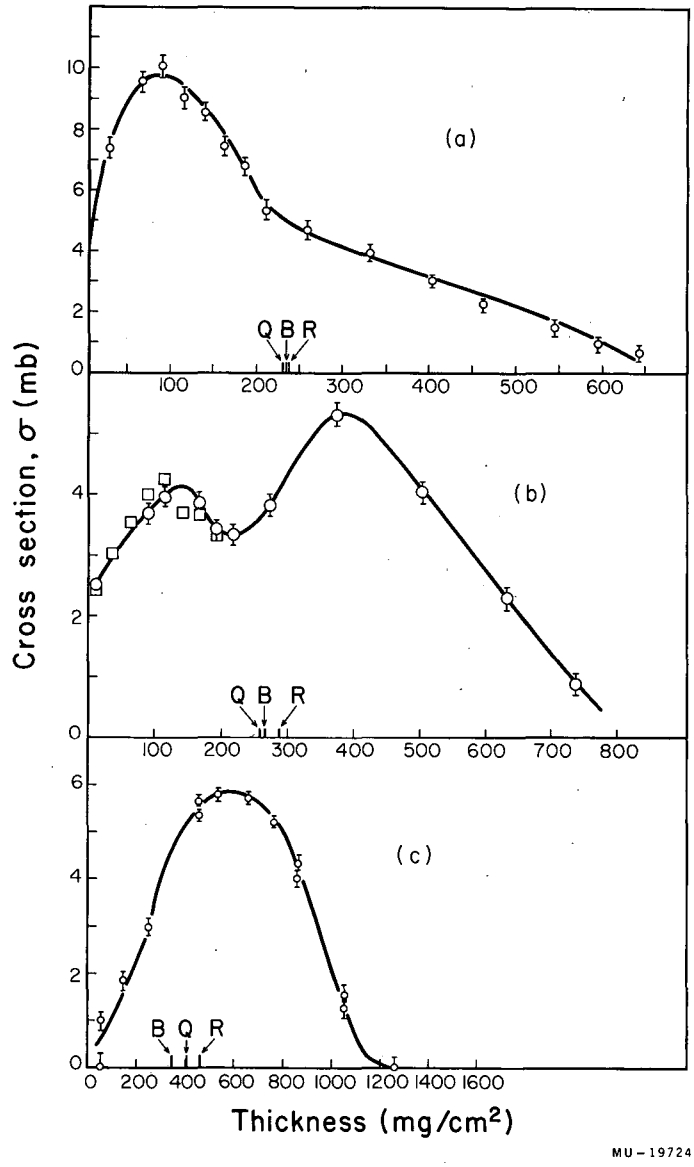

Fig. C.15-1. (a) Apparent excitation function for the $Al^{27}(\alpha, t)Si^{28}$ reaction.
(b) Apparent excitation function for the $Cu^{63,65}(\alpha, t)Zn^{64,66}$ reaction.
(c) Apparent excitation function for the $Au^{197}(\alpha, t)Hg^{198}$ reaction.

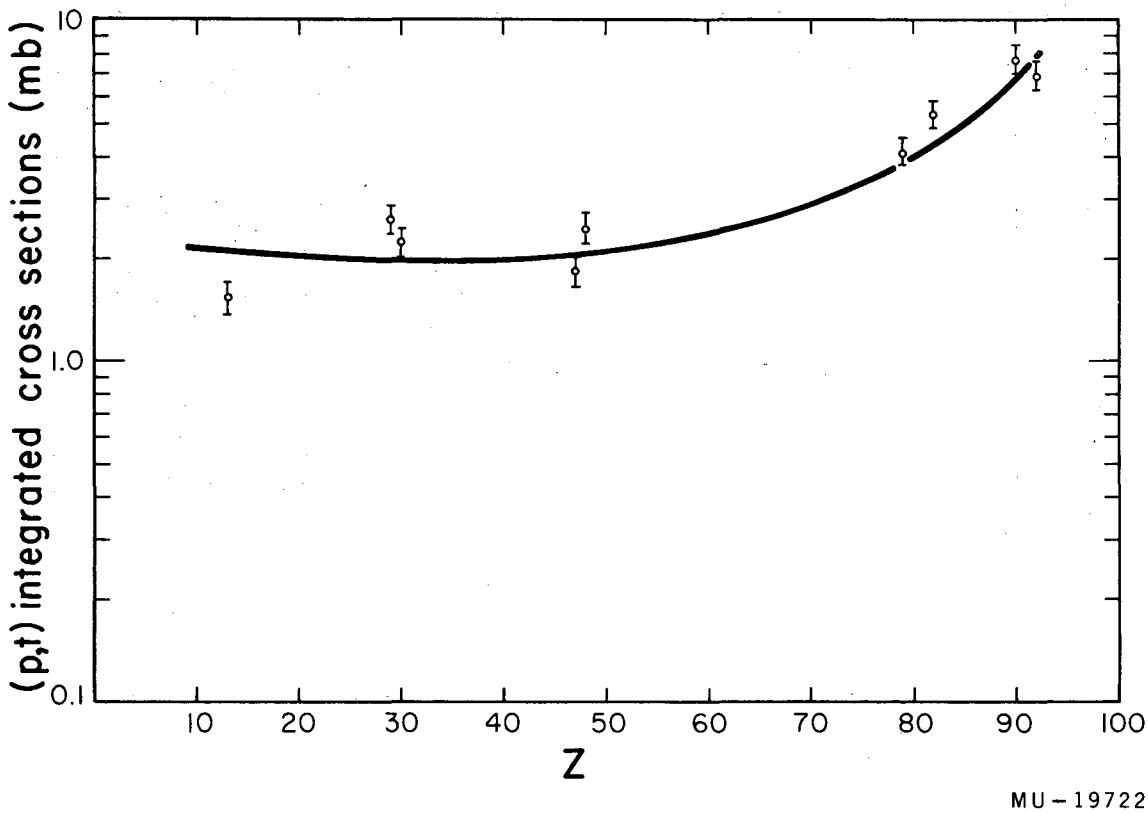

Fig. C. 15-2. Integrated cross section (in mb) for the p, t reaction vs atomic number Z.

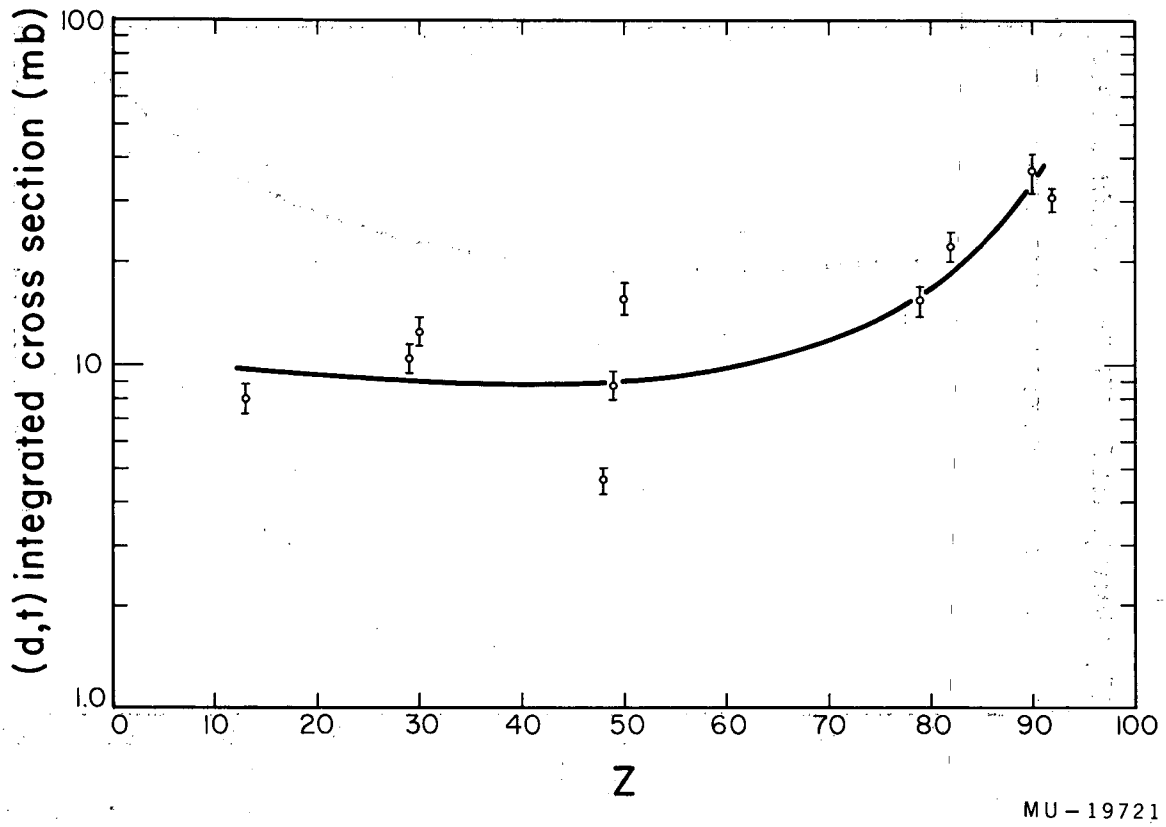

Fig. C.15-3. Integrated cross section in mb for the d, t reaction vs atomic number Z.

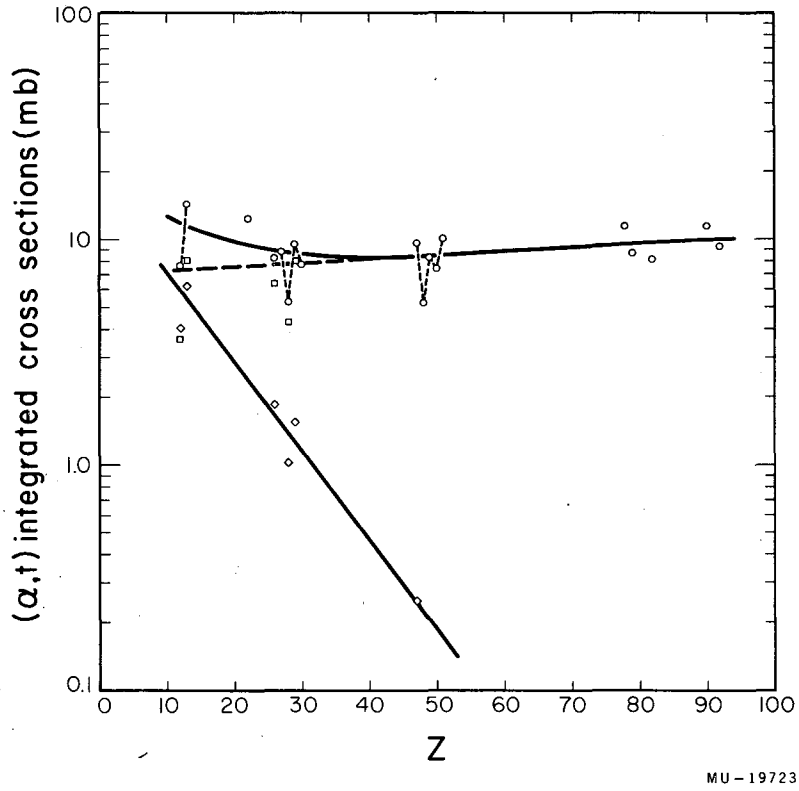

Fig. C. 15-4. Integrated cross section in mb for the α, t reaction vs atomic number Z.
O total integrated cross section
◇ compound-nucleus contribution
□ direct-interaction component.

α, t Reactions

The most striking result of the apparent excitation functions is the presence of tritons in foils that the beam cannot reach. This observation can have only one interpretation: tritons must be emitted in the forward direction with velocities comparable to those of the α particles. That is by direct interaction. At low Z, however, there is a large number of low-energy tritons; these have been ascribed to compound-nucleus processes. This interpretation seems in line with the behavior of the curve for total yield vs Z.

In all these reactions the direct-interaction part of the process appears to be a major component of the reaction mechanism.

16. SELF-TRANSFER OF CALIFORNIUM-252

Raymond C. Gatti, Llad Phillips, Harry R. Bowman, and Stanley G. Thompson

It has previously been observed that when an electroplated sample of Cf^{252} is placed parallel to a negatively charged collecting plate in vacuum Cf^{252} transfers from the sample to the collector plate.[1] This process of self-transfer has been used extensively in sample-preparation work. It was thought to be of sufficient interest to warrant studying the transfer mechanism further.

There is a maximum self-transfer rate for Cf^{252} samples that is a function of the source density in $\mu g/cm^2$ (Fig. C. 16-1). This maximum self-transfer rate can be achieved without applying a potential difference to the collecting foil if the pressure is reduced (Fig. C. 16-2). A study of transfer rate at pressures varying from 20 to 50 microns and using collecting foils at separation distances of 1/4, 5/8, 7/8, 2-1/8, and 4-1/8 in. indicates that the Cf^{252} leaves the electroplated source in a cone. This conclusion has been re-enforced by examining radioautographs of the collecting foils to determine in what pattern the Cf^{252} was transferred to the collecting foil.

At atmospheric pressure the maximum transfer rate is approached by increasing the negative potential difference on the collecting foil (Fig. C. 16-3). We have concluded that increasing the voltage or decreasing the pressure results in increasing the collecting efficiency up to the maximum transfer rate achievable with a source of a given density ($\mu g/cm^2$ of Cf^{252}).

Nuclear emulsion plates with metallic backing were substituted for platinum collecting foils and Cf^{252} was transferred to the emulsion plates in vacuum and with a potential of 300 v applied between the source holder and the metallic backing. The separation distance between the Cf source and the emulsion was 3 in. The emulsion plates after transferring Cf^{252} were allowed to stand for periods up to 1 month before development. Examination of the emulsion plate revealed that the Cf^{252} is transferred in groups of atoms.

[1] Chemistry Division Semiannual Report, UCRL-9093, Feb. 1960, p. 38.

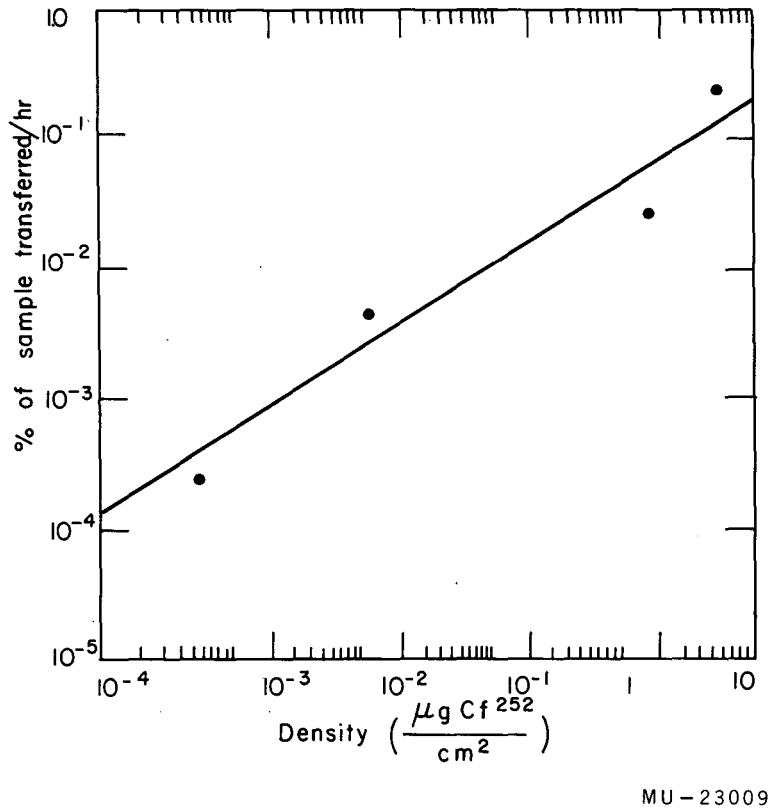

Fig. C.16-1. Percent of sample transferred per hour vs density. Distance from source to catcher 0.25 in.; pressure 50 μ; negative charge on catcher.

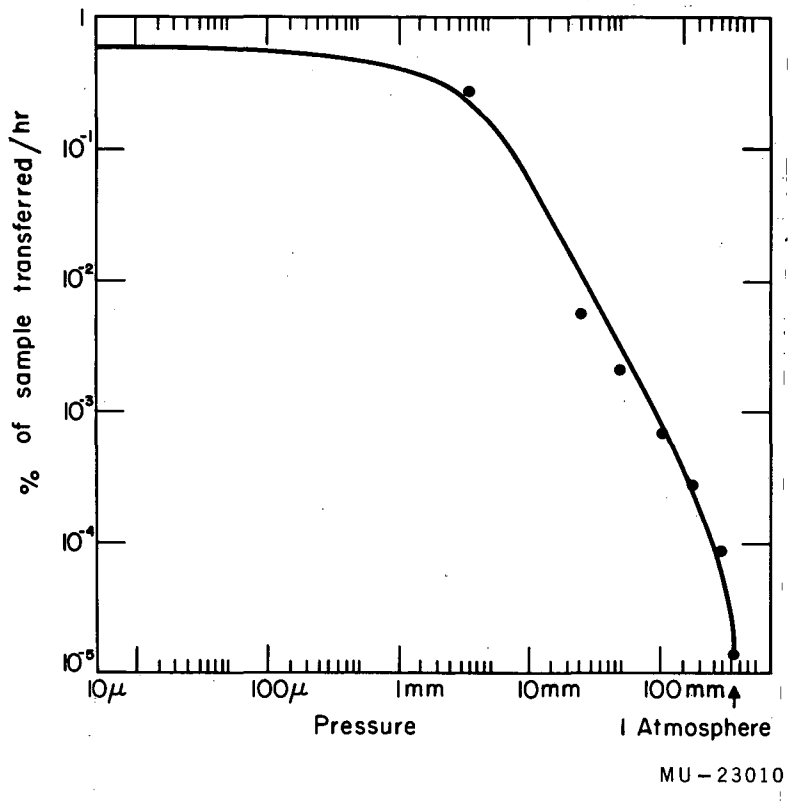

Fig. C. 16-2. Percent of sample transferred per hour vs pressure. Distance from source to catcher 0.25 in.; no charge on catcher.

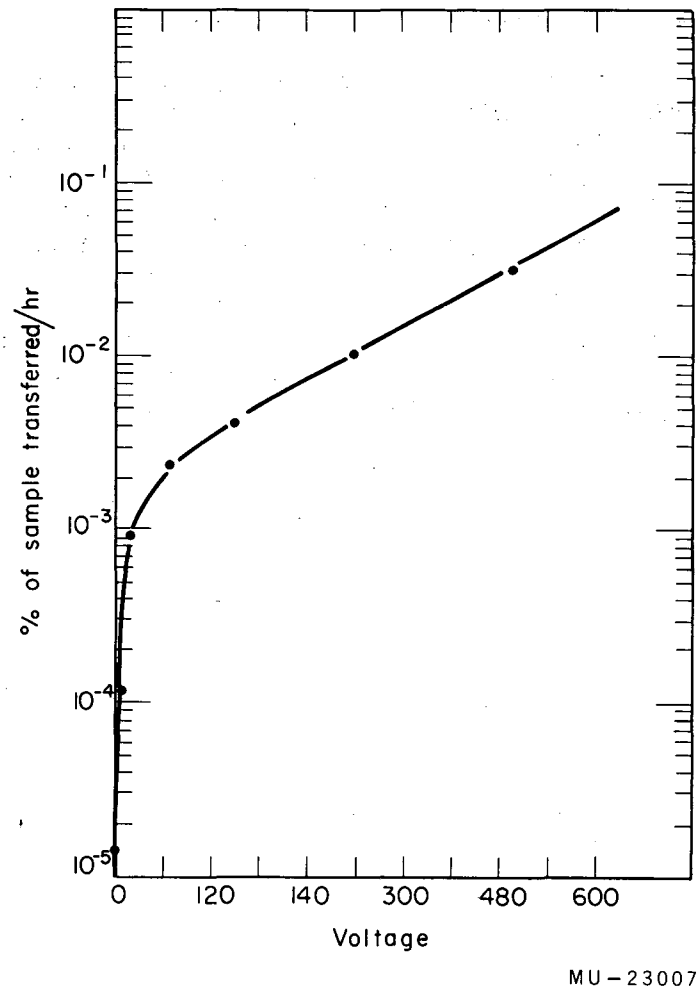

Fig. C. 16-3. Percent of sample transferred per hour vs charge. Distance from source to catcher 0.25 in.; atmospheric pressure; negative charge on catcher.

Approximately 60% of the atoms transferred were in clumps of 600 atoms or more. The largest clump observed was 13,000 atoms.

An electrostatic lens was used to focus Cf^{252} from a source 0.317 cm^2 in area to a collection deposit 0.031 cm^2 in area.

It is interesting to note that the transfer of Cf^{252} onto a 4-microinch nickel foil with a deposit density of 0.59 $\mu g/cm^2$ has caused the disintegration of the foil in a period of 9 months. The foil became progressively more transparent until only a sheer film was left before destruction. An electroplated source of Cf^{252}, deposited with a density of 5.5 $\mu g/cm^2$ on 5-mil platinum foil, has changed from a barely visible deposit to a discolored and enlarged deposit.

Further research is in progress to determine the distribution of charge size under different conditions of pressure and voltage, and to study the effect of fission fragments on the surfaces of metal.

D. PHYSICAL CHEMISTRY

1. REACTIONS OF ACCELERATED CARBON-14 IONS WITH BENZENE

Richard M. Lemmon, R. Terrance Mullen, and F. L. Reynolds

This work is an outgrowth of studies that have been made at several laboratories on the interaction of recoiling carbon atoms on organic molecules.[1, 2, 3] In this work we have substituted a controlled-energy (max 5 kv) C^{14} ion beam for the recoiling atoms ($N^{14}(n, p)C^{14}$) born in a nuclear reactor. Earlier work along these lines has been reported by Aliprandi[4] and Lemmon.[5]

This paper records the state of our knowledge of the distribution of labeled products from C^{14}-ion-irradiated benzene, and some data concerning the distribution of radioactivity between the methyl group and the ring in toluene formed from the irradiated benzene.

A brief description of the isotope separator has been previously given.[6] Benzene is slowly introduced to a cold-trap target area at a rate near 0.06 ml/hr. The target area is approximately 60 cm^2. The target is maintained at about -160°C by means of a slurry of isopentane. At this temperature benzene has a low vapor pressure, but the source gases $C^{14}O_2$, $C^{14}O$, and argon do not condense on the target.

During most of the bombardments a beam of C^{14} ions of a few tenths of a microampere was directed onto the benzene target. After several hours' irradiation the target area is valved off and allowed to come to room temperature. Carrier hydrocarbons such as toluene or cycloheptatriene are admitted into the target chamber preparatory to analysis by gas chromatography.

The gas-liquid partition chromatography was performed on a Wilkens "Aerograph." Two types of columns were used. One column was 5 ft long and 1/4 in. in diameter, filled with crushed firebrick and coated with "Apiezon" hydrocarbon. The carrier gas was pure methane. This column and a proportional counter tube were operated at 70°C. The other column was charged with dimethylsulfolane and used at room temperature. This second column was used to separate the pre-benzene group. The counter

---

[1] J. I. Yang and A. P. Wolf, J. Am. Chem. Soc. 82, 3315 (1960).

[2] A. P. Wolf, "Radioisotopes in Scientific Research" in Proceedings of the First (UNESCO) International Conference, 1957, Vol. II, p. 114.

[3] A. G. Schrodt and W. F. Libby, J. Am. Chem. Soc. 78, 1267 (1956).

[4] B. Aliprandi et al., "Radioisotopes in Scientific Research" in Proceedings of the First (UNESCO) International Conference, 1957, Vol. II, p. 146.

[5] R. M. Lemmon et al., J. Am. Chem. Soc. 78, 6414 (1958).

[6] F. L. Reynolds, in Chemistry Division Semiannual Report, UCRL-8618, Jan. 1959, p. 76.

output was fed to scaler-ratemeter equipment. A second signal from the thermal conductivity cell was fed to a dual pen recorder so that both mass peaks and radioactivity peaks could be recorded simultaneously.

In Fig. D. 1-1 are presented the results of a typical record of mass peaks and activity peaks after C^{14}-ion irradiation of benzene. The activity trace (solid line) shows several peaks emerging from the column before benzene. In all experiments completed, the major portion of the radioactivity emerges from the gas chromatograph ahead of benzene. The spectra of these different compounds seem sensitive to postirradiation treatment such as oxidation or bromination. These early peaks include such compounds as allene, propyne, 1-butyne, 1, 3-butadiene, 1-butene, and isobutylene. No two-carbon compounds were found.

The mass peaks and radioactivity peaks for benzene, toluene, and cycloheptatriene coincide very well, their radioactivity ratio being about 1:0.2:0.2. This ratio is subject to variation, but benzene seems to be the most labeled compound present. Estimates of the fractions of the total number of carbon ions striking the benzene target that appear as labeled benzene, toluene, and cycloheptatriene are also subject to some variation, benzene being approximately 2%, toluene 1%, and cycloheptatriene 2%.

The C^{14}-labeled toluene formed from one of the benzene irradiations was degraded only as far as a determination of the amounts of activity in the methyl group and in the ring. The value for the methyl group was found to be 87±5 % and for the ring carbons 18±25 % of the total activity in the toluene.

2. THE RADIOLYSIS OF BIACETYL VAPOR

Gilbert J. Mains and Amos S. Newton

The radiolysis of biacetyl vapor by using high-energy electrons has been investigated to determine whether the kinetics of the reactions of methyl radicals in radiolysis can be correlated to the kinetics of methyl radical reactions observed in photolysis. Some data from acetone radiolysis suggests that in simple ketones the yield of methane is too high to be ascribed completely to reactions of thermal methyl radicals.

For thermal methyl radical reactions, it can be shown that the ratio of the rates $CH_4/(C_2H_6)^{1/2}$(biacetyl) is a constant at low intensities. However, in the electron radiolysis of biacetyl, at 25°, rather than the above function's being constant as a function of pressure (i.e., conc. of biacetyl),

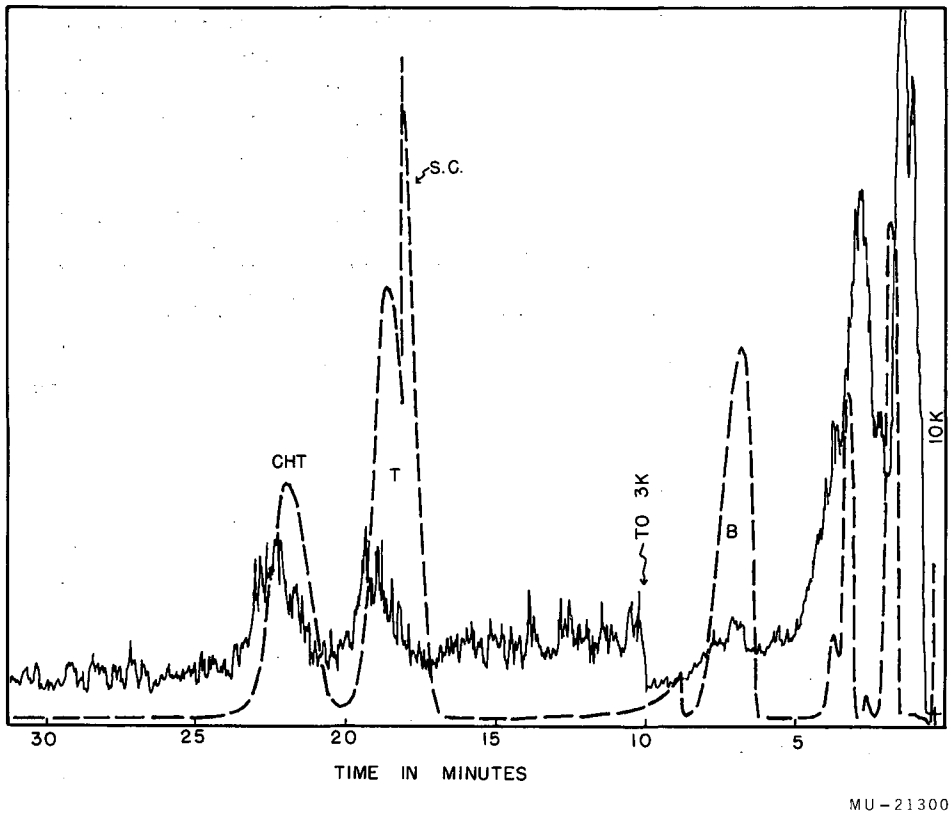

Fig. D. 1-1. Mass (dashed line) and radioactivity (full line) record of the gas-chromatographic separation of the products of the $^{14}C^{+}$ irradiation of benzene.

Legend: CHT = cycloheptatriene, T = toluene, B = benzene; 10K and 3K signify 10-kilovolt and 3-kilovolt full-scale deflection on the radioactivity record, S. C. = scale change on the mass record.

the direct ratio CH_4/C_2H_6 is nearly constant and independent of pressure, dose rate, and total dose. At higher temperatures, 200°C, the ratio of rates, $CH_4/(C_2H_6)^{1/2}$ (biacetyl), becomes constant with pressure but its value is higher than the value observed in photochemistry. Iodine scavenging experiments show that the bulk of the methane at 200° arises from thermal radicals, while at room temperature only about 80% arises from thermal radicals and the rest by a nonradical or hot-radical mechanism. A number of possibilities exist for such reactions, which might occur in radiolysis but not in photolysis. These include: (a) "Hot" radical reactions. (b) A molecular rearrangement from some excited state to produce methane directly without radical precursors. No decision as to the mechanism of this nonthermal-radical-produced methane is possible from the present experimental results. The yields of products formed in the radiolysis of biacetyl at 25, 120, and 200° are shown in Table I.

Table I. Yields[a] of products from electron irradiation of biacetyl vapor (in G(mol/100 ev) of product at temperature specified

	Temperature		
Product	25°	120°	200°
H_2	0.55	0.55	0.55
CH_4[(b)]	0.22	1.4	5.9
C_2H_2	0.15	0.2	0.2
C_2H_4	0.06	0.1	0.2
C_2H_6	2.0	2.2	2.0
CO	7.4	9.5	16.0
C_3H_6	0.03		
C_3H_8	0.08		
CO_2	0.1	0.4	0.6
CH_2CO[(b)]	0.5[(c)]	0.7	2.0
CH_3CHO	0.3	0.4	0.3
$CH_3CO\ CH_3$[(b)]	1.1	1.1	2.7
$C_2H_5COCOCH_3$	0.3	0.5	0.7
CH_3COOH	0.3		

(a) Data for irradiation at 20 mm pressure, 30 pulses/sec, 50 ma/pulse, and for 90 min bombardment. Values normalized for H_2, which does not appreciably change in yield with changes in irradiation parameters.
(b) Value dependent on pressure, dose rate, pulse rate, and total dose.
(c) Not always seen in 25° irradiations.

3. THE MERCURY-SENSITIZED RADIOLYSIS AND PHOTOLYSIS OF METHANE (*)

Gilbert J. Mains and Amos S. Newton

We have found that there is a remarkable similarity in the products from the radiolysis of methane at 260° with a high-energy electron beam and from the mercury-sensitized photolysis of methane at 260° using 2537-Å uv light. The same chemical products are found in both types of experiments, and differences in the distribution of these products can be ascribed to differences in radiation intensity rather than any basic difference in reaction mechanism after the initial transfer of the energy to the methane.

A typical analysis of the radiolysis and photolysis products of methane at 260° is given in Table I.

Table I. Methane radiolysis and photolysis–typical analyses[a]

Dose Product[b]	7.2×10^4 e^- at 260° (%)	8.1×10^4 Hg + e^- at 260° (%)	c Hg + hν at 260° (%)	10.8×10^4 e^- at 25° (%)
Hydrogen	3.94	4.37	4.83	4.49
Ethane	1.26	2.10	1.48	1.62
Propane	.41	.47	.27	.31
n-Butane	.05	.05	.02	.05
Isobutane	.10	.14	.13	.05
Neopentane	.12	.12	.58	.03
Isopentane	.04	.03	.02	.03
Neohexane	.03	.04	.09	.05
Heptane	.01	.01	.02	.01
Ethylene	.15	.20	.08	.04
Isobutene	.03	.02	.02	.03
Isopentene	.01	.01	.01	...

[a]Product yields expressed as per cent of total gas.

[b]Total number of 50-ma, square-wave electron pulses, 5 μsec in duration.

[c]Irradiated for 4-min using three 4-watt low-pressure mercury lamps.

As no ionic species can be formed in the photolysis, where the energy transfer is through the $Hg(^3P_1)$ excited state of mercury, and this leads to the same products as the radiolysis, one must conclude that ions are not necessary in describing the radiolysis products of methane, as has been postulated.[1,2] It supports the position of Yang and Manno[3] that most of the ethane and all of the higher products must be ascribed to a radical mechanism.

*Communication to the Editor, J. Phys. Chem. 64, 511 (1960). Full paper in J. Phys. Chem. 65, 212 (1961).

[1]F. W. Lampe, J. Am. Chem. Soc. 79, 1055 (1957).

[2]G. G. Meisels, W. H. Hamill, and R. R. Williams, Jr., J. Phys. Chem. 61, 1456 (1956).

[3]K. Yang and P. J. Manno, J. Am. Chem. Soc. 81, 3507 (1959).

The methane radiolysis at 25° was also compared. The results show the approximate yields of the products found to be in agreement with other authors,[1-4] though we find a large yield of neopentane, which was not previously reported and probably was included in the n-butane yield by others.

The hydrogen yield in the radiolysis experiments is linear with dose and shows almost no temperature coefficient. Within fairly wide limits of error in the analysis for the higher products, the yield of these increases with dose in approximately a linear relation. In the photolysis at 260°, however, a steady state is rapidly formed for ethane, propane, iso-butane and n-butane; the products found to increase with dose are neopentane and neohexane.

A free-radical process has been proposed for the photolysis of methane[5] to yield ethane and propane, and it appears reasonable to generalize this to account for the higher products.

Free-radical formation in photolysis

Primary

$$Hg \xrightarrow{h\nu} Hg^*(^3P_1) \quad (1)$$

$$Hg^*(^3P_1) + CH_4 \longrightarrow Hg + CH_3 + H \quad (2)$$

$$Hg^*(^3P_1) + RH \longrightarrow Hg + R + H \quad (3)$$

$$Hg^*(^3P_1) + H_2 \longrightarrow Hg + H + H \quad (4)$$

Secondary

$$H + CH_4 \longrightarrow H_2 + CH_3 \quad (5)$$

$$H + RH \longrightarrow H_2 + R \quad (6)$$

$$CH_3 + RH \longrightarrow CH_4 + R \quad (7)$$

Product Formation

$$2\ CH_3 \longrightarrow C_2H_6 \quad (8)$$

$$H + H \xrightarrow{M} H_2 \quad (9)$$

$$CH_3 + R \longrightarrow CH_3R \quad (10)$$

$$C_2H_5 + R \longrightarrow C_2H_5R \quad (11)$$

The rates of (2), (3), and (4) can be estimated from the cross sections for chemical quenching of the $Hg(^3P_1)$ fluoresence.[6] Because Reaction (4)

[4] M. A. El-Sayed, P. J. Estrup, and R. Wolfgang, J. Phys. Chem. 62, 1356 (1958).

[5] K. Morikawa, W. S. Benedict, and H. S. Taylor, J. Chem. Phys. 5, 212 (1937).

[6] K. J. Laidler, Chemical Kinetics of Excited States (Oxford University Press, 1955).

has a cross section about 100 times as large as Reaction (2), it is clear that after about 1% H_2 is formed, Reaction (4) will predominate. Reaction (3) may also become competitive. Reactions (5), (6), and (7) involve activation energies, but if the H atoms possess excess kinetic energy, the observed activation energy may be small. Reactions (3), (5), and (6) lead to the formation of radicals which yield higher products, and the specific rates of these are not known. In general one may show that the product build-up occurs as one-carbon additions except for a small amount of two-carbon branching due to ethyl radical reactions. The reaction effectively stops at neopentane because of its low quenching cross section for $Hg^*(^3P_1)$ and its low cross section for reaction with H atoms. The build-up may be sketched diagramatically as follows. Arrows represent an H atom abstraction and a radical addition to the previous compound.

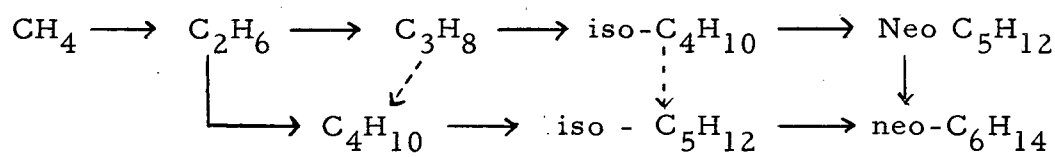

The olefins result from radical disproportionation reactions.

Mercury-sensitized radiolysis at 260° can be explained by the same sequence of reactions. In the radiolysis in the absence of mercury, one must assume the primary excitation to be analogous to Reaction (2), with the electron interaction giving the energy to the methane. One cannot exclude a free-radical mechanism for product build-up at 260°. The almost identical distribution of products of radiolysis at 260° with or without the presence of mercury shows methane ions, which should be scavenged in the presence of mercury, to lead to no products different than if they were not scavenged. It is therefore concluded that if ion-molecule reactions are occurring, they act as radical precursors and do not lead directly to higher products in the radiolysis.

Acknowledgment

The authors acknowledge their indebtedness to Mr. Aldo F. Sciamanna for the mass spectrometer runs and for making photolysis runs and to Mrs. Sylvia Waters for reading the mass spectra.

4. THE RADIATION CHEMISTRY OF THE SYMMETRICAL DICHLOROETHYLENES (*)

Jean H. Futrell and Amos S. Newton

The liquid-phase radiolysis of cis- and trans-1, 2-dichloroethylene by helium ions, γ rays, and electrons has been investigated. The gaseous products found were H_2, acetylene, monochloroacetylene, dichloroacetylene, vinyl chloride, and HCl. Among the higher-boiling products identified were 1, 1, 2, 2-tetrachloroethane, 1, 3, 4, 4-tetrachlorobutene-1, other tetrachlorobutenes, 1, 2, 3, 4, 4-pentachlorobutene-1, isomers of hexachlorohexene, and higher-boiling products which were not identified.

A free-radical process was invoked to explain the mechanism of polymer product formation, and the mechanism was shown to be consistent with the effects of changes of rates of linear energy transfer on the various product yields. The reactions may be summarized as follows:

Primary Processes

$$C_2H_2Cl_2 \rightsquigarrow \underset{(R_1)}{CHCl{=}CH\cdot} + Cl\cdot \qquad (1)$$

$$C_2H_2Cl_2 \rightsquigarrow HC{\equiv}CCl + HCl \qquad (2)$$

$$C_2H_2Cl_2 \rightsquigarrow ClC{\equiv}CCl + H_2 \qquad (3)$$

$$C_2H_2Cl_2 \rightsquigarrow \underset{(R_2)}{CHCl{=}CCl\cdot} + H\cdot \qquad (4)$$

Reaction (1) must be the principal primary process. This was also the primary reaction postulated in the photolysis of the dichlorethylene isomers at 1900 Å.[1] The absence of any large effect on the yields of monochloroacetylene and dichloroacetylene with changes in rates of linear energy transfer (particle effect) by comparison of radiolysis with helium ions and γ rays indicates Reactions (2) and (3) to be important in the production of these two compounds. Reaction (4) is necessary to account for the excess hydrogen found.

Secondary processes

$$CHCl{=}CH\cdot{}^{*} \longrightarrow C_2H_2 + Cl\cdot \qquad (5)$$

$$H\cdot + C_2H_2Cl_2 \longrightarrow H_2 + CHCl{=}CCl\cdot \qquad (6)$$

$$Cl\cdot + C_2H_2Cl_2 \longrightarrow R_2 + HCl \qquad (7)$$

*Brief version of published paper, J. Am. Chem. Soc. 82, 2676 (1960).

[1] H. E. Mahncke and W. A. Noyes, Jr., J. Phys. Chem. 58, 932 (1936).

Reaction (5) is the elimination of another chlorine radical from an excited R_1 radical to yield acetylene. A direct elimination of a chlorine molecule from dichloroethylene would yield the same result, but no chlorine was found as a product. Reactions (6) and (7) account for the H_2 and HCl not formed by Reactions (2) and (3).

The largest yields of products are those loosely designated as polymer, i. e., those products boiling higher than the dichloroethylenes. These are formed by radical addition to the dichloroethylene molecule.

$$Cl\cdot + C_2H_2Cl_2 \longrightarrow \underset{(R_3)}{CHCl_2\text{-}CHCl\cdot} \quad (8)$$

$$R_3 \longrightarrow C_2H_2Cl_2 + Cl\cdot \text{ (isomerization)} \quad (9)$$

$$R_3 + Cl\cdot \longrightarrow CHCl_2CHCl_2 \quad (10)$$

$$R_3 + C_2H_2Cl_2 \longrightarrow \underset{(R_4)}{CHCl_2CHClCHClCHCl\cdot} \quad (11)$$

$$R_4 \longrightarrow CHCl_2CHClCH{=}CHCl + Cl\cdot \quad (12)$$

$$R_4 \longrightarrow C_2H_2Cl_2 \quad \underset{(R_5)}{CHCl_2(CHCl)_4CHCl\cdot} \quad (13)$$

$$R_5 \longrightarrow CHCl_2(CHCl)_3CH{=}CHCl + Cl\cdot \quad (14)$$

$$R_5 + C_2H_2Cl_2 \longrightarrow \text{higher polymers}$$

This represents the main sequence of polymerization. Reactions (8), (11), and (12) are those suggested by Bauer[2] for the free-radical-induced dimerization of dichloroethylene. Such reaction sequences of polyhalo radicals of relatively low reactivity are not uncommon.[3]

Reactions involving R_1 and R_2 can explain the difference between tetrachlorobutene isomers observed in radiolysis and those found in benzoyl peroxide initiation.

The pentachlorobutene observed can arise by a direct combination of R_2 and R_3,

$$CHCl{=}CCl\cdot + CHCl_2\text{-}CHCl\cdot \longrightarrow CHCl_2\text{-}CHCl{=}CHCl, \quad (15)$$

but this cannot account for all the pentachlorobutene. Radical disproportionation reactions involving R_4 would yield pentachlorobutene:

---

[2] W. Bauer, U. S. Patent 2,267,712 (Dec. 30, 1941).

[3] Cheves Walling, Free Radicals in Solution (John Wiley and Sons, Inc., New York, N. Y., 1957), p. 270.

$$CHCl_2CHClCHClCHCl\cdot \longrightarrow CHCl_2CHClCCl{=}CHCl + HCl \qquad (16)$$

Such a reaction is consistent with the absence of pentachlorobutene in benzoyl-peroxide-initiated reactions, and with a lower yield in γ-ray radiolyses than in helium-ion radiolyses.

These results are consistent with earlier results of Cooper and Stafford on the polymer products found.[4]

Acknowledgments

The authors acknowledge their indebtedness to Mr. W. B. Jones and the crew of the Crocker Laboratory cyclotron for the helium-ion irradiations; to Dr. Lynn Hall of the California Research Corporation for irradiations with the Van de Graaff accelerator; to Mr. W. L. Everette for irradiations with the microwave linear accelerator; to Dr. Charles Koch for microanalysis data, and to Mr. Aldo F. Sciamanna and Mrs. Sylvia Waters for obtaining the mass spectra. One of us (J. H. F.), expresses his appreciation to Professor David H. Templeton for advice and encouragement tendered as his research advisor.

[4] W. Cooper and W. H. Stafford, in Proceedings of the Second United Nations International Conference on the Peaceful Uses of Atomic Energy (United Nations, New York, N. Y., 1959), Vol 29, p. 218.

5. CRYSTAL AND MOLECULAR STRUCTURE OF THE COMPOUND OF TRIETHYL PHOSPHINE AND CARBON DISULFIDE (*)

Thomas N. Margulis and David H. Templeton

Red monoclinic prismatic crystals are formed when triethyl phosphine reacts with carbon disulfide in benzene or other solvents.[1] Analogous compounds are known for several other tertiary phosphines. The conflicting proposals for the molecular structures of these substances are reviewed by Issleib and Brack,[2] who concluded incorrectly that they are loose molecular compounds. We have determined the structure of the triethyl compound by x-ray diffraction, and find that there is a chemical bond between phosphorus and the carbon atom of CS_2. The molecule is a zwitterion of a quaternary phosphonium derivative of dithioformate as proposed by Jensen,[3] $(CH_3CH_2)_3P^+\text{-}CSS^-$.

*Brief version of paper submitted to J. Am. Chem. Soc.

[1] A. W. Hofmann, Ann. Suppl. 1, 1 (1861).

[2] K. Issleib and A. Brack, Z. anorg. u. allgem. Chem. 277, 271 (1954).

[3] K. A. Jensen, J. prakt. Chem. 148, 101 (1937).

Single-crystal diffraction patterns were recorded with CuKα radiation by Weissenberg and precession techniques. The crystals are monoclinic, space group $P2_1/c$, with 4 molecules in the unit cell, of dimensions

$$a = 7.50 \pm .02 \text{ A},$$
$$b = 11.97 \pm .02 \text{ A},$$
$$c = 13.82 \pm .05 \text{ A},$$
$$\beta = 123.1 \pm .2 \text{ deg}.$$

The density is calculated to be 1.24 g/cm^3.

Atomic coordinates of P and S were found with the three-dimensional Patterson function. Electron-density calculations revealed the carbon atoms and accomplished some refinement of the heavy-atom coordinates. Further refinement by full-matrix least squares with isotropic individual temperature parameters and 610 observed independent reflections reduced the conventional unreliability factor R to 0.11. The resulting atomic parameters are listed in Table I. Hydrogen atoms are omitted from these calculations. The phosphorus and sulfur atoms are not clearly distinguished by the x-ray data, but are identified on the basis that phosphorus is the atom bonded to the ethyl groups.

Table I. Atomic coordinates and temperature parameters

Atom	x	y	z	B, A^2
S_1	0.127	0.114	0.141	6.3
P_2	0.132	0.244	0.329	4.4
S_3	0.089	0.840	0.401	5.7
C_4	0.056	0.231	0.183	5.4
C_5	0.104	0.751	0.169	5.1
C_6	0.300	0.128	0.416	5.6
C_7	0.279	0.376	0.392	5.9
C_8	0.348	0.372	0.042	6.3
C_9	0.479	0.377	0.380	6.7
C_{10}	0.249	0.645	0.218	7.8

The bond distances and some of the bond angles are shown in Fig. D. 5-1. Standard deviations are about 0.03 A for P-C and S-C bonds and 0.04 A for C-C bonds. The thioformate carbon (C_4) is coplanar with its three neighbors, and its bond angles (σ = 1 deg) are typical of those of salts of carboxylic acids. The bond angles at the phosphorus atom range from 108 deg to 111 deg (σ = 1 deg). The bond angles at the methylene carbon atoms (C_5, C_6, C_7) are 115, 113, and 109 deg (σ = 2 deg).

We thank Dr. George A. Wiley for preparing the crystals which we used.

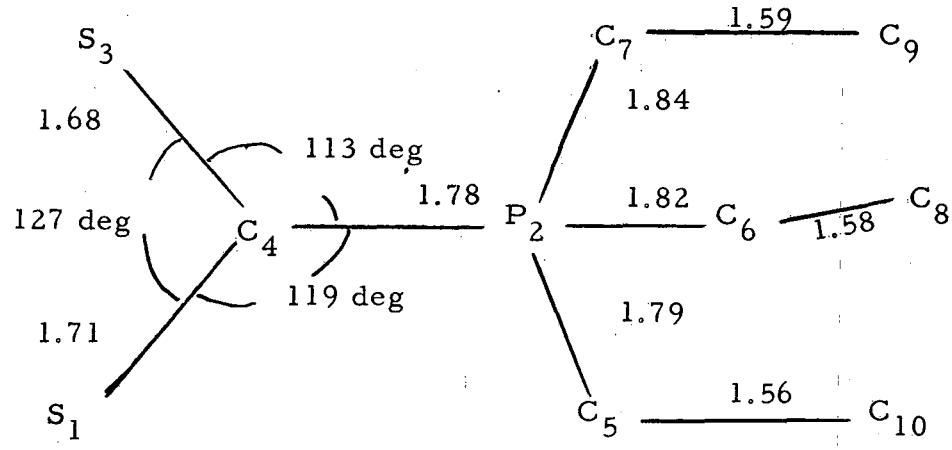

Fig. D. 5-1. Bond distances in A and bond angles (not to scale).

6. CRYSTAL STRUCTURE OF HYDROGEN PEROXIDE DIHYDRATE (*)

Ivar Olovsson† and David H. Templeton

The melting-point diagram of the system hydrogen peroxide–water indicates only one intermediary compound, $H_2O_2 \cdot 2H_2O$. Because of interest in its hydrogen bonding, we have determined its structure from single-crystal x-ray diffraction data obtained at -190°C. The crystals are monoclinic (space group C2/c) with four molecules in a unit cell of dimension

$$a = 9.400 \pm .002 \text{ A},$$
$$b = 9.479 \pm .002 \text{ A},$$
$$c = 4.51 \pm .01 \text{ A},$$
$$\beta = 121.33 \text{ deg}.$$

The calculated density is 1.36 g/cm^3 at -190°. Giguere, Knop, and Falk[1] report a preliminary value of 1.20 for the density at the melting point, about -51°. X-ray photographs taken at -70° indicate the same structure.

*Brief version of published paper, Acta Chem. Scand. 14, 1325 (1960).

†Present address: Institute of Chemistry, University of Uppsala, Uppsala, Sweden.

[1] P. A. Giguere, O. Knop, and M. Falk, Can. J. Chem. 29, 123 (1951).

The asymmetric unit consists of two oxygen atoms and three hydrogen atoms, each in general positions. The oxygen atoms were located by the Patterson function. About 20 cycles of least-squares refinement reduced the "unreliability factor" R to 0.091, based on oxygen atoms only, and gave, as the coordinates,

Atom	x	y	z
$O_1(H_2O)$	0.2980	0.0822	0.2850
$O_2(H_2O_2)$	-0.0075	0.1809	0.0785

The distances between these atoms correspond to three hydrogen bonds in the asymmetric unit. The electron density difference function, calculated with oxygen atoms subtracted out, shows the hydrogen atoms in locations near these bonds (Fig. D. 6-1).

The hydrogen peroxide molecule is nonplanar. Its dihedral angle (the angle between the two planes each containing two oxygen atoms and one hydrogen atom) is about 90 deg in pure solid H_2O_2 according to neutron diffraction data.[2] In this hydrate structure, the dihedral angle is 139 deg if hydrogen is assumed on the line between oxygen atoms and about 130 deg according to the hydrogen positions actually observed. Thus the hydrogen peroxide molecule, which is known to have little resistance against twisting,[3] is twisted out of its normal shape, but not as much as if the hydrogen atoms were on the line between the two oxygen atoms of the hydrogen bond. The hydrogen atoms of the water molecule are also observed to be displaced from the lines of the respective hydrogen bonds in the directions corresponding to a more normal H-O-H angle.

The O-O distance in the peroxide molecule is 1.481±.009 A. The three hydrogen bonds have O-O distances of 2.741±.005 and 2.761±.004 A for the two involving the hydrogen atoms of water, and 2.685±.004 A for the one involving the hydrogen atom of H_2O_2.

[2] W. R. Busing and H. A. Levy, Reports from the meeting of the American Crystallographic Association in Milwaukee, June 1958.

[3] P. A. Giguere and K. B. Harvey, J. Mol. Spect. 3, 36 (1959).

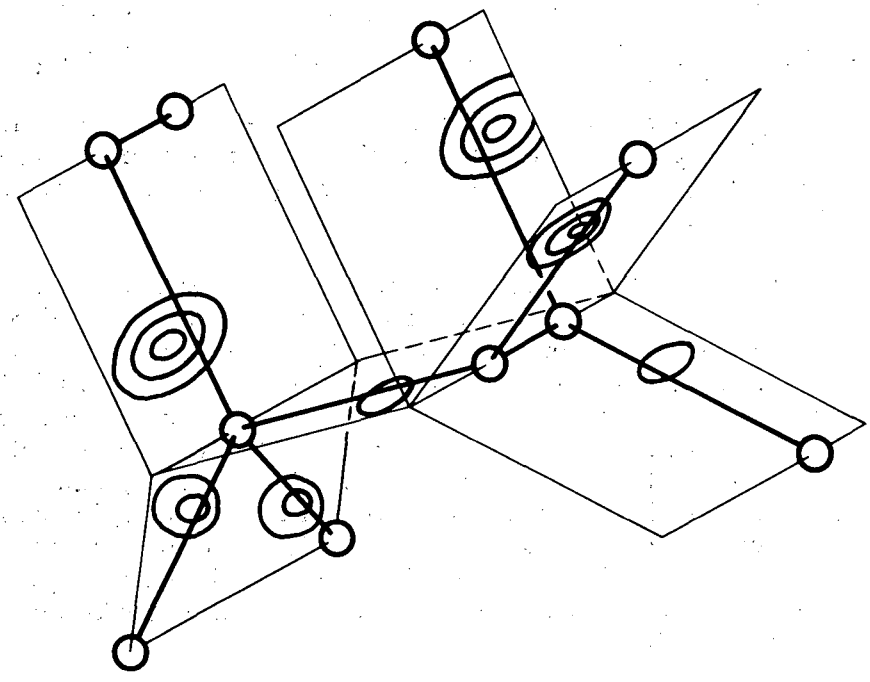

MU-23120

Fig. D.6-1. Schematic representation of the difference synthesis in various sections. The contours are drawn at 0.70, 0.85, and 1.00 e A^{-3}.

7. CRYSTAL STRUCTURE OF VANADYL BISACETYLACETONATE: GEOMETRY OF VANADIUM IN FIVEFOLD COORDINATION (*)

Richard P. Dodge, David H. Templeton, and Allan Zalkin

The crystal structure of vanadyl bisacetylacetonate,

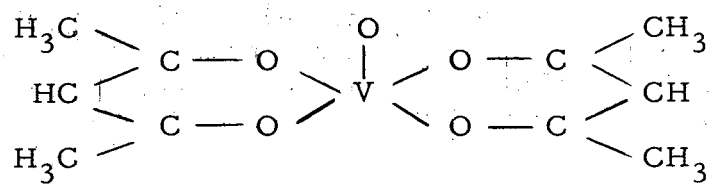

has been determined to establish the geometry of the bonds about five-coordinated vanadium (IV). In his discussion of this compound and its reactions, Jones assumed a square planar arrangement of four oxygen atoms about the vanadium atom, with the bond of the fifth oxygen presumably perpendicular to the plane of the other four.[1] From the chemical evidence, it was impossible to rule out the trigonal bipyramidal arrangement of the five bonds. The work of Feltham on the electron spin-resonance spectra of the compound indicates that the bipyramidal structure is improbable.[2] The work reported here shows that the five oxygen atoms are at the corners of an approximately square pyramid, but that vanadium is near the center of gravity of this pyramid rather than at the center of its base.

The structure was determined from x-ray diffraction data recorded by the Weissenberg and precession methods with CuKα radiation. The crystals are triclinic, space group $P\bar{1}$, with two molecules in the unit cell with dimensions

a = 7.53±.02 A,	α = 73.0 deg,
b = 8.23±.03 A,	β = 71.3 deg,
c = 11.24±.04 A,	γ = 66.6 deg.

The molecule has no crystallographic symmetry, but its dimensions correspond to the symmetry mm2 (C_{2v}) within the accuracy of the results.

The atomic coordinates of vanadium were determined from the Patterson function. Electron density calculations with signs based on vanadium revealed the approximate locations of the oxygen and carbon atoms. These atomic coordinates were refined by five cycles of diagonal least squares, using the IBM-650 computer. The "unreliability factor" R was reduced to 0.114 (observed reflections only). The resulting structure is described in a thesis by Dodge.[3]

---

*Brief version of paper submitted to J. Chem. Phys.

[1] M. M. Jones, J. Am. Chem. Soc. 76, 5995 (1954).

[2] R. D. Feltham, Ph. D. Dissertation, UCRL-3867, 1957.

[3] R. P. Dodge, Ph. D. Dissertation, UCRL-8225, 1958.

Examination of the records of these refinement cycles suggested that the best fit had not been achieved. Four additional cycles of refinement were carried out with the IBM-704 computer and the full-matrix program of Busing and Levy,[4] reducing R to 0.092. The results confirm that the earlier refinement had not adequately converged, and that the full-matrix method was considerably superior in this problem. The largest change in a bond distance was that of the $V--O_6$ bond (the bond of the vanadyl ion), which was 1.59 A after the diagonal refinement and 1.56 A in the final structure. The changes do not affect the chemical interpretation of the results, but do show that the accuracy of the earlier results was not as great as it was then estimated.

The shape of the molecule is shown in Fig. D. 7-1. The dimensions shown there are the average values for each chemically equivalent set of bond distances and bond angles. Each acetylacetone skeleton is accurately planar, as expected, but not quite coplanar with the other acetylacetone skeleton of the same molecule. The planes of these two parts of the molecule meet at an angle of 163 deg. It is interesting that these planes are a compromise between those that would contain the vanadium atom and those that would be coplanar, assuming no change in the oxygen and vanadium positions. We interpret this fact as evidence for conjugation effects between the two rings.

We know of no other measurement of the bond distance in the vanadyl ion. In the crystal V_2O_5, vanadium (V) has a coordination geometry which is related to this square pyramid, with one neighbor at 1.54 A and four others at 1.77, 1.88, 1.88, and 2.02 A.[5]

[4] W. R. Busing and H. A. Levy, ORNL Central Files Memorandum 59-4-37, April 1959.

[5] A. Byström, K. A. Wilhelmi, and O. Brotzen, Acta Chem. Scand. 4, 1119 (1950).

8. SINGLE-CRYSTAL TUNGSTEN RIBBON (*)

F. L. Reynolds

In preparing single crystals from polycrystalline tungsten ribbon by strain-annealing methods[1] it was found that the axis of the ribbon was within 10 deg of being always in the [110] direction. This has been previously

(*) Letter to the Editor, J. Chem. Phys. (submitted Jan. 1961).

[1] M. H. Nichols, Phys. Rev. 57, 297 (1940); F. L. Hughes, H. Levinstein, and R. Kaplan, Phys. Rev. 113, 1023 (1959); M. Tanenbaum, in Methods of Experimental Physics, Vol. 6, Solid-State Physics, Part A Ed. by Marton (Academic Press, New York, 1959) p. 86.

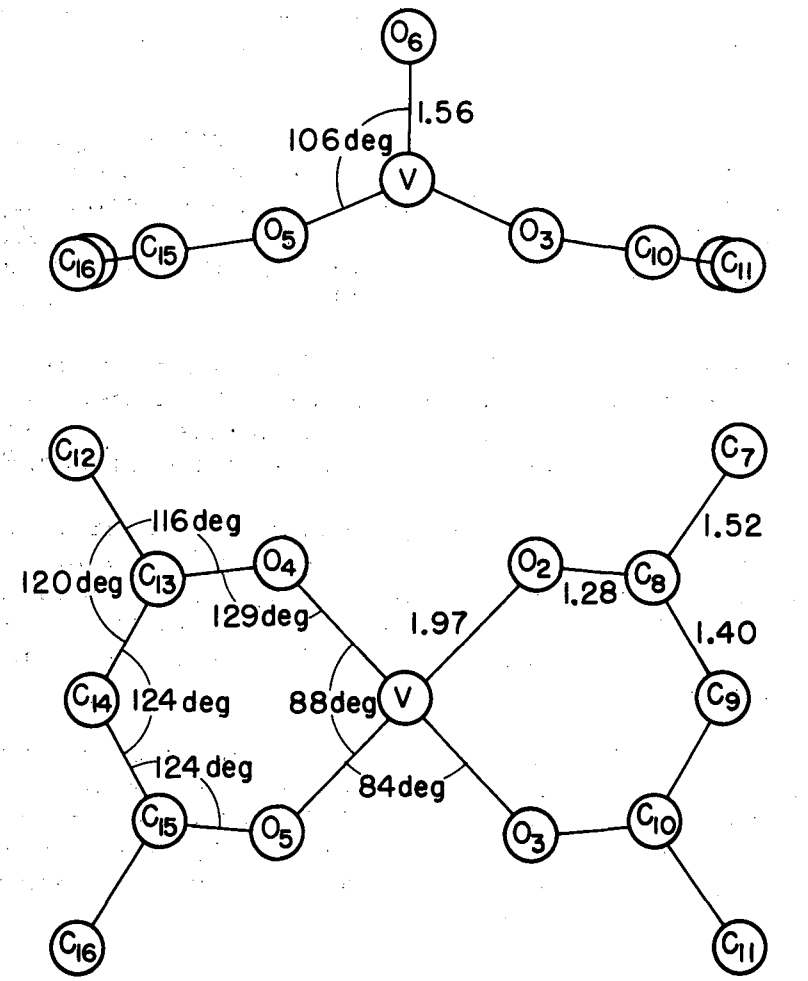

Fig. D.7-1. Average bond distances and bond angles in the molecule of vanadyl bisacetylacetonate.

pointed out by Rieck[2] and a number of other workers.[3] Their work was done on tungsten wires. Eisinger, working with tungsten ribbon, also found that the surface normal lay in the [110] zone or within 5 deg of it and that the crystal plane most commonly found to be parallel to the surface of the ribbon was 113 or within 10 deg of this direction.[4] This occurred in six crystals studied.

A number of polycrystalline ribbons have been treated to grow single-crystal material for further mass spectrometer surface-ionization experiments, and it was ascertained that within 10 deg all these ribbon single crystals were oriented along the drawing axis in the [110] direction. The surface normal, however, migrated on a zone which included the 113 crystal plane. Such a zone includes planes near 117, 115, 113, 112, 221, and 331.

A stereographic plot (Fig. D. 8-1) of the surface normal positions of these crystals on a (111) standard projection indicates the zone, and also that the pole of these points lies close to a [110] axis direction. Orientation was ascertained by standard back-reflected Laue x-ray techniques.[5]

It is interesting to note that Sample B, a crystal grown from an independent supply source,[6] falls on this zone. Also, Sample 24 was not strain-annealed by recommended techniques, but was a 1-cm-long ribbon filament heated for many hours at 2200°K. In previous work[7] on surface ionization data from hot tungsten surfaces it was thought that some of the filaments showed single-crystal properties.

The [110] axis orientation apparently is quite universal to drawn tungsten wire, but in making ribbon from wire the surface normal may be subject to specific orientation during rolling. This influences the crystal growth orientation of the single crystal formed in the ribbon during strain-annealing. With all crystals studied, none produced surface planes normal to the axis of simple index such as 100, 111, or 110.

---

[2] G. D. Rieck, Philips Research Reports 12, 423 (1957).

[3] R. P. Johnson and W. Shockley, Phys. Rev. 49, 439 (1936). See also Hughes, Ref. 1.

[4] J. Eisinger, J. Chem. Phys. 29, 1154 (1958).

[5] The author is indebted to Helena Rubin for taking the Laue photographs.

[6] Sample "B" supplied by J. A. Becker, Bell Telephone Laboratories.

[7] J. R. Werning, Thermal Ionization at Hot Metal Surfaces (thesis), UCRL-8455, Sept. 1958.

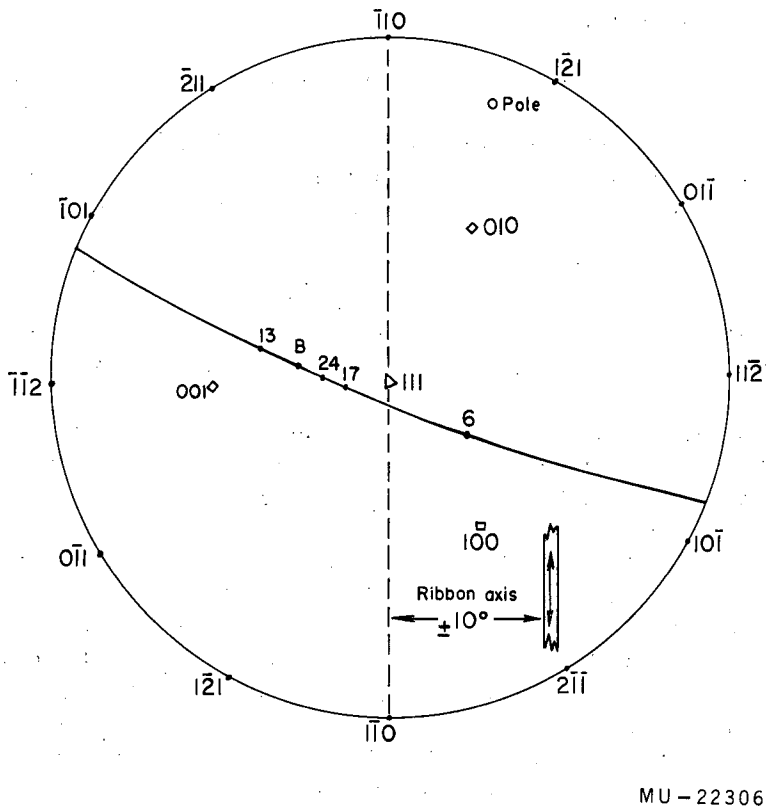

Fig. D.8-1. Stereographic plot of surface normals in tungsten ribbon single crystals.

9. MECHANISMS OF ION EXCHANGE

David C. Whitney and Richard M. Diamond

Many different theories have been advanced concerning the mechanisms of ion exchange.[1-7] This work is concerned with the effect of intermolecular water structure on ion-exchange behavior.

In pure water at room temperature each water molecule is linked tetrahedrally by hydrogen bonds to, on the average, three other water molecules. In an ion-exchange resin, however, the water structure is disrupted, owing to the intrusion of the organic matrix, so that each water molecule is most likely bonded to, on the average, fewer water molecules than in pure water.

If a large, relatively nonhydrated ion--e.g., butyrate ion--is introduced into pure water, a large number of water hydrogen bonds must be broken to accommodate the hydrocarbon chain. If, however, the same ion were introduced into the resin phase, fewer hydrogen bonds would be broken, and thus butyrate ion might be expected to enter into an ion-exchange resin more readily than a smaller ion of the same type. In order to confirm this hypothesis and obtain a measure of the effect of size on the relative amount of exchange, the following experiment was performed.

Acetate, butyrate, valerate, and caproate ions form a homologous series of anions whose only difference is the length of the hydrocarbon chain attached to the carboxylate group. The distribution coefficient (i.e., the ratio of milliequivalents of anion per gram of resin to milliequivalents of anion per milliliter of solution) of each anion was determined at several different concentrations by using an anion-exchange resin (Dowex-1X8, 100 to 200 mesh) in the chloride form, and a family of curves was obtained (see Fig. D.9-1) which shows that a definite size dependence does exist, the ion which causes the most disruption of the water structure being that which exchanges to the greatest extent.

In a similar manner, the effect of extent of hydration by the aqueous phase on the distribution coefficient of an ion can be investigated. Since the chloro and methyl groups are approximately the same size, the series trimethylacetate, chlorodimethylacetate, dichloromethylacetate, and trichloroacetate contains members which differ only in the extent of hydration, as exhibited by the decreasing hydrolysis constants. By carrying out the same

---

[1] H. P. Gregor, J. Am. Chem. Soc. 73, 642 (1951).

[2] S. A. Rice and F. E. Harris, Z. physik. Chem. 8, 207 (1956).

[3] J. L. Pauley, J. Am. Chem. Soc. 76, 1422 (1954).

[4] H. P. Gregor, J. Belle, and R. A. Marcus, J. Am. Chem. Soc. 77, 2713 (1955).

[5] J. Aveston, D. A. Everest, and R. A. Wells, J. Chem. Soc. 231, (1958).

[6] R. A. Horne, J. Phys. Chem. 62, 873 (1958).

[7] R. Kunin, Elements of Ion Exchange (Reinhold Publishing Company, New York, 1960), p. 10.

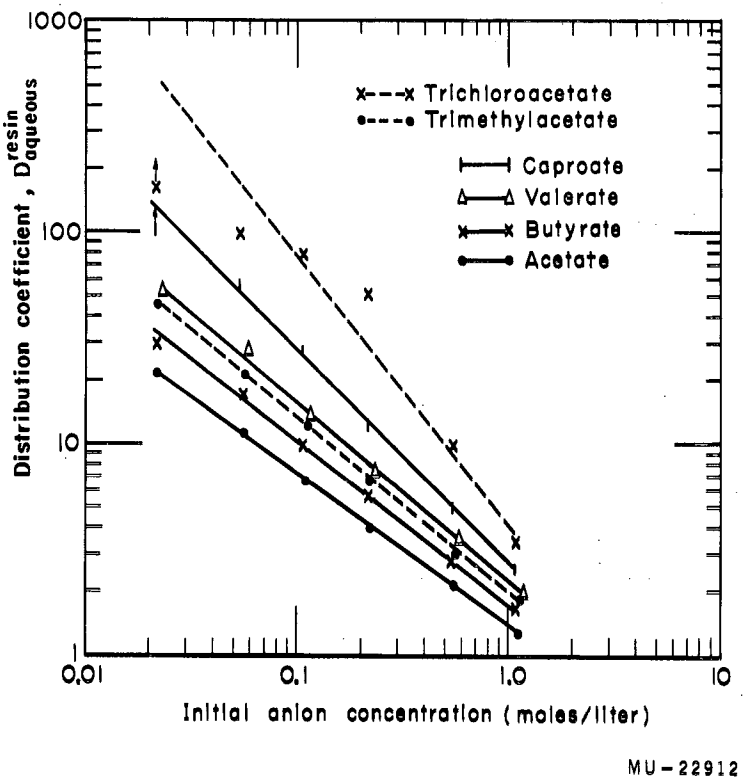

Fig. D. 9-1. Size dependence of ion exchange.

type of experiment as above, the distribution coefficients for the first and last members of the series have been determined at several different concentrations (see Fig. D. 9-1) and the order is as would be predicted--i. e., the greater the hydration, the greater the attraction of the ion for the aqueous phase, and the smaller the distribution coefficient.

The determination of the distribution coefficients for the two middle anions of the latter series and for γ-chlorobutyrate (to be compared with valerate in order to demonstrate the equivalence of the chloro and methyl groups) will be completed shortly.

10. SUBMICROGRAM METHODS USED IN STUDIES OF THE SYNTHETIC ELEMENTS

Burris B. Cunningham

The program of chemical research on the macroscopic properties of the synthetic elements, which began with the first studies of plutonium in 1942, has involved a progressive refinement of experimental techniques. At present, a number of methods used in this program are suitable for quantities of material well below the microgram range. It is the purpose here to describe these methods as they now exist.

I. Magnetic Susceptibility Measurements on a Submicrogram Scale

A magnetic susceptibility apparatus was constructed so that the magnetic force was exerted in a horizontal plane, perpendicular to the direction of gravitational force. The principle of the modified apparatus may be understood by reference to the diagram, Fig. D. 10-1.

Under the action of simultaneous gravitational and magnetic forces the sample of mass M_s and gram susceptibility χ_{gm} assumes an equilibrium position, such that

$$M_s \, g \, d\,\theta = M_s \, \chi_{gm} \, H \, \frac{dH}{dx} \, L = M_s \, g \, L \sin\theta, \qquad (1)$$

where L is the length of a suspension fiber having a mass negligibly small with respect to the mass of the sample, M_s, d is the deflection, θ is the angle of deflection, H is the magnetic field, and $\frac{dH}{dx}$ its gradient in the horizontal plane.

Since M_s appears on both sides of the equation, the deflection of a sample of given susceptibility is independent of its mass. In principle, therefore, the apparatus is capable of measuring susceptibilities of indefinitely small quantities of material.

There are practical difficulties, however, in keeping the mass of the suspension fiber negligibly small with respect to the mass of the sample as the latter is reduced to very small values. For practical purposes Eq. (1) must be modified to show the influence of the mass of the suspension

fiber, M_f,

$$M_f \cdot g \frac{L}{2} \sin\theta + M_s\, g\, L \sin\theta =$$

$$M_s\, \chi_{gm}\, H \frac{dH}{dx}\, L. \qquad (2)$$

The magnetic susceptibilities of the tripositive ions of Bk^{+3} and Cf^{+3}, sorbed on single beads of Dowex-50, were measured in 1957, by use of equipment based on this principle. A description of the apparatus has been published. Only 56 nonograms of Cf were used in these measurements. In 1959 the apparatus was slightly modified again by directly cementing a 1-μg bead of Dowex-50 to a very fine suspension fiber, and used to make susceptibility measurements on 3 nanograms of einsteinium.

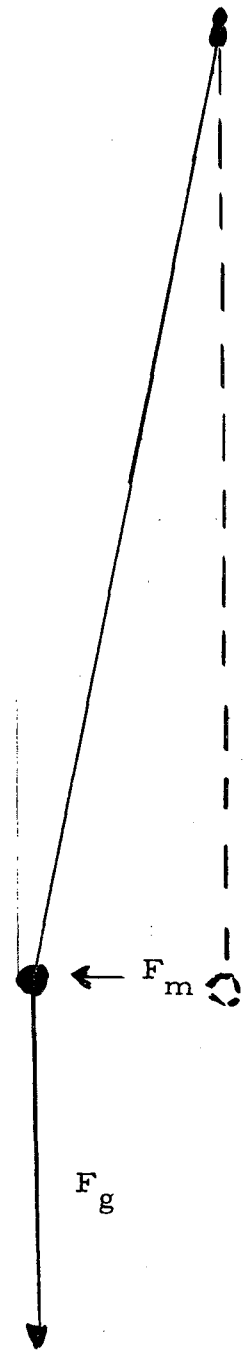

Fig. D. 10-1. Principle of magnetic susceptibility apparatus.

II. Absorption Spectroscopy Using Single Beads of Exchange Resins

Much of the interest in the susceptibility data on the actinide elements arises because these data provide information concerning the electronic configurations of the ions. Similar information may be derived from the determination and analysis of the absorption spectra of the ions.

The carefully purified Dowex-50 ion-exchange resins used in work with the synthetic elements show very little absorption in the visible region of the spectrum. They are therefore suitable for the observation of the absorption spectra of sorbed ions.

The technique employed for very small samples of the synthetic elements is illustrated in Figs. D. 10-2 and D. 10-3. The bead, which is saturated (or nearly saturated) with the ion of interest is placed in a closely fitting hole drilled in a thin sheet of platinum, sandwiched between a slide and cover slip. The mount is then placed on the stage of a microscope, and the bead is illuminated with an intense source of light such as that from a carbon arc. The spectrum is observed with a direct-vision spectroscope inserted in the microscope in place of the ocular. It may also be recorded photographically. The 503-mμ absorption line of americium ($\epsilon \approx 300$) has been easily observed with as little as one nanogram of Am.

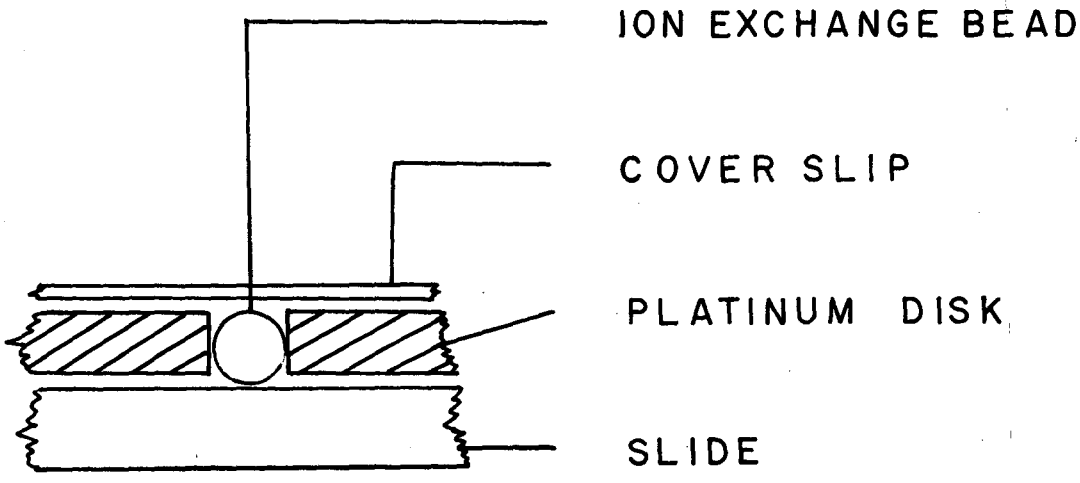

MU-22115

Fig. D.10-2. Mounting of ion-exchange bead for absorption spectroscopy.

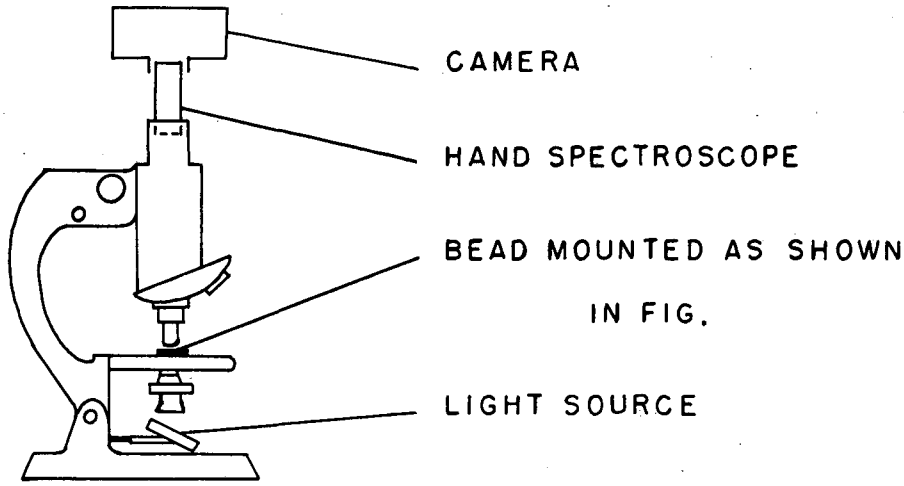

MU-22113

Fig. D. 10-3. Apparatus for ion-exchange bead absorption spectroscopy.

III. X-Ray Diffraction Work on Submicrogram Quantities of Crystalline Powders

X-ray diffraction methods have played and will continue to play an extremely important role in many phases of research on the synthetic elements. In the rarer elements, it is in general not feasible to produce single crystals of the materials of interest of sufficient size for single-crystal x-ray work. The less elegant powder methods, therefore have been used in almost all cases. Much work on the crystallography of the heavy-element compounds was done by W. H. Zachariasen and his collaborators during World War II, using a few micrograms of crystalline powders.

We have recently adapted diffraction methods to work with samples in the range from 0.1 to 0.01 μg, using ordinary x-ray diffraction equipment. Extensive work has been done on the crystallography of various compounds of californium, using samples of 0.1 to 0.2 μg weight.

The x-ray equipment used in this work employs the North American Philips Company x-ray tube, utilizing Cu Kα radiation. A 5.73-cm-diameter Norelco camera was used to obtain photographs of the diffraction patterns, which were taken on fast Ilford Industrial G film. The beam collimator of the camera was modified by insertion of a lead plug, sheathed in a section of hypodermic needle, pierced by a 0.07-mm-diameter hole. Exposure times varied from 4 to 24 hr. In most cases the x rays were filtered through 0.3-mil nickel foil, placed either at the x-ray tube port or in front of the film.

Success in obtaining good patterns is strongly dependent on the method of preparing and mounting the samples. Again it has proven extremely useful to employ single beads of ion-exchange resins in the initial stages of the x-ray work.

The steps followed in the preparation of submicrogram samples of the oxide, oxychloride, and trichloride of californium for x-ray diffraction work are illustrated in Fig. D. 10-4.

It is important that the wall thickness of the quartz capillary used to contain the sample be no more than about 1/5 the diameter of the sample, and that the x-ray beam diameter by no greater than about three times the sample diameter. Otherwise excessive scattering of the beam occurs and contrast with the diffraction lines from the sample is lost.

IV. Preparation of Metals on a Submicrogram Scale

Studies of the properties of the actinide metals constitute an extremely interesting and challenging area of investigation. Plutonium is one of the most complex metals known, and many of its properties continue to puzzle the theoretical metallurgist.

Elements beyond plutonium appear to be somewhat more normal in their properties, but as yet have been very little investigated. Small-scale techniques for producing the rarer synthetic elements are essential preliminary steps in such studies. A technique used successfully for making 0.1-μg amounts of the heavier elements is illustrated in Fig. D. 10-5.

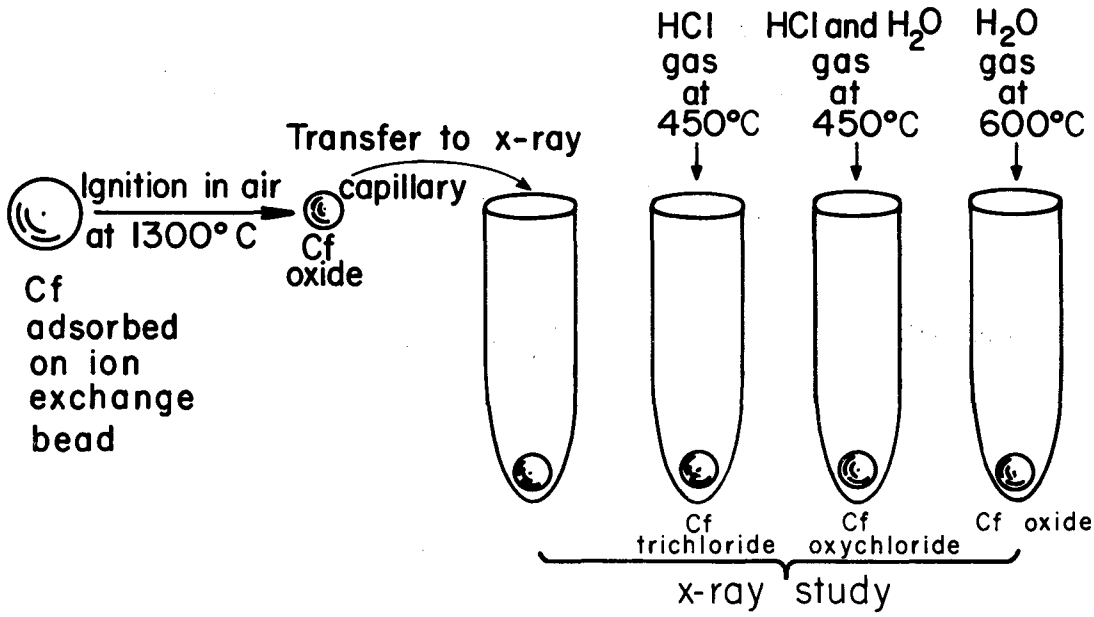

MU-22031

Fig. D. 10-4. Submicrogram scale preparation of heavy element compounds for x-ray diffraction investigation.

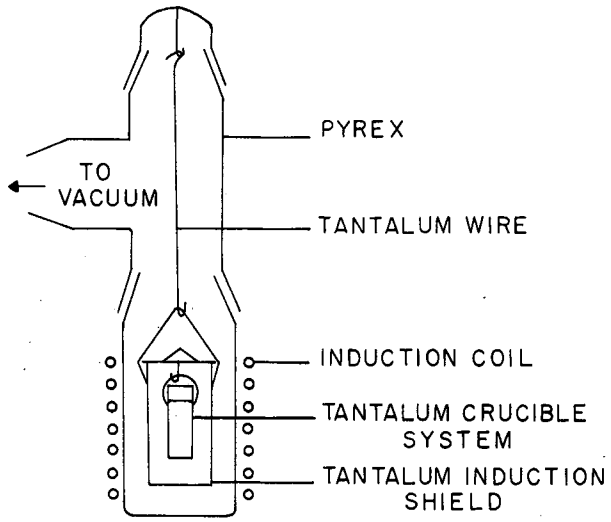

MICROSCALE METAL PRODUCTION APPARATUS

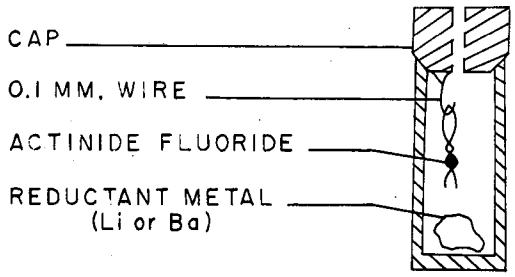

TANTALUM CRUCIBLE SYSTEM

MU-22112

Fig. D. 10-5. Apparatus for metal production.

A piece of the heavy-element trifluoride is inserted in one of the interstices of a twisted tantalum wire of 1 to 3 mils diameter. The trifluoride is reduced to the metal by reaction with barium vapor in an evacuated system. If the reduction temperature is properly chosen, the metal is obtained as a single globule adhering to the wire, from which it may be freed by gentle pressure and recovered intact. The sample may then be used for x-ray diffraction studies, or for other purposes. (The metal wire chosen to support the trifluoride should not form an alloy with the heavy-element metal formed, of course. Tantalum is suitable for americium and curium.)

V. Maintenance of Purity of Samples in Submicrogram Experimentation

The chance of random contamination of samples increases with decreasing sample size. Standards of cleanliness which are entirely satisfactory on a macro scale may be quite unsuitable with microgram samples.

One of the important technical advantages of the use of single beads of ion-exchange resins is that chance contamination in mechanical handling and transfer is much less than in more conventional methods of manipulation. In effect, the heavy elements are present in high concentration in very small containers of spherical shape which present minimal contact area to supporting surfaces. Solid impurities adhering to the beads may be removed mechanically or rinsed off with distilled water without loss of the sorbed materials.

Of course, some work must be done in aqueous solutions and some transfers carried out by ordinary pipetting. For such work containers or pipets made only from clean, freshly drawn silica tubing are employed, since it has been found that pyrex introduces significant amounts of Ca, Mg, Al, and Fe into either acidic or basic solutions in contact with it.

Reagents such as water, HCl, and HNO_3 are all freshly distilled below their boiling points onto quartz condensers.

The contamination of samples is one of the major problems in current work on the submicrogram scale, and it undoubtedly will become increasingly difficult to control in the future as the quantities of experimental materials are reduced still further.

11. PREPARATION AND CRYSTAL STRUCTURE OF AMERICIUM METAL (*)

Denis B. McWhan, James C. Wallmann, and Burris B. Cunningham
(with L. B. Asprey and F. H. Ellinger, Los Alamos Scientific Laboratory, Los Alamos, New Mexico, and W. H. Zachariasen, University of Chicago, Chicago, Illinois)

The crystal structure of americium has been studied by using metal produced by two methods. The first method consisted of the reduction of approximately 20-mg quantities of americium trifluoride with barium vapor in an all-tantalum double crucible system. The products were allowed to cool without controlled annealing. Spectrographic analysis of the resulting metal showed 2 weight % of impurities. In the second method americium dioxide, prepared by the decomposition of the oxalate in air was reduced with lanthanum metal. The large difference in the volatility of americium and lanthanum metals allows the product to be separated by distillation. The americium was effused through a hole in the crucible cap and collected on a rotatable tantalum wire or quartz fiber located $\leqslant$ 2 mm above the effusion orifice. Twenty to 100 μgm of americium, typically containing less than 0.5 weight % of lanthanum, was thus collected.

X-ray diffraction patterns were obtained by using Cu Kα radiation and 90-mm- and 114.6-mm-diameter cameras. The powder patterns of the microcrystalline metal from the fluoride reductions have been indexed as double hexagonal, close-packed, with a = 3.474±.005 A and c = 11.25±.02 A. The proposed structure yields a calculated density of 13.61±.05 g/cm^3 and a metallic radius of 1.73 A.

The powder patterns from the metal produced by the vaporization technique can be interpreted in terms of small amounts of AmO (fcc, a = 5.05),[1] and an intimate mixture of the cubic and hexagonal forms of of close-packed atoms, resulting from faults in the stacking of the close-packed layers. This type of stacking fault has been treated by Wilson.[2] The hexagonal reflections with (h-k)/3 = integral and ℓ = even superimpose on the cubic reflections and are sharp. The remaining lines are broadened because of the stacking faults. The above preparations were predominantly cubic, and the average face-centered cubic unit cell constant, on the basis of four preparations, is a = 4.894±.005 A. The calculated density is 13.65±.05 g/cm^3, and the metallic radius is 1.73 A.

---

*Brief version of published paper, J. Inorg. and Nuclear Chem. 15, 185 (1960).

[1] Yumi Akimoto, Burris B. Cunningham, Denis B. McWhan, and James C. Wallmann, Preparation of Americium Metal, Curium Metal, Americium Nitride, and Americium Monoxide, in Chemistry Division Semiannual Report, UCRL-8867, July 1959, p. 59.

[2] A. J. C. Wilson, X-Ray Optics (Methuen, London, 1949).

After one of the vaporized samples, which had been indexed as fcc, was kept at dry ice temperature for a week, the pattern was predominantly hexagonal and agreed with the double-hexagonal close-packed structure above. As the large-scale reduction yields dhcp structure, and the fcc phase goes to the dhcp phase on cooling, the dhcp phase is probably the α or room-temperature form, and the fcc phase becomes stable at a higher temperature.

Graf et al. have reported a dhcp phase of americium with $a = 3.642 \pm .005$, $c = 11.76 \pm .01$ A, and metallic radius 1.82 A,[3] but in this work no metal with the larger cell dimensions has been obtained. It should be pointed out, however, that the results of Graf and co-workers were reproduced in many successful reductions using both Am^{241} and Am^{243}, and that his metal appears to have been as pure as ours. It may be that americium, like cerium, exists in a "collapsed" as well as an expanded phase of the same structure type.

It must also be emphasized that spectrographic analysis is inadequate for the detection of all impurities, and particularly anionic impurities, small amounts of which may have an important effect on the structure.

Magnetic-susceptibility measurements and high-temperature x-ray studies are now in progress and will be reported in the future.

[3] P. Graf, B. B. Cunningham, et al., J. Am. Chem. Soc. 78, 2340 (1956).

12. ATOMIC BEAM RESEARCH

Richard Marrus

The electronic and nuclear properties of atoms can be very conveniently investigated by observing the magnetic resonance of these atoms in an atomic beam apparatus. In brief, the method is to pass the atoms through two inhomogeneous magnetic fields whose field gradients are in the same direction. In between the two inhomogeneous fields is a homogeneous field in which the magnetic resonance is performed. If the frequency of the radiation is such as to induce a change in sign of the high-field magnetic moment, an increase in intensity is noted at the detector and the resonance is observed.

The resonant frequency can be related to several important properties of the observed electronic state. The spectroscopic splitting factor g_J and the electronic angular momentum J can both be measured. From them it is possible to infer the electronic configuration and the details of the electronic coupling in the state. In addition, the magnetic dipole (A) and electric quadrupole (B) hyperfine-structure coupling constants can be measured and can be made to yield information about both the electronic and nuclear properties of the ground state.

The nuclear properties directly obtainable from beam measurements are the nuclear spin (I), the magnetic dipole moment (μ_I), and the hyperfine-structure anomaly (Δ). In addition, it is possible to infer the electric quadrupole moment (Q) and the magnetic octupole moment (Ω). Measurements of this kind have been made in all regions of the periodic table and have contributed much to our understanding of nuclear structure.

13. HYPERFINE STRUCTURE AND NUCLEAR MOMENTS OF PROTACTINIUM-233 (*)

Richard Marrus, William A. Nierenberg, and Joseph Winocur

By means of the atomic-beam magnetic resonance method using radioactive detection, the hyperfine structure of $_{91}Pa^{233}$ ($T_{1/2}$ = 27.4 days) has been investigated. Three low-lying states are found to be present in the beam, characterized by electronic angular momenta J = 11/2, 9/2, and 7/2, and g values g_J = -0.8141(4), -0.8062(15), and -0.7923(15) respectively. From these results it is inferred that the ground-state configuration of protactinium is almost certainly $(5f)^2\ (6d)^1\ (7s)^2$. The nuclear spin was measured and found to be I = 3/2 and the magnetic dipole and electric quadrupole hyperfine-structure coupling constants were measured as A = ± 595(40) Mc and B = ∓ 2400(300) Mc respectively. From a direct measurement, the nuclear moment is found to be μ_I = + 3.4(1.2) nm. From the hyperfine-structure constants and detailed calculations involving the electronic wave functions, the quadrupole moment is inferred to be Q = -3.0 barns.

*Abstract of paper (UCRL-9315) submitted to Phys. Rev.

14. THE MAGNETIC DIPOLE AND ELECTRIC QUADRUPOLE INTERACTION CONSTANTS OF BISMUTH-210 (*)

Seymour S. Alpert, Edgar Lipworth, and Matthew B. White, and K. F. Smith,†

The magnetic dipole interaction constant, a, and the electric quadrupole interaction constant, b, were measured for Bi^{210} (I=1, $T_{1/2}$= 5.0 days) by the method of atomic beams. These results were a = 21.78±.03 Mc and b = 112.38±.03 Mc. Sixteen "flop-in" resonances were observed, including the three direct transitions (F=5/2, m = 1/2 ↔ F = 3/2, m = 1/2), (F = 3/2, m = 1/2 ↔ F = 1/2, m = - 1/2), and (F = 3/2, m = -1/2 ↔ F = 1/2, m = 1/2). The radioactive isotope was produced from the stable metal by the reaction $Bi^{209}(n, \gamma)Bi^{210}$ in the Livermore pool-type reactor. Detection was by collection on sulfur-coated "buttons" which were counted in continuous-flow β counters.

*Abstract for American Physical Society Meeting, New York, Jan. 31–Feb. 4, 1961.

†On leave from the Cavendish Laboratory, Cambridge, England.

15. NUCLEAR MOMENTS OF IODINE-133

Seymour S. Alpert, Edgar Lipworth, and Matthew B. White

The magnetic dipole interaction constant, a, and the electric quadrupole interaction constant, b, of 21-hr I^{133} have been measured by a "flop-in" atomic-beam magnetic-resonance experiment. The spin of I^{133} is known to be 7/2.[1] The results are a = 596.8±1.0 Mc and b = 385.8±7.4 Mc. From these results and the known magnetic dipole moment of I^{127}, the magnetic dipole moment (uncorrected for diamagnetism) and the electric quadrupole moment (corrected for core polarization) of I^{133} were calculated and found to be $|\mu_{133}| = 2.821 \pm .005$ nm and $|Q_{133}| = 0.27 \pm .01$ barn. The electric and magnetic moments must have opposite signs; the sign of μ_{133} is very probably positive. A total of 14 resonances was observed in fields ranging from 26 gauss to 300 gauss, the observed transitions being ($F = 5$, $m_f = -3 \rightarrow F = 5$, $m_f = -4$) and ($F = 4$, $m_f = -2 \rightarrow F = 4$, $m_f = -3$).

[1] H. L. Garvin and E. Lipworth, The Nuclear Spin and Magnetic Moments of Iodine-133, to be submitted to Nuclear Phys.

16. NUCLEAR MOMENTS OF IODINE-132 (*)

Matthew B. White, Seymour S. Alpert, Hugh L. Garvin, and Edgar Lipworth

The magnetic dipole interaction constant, a, and the electric quadrupole interaction constant, b, have been measured in 2.3-hr I^{132} (I = 4) by an atomic-beam resonance experiment. The results are $|a| = 567.6 \pm 1.3$ Mc, $|b| = 128.2 \pm 10.3$ Mc, with b/a positive. These results, when combined with the known values of a, b, μ, and I of stable I^{127}, yield the nuclear magnetic moment and nuclear quadrupole moment of I^{132}. We find $|\mu_{132}| = 3.084 \pm .007$ nm (diamagnetically corrected), and $|Q| = .09 \pm .01$ barn, where a small core polarization or Sternheimer correction has been included. The sign of μ is not determined, but μ and Q must have opposite signs. The I^{132} was obtained by a milking process from Te^{132} supplied by Brookhaven National Laboratory. A total of 16 resonances was observed at magnetic fields ranging from 6.9 to 374.7 gauss. At each field the two flop-in resonances $(11/2, -7/2) \leftrightarrow (11/2, -9/2)$ and $(9/2, -5/2) \leftrightarrow (9/2, -3/2)$ were observed.

*Abstract for American Physical Society meeting, Berkeley, California, Dec. 29-31, 1960.

17. NUCLEAR SPIN AND HYPERFINE STRUCTURE OF LUTETIUM-176m

Matthew B. White, Seymour S. Alpert, and Edgar Lipworth

The nuclear spin of 3.7-hr Lu^{176m} has been measured by an atomic-beam magnetic-resonance flop-in experiment using radioactive detection. Observations were made by using Lu^{176m} atoms in the $^2D_{5/2}$ atomic ground state. The value I = 1 was measured by observing transitions in the states F = 7/2 and F = 5/2 at three different values of the applied magnetic field. The Lu^{176m} was prepared by the reaction $Lu^{175}(n\gamma)Lu^{176m}$. A total of 14 resonances was observed in fields ranging from 26 to 350 gauss.

18. NUCLEAR SPINS OF PROMETHIUM-149, PROMETHIUM-151, AND TERBIUM-160 (*)

Amado Y. Cabezas, Ingvar Lindgren,† Richard Marrus, and Mark Rubinstein

The atomic-beam magnetic-resonance method has yielded the ground-state nuclear spins of three radioactive rare earths. The results are I = 7/2 for 50-hr Pm^{149}, I = 5/2 for 27-hr Pm^{151}, and I = 3 for 72-d Tb^{160}. Zeeman transitions in the J = 7/2 level of promethium were observed with a previously measured electronic g value.[1] The g values used for terbium were obtained from an atomic-beam experiment on stable Tb^{159}.[2] The nuclear spins are interpreted on the basis of existing nuclear models.

*Abstract for American Physical Society Meeting, Berkeley, California, Dec. 29-31, 1960.

†Now at the Institute of Physics, University of Uppsala, Uppsala, Sweden.

[1]A. Cabezas, I. Lindgren, E. Lipworth, R. Marrus, and M. Rubinstein, Nuclear Spins of Neodymium-147 and Promethium-147 (UCRL-9122, March 1960), submitted to Nuclear Phys.

[2]S. Penselin and K. Schlüpmann (University of Heidelberg), private communication).

19. ELECTRONIC ENERGY LEVELS AND CRYSTAL QUANTUM STATES OF Tm (IV) (*)

John B. Gruber and John G. Conway

The electronic configuration of Tm IV in the ground state is sometimes written as [Xe core] $4f^{12}$, where there are essentially two "holes" in the 4f shell.

*Brief version of published paper, J. Chem. Phys. 32, 1178 (1960).

Following the coupling scheme of Russell and Saunders, one may couple 12 equivalent f electrons to obtain

$$^1S\,^3P\,^1D\,^3F\,^1G\,^3H\,^1I\,.$$

The calculations for pure electrostatic interactions for Tm IV (f^{12}) are the same as for Pr IV (f^2). The electrostatic results are given in Table I.

Table I. Pure electrostatic energy levels--f^{12} configuration

Level	Electrostatic equations in terms of Slater integrals	Electrostatic equations in terms of F_2 (a)	Energy levels normalized to $^3H = 0$
^3H	$F_0 - 25\,F_2 - 51\,F_4 - 13\,F_6$	$F_0 - 32.3\,F_2$	$0.00\,F_2$
^3F	$F_0 - 10\,F_2 - 33\,F_4 - 286\,F_6$	$F_0 - 18.9\,F_2$	$13.4\,F_2$
^1G	$F_0 - 30\,F_2 + 97\,F_4 + 78\,F_6$	$F_0 - 15.5\,F_2$	$16.8\,F_2$
^1D	$F_0 + 19\,F_2 - 99\,F_4 + 715\,F_6$	$F_0 - 16.3\,F_2$	$48.4\,F_2$
^1I	$F_0 + 25\,F_2 + 9\,F_4 + F_6$	$F_0 + 26.3\,F_2$	$58.6\,F_2$
^3P	$F_0 + 45\,F_2 + 33\,F_4 - 1287\,F_6$	$F_0 + 30.3\,F_2$	$62.6\,F_2$
^1S	$F_0 + 60\,F_2 + 198\,F_4 + 1716\,F_6$	$F_0 + 113.2\,F_2$	$145.5\,F_2$

(a) $F_4 = 0.138\,F_2$, and $F_6 = 0.0151\,F_2$.

When the electrostatic equations in terms of F_2 were normalized to ^3H as the ground state, the results were found to be complete agreement with those obtained by Elliott, Judd, and Runciman.[1]

Spedding has given the secular equations for f^2.[2] For the f^{12} configuration, one need only change the sign in front of each ζ value. The authors divided each term and ζ value in Spedding's equation by F_2 and used the variable $\chi = \zeta/F_2$. The secular equations may be solved for energy/F_2 as a function of χ. The results of the calculations appear in Fig. D. 19-1.

$^3H_4$ and $^3H_5$ levels

The spectrum of 203.0 mg of anhydrous $TmCl_3$ in 10.0 ml of 0.10 M DCl in > 98.5% D_2O was measured between 1 and 2 μ on a recording Cary 14 spectrophotometer. An acid solution was necessary in order to prevent the hydrolysis of the Tm^{+3} ion. Absorption bands for ordinary water appear

[1] Elliott, Judd, and Runciman, Proc. Roy. Soc. (London) A240, 509 (1957).

[2] F. H. Spedding, Phys. Rev. 58, 255 (1940).

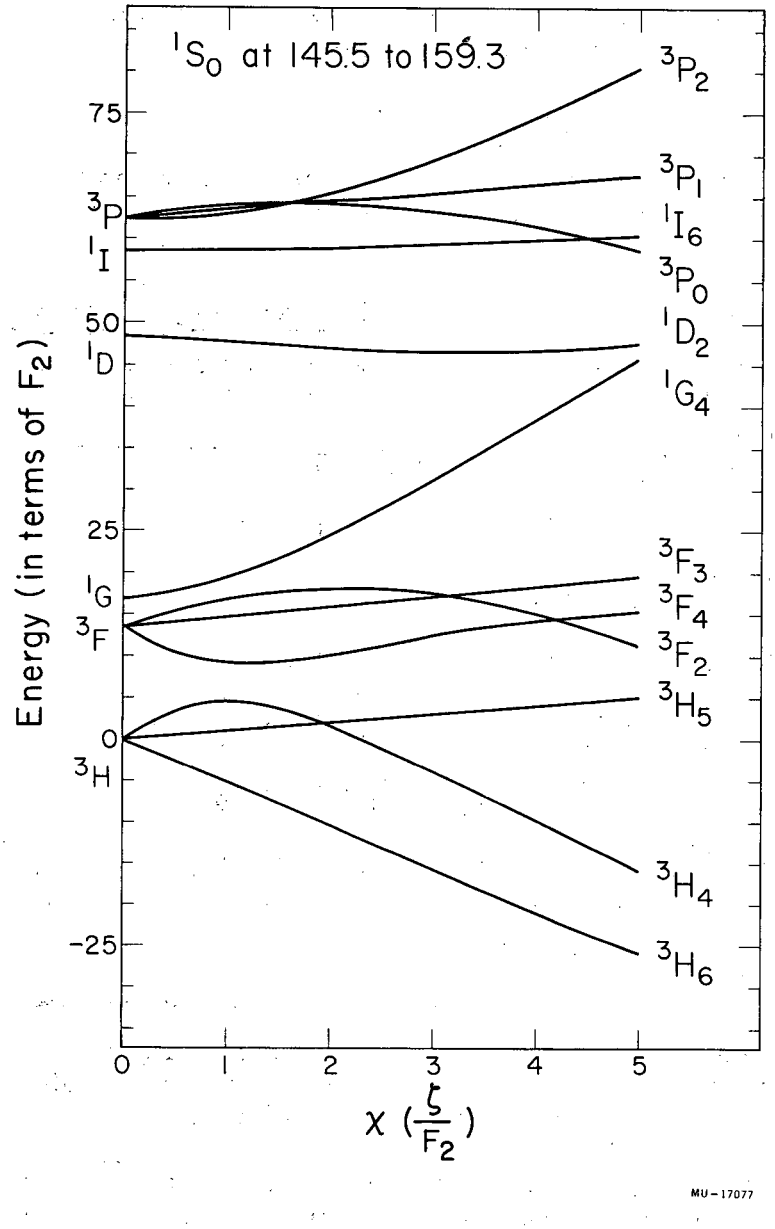

Fig. D.19-1. Energy-level diagram for Tm IV in intermediate coupling. The $^1S_0$ varies from 145.5 for $\chi = 0$ to 159.3 for $\chi = 5$.

around 1.4 μ and 1.8 μ, making it difficult to employ H_2O as a solvent for absorption studies in the region from 1 to 2 μ. In D_2O, the isotope shift is far enough to the red (to about 2.2 μ) to make D_2O a useful solvent for studies in the region where the $^3H_5$ and $^3H_4$ levels are expected. Two peaks (1.175 μ and 1.206 μ) and one shoulder (1.217 μ) were found for the $^3H_5$, and one peak (1.668 μ) and one shoulder (1.715 μ were found for the $^3H_4$. The theoretical values calculated for $^3H_5$ and $^3H_4$ are 8520 cm^{-1} and 5320 cm^{-1}, which may be compared with the mean experimental values 8,390 cm^{-1} and 5,900 cm^{-1}, respectively.

RESULTS

Johnsen has identified the 0 and ±1 crystal quantum levels of the $^3H_6$ ground-state multiplet and the upper multiplets of $^3F_{2,3,4}$ and $^1G_4$.[3] Our work confirms these ground-state assignments for transitions to the ultraviolet multiplets of $^3P_{0,1,2}$ and $^1D_2$.

The symmetry of the Tm^{+3} ion in the ethylsulfate crystal is C_{3h} as given by Johnsen and by Ketelaar.[4] The crystal-quantum selection rules for this symmetry have been discussed previously.[5] The ultraviolet multiplets appear sharper than the $^3F_{2,3,4}$ group. As a result, one observes transitions from additional ground-state crystal quantum levels to excited states. At 77°K, 194°K, and 273°K, the 3 and ±2 crystal quantum levels of the $^3H_6$ are populated. Transitions from these levels appear more intense as one goes from N_2 temperature (77°K) to CO_2 temperature (194°K). From the 3 and ±2 crystal quantum states the position of the μ = 0 level in $^1G_4$ was determined.

Figure D. 19-2 gives the energy level diagrams for the $^3P_0$, $^3P_1$, $^3P_2$ multiplets; Figure D. 19-3 gives the diagram for the $^1D_2$ and $^1G_4$. The $^3F_{2,3,4}$ lines are too broad to permit an extension of the analysis. Polarized lines are observed between the $^3P_0$ and $^3P_1$ multiplets which are not due to impurities. These lines are probably due to the $^1I_6$ multiplet. The lines are faint and difficult to distinguish from vibrational lines of the $^3P_0$ and $^3P_1$. As many as 10 vibrational lines per multiplet appear to the violet side of the $^3P_2$ and $^1D_2$.

Holmium and erbium ethylsulfate crystals were prepared and polarization spectra taken to determine if these impurities appeared in the Tm spectra. No lines of Er or Ho were observed in the Tm spectra taken.

The experimental data, including Johnsen's, were fitted to Fig. D. 19-1 and a good fit was obtained for $\chi = 3$, $F_2 = 450$ cm^{-1}, and ζ_{4f} 2700 cm^{-1}. The spin-orbit interaction term, ζ, as used in Fig. D. 19-1 and in Spedding's work is one-half this value. From these parameters the calculated positions were obtained and are listed in Table II.

---

[3] U. Johnsen, Z. Physik 152, 454 (1958).

[4] J. A. A. Ketelaar, Physica (Haag) 4, 619 (1937).

[5] Sayre, Sancier, and Freed, J. Chem. Phys. 23, 2060 (1955); ibid. 29, 242 (1958).

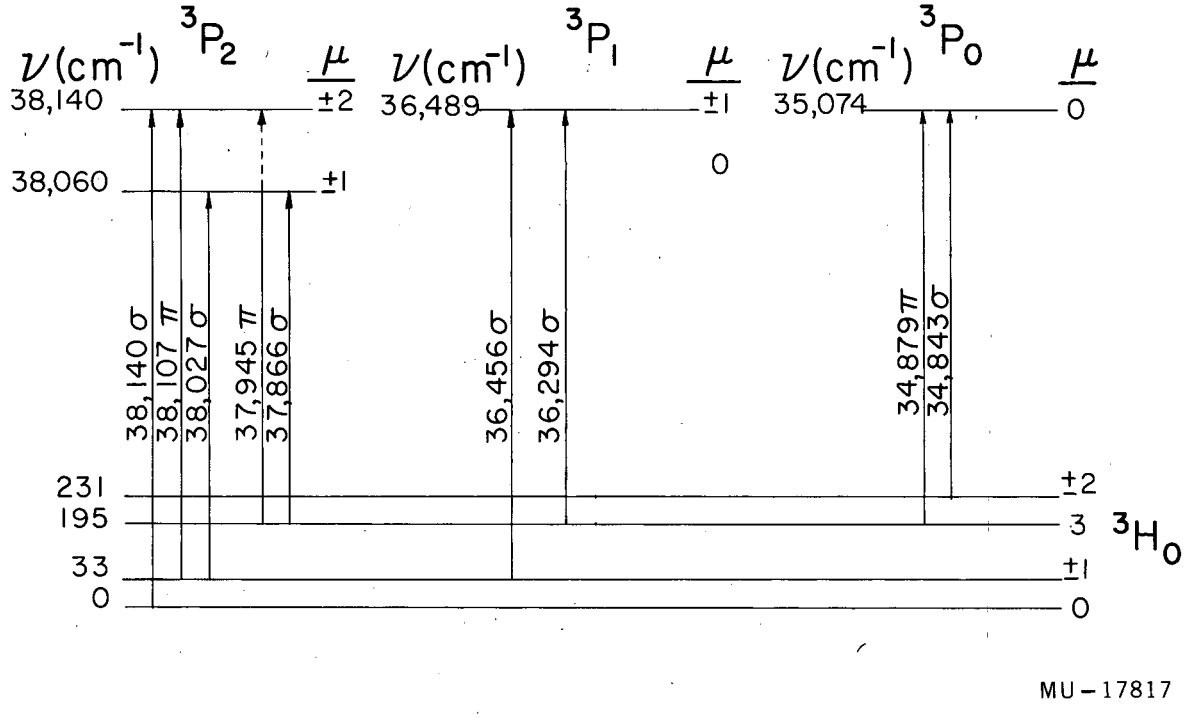

Fig. D. 19-2. Transitions from ground states to $^3P_{2,1,0}$ of $Tm(C_2H_5SO_4)_3 \cdot 9H_2O$. Spectra of single crystal at 77°K; electromagnetic radiation transmitted perpendicular to unique Z axis of crystal. Forbidden transition $3 \rightarrow \pm 2$ observed in $^3P_2$ group.

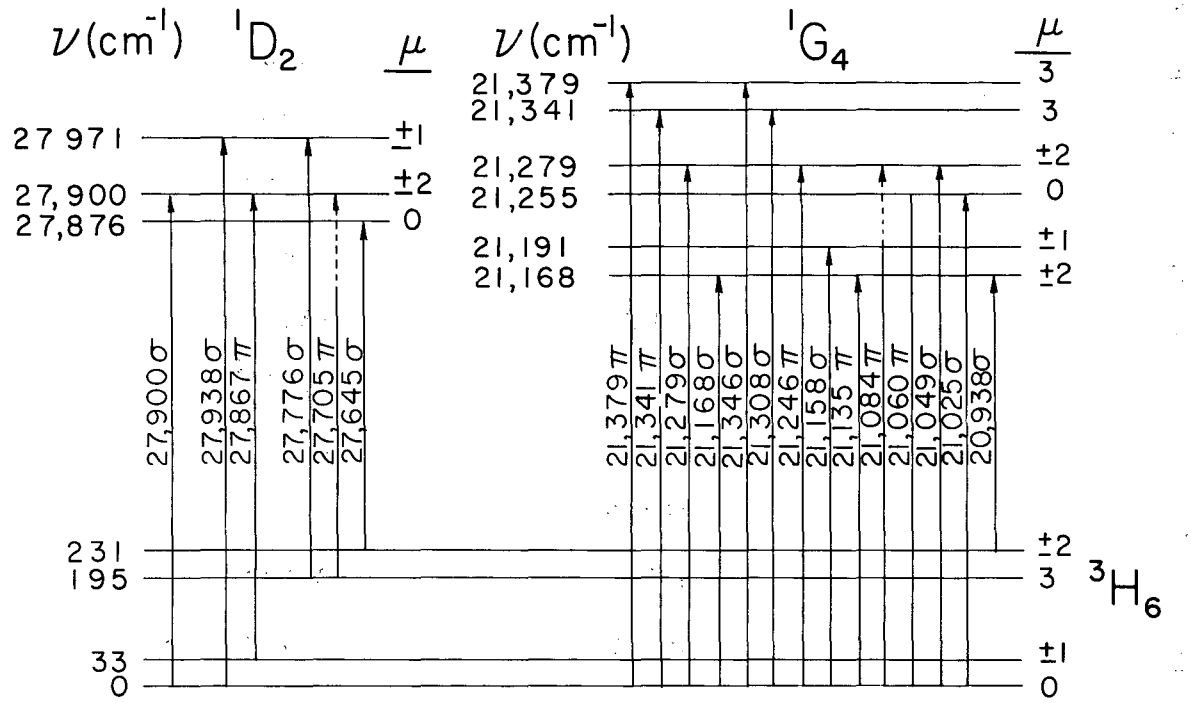

MU-17818

Fig. D. 19-3. Transitions from ground states to $^1D_2$ and $^1G_4$ of $Tm(C_2H_5SO_4)_3 \cdot 9H_2O$. Spectra of single crystal at 77°K; electromagnetic radiation transmitted perpendicular to unique Z axis of crystal. Forbidden transition $3 \rightarrow \pm 2$ observed in $^1D_2$ and $^1G_4$ groups.

Table II. Comparison of theory with experiment

Levels	Values for energy levels (cm^{-1}) Theory	Experiment
$^3H_6$	100	105
$^3H_4$	5320	5900
$^3H_5$	8520	8390
$^3F_4$	12730	12673[a]
$^3F_3$	14550	14446[a]
$^3F_2$	15000	15092[a]
$^1G_4$	21120	21275[a]
$^1D_2$	28090	27926
$^1I_6$	33850	--
$^3P_0$	35600	35074
$^3P_1$	36640	36443
$^3P_2$	38440	38100
$^1S_0$	75030	--

a. From Ref. 3.

20. EVALUATION OF ELECTROSTATIC ENERGY LEVELS OF f^6 (*)

John B. Gruber and John G. Conway

INTRODUCTION

The absorption and fluorescence spectra of Eu IV and Am IV have been reported in a number of papers.[1-5] However, a theoretical analysis of the absorption-spectra data (arising from 4f → 4f transitions) has not been

*Brief version of paper submitted to J. Chem. Phys. 34, 632 (1961).

[1] H. Gobrecht, Ann. Phys. 28, 673 (1937).

[2] O. Deutschbein, Ann. Phys. 36, 183 (1939).

[3] E. V. Sayre and S. Freed, J. Chem. Phys. 24, 1211 (1956).

[4] D. M. Gruen, J. G. Conway, R. D. McLaughlin, and B. B. Cunningham, J. Chem. Phys. 24, 1115 (1956).

[5] B. Stover and J. G. Conway, J. Chem. Phys. 20, 1490 (1952).

attempted, and only a complete analysis of the ^7F ground term and ^5D term by Judd[6] has been made from the fluorescence data of Sayre and Freed.[3] As a start in analyzing the absorption spectra, we have evaluated the 119 pure electrostatic energy levels for an nf^6 configuration. Tentative theoretical assignments can then be made for Eu IV and Am IV based on several assumptions. The necessary theory to handle such a problem is available in the papers of Racah, who has shown how states of f^n may be classified by group-theoretical methods.[7] Several papers are now available which describe how Racah's theory can be used.[8]

Elliott, Judd, and Runciman have re-evaluated all the pure electrostatic energy levels from f^2 to f^4 and the two lowest multiplicities of the f^5 and f^6 configurations.[8] Also Wybourne has calculated the doublet electrostatic energy matrices for f^5 and triplet and singlet matrices for f^6.[9] In this paper, a complete evaluation of the f^6 configuration energy matrices has been made independently by the authors, and actual energy levels in terms of F_2, the Slater radial integral, are presented on the assumption of various Slater F_k ratios.

Electrostatic Energy Levels

Three different Slater F_k ratios were used in our calculations. For $4f^6$, the 4f hydrogenic radial-distribution function yields $F_4/F_2 = 0.1381$ and $F_6/F_2 = 0.01511$; for $5f^6$ the 5f hydrogenic radial distribution function yields $F_4/F_2 = 0.1422$, and $F_6/F_2 = 0.01610$; and from Cohen's relativistic Hartree-Fock calculation for the normal uranium atom, Marrus et al. obtained (from an IBM-704 program) $F_4/F_2 = 0.159$ and $F_6/F_2 = 0.0204$.[10] The additional assumption is made that the F_k ratios obtained from the Hartree-Fock calculation will not change appreciably in going from the uranium atom with three f electrons to the Am IV, $5f^6$, for example.

The theoretical results are given in Tables I, II, and III. Each table gives the configuration considered and the assumption made for that calculation. It should be noted that several numerical errors were found under the f^6 column in Table III of Elliott et al. These errors have been corrected and all other energy levels for nf^6 rechecked.

TERM ANALYSIS

There is no question that an intermediate-field calculation of the 301J levels for f^6 is necessary in order to completely interpret the absorption

[6] B. R. Judd, Mol. Phys. 2, 407 (1959).

[7] G. Racah, Phys. Rev. 76, 1352 (1949).

[8] J. P. Elliott, B. R. Judd, and W. A. Runciman, Proc. Roy. Soc. (London) A, 240, 509 (1957).

[9] B. G. Wybourne (Johns Hopkins University, Baltimore, Md.), private communication, 1960; to be published.

[10] Richard Marrus, William A. Nierenberg, and Joseph Winocur, Phys. Rev. 120, 1429 (1960).

TABLE I

Pure Electrostatic Energy Levels for the $4f^6$ configuration.

Assumption: 4f hydrogenic radial distribution function.

Energy levels in terms of F_2.

Term	Energy	Term	Energy	Term	Energy	Term	Energy	Term	Energy
^7F	0	^1I	114.5	^3H	148.3	^3H	181.7	^3H	250.4
^5D	51.70	^3D	114.6	^5F	148.6	^1L	183.6	^1G	251.4
^5L	57.64	^1N	117.5	^1M	148.7	^1H	185.0	^3G	253.6
^5G	60.69	^3H	118.2	^3D	151.3	^3M	186.7	^1I	257.7
^5H	68.93	^3G	118.9	^1I	151.6	^3L	194.3	^3G	268.3
^5I	78.03	^3M	121.7	^1F	153.4	^3I	198.8	^3P	269.1
^5F	78.89	^3K	121.8	^1G	154.5	^3K	199.3	^1S	269.7
^5K	88.05	^1L	122.6	^1K	155.8	^3P	200.0	^1D	277.2
^3P	88.57	^3I	126.7	^3I	157.6	^1G	202.6	^1L	277.6
^3O	95.37	^1G	126.8	^3K	162.3	^1L	203.4	^1G	277.7
^5G	96.52	^3L	128.2	^3F	163.6	^3G	204.0	^3D	278.7
^3M	97.67	^3H	130.1	^1F	164.5	^1N	208.2	^1F	279.4
^3K	99.56	^1M	130.8	^3H	167.1	^3F	213.4	^3F	300.4
^5D	99.73	^3F	131.2	^1S	168.4	^1F	221.7	^1D	304.4
^3F	101.2	^5S	132.2	^1G	170.1	^1P	222.5	^1G	322.8
^3H	101.4	^3P	132.7	^3P	170.6	^3H	222.8	^1H	325.5
^3I	101.5	^1H	133.2	^1D	171.4	^3D	228.3	^3F	334.3
^5P	104.5	^3I	135.6	^3D	174.9	^1H	233.9	^3P	337.2
^3N	106.7	^3L	136.1	^3G	175.0	^1D	236.4	^1I	337.4
^3G	107.5	^1D	136.7	^5G	177.3	^3I	237.5	^3H	337.9
^5H	110.1	^3F	137.7	^3F	178.6	^3F	241.1	^1G	372.3
^3K	112.6	^1I	142.1	^5D	180.7	^1I	241.3	^1D	395.3
^1S	113.9	^5I	144.4	^1K	180.9	^3K	242.6	^1S	462.2
^1Q	114.1	^3G	145.7	^1I	181.4	^1K	246.5		

TABLE II

Pure electrostatic energy levels for the $5f^6$ configuration.

Assumption: 5f hydrogenic radial distribution function.

Energy levels in terms of F_2.

Term	Energy	Term	Energy	Term	Energy	Term	Energy	Term	Energy
^7F	0	^1S	120.2	^5F	150.8	^1L	188.1	^1G	255.1
^5D	54.76	^1I	120.5	^3H	151.7	^1H	189.3	^3G	255.7
^5L	60.04	^3H	122.6	^1M	152.9	^3M	190.4	^1I	261.8
^5G	63.56	^3G	122.9	^3D	154.7	^3L	197.7	^3G	270.9
^5H	71.03	^1N	123.2	^1I	156.4	^3I	202.0	^3P	272.6
^5I	80.21	^3K	125.6	^1F	158.4	^3P	203.8	^1S	273.8
^5F	81.29	^3M	125.7	^1G	159.2	^3K	204.4	^1D	280.7
^5K	90.06	^1L	127.9	^1K	160.7	^1G	206.5	^3D	280.7
^3P	94.53	^3I	130.5	^3I	161.0	^3G	207.6	^1L	281.0
^5G	98.73	^1G	131.9	^3K ^3F	166.5 167.3	^1L	207.7	^1G	282.0
^3O	99.50	^3L	132.0	^1F	168.5	^1N	212.4	^1F	282.1
^5D	101.8	^3H	133.8	^3H	170.7	^3F	216.6	^3F	303.8
^3M	102.0	^3F	134.7	^1S	172.6	^1F	225.2	^1D	307.5
^3K	104.0	^5S	135.0	^3P	173.9	^1P	225.6	^1G	326.4
^3I	105.7	^1M	135.3	^1G	174.4	^3H	226.0	^1H	328.3
^3F	105.8	^3P	136.6	^1D	175.4	^3D	231.3	^3F	336.3
^5P	106.1	^1H	137.6	^3G	178.1	^1H	238.1	^3P	338.8
^3H	106.2	^3I	139.6	^3D	178.3	^3I	240.0	^1I	341.2
^3N	110.6	^3L	140.1	^5G	178.7	^1D	240.7	^3H	341.4
^5H	111.8	^3F	141.6	^5D	181.7	^3K	243.5	^1G	374.6
^3G	112.0	^1D	142.4	^3F	181.8	^3F	244.1	^1D	399.1
^3K	115.8	^1I	147.0	^1K	184.5	^1I	244.8	^1S	467.7
^3D	118.5	^5I	147.0	^3H	185.4	^1K	250.0		
^1Q	119.0	^3G	148.9	^1I	185.4	^3H	253.4		

TABLE III

Pure electrostatic energy levels for the $5f^6$ configuration.

Assumption: Slater ratios from Hartree-Fock calculation for the normal uranium atom.

Energy levels in terms of F_2.

Term	Energy	Term	Energy	Term	Energy	Term	Energy	Term	Energy
^7F	0	^3H	140.4	^3H	166.3	^1I	205.9	^1K	266.5
^5D	67.21	^3G	140.6	^1I	168.0	^3M	206.9	^3H	266.9
^5L	70.14	^3K	141.2	^3D	169.6	^1L	207.6	^1G	272.0
^5G	72.24	^3M	142.8	^1M	171.4	^1H	208.0	^1I	280.0
^5H	80.01	^1I	144.8	^3I	176.0	^3L	213.1	^3G	283.6
^5I	89.52	^1S	145.5	^1I	176.7	^3I	216.7	^3P	288.5
^5F	91.36	^3I	146.2	^1F	179.0	^3K	217.5	^3D	291.3
^5K	98.83	^1N	147.2	^1G	179.6	^3P	220.5	^1S	292.7
^5G	108.4	^5S	147.6	^3K	180.2	^3G	223.5	^1F	295.1
^5D	111.2	^3L	147.9	^1K	181.9	^1G	223.9	^1D	296.7
^5P	113.4	^3F	149.8	^3F	183.1	^1L	226.7	^1L	296.8
^3O	116.8	^3H	149.9	^5G	185.3	^3F	231.0	^1G	301.3
^3P	118.5	^1L	149.9	^3H	185.7	^1N	231.5	^3F	319.6
^5H	119.4	^3P	152.5	^1F	186.2	^1P	239.8	^1D	322.6
^3M	119.9	^1G	153.1	^5D	187.7	^3H	240.6	^1H	342.0
^3I	123.5	^1M	154.2	^3P	188.2	^1F	240.6	^1G	343.6
^3K	123.5	^1H	156.2	^1S	191.1	^3D	244.7	^3F	347.3
^3F	124.5	^3I	157.3	^3G	192.1	^3I	252.2	^3P	348.5
^3H	125.5	^3L	157.5	^1D	192.6	^1H	256.8	^3H	357.8
^3N	127.0	^3F	158.5	^3D	193.0	^3F	257.7	^1I	359.7
^3G	130.4	^5I	158.7	^1G	193.3	^3I	259.4	^1G	387.6
^3K	131.6	^5F	160.7	^3F	195.8	^1D	259.8	^1D	418.2
^3D	134.6	^3G	162.8	^1K	201.3	^1I	260.6	^1S	494.6
^1Q	139.9	^1D	166.3	^3H	202.0	^3G	266.0		

spectra of Eu IV and Am IV. However, until the intermediate-field matrices are completed, we can use some pieces of experimental and theoretical information now at our disposal to give us at least a tentative term assignment for some of the J levels of Eu IV.

The Sayre and Freed J-level assignments for Eu IV are based on the polarized and axial absorption spectra of $Eu(C_2H_5SO_4)_3 \cdot 9H_2O$[3]. Such polarized data, consistent with a given point symmetry, identified J levels 1, 2, and 3 uniquely and larger J values only indicatively.

We have found the 5f hydrogenic ratios to give the best values to the electrostatic energy levels for Eu IV. From a least-squares fit, Wybourne in his analysis of Nd IV, $4f^3$ also obtained Slater ratios close to the 5f hydrogenic ratios.[11] If the reasonable values of $\zeta = 1360\ cm^{-1}$ (Ref 12) and $F_2 = 370\ cm^{-1}$ are used for Eu IV, we obtain an L-S plot of energy levels in units of F_2 which appears in Fig. D. 20-1.

It should be pointed out that a term assignment in intermediate field is based on that L-S level which provides the largest eigenvector contribution to a given J level. In Fig. D. 20-1, however, for Eu IV we have made the assignments in terms of the parent L-S level, since the exact eigenvectors are not known. The goodness of fit in some cases would indicate that the L-S level will probably also be the intermediate level. Several of the theoretical levels have been evaluated according to first-order perturbation theory. Judd has calculated the depression of the $^7F_0$ by the $^5D_0$ and obtains $1324\ cm^{-1}$.[13] This correction has been made to the experimental data of Sayre and Freed.

On the basis of the data and assumptions just considered, we can make a limited number of assignments. The $^5D_{0,1,2}$ which have been studied and identified by various workers agree fairly well with our plot.[14,15] Also we presume to identify the $^5G_2$, $^5G_3$, $^5F_2$, $^3P_2$, and possibly the $^5H_3$ from the Sayre and Freed data. However, it is impossible to unequivocally identify such levels as the $^5I_{4,5,6,7}$, $^5L_{6,7}$, and $^5H_{4,5,6,7}$ because of the complex absorption-spectra pattern. Zeeman experiments must be done on such levels if further analysis is to be made. Complications in the analysis of the Eu IV data result from the intermixing of crystal quantum sublevels of different near-by J levels. Also F_k ratios should be determined from the experimental data.

---

[11] B. G. Wybourne, J. Chem. Phys. 32, 639 (1960).

[12] B. R. Judd, Proc. Phys. Soc. (London) A 69, 157 (1956).

[13] Brian R. Judd (Lawrence Radiation Laboratory), private communication, 1960.

[14] K. H. Hellwege, U. Johnsen, H. G. Kahle, and G. Schaack, Z. Physik 148, 112 (1957).

[15] H. G. Kahle, Z. Physik 155, 145 (1959).

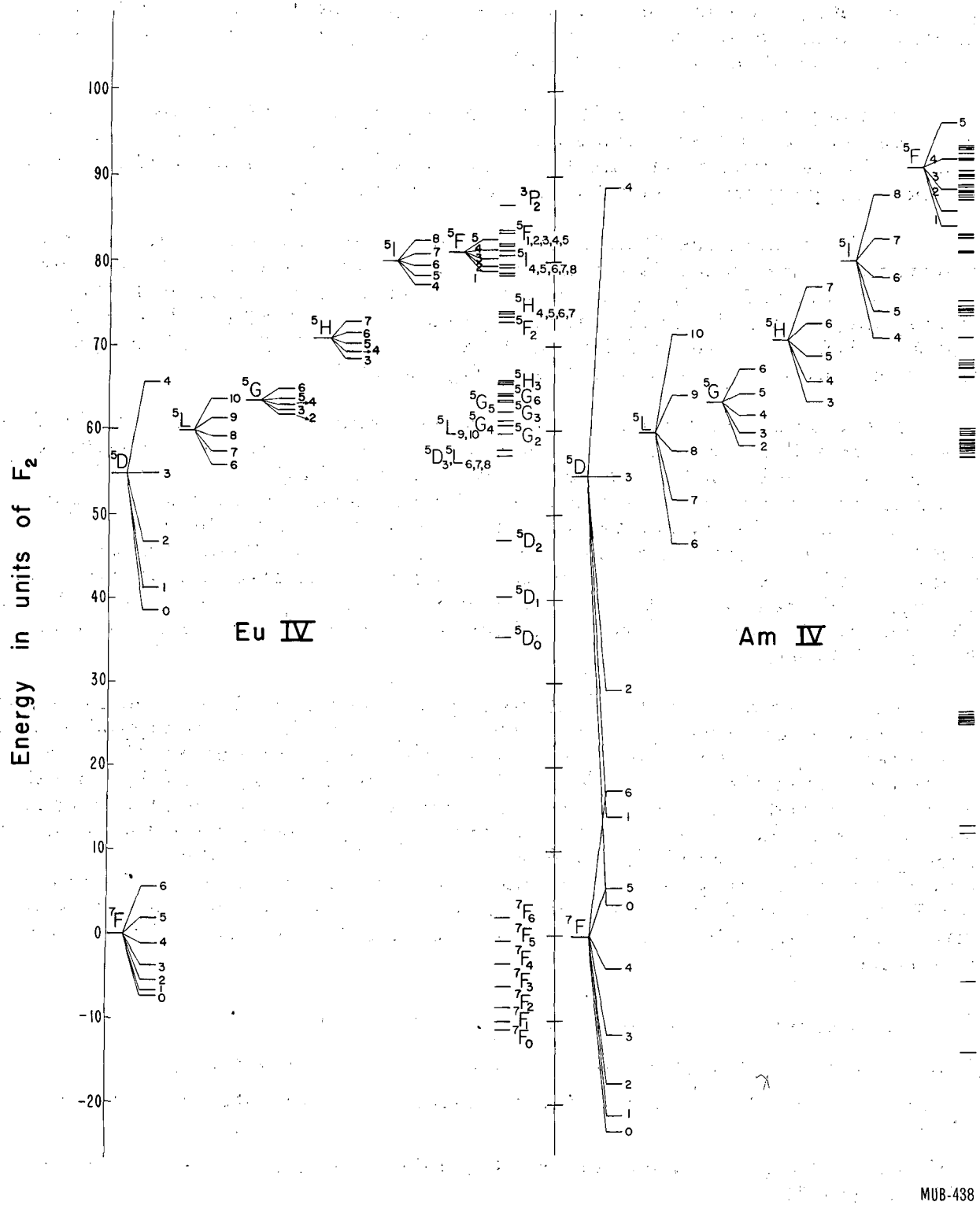

Fig. D. 20-1. Comparison of the L-S, Landé energy levels with experimental levels for Eu IV and Am IV.

The right-hand side of Fig. D. 20-1 represents Am IV energy levels based on values of 2600 cm^{-1} for ζ and 225 cm^{-1} for F_2. The experimental infrared energy levels are unpublished work of the authors; other levels shown are from Stover and Conway.[5] It is apparent that nothing can be derived from the L-S model even in the ground state of Am IV. However, the polarized absorption spectra of Am IV in $LaCl_3$, which allow experimental identification of the ^7F levels, will be made available shortly for an intermediate-field calculation of Am IV energy levels.

21. THEORY OF ZEEMAN EFFECT IN THE GROUND MULTIPLETS OF RARE EARTH ATOMS

B. R. Judd

The purpose of this note is to summarize the paper of the same title written with I. Lindgren,[1] and also to compare the predictions made there to the recent experimental results of Woodgate[2] for SmI.

As a first approximation, the effect of an external magnetic field $\underset{\sim}{H}$ on the energy levels of a free atom is taken into account by including the term

$$\mathcal{H} = \mu_0 \underset{\sim}{H} \cdot (\underset{\sim}{L} + 2\underset{\sim}{S}) \tag{1}$$

in the Hamiltonian, where $\underset{\sim}{L}$ is the orbital angular momentum of the electron system, and $\underset{\sim}{S}$ is that of the spin; μ_0 is the Bohr magneton. Since $\underset{\sim}{L} + 2\underset{\sim}{S}$ is a vector, its matrix elements are proportional to those of $\underset{\sim}{J}$, the total angular momentum of the atom. The factor of proportionality is called the Landé g factor, and if L and S are good quantum numbers, is given by

$$g = 1 + \frac{J(J+1) + S(S+1) - L(L+1)}{2J(J+1)} .$$

This approach is sufficiently accurate for most purposes, but the high precision of atomic beam measurements leads us to attempt a number of improvements. They are essentially of two kinds: the first elaborates the simple perturbation $\mathcal{H}$; the second allows for the fact that Russell-Saunders coupling may not be obeyed rigorously, so that S and L are not good quantum numbers. The Schwinger correction, which replaces the factor 2 in Eq. (1) by 2.00232, is of the first category. In addition, there is the Breit[3]-Margenau[4] correction, which adds to $\mathcal{H}$ the term

[1] B. R. Judd and I. Lindgren (same title) (UCRL-9188, May 1960), submitted to Phys. Rev.

[2] K. M. Woodgate, private communication.

[3] G. Breit, Nature 122, 649 (1928).

[4] H. Margenau, Phys. Rev. 57, 383 (1940).

$$-\alpha^2 \mu_0 \sum_i \underset{\sim}{H} \cdot (\underset{\sim}{\ell}_i + 2\underset{\sim}{s}_i) T_i - \underset{\sim}{s}_i \cdot (\nabla_i V_i \times \underset{\sim}{A}_i) , \qquad (2)$$

where T_i is the kinetic energy operator, and V_i is given by

$$V_i = -\frac{Z}{r_i} + \sum_{k \neq i} \frac{1}{r_{ik}} .$$

Here α is the fine-structure constant. This correction is essentially a relativistic correction, since it derives from the Dirac theory of the electron. Breit's equation for electron-electron interactions[5] gives to the further correction

$$\alpha^2 \mu_0 \sum_{i \neq k} \left[2\underset{\sim}{s}_i \cdot (\nabla_k \frac{1}{r_{ik}} \times \underset{\sim}{A}_k) - \frac{\underset{\sim}{A}_k \cdot \underset{\sim}{p}_i}{r_{ik}} - \frac{(\underset{\sim}{r}_{ik} \cdot \underset{\sim}{A}_k)(\underset{\sim}{r}_{ik} \cdot \underset{\sim}{p}_i)}{r_{ik}^3} \right] \qquad (3)$$

This term depends on the electron density in the core, and is called the diamagnetic correction. The method of Abragam and Van Vleck[6] is used to throw Eqs. (2) and (3) into more tractable forms; eventually their expectation values depend on various radial integrals.

For rare earth atoms, various data suggest that the lowest configurations are usually of the type $4f^n$. The radial integrals are calculated by using the modified hydrogenic eigenfunction of the form $r^n e^{-ar} \cosh k(ar-n)$. The parameter k is estimated to be approximately 0.42 over the rare earth series by comparison with available Hartree SCF eigenfunctions. The second parameter, a, is chosen to give a fit with the spin-orbit coupling constants, which are investigated and evaluated from the existing raw data where necessary. As a subsidiary topic, accurate values of $\langle r^{-3} \rangle$ for neutral and triply ionized rare earth ions are presented to facilitate the calculation of nuclear moments of rare earth atoms.

To calculate the breakdown of RS coupling, the Coulomb integrals F_k are required, since it is necessary to know where the perturbing levels are located. This calculation is forced upon us because no experimental data are available for these levels. Except for some special cases, the complexity of configurations of the type $4f^n$ makes it feasible to pursue the calculations to second order in perturbation theory only. Correlation effects are allowed for by using different eigenfunctions from those assumed when estimating the radial integrals of the single particle operators. Tables are given of the g values for all levels of the lowest multiplets of the rare earth atoms;

[5] G. Breit, Phys. Rev. 34, 553 (1929).

[6] A. Abragam and J. H. Van Vleck, Phys. Rev. 92, 1448 (1953).

the equation

$$\Delta = (J+1)g_J - (J-1)g_{J-1} = a\,J^2 + b$$

proved useful in checking results for a given multiplet. Agreement in all cases is extremely good, confirming that the ground configurations of PrI, NdI, PmI, SmI, EuI, DyI, HoI, ErI, and TmI are of the type $4f^n$, and that such a configuration is very low-lying in TbI.

The new experimental data of Woodgate for SmI are displayed in Fig. D. 21-1, and compared to the predictions of the theory. The slight discrepancies between experiment and theory which still remain are to be ascribed to third- and higher-order spin-orbit coupling effects.

22. CRYSTAL-FIELD SPLITTING OF ENERGY LEVELS OF THULIUM ETHYLSULFATE (*)

John B. Gruber and John G. Conway

In a $Tm(C_2H_5SO_4)_3 \cdot 9\,H_2O$ single crystal, where the Tm^{+3} configuration is $4f^{12}$, the perturbing influence of the water and ethylsulfate groups on the energy-level system of the free ion can be calculated by expanding the crystal-field electric potential in a series of spherical harmonics. A first-order perturbation treatment is possible, since the crystal-field splitting of the various electronic levels is of the order of 100 cm^{-1}, whereas the spin-orbit splitting between adjacent levels is generally greater than 1000 cm^{-1}. The work of Ketelaar has shown that the point symmetry at the metal-ion site in rare earth ethylsulfates is predominantly C_{3h}.[1] Johnsen[2] and these authors[3] have found C_{3h} point symmetry to be consistent with the interpretation of the $Tm(C_2H_5SO_4)_3 \cdot 9\,H_2O$ absorption spectra. However, a few transitions were observed that are forbidden in C_{3h} symmetry but are allowed in C_{3v} symmetry. The theoretical splitting of $^3H_6$, $^3F_4$, $^3F_3$, $^3F_2$, $^1G_4$, $^1D_2$, and $^3P_2$ levels presented here is based on the experimental work of these investigators.

In an earlier paper[3] the electronic energy levels for Tm^{+3} in the intermediate field were obtained from a plot of E/F_2 vs χ, where $\chi = \zeta/F_2$, ζ is the spin orbit parameter used by Spedding,[4] and F_2 is a Slater integral. The best fit of theory to experiment was obtained at $\chi = 3$. The eigenvectors at $\chi = 3$ for $^3H_4$, $^3F_4$, $^1G_4$, and $^3F_2$, $^3P_2$, $^1D_2$, used in calculating α, β, and γ in the intermediate field, were obtained from an IBM 650 program. The eigenvectors for $^3H_6$ and $^1I_6$ were calculated by hand by using Spedding's equations. Table I includes values of operator equivalents for $Tm(C_2H_5SO_4)_3 \cdot 9\,H_2O$ with intermediate-field corrections in brackets.

---

*Condensed version of published paper, J. Chem. Phys. 32, 1531 (1960).

[1] J. A. A. Ketelaar, Physica (Haag) 4, 619 (1937).

[2] U. Johnsen, Z. Physik 152, 454 (1958).

[3] J. B. Gruber and J. G. Conway, Electronic Energy Levels and Crystal Quantum States of Tm(IV), J. Chem. Phys. 32, 1178 (1960).

[4] F. H. Spedding, Phys. Rev. 58, 255 (1940).

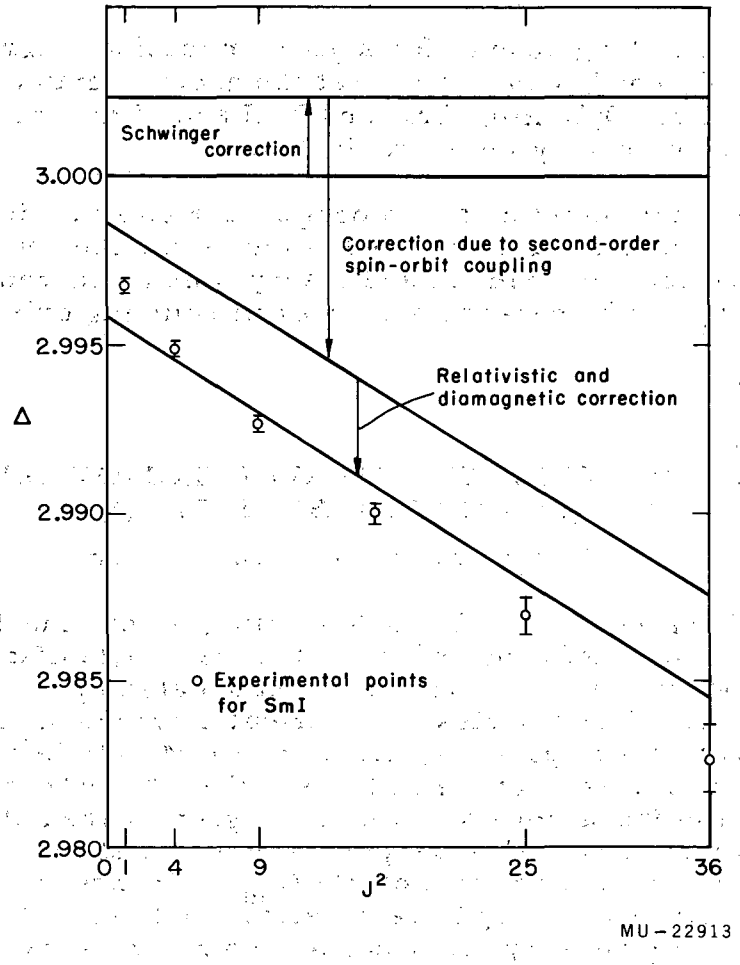

Fig. D.21-1. A plot of Δ against J^2.

Table I. Operator equivalents in the intermediate field, $Tm^{+3}(4f^{12})$

Level	$\langle J \| \alpha \| J \rangle$		$\langle J \| \beta \| J \rangle$		$\langle J \| \gamma \| J \rangle$	
$^3P_1$	$\frac{1}{5}$	[1.000]	0		0	
$^3P_2$	$\frac{-1}{15}$	[1.095]	$\frac{-4}{7\cdot 27}$	[0.629][a]	0	
$^1D_2$	$\frac{-22}{15\cdot 21}$	[0.678]	$\frac{-4}{7\cdot 27}$	[-0.105]	0	
$^3F_2$	$\frac{-8}{21\cdot 15}$	[1.636]	$\frac{2}{7\cdot 81}$	[-1.859]	0	
$^3F_3$	$\frac{-1}{90}$	[1.000]	$\frac{1}{45\cdot 99}$	[1.000]	$\frac{1}{39\cdot 99}$	[1.000]
$^3F_4$	$\frac{-1}{126}$	[-1.357]	$\frac{1}{45\cdot 77}$	[1.527]	$\frac{-1}{13\cdot 63\cdot 99}$	[5.945]
$^1G_4$	$\frac{2}{11\cdot 35}$	[1.799]	$\frac{46}{11\cdot 45\cdot 77}$	[0.866]	$\frac{4}{13\cdot 33\cdot 77}$	[0.537]
$^1I_6$	$\frac{2}{99}$	[0.995]	$\frac{-4}{11\cdot 15\cdot 99}$	[0.984]	$\frac{2}{13\cdot 33\cdot 21\cdot 99}$	[0.967]
$^3H_6$	$\frac{1}{99}$	[1.010]	$\frac{8}{3\cdot 11\cdot 1485}$	[0.976]	$\frac{-5}{13\cdot 33\cdot 2079}$	[0.986]

[a]The pure L-S operator equivalent, β, is zero for $^3P_2$, since the corresponding Racah coefficient is zero. However, if we allow for intermediate coupling effects, the entry becomes $(-4/7\cdot 27)$ [0.629].

Having found α, β, and γ for a particular level, we can now express the crystal splitting in terms of parameters $A^m_n \langle r^n \rangle$. These parameters were defined earlier. The values that these parameters can assume must be consistent with the point symmetry at the rare earth ion in the lattice. The structure of $^3P_1$ (split into two sublevels $\mu = 0, \pm 1$) gives at once a preliminary value for $A^0_2 \langle r^2 \rangle$. Unfortunately, our photographic plates unambiguously confirmed only the position of the $\mu = \pm 1$ sublevel in $^3P_1$. Another line appearing in both σ and π polarization with a line width of some 10 cm^{-1} may have been two lines close together. More careful polarization experiments, in which the σ and π spectra are taken as a function of the rotation of the crystal, are necessary to confirm the actual energy value of the splitting. Parameters $A^6_6 \langle r^6 \rangle$ and $A^0_6 \langle r^6 \rangle$ were chosen so as to give the proper splitting of the $\mu = 3$ and $\mu = \pm 2$ sublevels in $^3F_4$, $^1G_4$, and $^3H_6$. Parameter $A^0_4 \langle r^4 \rangle$ was chosen so as to give reasonable splitting of the $^3P_2$, $^3F_2$, and $^3H_6$ levels. The best over-all fit for this first-order perturbation treatment was obtained by using $A^0_2 \langle r^2 \rangle = 13$ cm^{-1}, $A^0_4 \langle r^4 \rangle = -80$ cm^{-1}, $A^0_6 \langle r^6 \rangle = -32$ cm^{-1}, and $A^6_6 \langle r^6 \rangle = 300$ cm^{-1}.

Fitting to Experimental Data

A. The $^3H_6$ Level

The theoretical predictions for $\mu = 0, \pm 1, 3$ are in good agreement with those crystal quantum states reported by experiment. (See Fig. D. 22-1.) The prediction of additional states between ± 1 and 3 has led us to restudy our plates. Our reported analysis included only those intense lines in which polarization was complete.[3] As many as three or four weak lines appear between those due to transitions from the ± 1 and 3, but these are not well polarized. These lines may be due to sublevels $\mu = 0', \pm 1'$, and $\pm 2'$ in $^3H_6$, as the theory predicts, or satellite levels, but our experiments cannot really confirm this. Forbidden transitions observed in $^3P_2$, $^1D_2$, and $^1G_4$ may also confirm these predicted states in the $^3H_6$ level.

B. The $^3F_4$ Level

The splittings of the $\mu = \pm 2$ and 3 are in reasonable agreement with experiment. (See Fig. D. 22-2.) However, the presence of the $^3F_3$ some 200 cm^{-1} away will cause certain states to be depressed more than others. This may explain the relative position of the theoretical value of $\mu = \pm 1$.

C. The $^3F_3$ and $^3F_2$ Levels

Since $^3F_3$ and $^3F_2$ are separated by 400 cm^{-1}, a simultaneous perturbation treatment is necessary in order to get better fit. Such a treatment may reverse the positions $\mu = \pm 1$, $\mu = \pm 2$ in $^3F_2$, now given as a result of first-order methods. (See Figs. D. 22-3 and D. 22-4.) As yet, $\mu = 0$ has not been reported for either of these levels.

D. The $^1G_4$ Level

The splitting between the lower $\mu = 3$ and $\mu = \pm 1$, between $\mu = \pm 2$ and $\mu = \pm 1$, and between $\mu = \pm 1$ and lower $\mu = \pm 2$ fits that found by experiment. (See Fig. D. 22-2.) The experimental positions of both $\mu = 3$ sublevels are reasonably well established. The theoretical value of upper $\mu = 3$ cannot be brought into better agreement by this present treatment. A slightly different set of parameters, $A_2^0 \langle r^2 \rangle = 13\ cm^{-1}$, $A_4^0 \langle r^4 \rangle = -80\ cm^{-1}$, $A_6^0 \langle r^6 \rangle = -20\ cm^{-1}$, and $A_6^6 \langle r^6 \rangle = 200\ cm^{-1}$ gives the following somewhat better agreement: $\mu \pm 2 = -79\ cm^{-1}$, $\mu \pm 1 = -50\ cm^{-1}$, $\mu \pm 2' = 23\ cm^{-1}$, $\mu\ 3 = 101\ cm^{-1}$, $\mu\ 3' = 166\ cm^{-1}$.

That a slightly different set of parameters better fits theory to data may be due to increased importance of configuration interaction on excited levels. However, the internal inconsistency within the $^1G_4$ may be due to interactions between crystal quantum states of $^1G_4$ with those in $^3F_2$, $^3F_3$, and $^1D_2$.

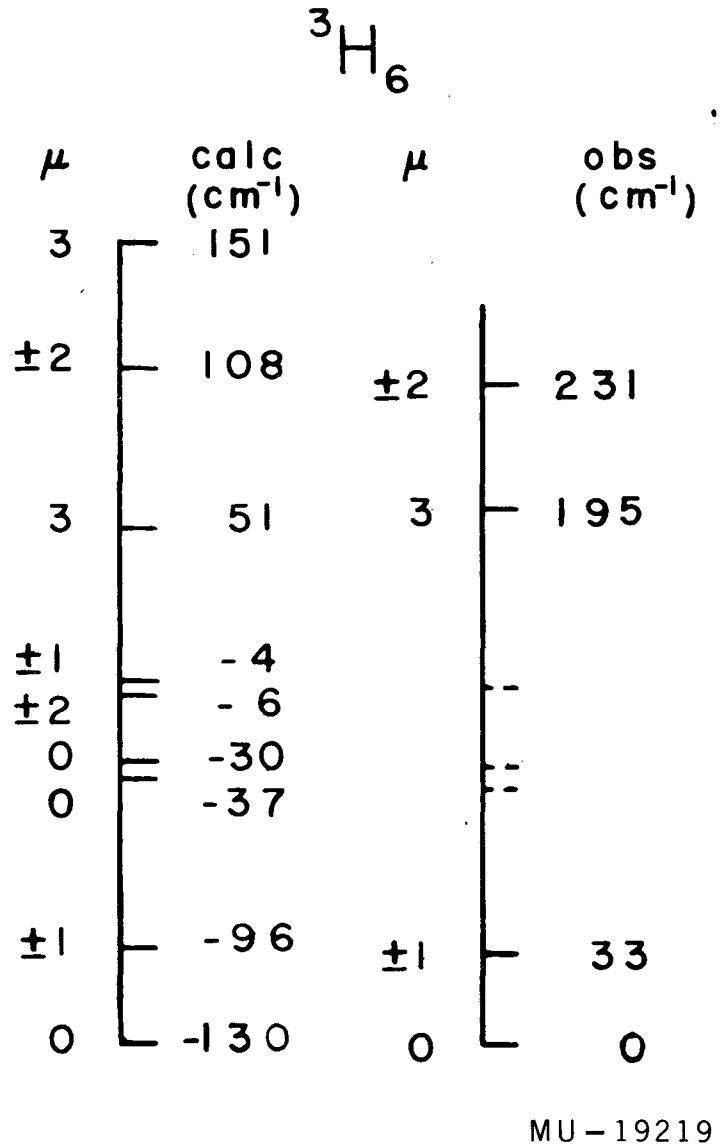

Fig. D. 22-1. The ground state, $^3H_6$ level.

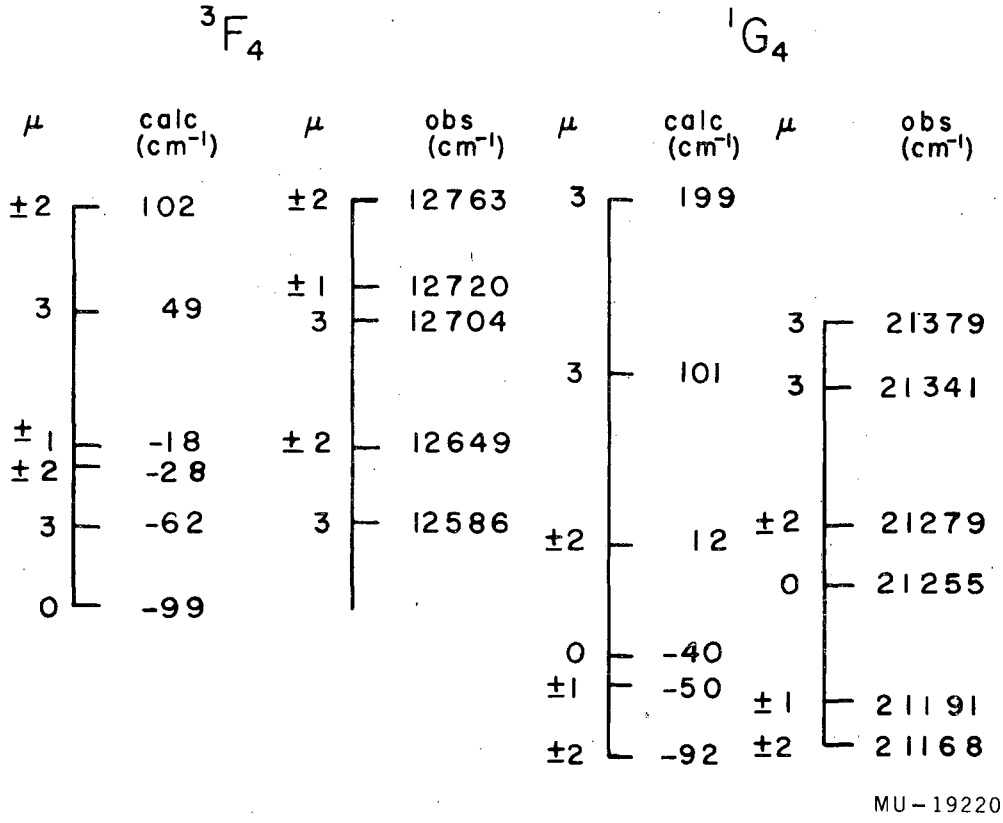

Fig. D. 22-2. The $^3F_4$ and $^1G_4$ levels.

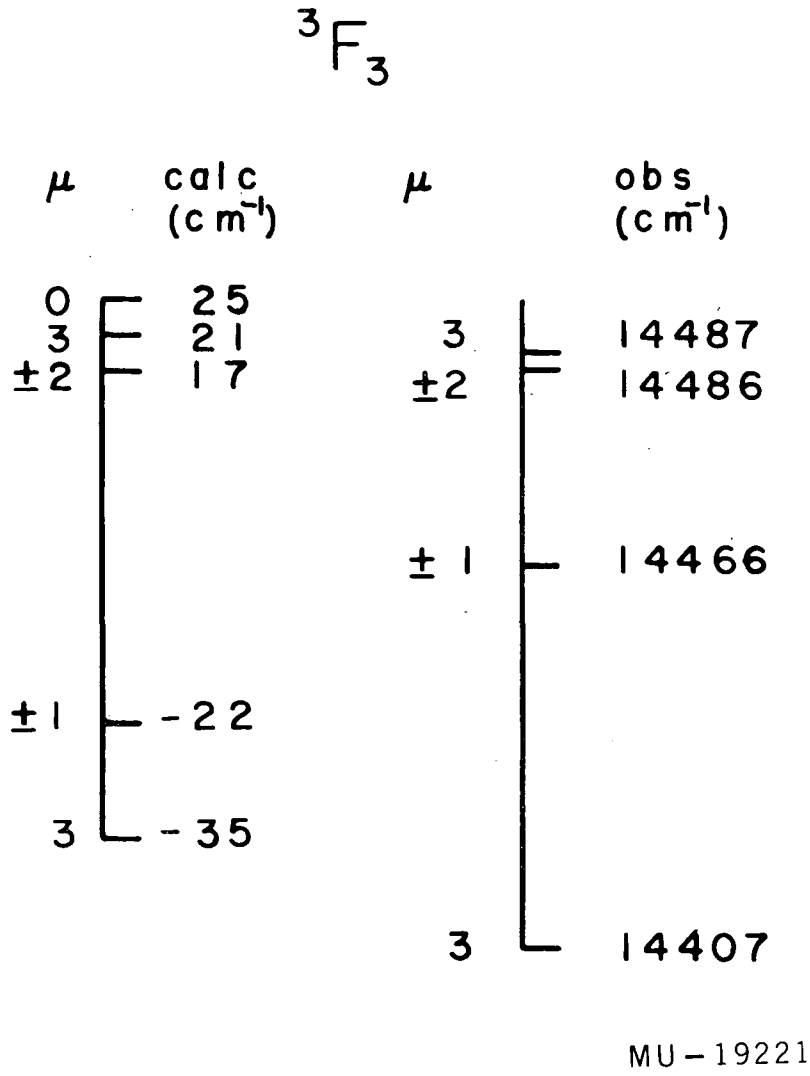

Fig. D.22-3. The $^3F_3$ level.

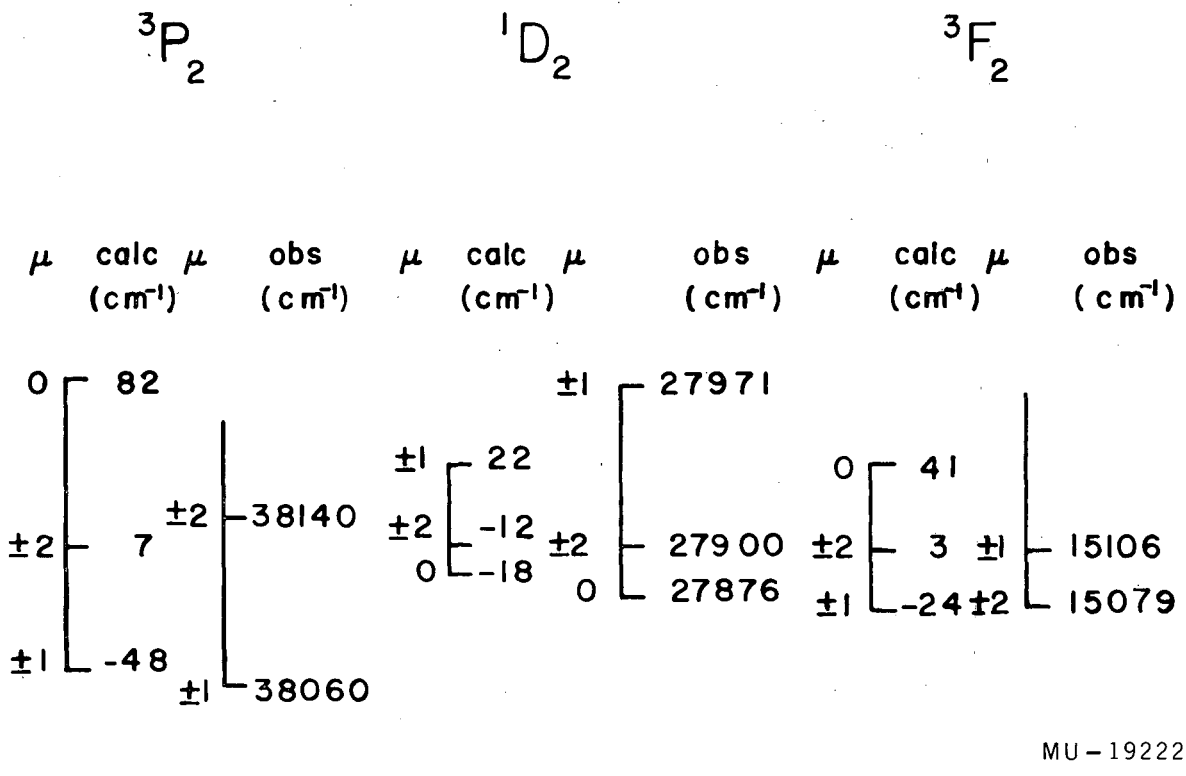

Fig. D.22-4. The $^3P_2$, $^1D_2$, $^3F_2$ levels. The theoretical splitting of a particular J level is given on the left; the observed energy-level scheme on the right. Here μ is the crystal quantum number.

E. The $^1D_2$ Level

The poor agreement can be partially remedied by considering interaction of $^1D_2$ with $^1I_6$. Our plates reveal lines between $^3P_1$ and $^3P_0$ and to the red side of $^3P_0$ as possibly due to the $^1I_6$. The energy of $^1I_6$ above $^1D_2$ was taken to be 6000 cm^{-1}. Even when the total matrix of the crystal field interaction between $^1D_2$ and $^1I_6$ is considered, it is impossible to obtain good agreement with $^1I_6$ this far removed from $^1D_2$. (See Fig. D. 22-4.)

Judd has also obtained a poor fit for $^1D_2$ in the analysis of $PrCl_3$ (Pr^{+3}, $4f^2$).[5] Although configuration interaction is known to be important for $^1D_2$, it is difficult to see in detail why this poor agreement occurs again in Tm^{+3}.

F. The $^3P_2$ Level

Actually good agreement exists between theory and experiment. (See Fig. D. 22-4.) The experimental error in measuring the broad lines in the ultraviolet is some 13 cm^{-1} in magnitude.

[5] B. R. Judd, Proc. Roy. Soc. (London) A 241, 414 (1957).

23. PARAMAGNETIC RESONANCE HYPERFINE STRUCTURE OF TETRAVALENT Pa^{231} IN Cs_2ZrCl_6

John D. Axe, H. J. Stapleton,* and C. M. Jeffries*

Paramagnetic resonance absorption at 3 cm wavelength is observed for tetravalent Pa^{231} in a single crystal of Cs_2ZrCl_6 at helium temperatures. The observed spectra correspond to the allowed transitions ($S_z, I_z \rightarrow S_z \pm 1, I_z$) and the forbidden transitions ($S_z, I_z \rightarrow S_z \pm 1, I_z \mp 1$) of a system described by the spin Hamiltonian

$$H_s = gS\underset{\sim}{H}\cdot\underset{\sim}{S} + A\underset{\sim}{I}\cdot\underset{\sim}{S} - g_n'\,\beta\underset{\sim}{H}\cdot\underset{\sim}{I},$$

with $S = 1/2$, $I = 3/2$, $|A|/h = 1{,}578.6 \pm 1.4$ Mc, $|g| = 1.1423 \pm .0014$, and $|g_n'| \approx 8 \times 10^{-4}$. The errors indicate a small deviation from isotropy. It is further observed that $g'_n/g < 0$, indicating that if g'_n is positive, as is strongly indicated by the nuclear shell model, then g is negative. An additional electron-nuclear double-resonance experiment is used to determine directly the nuclear magnetic moment $\mu(Pa^{231}) = 1.96$ nuclear magnetons. This value includes a correction of 9% due to perturbations of an excited state about 1900 cm^{-1} above the ground-state doublet of Pa^{4+} in its octahedral crystal field. A lower-frequency double-resonance experiment is used to measure the weak hyperfine interaction of the Pa^{4+} ion with its Cs^{133} neighbors, of order $A''/h \approx 0.5$ Mc.

*Department of Physics.

24. PARAMAGNETIC RESONANCE IN TETRAVALENT PROTACTINIUM-231 (*)

John D. Axe, Ru-tao Kyi, and H. J. Stapleton

The paramagnetic-resonance spectrum of tetravalent Pa^{231} has been observed in a single crystal of Cs_2ZRCl_6. A melt of Cs_2ZrCl_6 was "doped" with approx 500 μg of anhydrous $Pa^{231}Cl_4$ [1] and allowed to crystallize in an atmosphere of hydrogen by slow passage through a furnace. At 4.2°K and a frequency of 9457 Mc, the observed resonance pattern consisted of four widely separated hyperfine components. The spectrum was isotropic to within the accuracy of the field measurements (approx 1/2%). These features are interpreted as the usual $\Delta M_S = \pm 1$, $\Delta M_I = 0$ transitions between the eigenstates of the spin Hamiltonian

$$\mathcal{H} = g \beta H \cdot S + A I \cdot S,$$

with $S = 1/2$, $I = 3/2$, $|g| = 1.15 \pm .02$, and $|A| = 0.0518 \pm .001)$ cm^{-1}. The large hyperfine interaction necessitates the use of exact solutions for the energy levels. [2] No resonance was detected at 77°K.

The nuclear spin value of 3/2 is verified. [3] The paramagnetism can be most plausibly ascribed to a single 5f electron. A magnetically isotropic Kramers' doublet is expected to be the lowest-lying as the result of the octahedral perturbation present at the zirconium site. [4, 5] As an alternative, a $6d^1$ configuration is expected to give rise to a fourfold degenerate magnetically anisotropic level if octahedral symmetry is preserved, [6] or an anisotropic doublet if distortion is present. [7] Further work on the optical absorption spectra of this system is in progress and should allow amplification of the above conclusions. An attempt to measure the nuclear magnetic moment of Pa^{231} by a "double-resonance" technique is likewise in progress. We wish to thank Professors C. D. Jeffries and B. B. Cunningham for their invaluable advice.

---

*Published in J. Chem. Phys. 32, 1261 (1960) and embodying abstract of thesis by Ru-tao Kyi (UCRL-9109, March 1960).

[1] Prepared by the method of Sellers, Fried, Elson, and Zachariasen, J. Am. Chem. Soc. 76, 5935 (1954).

[2] B. Bleaney, Phil. Mag. 42, 441 (1951).

[3] H. Schuler and H. Gollnow, Naturwiss. 22, 511 (1934).

[4] See, for example, J. S. Griffith and L. E. Orgel, J. Chem. Phys. 26, 988 (1956).

[5] C. A. Hutchison and B. Weinstock, to be published in J. Chem. Phys. These authors discuss paramagnetic resonance in another f^1 octahedral system, NpF_6.

[6] B. Bleaney, Proc. Phys. Soc. (London) 73, 939 (1959).

[7] Griffiths, Owen, and Ward, Proc. Roy. Soc. (London) A219, 526 (1953).

25. NUCLEAR QUADRUPOLE RESONANCE STUDIES (*)

Allan H. Reddoch

The chlorine nuclear quadrupole resonance in titanium tetrachloride has been re-examined, confirming the existence of four resonances.

A chlorine-35 resonance in thorium tetrachloride has been discovered, consisting of a single resonance line at about 6 Mc. The frequency suggests highly ionic bonding, at variance with earlier conclusions reached by x-ray studies. Some double-bond character may be present in the Th-Cl bond.

Niobium and chlorine resonances have been discovered in niobium pentachloride. The niobium resonances are described by a single set of parameters, the coupling constant eq Q being approximately 78 Mc, and the asymmetry parameter $\eta = 0.32$. Because of the large asymmetry parameter, it was possible to observe two $\Delta M = 2$ transitions and one $\Delta M = 3$. Only a single Cl^{35} resonance was found at about 13 Mc, although two more chlorine resonances would be expected on the basis of crystal structure. The frequency of the chlorine resonance suggests appreciable covalency in the niobium-chlorine bond in niobium pentachloride.

A single resonance has been found in tantalum pentachloride at about 13 Mc. It is believed to be a Cl^{35} resonance.

A fairly simple method was developed for determining the asymmetry parameter of the electric field gradient from the observed transition frequencies without directly solving the secular equations.

---

*Abstract from Nuclear Quadrupole Resonance in $TiCl_4$, $ThCl_4$, $NbCl_5$, and $TaCl_5$ (UCRL-8972 Rev., Nov. 1960), submitted to J. Chem. Phys.

E. INSTRUMENTATION

1. USE OF SILICON p-n JUNCTION DETECTORS IN STUDIES OF NUCLEAR REACTIONS INDUCED BY HEAVY IONS

Almon E. Larsh, Glen E. Gordon, and Torbjørn Sikkeland

We have used silicon p-n junctions and gold-silicon junctions as detectors of fission fragments and elastically scattered heavy ions in experimental studies of fission induced by heavy ions. In the course of our experiments we have studied some of the properties of the detectors.

Experimental Procedures

Properties of the detectors used in obtaining the results described herein are given in Table I. These detectors were formed by diffusion of one type of impurity into one face of a silicon wafer containing an excess of the opposite type of impurity, or by evaporation of gold onto the face of a wafer of n-type silicon.

Heavy-ion beams used in these experiments were obtained from the Berkeley heavy-ion linear accelerator. Experiments were performed in a vacuum tank that contained the detectors, targets, and a Cf^{252} α-SF source. The energy of the beam particles was varied by placing weighed aluminum foils in the beam path ahead of the target. The width of the peak obtained with 103.6-Mev C^{12} particles is 2.2%. This figure includes inherent resolution of the detector, spread in pulse heights due to noise in the electronic system, and energy spread in the degraded carbon beam.

Table I. Properties of Si detectors

Detector	Base material type	Resistivity (Ohm-cm)	Diffusant type	Window thickness ($\mu g/cm^2$)
Ha-2	n	100	p	475
Hu-18	p	1000	n	350
L-.1501	n	15	Au	< 15
L-820	n	800	Au	30

Discussion

A. Pulse Height versus Applied Potential

The relative pulse heights produced by 121.3-Mev C^{12} particles and Cf^{252} alpha particles in the Hu-18 detector as a function of reverse bias are shown in Fig. E.1-1. The rapid rise in the curve for α-particle pulses is due mainly to a decrease in capacitance of the detector with increasing reverse

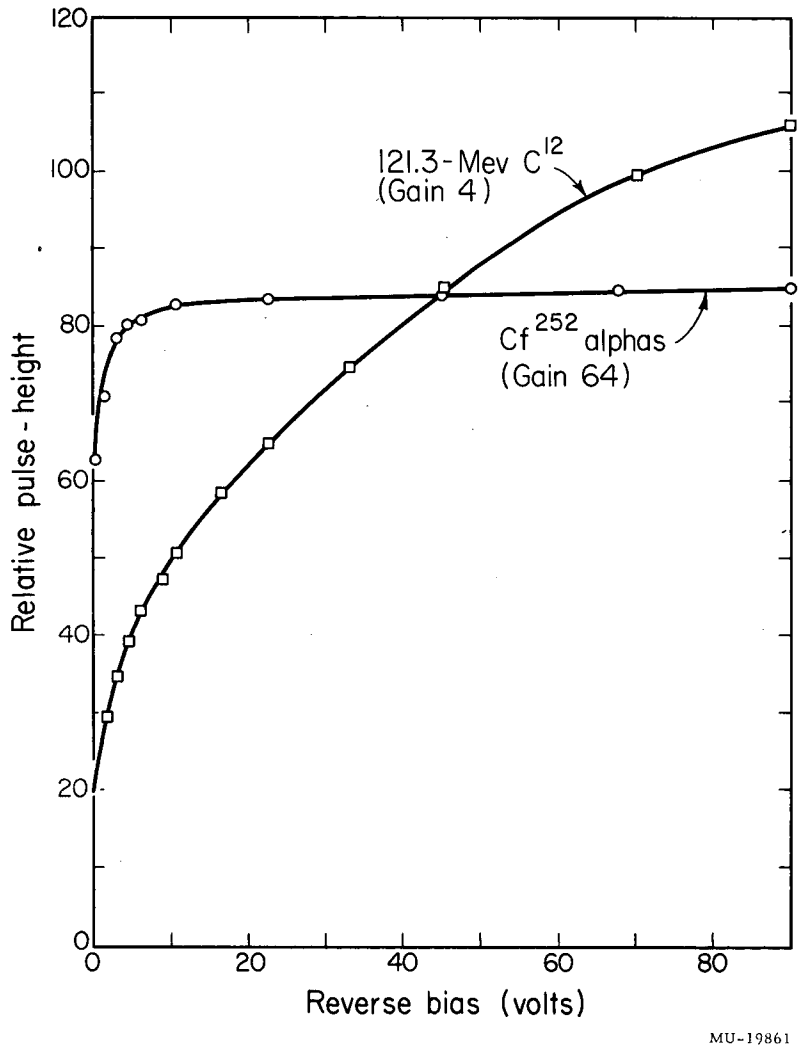

Fig. E. 1-1. Pulse heights produced by 121.3-Mev C^{12} particles and Cf^{22} alpha particles in the Hu-18 detector as a function of reverse bias. Amplifier gain factors shown in the figure are only approximate values.

bias. At very low reverse bias, the range of the α particles may be slightly longer than the thickness of the sensitive counting region. Therefore, some of the rise in the pulse height may be due to extension of the sensitive counting region, and increase in the amount of energy deposited in it by the α particles.

The relative pulse heights produced by 120-Mev Ne^{20} ions and a constant-amplitude pulse generator, as a function of reverse bias on detector L-820, are shown in Fig. E. 2-2.

B. Pulse Height as a Function of Energy

Data from Hu-18 have been used to construct the curve of pulse height versus energy shown in Fig. E.1-3. A pulse-generator calibration of the electronic system was used to determine the position of zero pulse height on the pulse-height analyzer scale. Points for the α particles and the two mass groups of spontaneous fission fragments of Cf^{252} have also been included in Fig. E.1-3.

In the case of fission fragments, a correction has been applied for loss of energy in passing through the insensitive front surface of the detector. Two different approaches have been used in making this correction.

On one hand, one may assume that the pulse-height-versus-energy relationship is the same for fission fragments as for carbon particles. The positions of the peaks for the two mass groups of fission fragments correspond to energies of 91.4 and 65.6 Mev on the curve of Fig. E. 1-3. From Fraser and Milton's time-of-flight data,[1] the energies of the two fragment groups before passage through the window are known to be 104.7 and 79.8 Mev for the light- and heavy-mass groups, respectively. The "window" thickness is then determined from the energy loss by the light-fragment group and the range-energy data of Schmitt and Leachman,[2] for fission fragments in aluminum. The check on the self-consistency of this approach is to use the window thickness determined for the light fragments to correct the energy of the heavy group. This procedure yields an energy of 80.4 Mev for the heavy group, in good agreement with the expected value of 79.8 Mev.

The second method is to assume that the curve of pulse height versus energy deposited by the fragments is linear and passes through the origin. Various window thicknesses are assumed, and energy corrections are made until the ratio of corrected energies is 1.31 (= 104.7/79.8). The results of this analysis of the data are identical with those of the first method. In each case the window thickness is found to be approximately 350 $\mu g/cm^2$. The estimated window thicknesses listed in Table I were obtained by this procedure. The fission-fragment deposition energies obtained by this method are plotted in Fig. E.1-3.

---

[1] J.S. Fraser and J.C.D. Milton, in Proceedings of the Second United Nations International Conference on the Peaceful Uses of Atomic Energy 1958, Vol 15, p. 216 (United Nations, Geneva, 1958).

[2] H.W. Schmitt and R.B. Leachman, Phys. Rev. 102, 183 (1956).

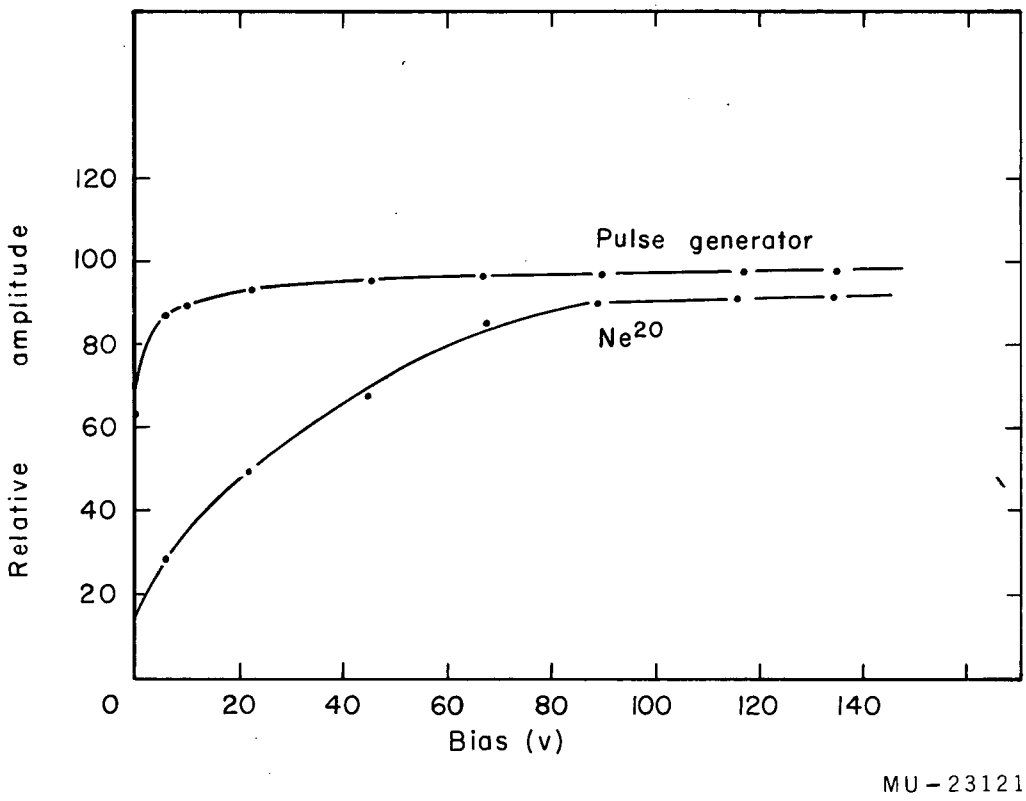

Fig. E. 1-2. Pulse heights as a function of reverse bias (detector L-820, Si-Au).

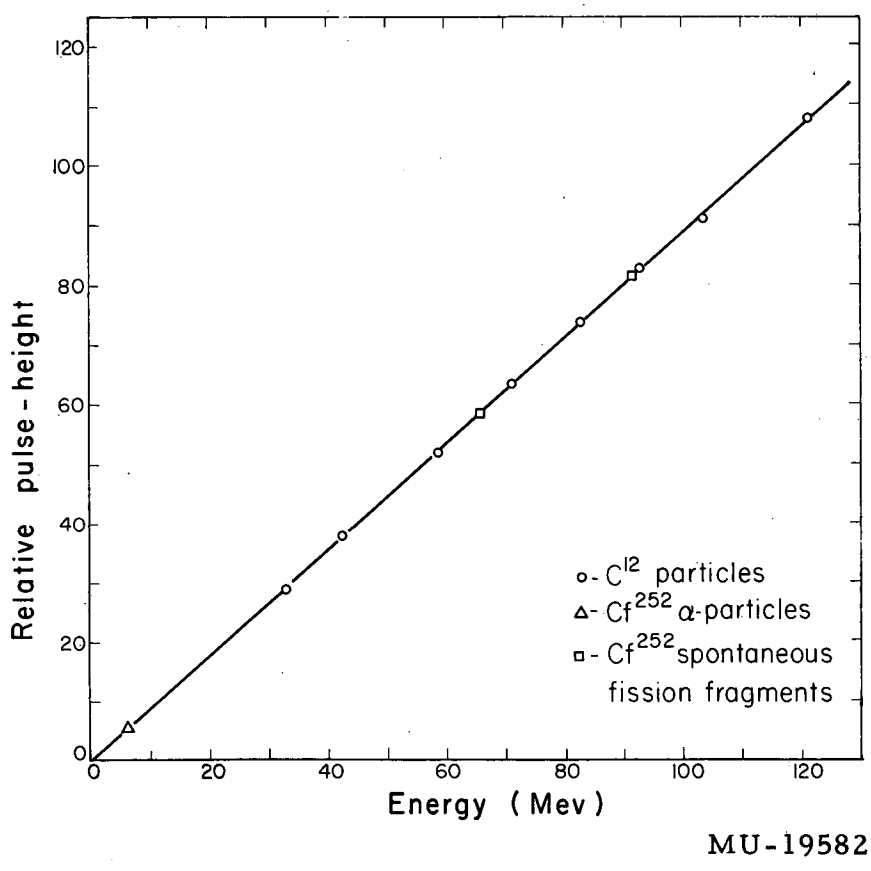

Fig. E. 1-3. Pulse heights produced by C^{12} particles of various energies and Cf^{252} alpha particles and fission fragments observed with the Hu-18 detector reverse-biased by 94 v.

These observations may be made from the results presented in Fig. E.1-3: (a) Pulse height is proportional to the energy deposited by the particle in the sensitive counting region. (b) Alpha-particle and fission-fragment points fall on the curve determined by the carbon-particle points.

C. Thickness of the Sensitive Counting Region

For all the detectors that we have studied, the fission-fragment data indicate that the thicknesses of the insensitive layers on the front surfaces stay very nearly constant with increasing reverse bias. The existence of these "windows" indicates that holes (in the case of p-type base, n-type diffusant) produced in the front surface outside the depletion layer are not efficiently collected in the pulse. Apparently this is because the holes have only a very short lifetime in the region of high impurity concentration on the front surface, and therefore do not migrate far before being trapped. Also, the constancy of the window thickness with increasing applied potential shows, in agreement with semiconductor theory, that the increase in depletion-layer thickness is almost entirely in the direction of the material containing the lower concentration of impurities, or the base material in the body of the detector.

Applicability of Solid-State Detectors in Nuclear Reaction Studies

The silicon p-n junction detectors have been very useful in our studies of heavy-ion-induced nuclear reactions. The main purpose of our research has been to observe fission-fragment kinetic energy distributions at various angles to the Hilac beam. In order to determine absolute fission cross sections, we relate the number of fragment counts to the number of elastically scattered beam particles observed at small angles to the beam. One of the main advantages of the solid-state detectors is that one can use the same detector for both types of measurements. When observing fragment kinetic energy distributions, we apply very small potentials to the detectors; thus, the sensitive counting region is longer than the paths of the short-range densely ionizing fission fragments, but short enough that the scattered beam particles and light reaction products deposit only small fractions of their energies in the sensitive region. This yields a clear distinction between pulses produced by fragments and those produced by light particles. For observation of scattered beam particles, the reverse bias is increased, thus increasing the size of the pulses produced. The detectors have proved quite stable over the period of each series of experiments (normally about 8 hr), as shown by calibrations done before and after the other experiments. Also they appear to have fairly long lifetimes. We have used one detector over a period of 18 months and, as yet there have been no signs of deterioration.

An important feature of the detectors for counting experiments conducted near the heavy-ion beam is their insensitivity to the large neutron and γ-ray background that is always present. We have had some difficulty with electrons that are knocked out of the target, collimators, etc. by the heavy ions. Although individual pulses produced by these electrons are quite small, "pileup" of the pulses made the resolution of the pulse generator and scattered particle peaks quite poor. This difficulty was eliminated by placing a magnet near the front surface of the detector, thereby deflecting the electrons away from it

but having little effect upon the fission fragments and scattered beam particles. We observed no effect of the magnetic field (approx. 1000 gauss) upon the detector.

Acknowledgments

The detectors used in these tests were made by William L. Hansen and Robert M. Latimer of Lawrence Radiation Laboratory and Hughes Aircraft Company.

2. A MODIFICATION OF THE SUPER-SNAPPER PULSE-HEIGHT ANALYZER

Duane F. Mosier and Richard G. Leres

A number of Super-Snapper Analyzers[1] in use at Berkeley for the past several years have demonstrated the difficulty of maintaining uniform channel widths in "stacked discriminator" types of analyzers. In order to improve the performance of these analyzers, the development of a "height-to-time conversion" modification, which would be comparatively inexpensive, was undertaken. Another factor in the undertaking was the desire to re-use the memory-storage portion of the Super-Snapper, because of its costly nature.

For purpose of identification at the Laboratory, the described instrument is known as the "Echo Analyzer". A brief description and a block diagram (Fig. E.2-1 of the resulting Echo Analyzer follow.

Acceptance of a pulse for analysis requires a gate signal that exceeds the discriminator level. Self- or external gating is permitted by switching of the discriminator gate input, and is independent of other analyzer controls. The threshold circuit, unlike the discriminator, subtracts an equal amount from all pulses that exceed the threshold level. This determines the amplitude necessary for storage in Channel 1 without affecting channel width.

An analog-to-digital converter circuit (ADC) transforms the pulse amplitude into a gate, whose duration is proportional to the pulse amplitude. This gate, together with 500-kc oscillator pulses, and a 5-to-1 frequency divider, produces a train of 100-kc channel address pulses.

The block generator is triggered by the first pulse of the channel address train, and continues to develop a block signal for a fixed period after the last address pulse. This block signal is used to prevent gating of the input amplifier during analysis of a pulse. The initiation of the block signal generates an address-scaler reset pulse, and its termination produces a store-pulse trigger. A store-inhibit circuit prevents generation of a store pulse when the address scaler is advanced beyond "99." An upper bound circuit causes a rapid reset of the ADC for pulses which would produce an address beyond "100." Because of the erroneous address train generated, this circuit also actuates the store-inhibit circuit.

[1] Almon E. Larsh, Super-Snapper Pulse-Height Analyzer, UCRL-3945, Sept. 1957.

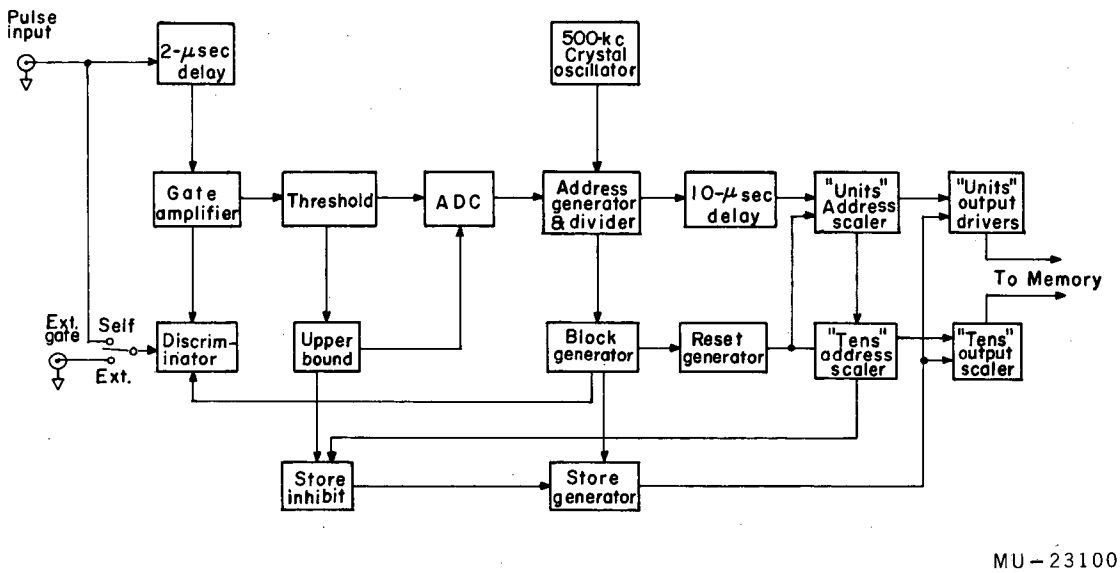

Fig. E. 2-1. Block diagram of Echo Analyzer.

The address pulse train is delayed to allow resetting of the channel address scaler. This scaler consists of two decade glow transfer tubes, which provide one hundred discreet channels, identified by a "tens" and a "units" address. The "units" tube is advanced by each pulse in the address train, and it produces a "tens" tube advance pulse for every tenth pulse received. In addition to the visual presentation of channel address, these tubes determine which "units" output driver and which "tens" output driver are actuated by the store generator to produce memory pulses.

The two memory pulses are used to drive one of the fifty individual Dekatron and Sodeco registers of the original Super-Snapper analyzer. These registers were conveniently arranged in a two-dimensional matrix, using the existing diode coincidence circuits within the Super-Snapper.

The circuits described were arranged on a single chassis and a second chassis, providing the power supplies for this circuitry and the Super-Snapper memory were developed. These chassis occupy the same space originally used by the Super-Snapper power supply and gate generator.

Characteristics of the resulting analyzer are as follows.

No. of address channels: 99
No. of storage channels: 49
Channel count capacity: 10^5-1 counts
Channel widths: Either 1 or 2 volts
Maximum input pulse amplitude: 200 volts
Dead time: 250 μsec + (channel no.×10) μsec

Performance of the prototype indicates substantial improvement in differential linearity, which will allow the Echo Analyzer to relieve more costly core-storage analyzers for higher count rate and more sophisticated applications. Initial estimates of cost indicate these modifications can be performed for approximately half the value of the reclaimed Super-Snapper memory. Six production units are undergoing initial tests, and more detailed description of circuits and performance will be covered in a subsequent report.

3. ENERGY RESOLUTION IN SEMICONDUCTOR PARTICLE DETECTORS

William L. Hansen and F.S. Goulding

The theoretical limits of noise in detector-amplifier combinations using semiconductor particle detectors have not been derived to date, because of unpredictable noise generators in existing detectors. These noise generators are always due to surface effects at the point where a semiconductor junction meets a surface, and are usually greater by orders of magnitude than the bulk effects of carrier diffusion and thermal generation. If the surface effects were not present, the signal-to-noise relations developed for gaseous ionization chambers would be directly applicable. Since it has been found possible to largely eliminate surface noise by means of a suitable geometry, the optimum signal-to-noise relations can be derived for semiconductor detecors. In the following presentation we assume that the detector is p-type silicon at 25°C.

It is convenient to divide the noise generators into those due to the amplifier and those due to the detector. Following the development by Gillespie,[1] the optimum time constant and signal-to-noise ratio can be derived for a pulse amplifier with equal integrating and differentiating time constants. The known noise generators are tube shot noise, tube flicker effect, tube grid current, detector leakage, and input resistance, of which only tube shot noise and detector leakage current are significant for presently available detector-amplifier combinations. If all other noise generators are ignored, the optimum time constant can be shown to be

$$T_{opt} = \frac{0.35\ C}{\sqrt{G_m i_L}} \tag{1}$$

and the minimum mean square noise to be

$$\langle \text{noise}^2 \rangle = 0.11\ C \sqrt{i_L/G_m}\ , \text{ in kev}^2, \tag{2}$$

where C is the total input capacity, in picofarads; i_L is the detector leakage current, in microamperes, G_m is the input tube transconductance, in ma/v; and T_{opt} is in microseconds.

When surface effects on the detector are eliminated, its noise contribution is due solely to its capacity and generation and diffusion currents. The detector capacity is given by

$$C_d = 3.3 \times 10^4\ (\rho V)^{-1/2}, \text{ in pf/cm}^2, \tag{3}$$

and the generation current by

$$I_g = 38\ (\rho V)^{1/2} / \tau_0, \text{ in m}\mu\text{a/cm}^2\ , \tag{4}$$

and for most practical detectors the diffusion current is negligible. In these equations ρ is the semiconductor resistivity, in ohms; V the applied voltage, in volts; and τ_0 is the minority carrier lifetime, in μsec.

Equations (3) and (4) can be combined with Eq. (2) to give the minimum noise for the detector amplifier combination, so that one has

$$\langle \text{noise}^2 \rangle = \left(\frac{A}{\tau_0 G_m} \right)^{1/2} \left\{ 0.7\ C_{in} (\rho V)^{1/4} + \frac{2.2 \times 10^4 A}{(\rho V)^{1/4}} \right\} \text{ in kev}^2, \tag{5}$$

where A is the detector area, in cm^2; and C_{in} is the amplifier input capacity. An optimum operating voltage can be derived from Eq. (5) such that

$$V_{opt} = \frac{10^9 A^2}{\rho\ C_{in}^2}\ , \text{ in volts.} \tag{6}$$

[1] A. B. Gillespie, Signal, Noise and Resolution in Nuclear Counter Amplifiers Pergamon Press, London (1953).

Inserting Eq. (6) into Eq. (5), we find the optimum performance that can be obtained from a detector-amplifier combination is

$$\langle \text{noise}^2 \rangle_{opt} = 250\ A \sqrt{C_{in}/\tau_0 G_m}, \qquad \text{in kev}^2. \tag{7}$$

The important point to observe about Eq. (7) is that if the detector is used at its optimum operating voltage and the amplifier at its optimum time constant, the noise is not a function of the resistivity of the detector semiconductor.

In order to realize this theoretical behavior, the surface effects must be eliminated. This has been accomplished with detectors with a guard-ring structure, as shown in Fig. E.3-1. These detectors have shown the theoretically predicted noise within limits of experimental error, indicating that all significant noise generators have been accounted for. The detectors used in these experiments have had detector areas of $1 cm^2$ with an etched ring 1 to 2 mils wide and 1μ deep, and have been made from 1500- and 5000-ohm-cm p-type silicon. Finished detectors have shown minority carrier lifetimes as great as 800 μsec when measured from the thermal generation current, and have shown the theoretically predicted C-V and I-V characteristics. The resistance between the guard ring and the detector is usually greater than 10^8 ohms at the operating voltage.

The theoretically predicted energy resolution for detectors of this area ($1 cm^2$) is about 10 kev full width at half maximum, depending upon the minority carrier lifetime obtained. Measurements with ionizing radiations show that this resolution is obtained with electrons, within limits of experimental error, but not with α particles. The best α-particle resolution obtained with these detectors is only 21 kev (Am^{241}). Monoenergetic α sources show evidence of multiple peaking which is area-sensitive, and the poor resolution could well be due to unresolved multiple peaks. A thorough investigation of effects just within the detector surface will probably be necessary before the ultimate α resolutions are realized.

As there is no voltage between the detector and the guard ring, no net current can flow, and noise due to ionic conduction and surface inversion cannot appear in the output signal. However, it is still possible for carrier injection to occur at the etched ring. When the detector is placed in a strongly p-type ambient (e.g., chlorine), a large and almost voltage-independent injection current is observed; in a strongly n-type ambient (e.g., ammonia) the impedance betweeen the guard ring and the detector drops, and the guard-ring leakage appears in the output signal. Methods of minimizing the surface injection are being studied.

4. A MULTIPLEX PUNCHED-TAPE PULSE-HEIGHT ANALYZER

A. A. Wydler

A system for the analysis, processing, and storage of pulse-height and time data has been constructed, using punched paper tape as the storage medium. This particular system is capable of recording the data and time of an

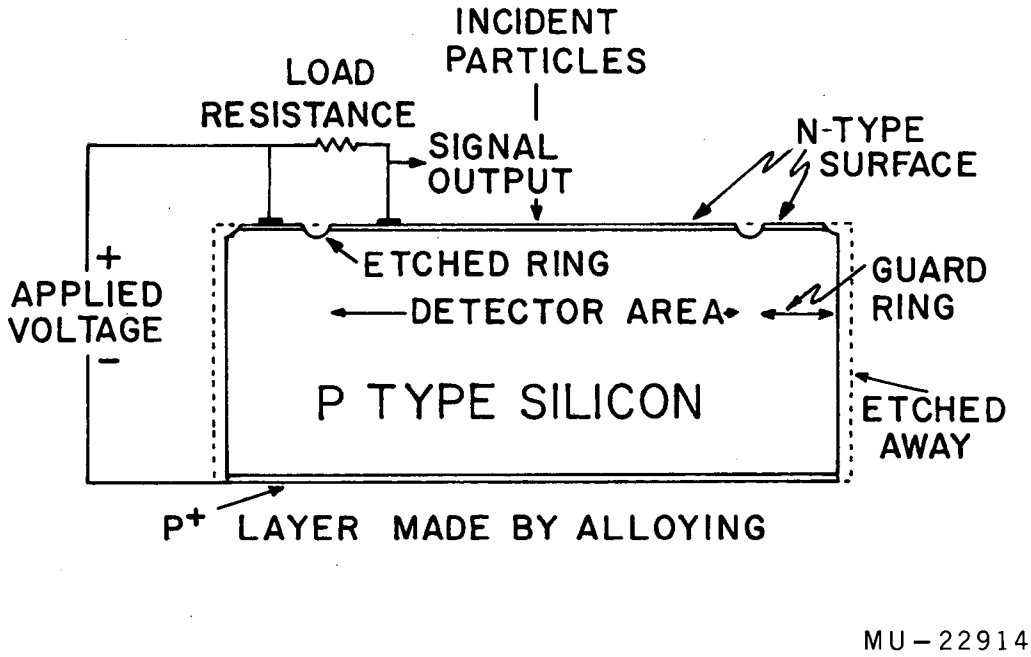

Fig. E. 3-1. Detector with guard-ring structure.

event from six detectors. Included is a device to read the punched tape and to assist in the evaluation of the recorded data.

This analyzer is similar to the one described by A. E. Larsh Jr.,[1] and was constructed primarily to allow for the retirement of the older and slower system. However, it is now being used as a unique growth-and-decay analyzer.

The system is such (see Fig. E.4-1) that signals originating in any detector are coded, then mixed in a resistive network and fed to a common height-to-time converter type of pulse-height analyzer. The output of the pulse-height analyzer is split, so as to provide immediate visual indication on a ten-by-ten register matrix and permanent storage on the paper tape, which has been previously identified by the originating detector. Each entry on the paper tape includes the time of origin of the signal.

The punches used are Fridén Model MCP 617, using 1-in.-wide oiled paper tape. They are capable of punching up to eight transversely spaced holes. This allows for the storage of 100 channels of information in binary form. The punching rate is 20 lines per second. Therefore, ten groups of pulse-height and time information may be encoded and punched each second. The punches are blocked individually upon receipt of data, hence several may be recording simultaneously.

The tape reader Model MR 690, a companion to the Fridén punches, with associated apparatus, is shown in Fig. E.4-2. This reading system is capable of decoding a previously punched tape as to data spectra, the time distribution of any part of the data, and, where applicable, the time of decay of any part of the spectra. The display is by means of a ten-by-ten register matrix or by the printer and plotter of an associated Penco Model PA-4 pulse-height analyzer.

This system provides a simple, relatively inexpensive method of multiplex analysis and storing of nuclear data produced from more than one detector.

[1] A. E. Larsh Jr., Multiplex Pulse-Height Analyzer, Nucleonics 17, No. 3, 92 (1959).

5. SUMMARY OF 1960 HILAC OPERATIONS

Edward L. Hubbard

During the year 1960, most emphasis was place on improving the reliability of the Hilac. As a consequence it has been possible to deliver relatively larger beams of heavy ions to the various experimenters with a consistency not before possible. Other improvements are possible, and many of these are planned for 1961. A simple listing of some of the changes made during the last year includes:

1. The pulse rate was increased from 10 to 15 pulses per sec.
2. Steel shielding was put over the top of the accelerator and along

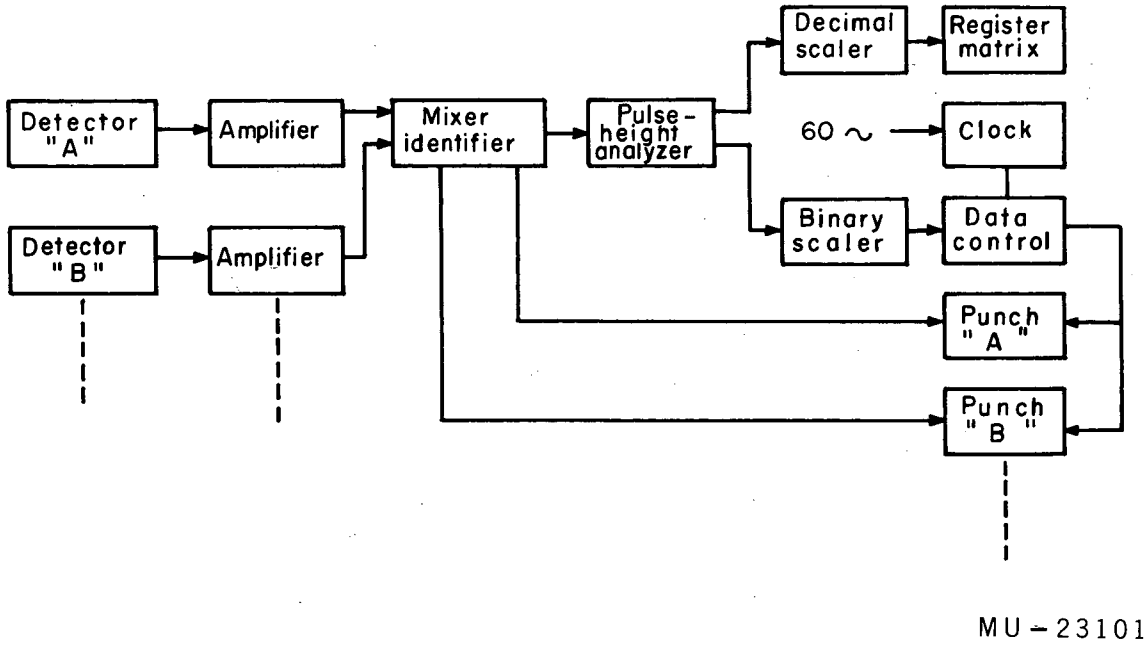

Fig. E. 4-1. Punch block diagram.

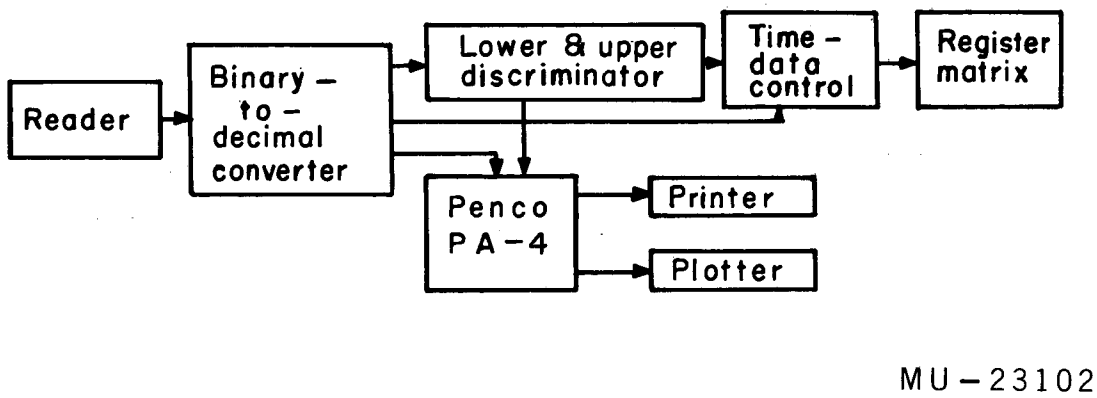

Fig. E. 4-2. Reader block diagram.

the south side. The new shielding reduced the monthly x-ray dose of the operating crew by a factor 2.5, and reduced the x-ray level in the driveway to a safe value.

3. A new room for pulse lines No. 5 and No. 6 was completed, and pulse line No. 5 and its firing equipment were installed. The completion of the rf crowbar in the prestripper cavity makes possible the use of amplifier No. 5 for producing beams of 1 Mev/A.

4. A new steering magnet was installed in the target area to deflect the beam into the heavy-element and Coulomb-excitation caves. The old steering magnet was moved back into the main cave and now provides five beam ports for other experimenters. A Rootes-type vacuum pump was added to the target area roughing system to reduce the time required to pump down experimental apparatus and to lessen the pressure surge in the accelerator when experimental equipment is opened into it. A current regulator for the drift-tube magnets and the target area quadrupoles was completed.

5. A highly variable attenuator was installed at the beam entrance to the prestripper cavity. This consists of two rotatable wheels with various openings closed by low-transmission Lectromesh grids. It is now possible to vary the beam intensity by many orders of magnitude, quickly and without disturbing the basic adjustments of the machine.

6. A sixth main rf amplifier was completed and is now in stand-by service. The oil tank in the rf power-supply cooling system was moved to make room for the transformer for the power supply for amplifier No. 6. The pulse-line room and the injector room were air-conditioned to eliminate failures of electronics components caused by overheating of these rooms.

7. Construction was started and nearly completed on an addition to Bldg. 71--Increment No. III. The addition provides 2,100 ft^2 of building space to be used for expanding the target area, new counting area, and an electronics shop. There will also be 2,100 ft^2 of office space on the second floor. Removal of offices and electronics shops from their present locations will allow expansion of the chemistry laboratories and the accelerator technicians' shop.

The accelerator was operated for experimenters two shifts a day, seven days a week except during the first half of the year, when one shift was used for maintenance, repairs, and modification. The experimental time was used as follows:

Chemistry		90.3%
Heavy Element (Ghiorso)	24.2%	
Coulomb Excitation (Diamond)	15.2	
Fission (Sikkeland)	8.8	
Fission (Viola)	4.3	
Rare Earth Alpha Activities (Macfarlane)	4.8	
Nuclear Reactions (Igo)	3.9	
Other	29.1	
Medical Physics		6.2
Physics		3.2
Health Physics		0.3

F. CHEMICAL ENGINEERING

1. CONDUCTIVITIES IN EMULSIONS (*)

Robert E. Meredith† and Charles W. Tobias

The dependence of the conductivity of water-propylenecarbonate emulsions on volume fraction f of the dispersed phase, on the conductivities of the continuous phase k_c, and of the discontinuous phase k_d, has been measured in the ranges of $0 < f < 0.5$ and $0.172 < k_d/k_c < 101$. The results indicate that for $f > 0.2$ neither Maxwell's equation nor Bruggemann's approximation represents the behavior of data satisfactorily. In an attempt to take into account the interaction of fields around particles of the dispersed phase, based on Maxwell's equation, a simple approximation is proposed. In the range of conductivities investigated in this study the new equation represents the conductivity of emulsions with reasonable accuracy.

*Abstract of published paper, J. Electrochem. Soc. (in press).

†Present address: Oregon State College, Corvallis, Oregon.

2. FRACTIONAL CRYSTALLIZATION FROM MELTS (*)

William R. Wilcox and C. R. Wilke

Studies of the separation process known as zone melting[1] were made on 10%-by-weight (10%w) mixtures of β-naphthol and of benzoic acid in naphthalene. These systems were chosen as representative of the two simplest types of binary solid-liquid phase behavior, namely isomorphous and eutectic-forming. The solid mixtures were enclosed in 5- to 10-mm glass tubes and pulled through a stationary heater, which generated a liquid zone. The separation attained in the process was significantly less than that predicted by assuming equilibrium between the bulk zone and the freezing solid. The separation increased as the zone travel rate decreased, as the size of the tube increased, and as the difference in liquid density between the bulk solid and the freezing interface increased. In addition, it was found that, for vertical tubes, the separation was much greater when the fluid of lower density (between the bulk zone and the freezing interface) was on the bottom than when it was on the top. Insertion of an axial tube or rod of metal or glass into the zone also increased the separation. These observations show conclusively that the separation was less than the equilibrium separation primarily because the zone was not completely mixed, especially near the freezing interface. Free-convection effects were found to be important in zone mixing.

*Abstract from thesis by William R. Wilcox, UCRL-9213, June 1960.

[1] W. G. Pfann, Zone Melting (John Wiley and Sons, Inc., New York, 1958).

A theoretical study of pure diffusional mass transfer in zone melting was also made. By using the experimental data, a correlation was developed which permits estimation of the separation for various situations in zone melting.

Equations and principles were also developed which allow estimation of the thermal requirements for zone melting. A correlation of zone position, relative to the heater, was also developed from experimental measurements for low zone-travel rates (less than 1 in./hr).

Economic calculations were made for a separation in the multistaged semicontinuous zone refiner known as a zone-void refiner. A cost on the order of $2.50 to $3.00 per pound was estimated for the separation of 500,000 pounds per year of 1% w β-naphthol in naphthalene into 0.1%w β-naphthol and 30% w β-naphthol. This is obviously uneconomical for a bulk chemical commodity, although it might be satisfactory for special, or ultra-high purity, chemicals. A capital investment of about four million dollars was also estimated to be necessary for this separation.

Exploratory experiments were made on a cooled-drum apparatus (modified drum-flaker), using NaCl-water as a system. These indicated that this equipment might be useful for large-scale industrial separations, although further research and development are needed.

3. DIFFUSION COEFFICIENTS IN MULTICOMPONENT SOLVENTS (*)

J. T. Holmes, D. R. Olander, and C. R. Wilke

The molecular diffusion coefficient of liquid systems has been found to be an important variable in processes such as absorption, extraction, distillation, and ion exchange. Correlation of mass-transfer coefficients requires a knowledge of the diffusion coefficient. Little is known about mass transfer by molecular diffusion in liquid mixtures of more than two components, although Gosting and others have studied the effects of interacting flows for systems of two solutes in one solvent.[1] However, there have been no data or specific theory published on the diffusion of a dilute solute in a multicomponent solvent.

The purpose of this study was to determine if diffusion in a mixed solvent could be related to the binary diffusion coefficients of the solute in each of the pure solvents and to the mixture viscosity.

Diffusion coefficients of very dilute toluene (5.0×10^{-3} mole per liter) in mixed hydrocarbon solvents were measured by using a stirred diaphragm cell technique. Counterdiffusion of the solvent was not measured, since the

*Summary of thesis by John T. Holmes, UCRL-9145, April 1960.

[1] R. L. Baldwin, P. J. Dunlop, and L. J. Gosting, J. Am. Chem. Soc. 77, 5235 (1955).

solvent is essentially stagnant when the solute is very dilute. Each system may thus be considered, for diffusion purposes, to be a binary of one solute and a two-component solvent.

The usual correction for nonideality, $1 + \left(\frac{d \ln \gamma_1}{d \ln x_1}\right)$, may be omitted, since the solute is very dilute. Here γ_1 is the activity of the solute and x_1 its mole fraction.

Johnson and Babb have presented an excellent review of current diffusion theory and data for binary nonelectrolytes.[2] For conditions under which the solute is very dilute, the Eyring, thermodynamic, Stokes-Einstein, and thermodynamics-of-irreversible-processes theories give the following form for correlation:

$$\frac{D\mu}{T} = \psi , \qquad (1)$$

where ψ is a correlation coefficient which is dependent on molecular size, shape, and other variables. It is generally assumed to vary linearly with mole fraction, with the end point fixed by the value at infinite dilution of each component.

Direct application of the gas-diffusion equation to liquid transport provides another possible means of correlating the diffusion of a dilute solute in a mixed solvent. For this case, the Maxwell-Stephan relation reduces to[3,4]

$$D = \frac{1}{x_2/D_{12} + x_3/D_{13}} , \qquad (2)$$

where x_2 and x_3 are the mole fractions of the two constituents of the mixed solvent, and D_{12} and D_{13} the binary diffusivities of the solute in each of the solvents. Unlike most theories of liquid diffusion, Eq. (2) makes no reference to the viscosity of the mixture.

The mixed solvents employed were

(a) n-hexane-tetradecane
(b) n-hexane-cyclohexane
(c) cyclohexane-n-decane

Diffusion coefficient and viscosities were determined over the entire composition range of the three mixed solvents. The results indicate that Eq. (2) predicts quite closely the variation of the mixture diffusivity with composition for solvents (a) and (c). However, it is in error by 30% for the middle composition region of solvent (b). It appears that the direct application

[2] P. A. Johnson and A. L. Babb, Chem. Revs. 56, 387 (1956).

[3] R. B. Bird, W. E. Stewart, and E. N. Lightfoot, Notes on Transport Phenomena (John Wiley and Sons., New York, 1958), pp. 571, 678.

[4] C. R. Wilke, Chem. Eng. Progr. 46, 95 (1950).

of gas-diffusion theory without considering the viscosity of the system is not a fruitful method of analyzing mixture diffusivities in liquids.

The Eyring method, however, provided a much more satisfactory method for correlating the results. For solvents (a) and (b), the $(D\mu/T)$ group was linear in mole fraction, as implied by the Eyring theory. For solvent (c) however, $(D\mu/T)$ exhibited a definite minimum between the pure component values, corresponding to the minimum in the viscosity-composition curve. However, even in this case, the maximum deviation from the linear relationship was less than 10%. The discrepancy was ascribed to a nonnegligible difference in the free energies of activities for viscosity and diffusion.

From the few data available from this study, the best method for estimating the diffusion coefficient of a dilute solute in a mixed solvent is as follows: From measured (or estimated) values of the binary diffusivities in each of the solvents, and the viscosities of the pure solvents and the mixture, obtain the diffusivity in the mixture by a linear mole fraction interpolation of the group $(D\mu/T)$.

4. FREE AND FORCED CONVECTION IN A DIAPHRAGM-TYPE DIFFUSION CELL

J.T. Holmes, D.R. Olander, and C.R. Wilke

The standard relation for calculating diffusion coefficients in a diaphragm cell is[1,2,3]

$$\ln\left(\frac{\Delta c_i}{\Delta c_f}\right) = \beta D t, \qquad (1)$$

where Δc_i and Δc_f are the initial and final concentration differences between the two compartments of the cell, D is the diffusivity, and t the time; β is the cell constant, determined by calibration with a substance of known diffusivity.

If all the transport resistance is the sintered glass diaphragm, then β is a function of the cell volumes and the dimensions of the pores within the disc.

However, if in addition, the fluid layers adjacent to the disc offer significant diffusional resistances, the cell constant is given by

[1] J.B. Lewis, J. Appl. Chem. (London) 5, 228 (1955).

[2] Pin Chang, Ph.D. Thesis, University of California (1954).

[3] R.H. Stokes, J.Am. Chem. Soc. 72, 763 (1950).

$$\beta = \left(\frac{1}{V_1} + \frac{1}{V_2}\right)\left[\frac{1}{2D/kA + \ell/A'}\right] , \qquad (2)$$

where V_1 and V_2 are the volumes of the two compartments, k is the mass-transfer coefficient for the fluid film, A the gross area of the disc, and ℓ/A' the effective length-to-area ratio of the pores within the disc. The 2D/kA group accounts for the external mass-transfer resistance due to laminar fluid layers on the diaphragm. Normally, by including this term one can correct for a cell constant which apparently varies with stirring speed and fluid properties. It may be omitted from the cell constant only when the cell is perfectly stirred and there is no external mass-transfer resistance. In actual practice these conditions are not fully realized.

Other users of the diaphragm cell have investigated the effect of stirring,[1,3,4] but have not actually considered 2D/kA in the cell constant.

Lewis[1] used a cell with very efficient stirring and found that above 120 rpm all the cell constants were constant. He concluded that the cells should be run at this speed to obtain reproducible results.

Other investigators[3,4] have essentially done the same thing and used some minimum speed, determined for their cell geometry, for all experiments. This procedure requires many calibration runs for each cell, and then the assumption that the minimum calibration speed works for all other fluid properties.

To use Eqs. (1) and (2), one needs to know k, the mass-transfer coefficient, as a function of stirring speed and fluid properties. A correlation of mass-transfer coefficients, for a specific cell geometry, as a function of stirring speed and fluid properties would provide a convenient means for estimating the external resistance term.

Electrochemical limiting-current experiments were performed to determine the mass-transfer coefficient for the cell geometry used in this study. A special half-cell was constructed and the limiting current for three different copper sulfate solutions was measured as a function of stirring speed. The limiting currents were used to calculate the mass-transfer coefficients.

The mass-transfer coefficients were correlated in the forced-convection range in the usual dimensionless group manner. The least-squares fit of 32 datum points gives

$$Nu' = 0.050\, Re^{0.79}\, Sc^{0.38} , \qquad (3)$$

where Nu' is the Nusselt number, Re the Reynolds number, and Sc the Schmidt group.

---

[4] I. E. Smith and J. A. Storrow, J. Applied Chem. (London) 2, 225 (1952).

It was assumed that the correct length parameter was the stirring-bar length, but this was not varied. Therefore the correlation should be applied only to this specific cell geometry. It was also assumed that the mass-transfer coefficient was the same for the sintered glass diaphragm as it was for the copper cathode.

A free-convection correlation was obtained from the limiting current measurements on each of the three copper sulfate solutions. It is

$$Nu' = 0.58 [Sc \cdot Gr]^{1/4} \quad . \tag{4}$$

It compares quite favorably with the equation given by Wilke et al.,[5,6] who obtained

$$Nu' = 0.66 [Sc \cdot Gr]^{1/4} \tag{5}$$

for free vertical plates, from electrochemical measurements and the dissolution of benzoic acid. The difference between the correlations is thought to be due to wall and shape effects.

The correction resulting from including 2D/kA for various systems is about 0.5% at 200 rpm and about 0.3% at 350 rpm, which is less than the precision of the diffusivity measurement.

Therefore one stirring speed was used (350 rpm) for all measurements and the correlations were not required to determine the cell constants or diffusion coefficients. One should note that 2D/kA is part of the cell constant and about the same, at one speed, for all fluids.

[5] C.R. Wilke, M. Eisenberg, and C.W. Tobias, J. Electrochem. Soc. 100, 513 (1953).

[6] C.R. Wilke, M. Eisenberg, and C.W. Tobias, Chem. Eng. Progr. 49, 633 (1953).

5. COALESCENCE AND DISPERSION RATES IN AGITATED LIQUID-LIQUID SYSTEMS (*)

James H. Vanderveen and Theodore Vermeulen

Agitated mixtures of immiscible liquids in stirred tanks are of interest in connection with rational design of mixer-settler extraction equipment. Previous work in this field[1] has shown that the drop diameter near the agitator

(*) Abstract from thesis by James H. Vanderveen UCRL-8733, Nov. 1960.

[1] J.L. Fick, (Thesis), H.E. Rea and T. Vermeulen, The Effects of Agitator Geometry in the Mixing of Liquid-Liquid Systems, UCRL-2545, April 1954.

impeller tip, in such mixtures, varies inversely with the 1.2 power of impeller speed (0.6 power of Weber number), and also increases linearly with volume fraction. This experimental result agrees with a theoretical analysis by Hinze.[2]

However, in systems with low interfacial tension and with large viscosity differences between the two phases, coalescence may take place to a major extent. This effect appears to have been encountered in measurements by Rea[3] and by Rodger, Trice, and Rushton.[4] In the study presented here, drop-diameter profiles have been measured for several immiscible mixtures. Figure F.5-1, for mixtures of cyclohexanone and water, is typical of the results obtained. The extrapolated values at zero distance (i.e., at the impeller tip) were calculated from the earlier correlation.

Correlation of the new experimental results, and of Rodger's, shows that the diameter increase (the increment due to coalescence between the impeller tip and the point of measurement) varies inversely with the 0.65 power of speed (i.e., it varies with the -0.45 power of Weber number and with the +0.25 power of Reynolds number), as well as with the 1.2 power of the ratio of tank diameter to impeller diameter, and with a complex function of viscosities and volume fractions. The proportionality constant in the expression increases in a general way with distance from the impeller, but needs to be redetermined for each new tank geometery.

[2] J.O. Hinze, A.I. Ch. E. Journal 1, 289 (1955).

[3] H.E. Rea, Jr. (Thesis) and T. Vermeulen, Effect of Baffling an Impeller Geometry on Interfacial Area in Agitated Two-Phase Liquid Systems, UCRL-2123, April 1953.

[4] W.A. Rodger, V.G. Trice, Jr., and J.H. Rushton, Chem Eng. Progr. 52, 515 (1956).

6. DOWNFLOW BOILING AND NONBOILING HEAT TRANSFER IN A UNIFORMLY HEATED TUBE (*)

Robert LeRoy Sani and L.A. Bromley

Local heat-transfer coefficients in forced convection, down-flow boiling, and nonboiling have been measured by use of an electrically heated type-304 stainless steel tube (0.7194 in. i.d.×0.7502 in. o.d.×68.0 in. long). Average forced-convection heat-transfer coefficients in turbulent one-phase flow and local total pressure gradients in two-phase flow were also determined.

Data have been obtained for the boiling of distilled water with mass fluxes of 51 to 165 lb/sec ft^2, heat fluxes from 13.8×10^3 to 49.8×10^3 BTU/hr ft^2, pressures from 15.8 to 30.9 psia, and qualities up to 14%.

*Abstract from M.S. Thesis by Robert LeRoy Sani, UCRL-9023, Jan. 1960.

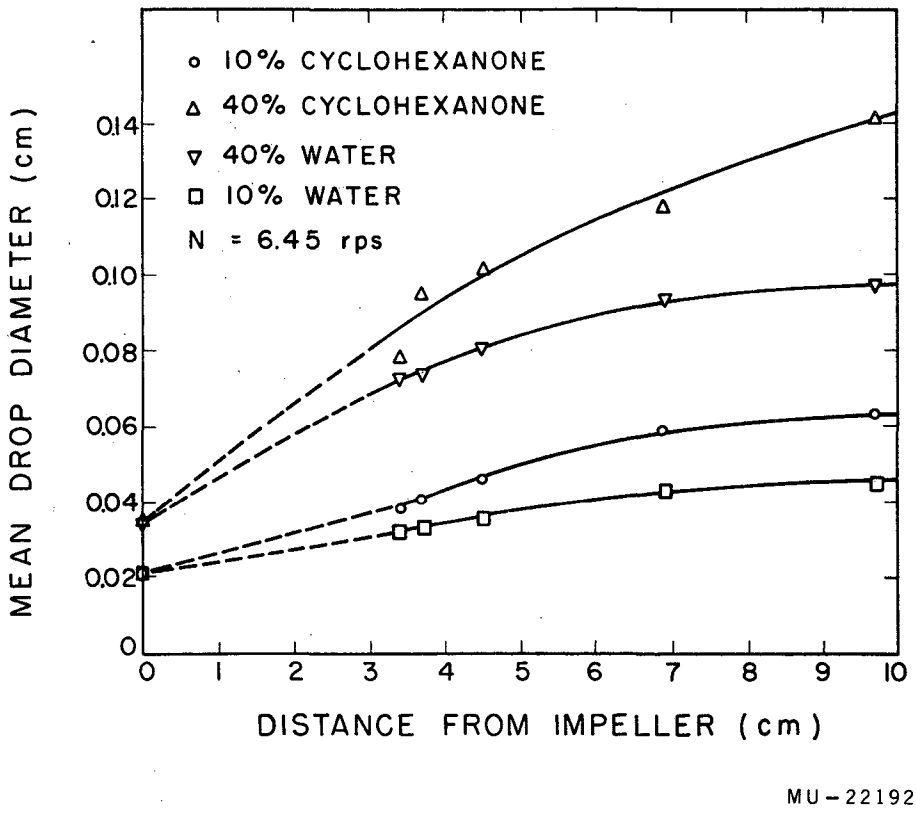

Fig. F. 5-1. Mean-drop-diameter profiles in a 10-inch baffled tank, using a four-bladed impeller of 5-inch diameter and 1-inch width, for cyclohexanone-water mixtures.

The boiling heat-transfer data were compared to the correlations proposed by Mumm, Dengler, Rohsenow, and Grossman and Schrock. No attempt was made to formulate a new correlation because of the limited range of conditions investigated. The nonboiling heat-transfer data were compared to the Dittus-Boelter and Sieder-Tate correlations. The local total pressure gradients in two phase flow were correlated by the Martinelli parameter, X_{tt}, for turbulent two-phase flow.

7. RESISTANCE TO POTENTIAL FLOW THROUGH A CUBICAL ARRAY OF SPHERES (*)

Robert E. Meredith and Charles W. Tobias

Precise conductivity measurements on models sectioned out from a cubic lattice of spheres in a continuous medium indicate that the effective conductance of such a system deviates from the values predicted by Lord Rayleigh's analytic solution of this potential distribution problem. Deviations become particularly significant when the spheres approach close packing, and when the conductance of spheres is much greater than that of the continuum. By use of a different function for potential, and by consideration of higher terms in the series expression for the potential in the continuous phase, Rayleigh's results are modified, yielding an analytical expression that represents effective conductance satisfactorily in the concentration region approaching close packing.

*Abstract of published paper, J. Appl. Phys. 31, 1270 (1960).

8. NONEQUILIBRIUM THERMODYNAMIC THEORY FOR CONCENTRATION PROFILES IN LIQUID EXTRACTION (*)

Alphonse Hennico and Theodore Vermeulen

The pattern or "profile" of concentration change in each of the two countercurrent streams, within a packed extraction column involving a three-component nonelectrolyte system, is generally assumed to follow either branch of the mutual-solubility curve for the system. In the work reported here, such concentration profiles have been computed for an idealized extraction process, and the profiles have been found to depart from the equilibrium curve.

The idealized extraction postulated here has the following characteristics: It involves a system with thermodynamically defined equilibrium behavior, rather than with known experimental behavior. Mass-transfer-coefficient ratios are held constant at any one steady-state condition of operation (or "run") but are varied in different runs. A modified activity gradient,

*Abstract from paper embodying M S. Thesis by Alphonse Hennico, UCRL-9415, Sept. 1960.

derived both for molecular diffusion and for penetration-theory conditions, is postulated to govern mass transfer and is used in place of the usual concentration driving potential.

The calculations show that the concentration profile for the raffinate will usually be carried into a metastable condition, represented by a locus inside the equilibrium curve. The extract compositions always remain appreciably outside the equilibrium curve. Solute depletion, mainly, is found to explain the result for the raffinate phase, in much the same way as temperature lowering leads to supersaturation in binary solutions. Solute enrichment is the cause of the extract-phase behavior. The distance between the calculated concentration paths and the equilibrium curve depends on the values of the mass-transfer coefficients, as shown in Fig. F.8-1. Raffinate streams for different runs, with a solute (C) mole fraction of 0.30, are shown on the left-hand side of the figure; the corresponding extract compositions start with pure solvent (B) as shown on the right.

Values of the number of transfer units obtained from the exact concentration profiles can differ as much as 10% from the values given by the usual equilibrium-curve approximation. Because the deviation is no greater than this, the usual approximation is a good one. Nevertheless, when either internal or outlet streams from an extraction column are sampled, a full composition analysis should be made without assuming that they correspond to the points on the equilibrium curve.

9. LONGITUDINAL DISPERSION IN TWO-PHASE CONTINUOUS-FLOW OPERATIONS: SOLUTION AND TABLES FOR CONCURRENT FLOW (*)

Terukatsu Miyauchi, Alice K. McMullen, and Theodore Vermeulen

The mathematical derivation of solutions for longitudinal dispersion in chemical-process equipment, carried out previously by Miyauchi for countercurrent flow, has been extended to the case of concurrent flow. These results are particularly applicable to certain types of heat exchangers, flash evaporators, and line-mixing solvent extractors. The extent of completion of the process, in dimensionless form, is given as an analytical function of rates of dispersion in the two phases, over-all heat- or mass-transfer coefficient, partition coefficient, rates of fluid flow, and fractional height in the equipment.

Numerical results for a large number of typical conditions, obtained on the IBM 701 computer, are given in tabular form in report UCRL-9112. Typical profiles, as plotted from the tables, are shown in Fig. F.9-1. In this figure, PB is a dimensionless number, for either phase x or phase y, which decreases as mixing increases; Λ is a phase-capacity ratio (or "extraction factor"); N_{ox} is the number of transfer units, based upon the true transfer

*Summary of UCRL-9112, March 1960.

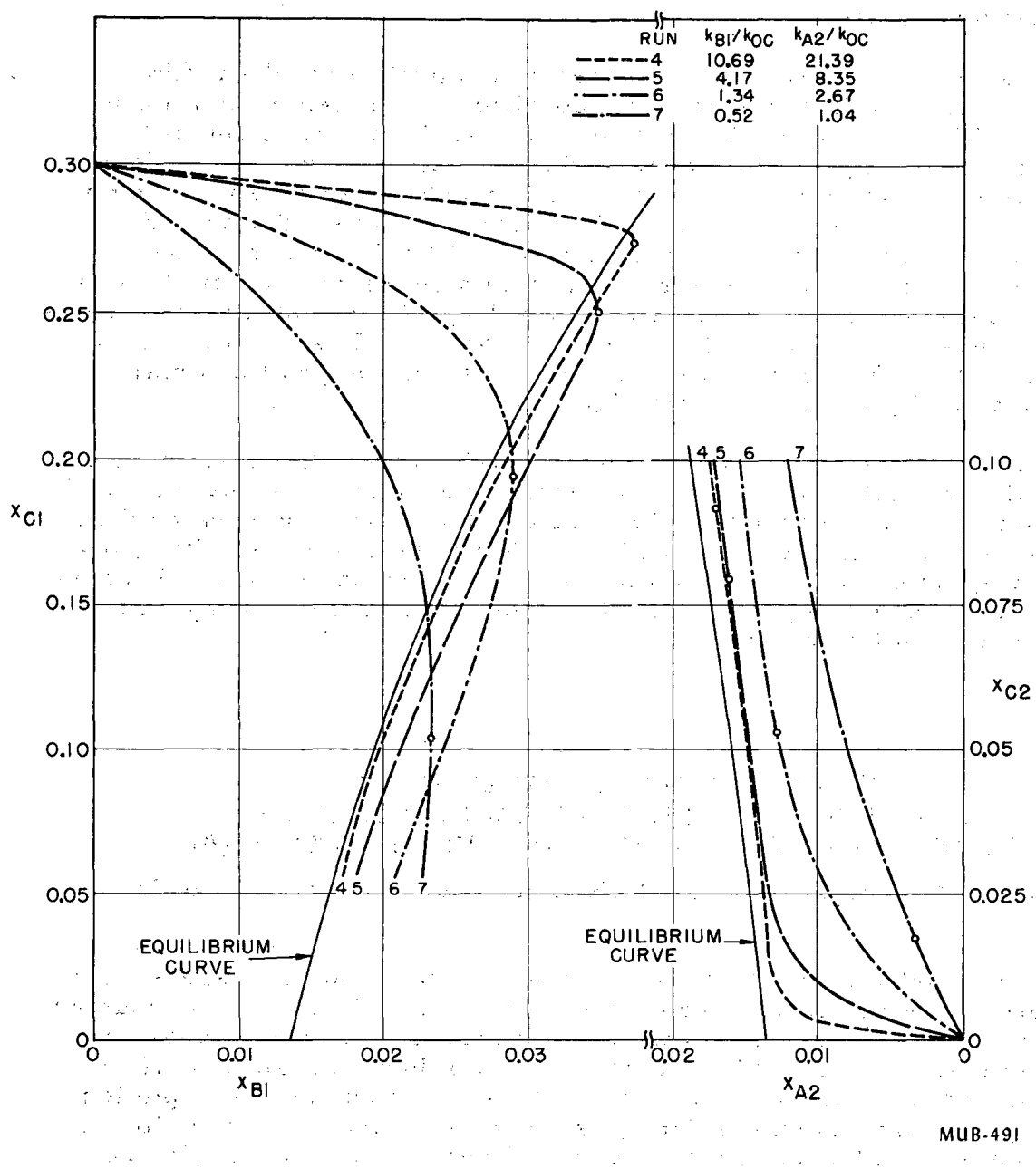

Fig. F.8-1. Calculated concentration profiles showing the effect of the k_{B1}/k_{0C} and k_{A2}/k_{0C} ratios.

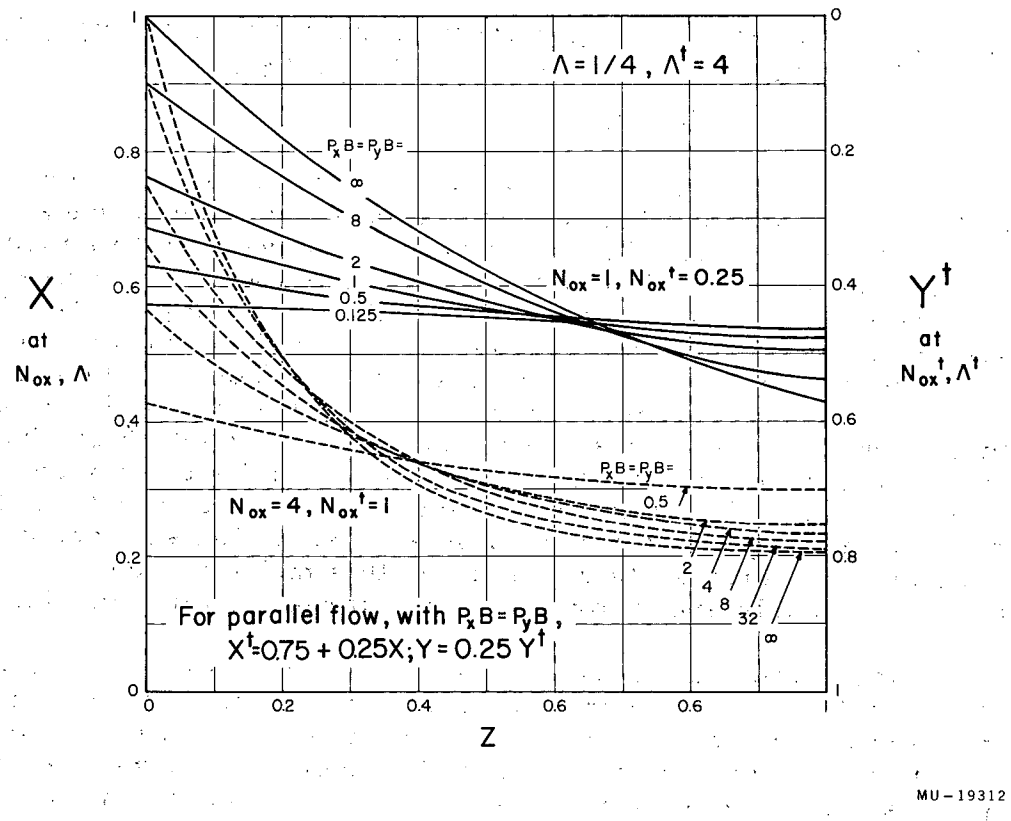

Fig. F. 9-1. Typical concentration or temperature profiles in cocurrent flow.

rate; X and Y are ratios of the transfer that has occurred (in the two phases) to the transfer that could ultimately occur under countercurrent conditions, with $1-X = Y/\Lambda$; and a dagger (†) indicates the values that would apply if the arbitrary designation of x and y phases were reversed.

10. A DIGITAL COMPUTER PROGRAM FOR TRIBUTYL PHOSPHATE SOLVENT-EXTRACTION COLUMN DESIGN

Donald R. Olander

The calculation of the number of theoretical stages required for the solvent-extraction separation of heavy-metal nitrates by tributyl phosphate-diluent mixtures is an extremely laborious affair. Conventional methods, which employ measured equilibrium data in conjunction with a graphical analysis, cannot cope with systems containing more than two components. Furthermore, the treatment of multicomponent systems invariably involves the time-consuming game of guessing raffinate concentrations of some of the components, the validity of which can be verified only after completion of the entire step-by-step column computations. This work describes a method which, by use of an analytical form for the distribution behavior, permits the evaluation of the correct unspecified raffinate concentrations and the determination of the number of theoretical stages in the scrubbing and extraction sections of a center-fed column. Because of its complexity, this multicomponent problem is virtually unapproachable except by means of a large digital computer.

The stagewise numerical procedure differs in one major particular from that employed for multicomponent distillation or extraction of organic solutes which do not dissociate or react in either phase; the variation of the distribution coefficients with composition, which necessitates the step-by-step technique, cannot be characterized solely by deviations from ideality expressed through Van Laar, Porter, or Margules equations. For the inorganic systems to be considered here, the distribution coefficients would be strongly concentration-dependent even for ideal solutes, because of the dissociation of the solute in the aqueous phase and its complexing with the tributyl phosphate (hereafter abbreviated TBP) in the organic phase. These two effects are expressed for the ith component by the over-all reaction

$$M^{+a_i}(aq) + a_i\, NO_3^-(aq) + b_i\, TBP(org) \rightleftharpoons M(NO_3)_{a_i} \cdot b_i\, TBP(org), \qquad (1)$$

for which the mass-action constant is

$$K_i = \frac{\left\{C_i\right\}_{org}}{\left\{M_i\right\}_{aq} \left\{NO_3^-\right\}_{aq}^{a_i} \left\{TBP\right\}_{org}^{b_i}} \qquad (2)$$

Equation (2) can be rearranged to a more useful form for the stage-wise computation, that is, as a distribution coefficient,

$$D_i = \frac{[C_i]}{[M_i]} = K_i \left[NO_3^-\right]^{a_i} \left[TBP\right]^{b_i} \quad . \tag{3}$$

Thus, the equilbria for each component can be described solely by three constants, K_i, a_i, and b_i. Furthermore, the effect of all other extractable solutes is implicitly included in the nitrate ion and TBP concentration terms.

The program assumes an aqueous feed consisting of a nitric acid solution of the heavy-metal nitrates, e.g., $UO_2(NO_3)_2$, $La(NO_3)_3$, $Th(NO_3)_4$. A maximum of 5 macro and 15 trace constituents can be accommodated.

The usual criterion for minimum flow rates--i.e., simultaneous attainment of equilibrium at the feed stage in both sections--has been shown to be inapplicable to these systems. However, no analytical method has been devised for determining the true limiting flow rates.

The reliability of the entire computation rests primarily upon the validity of the ideal equilibrium expressions represented by Eq. (3). There is no longer any serious doubt that complexing reactions between heavy-metal nitrates and oxygenated organic solvents such as TBP do in fact occur. However, the process is sufficiently involved that the simple approach represented by Eq.(3) (with concentrations replacing activities) does not yield complexing constants that are independent of concentration level. This could be partially remedied by including an activity coefficient term, which would convert the distribution coefficient expression to

$$D_i = K_i \left[NO_3^-\right]^{a_i} \left[TBP\right]^{b_i} \left[\frac{y_{\pm i}^{(1+a_i)} y_{TBP}^{b_i}}{y_{c_i}}\right] , \tag{4}$$

where $y_{\pm i}$ is the mean molar stoichiometric activity coefficient of the aqueous inorganic nitrate, and y_{TBP} and y_{c_i} the molar activity coefficients of the uncombined TBP and the complex in the inorganic phase. Equation (4) applies to every extractable component present, and separate $y_{\pm i}$ and y_{c_i} terms are required for each.

The omission of undeterminable activity coefficient terms in the equilibrium expression severely limits the usefulness of the method, which must be regarded solely as an order-of-magnitude approximation to the true number of theoretical stages.

The K_i values employed in the computation should be those corresponding as closely as possible to the concentration ranges encountered in the particular separation.

G. THESIS ABSTRACTS

On the following pages the abstracts of theses issued in 1960 are reproduced from the original documents.

Papers elsewhere in this report cover work described in theses by

John Gilmore (Paper B. 5),
John Thomas Holmes (Paper F. 3),
Ru-tao Kyi (Paper D. 24),
Allan Harvey Reddoch (Paper D. 25),
Robert LeRoy Sani (Paper F. 6), and
William R. Wilcox (Paper F. 2).

1. ELECTRONIC AND NUCLEAR PROPERTIES OF SOME RADIOACTIVE RARE-EARTH ELEMENTS

Amado Y. Cabezas

Lawrence Radiation Laboratory
University of California
Berkeley, California

August 9, 1960

ABSTRACT

Ground-state nuclear spins of thirteen radioactive rare earths (lanthanides) have been measured by the atomic-beam magnetic-resonance method. Ground levels (J) and corresponding g values of four rare earths have been determined. Ground-state electronic configurations have been inferred for the following elements:

Atomic number	Element	Observed ground levels	Ground-state electronic configuration
61	promethium	$^6H_{(5/2),\,7/2,\,9/2}$	$4f^5\,6s^2$
66	dysprosium	$^5I_8$	$4f^{10}\,6s^2$
67	holmium	$(^4I_{15/2})$	$(4f^{11}\,6s^2)$
68	erbium	$^3H_6$	$4f^{12}\,6s^2$

The configuration assigned to holmium is tentative in view of the measurement $I = 0$ for Ho^{166}, which does not allow an unambiguous determination of the J levels. The basis of the assumption is the close agreement between the measured g_J and the pure Russell-Saunders value for $^4I_{15/2}$.

In addition, these electronic properties have also been verified for the following rare earths:

Atomic number	Element	Observed ground levels	Ground-state electronic configuration
59	praseodymium	$^4I_{9/2}$	$4f^3\ 6s^2$
60	neodymium	$^5I_4$	$4f^4\ 6s^2$
62	samarium	$^7F_{(0),1,2}$	$4f^6\ 6s^2$
64	gadolinium	$^9D_{2,3,4,5}$	$4f^7\ 5d\ 6s^2$
65	terbium	$^6H_{15/2}$ and ($[^7F_6, {}^2D_{3/2}]_{15/2,13/2}$ $11/2$)	$4f^9\ 6s^2$ and ($4f^8\ 5d\ 6s^2$)
69	thulium	$^2F_{7/2}$	$4f^{13}\ 6s^2$

The following isotopes were used in these investigations. The half lives, nuclear ground-state spins, and J and g_J values are also stated:

Pr^{142} ($T_{1/2}$ = 19 hr) I = 2
with J = 9/2,* g_J = -0.7311(3)
$|a|$ = 67.5(1.0) Mc, $|\mu_I|$ = 0.30(2) nm
$|b|$ = 7(2) Mc, $|Q|$ = 0.035(15) barns

Nd^{147} ($T_{1/2}$ = 11.6 d) I = 5/2
with J = 4* g_J = - 0.6032(1)*

Pm^{147}	($T_{1/2}$ = 2.6 yr)	I = 7/2
	with J = 5/2,	g_J = - 0.286 (not observed)
	J = 7/2,	g_J = - 0.831(5)
	J = 9/2,	g_J = - 1.068 (4)
Sm^{153}	($T_{1/2}$ = 47 hr)	I = 3/2
	with (J = 0)	(not observed)
	J = 1*	g_J = - 1.495(15)
	J = 2*	g_J = - 1.497(15)
Gd^{159}	($T_{1/2}$ = 18 hr)	I = 3/2
	with J = 2*	g_J = - 2.6514(3)*
	J = 3*	g_J = - 2.0708(2)*
	J = 4*	g_J = - 1.8392(2)*
	J = 5*	g_J = - 1.725(7)*
Tb^{160}	($T_{1/2}$ = 72 d)	I = 3
	with J = 15/2*	g_J = - 1.3225*
	J = 15/2*	g_J = - 1.4563*
	J = 13/2*	g_J = - 1.4633*
	J = 11/2*	g_J = - 1.5165*
Dy^{165}	($T_{1/2}$ = 2.3 hr)	I = 7/2
Dy^{166}	($T_{1/2}$ = 82 hr)	I = 0
	with J = 8	g_J = - 1.2415(3)
Ho^{166}	($T_{1/2}$ = 27 hr)	I = 0 or I $\neq$ 0 with very small hfs (a<100 kc)
	with (J = 15/2)	g_J = - 1.1956(12)

Er^{169} ($T_{1/2}$ = 9.4 d) I = 1/2

Er^{171} ($T_{1/2}$ = 7.5 hr) I = 5/2
with J = 6 g_J = - 1.164(5)

Tm^{170} ($T_{1/2}$ = 129 d) I = 1
with J = 7/2* g_J = - 1.1412(2)
$|a|$ = 200(3) Mc, $|\mu_I|$ = 0.26(2) n.m
$|b|$ = 1,010(15)Mc, $|Q|$ = 0.61(5) barns

Tm^{171} ($T_{1/2}$ = 1.9 yr) I = 1/2.

The quantities measured elsewhere, but verified and directly involved in the experimental observations are marked by an asterisk. Our original results are unmarked. The numbers enclosed in the parenthesis denote the uncertainty in the last places of the figures quoted.

The magnetic dipole and electric quadrupole moments of the two odd-odd nuclei Pr^{142} and Tm^{170} are calculated from measurements of the hyperfine-structure separations.

2. A MASS-SPECTROMETRIC INVESTIGATION OF SULFUR VAPOR AS A FUNCTION OF TEMPERATURE

M. Charles Zietz
Lawrence Radiation Laboratory
University of California
June 15, 1960

ABSTRACT

A mass-spectrometric investigation was performed on sulfur vapor, which was in equilibrium with the condensed phase, in the temperature range of 120 to 210°C. The principal finding was that, in this temperature range, equilibrium sulfur vapor contains appreciable quantities of S_8, S_7, S_6, and S_5 only.

The sulfur vapor emanated as a small well-collimated molecular beam from a specially constructed source into an ionization chamber which was designed to exclude from analysis any sulfur vapor that had impinged on the walls or the hot electron filament. The ions were analyzed with a 6-in.-radius 60-deg.-deflection single-direction focusing mass spectrometer. The sulfur used for this study was purified by prolonged boiling with MgO followed by vacuum distillation.

In addition to establishing the principal species in the vapor phase, the results of this work provided essentially identical ionization potentials for S_8, S_7, S_6, and S_5 of 9.8 ± 0.4 ev. Also, the heat of vaporization of S_1 was calculated to be approximately 2.5 kcal greater than that of S_8. It was not possible to determine the quantitative composition of sulfur vapor. However, upper limits for S_8 and S_7 at 120°C of 86% and 14% respectively were obtained.

It is proposed that S_8 is the vaporizing species and that S_7, S_6, and S_5 result from dissociation of S_8, and that all four molecules have a ring configuration.

3. THE ELECTRONIC STRUCTURE OF OCTAHEDRALLY COORDINATED PROTACTINIUM (IV)

John D. Axe

Lawrence Radiation Laboratory and Department of Chemistry
University of California, Berkeley, California

July 1960

ABSTRACT

The compound of Cs_2ZrCl_6 has been used as a matrix for the study of certain magnetic and optical properties of tetravalent protactinium. The experimental procedures for the growth of Cs_2ZrCl_6 crystals and the incorporation of small amounts of other tetravalent ions into its structure are discussed in some detail.

The optical spectrum of tetravalent protactinium in this matrix has been investigated from 2000 A to 16 μ. Several features of the spectrum, as well as the results of para-mangetic-resonance absorption in these crystals, are attributed to single 5f electrons localized about the protactinium ions but subject to an octahedrally symmetric perturbation due to the crystal lattice.

4. I. BETA-SPECTROSCOPIC STUDIES IN THE PROMETHIUM REGION

II. THE CORIOLIS INTERACTION IN DEFORMED NUCLEI

Thomas V. Marshall
(Thesis)

May 1960

Lawrence Radiation Laboratory and Department of Chemistry
University of California, Berkeley, California

ABSTRACT

The new isotopes Sm^{142} and Pm^{142} have been produced by the reaction sequence: $Nd^{142}(\alpha,4n)Sm^{142} \xrightarrow{\beta^+,\ EC} Pm^{142}$. The decay characteristics of these isotopes have been determined.

The gamma, beta, and conversion-electron spectra of Pm^{149} have been measured and a decay scheme is proposed for this isotope.

A method for calculating the effect of the Coriolis interaction on the energies of the rotational levels of a generalized, spheroidally deformed nucleus has been developed using a simple nuclear model, and the general effect of this interaction on rotational bands is discussed. Part of the energy level schemes of Pa^{231} and Pa^{233} have been interpreted in terms of rotational bands perturbed by the Coriolis interaction.

5. CHEMICAL PROPERTIES OF ASTATINE

Evan H. Appelman
(Thesis)

Lawrence Radiation Laboratory and Department of Chemistry
University of California, Berkeley, California

January 1960

ABSTRACT

The aqueous solution chemistry of astatine has been investigated by extraction of the astatine into benzene and carbon tetrachloride and by its coprecipitation with insoluble iodides, iodates, and periodates. Some of the experiments of previous workers have been repeated and amplified.

A systematic study of the behavior of astatine as a function of the emf of an acid aqueous solution has been carried out. This study has confirmed the existence of the (-1), (0), and (+5) oxidation states, and of at least one intermediate positive state. A rough potential diagram for acidic astatine solutions has been proposed. No evidence for a (+7) state has been found. Iodine has been used as a nonisotopic carrier to fix the identity of the (0) state as AtI. In the course of this study photochemical reactions involving astatine have been observed for the first time.

The distribution of astatine between aqueous solutions and carbon tetrachloride in the presence of other halogens and halide ions has been investigated quantitatively, and evidence has been adduced for the species AtI, AtI_2^-, $AtIBr^-$, $AtICl^-$, AtBr, $AtBr_2^-$, and $AtCl_2^-$. The equilibrium constants relating these species have been determined. In connection with these studies the distribution of IBr between CCl_4 and aqueous bromide solutions has been accurately determined.

A report is given of an unsuccessful attempt to obtain quantitative information regarding the At (-1) -- At (0) couple from the reactions of astatine with the As (III) -- As (V) couple.

Incidental data is presented on the half-lives of At^{211} and Bi^{207}.

6. FISSION AND SPALLATION IN NUCLEAR REACTIONS INDUCED BY HEAVY IONS

Glen E. Gordon

Lawrence Radiation Laboratory and Department of Chemistry
University of California, Berkeley, California

May 1960

ABSTRACT

Several features of fission and spallation reactions proceeding through astatine compound nuclei formed by carbon-ion and nitrogen-ion bombardment have been investigated. The kinetic-energy spectra of the fission fragments were observed at various angles to the beam over a range of bombarding energies by use of two types of detectors, gas scintillation chambers and diffused p-n junctions. Cross sections for neutron-evaporation reactions were determined by radiochemical measurement of the production of astatine isotopes.

Analysis of the fission-fragment angular distributions according to the models by Halpern and Strutinski and by Griffin, together with the dependence of the fission and spallation cross sections on bombarding energy, suggests that fission is frequently preceded by evaporation of neutrons and charged particles. This result is explained on the basis of increasing probability for charged-particle emission with excitation energy and hindrance of neutron evaporation at low energies due to angular-momentum and level-density effects. The latter argument is also used to explain discrepancies between experimental and theoretical shapes of the excitation functions for neutron-evaporation reactions. Evidence has also been found that, in the astatine region, a larger total kinetic energy release is associated with symmetric fission than with the asymmetric modes. This is a reversal of the trend found in heavier elements.

In order to obtain the data presented in the main body of the thesis, several supplementary investigations were necessary. These are discussed in the appendices.

7. COINCIDENCE MEASUREMENTS IN NUCLEAR DECAY-SCHEME STUDIES

John P. Unik
(Thesis)
Lawrence Radiation Laboratory and Department of Chemistry
University of California, Berkeley, California

March 1960

ABSTRACT

The decay schemes of the isomers of Tc^{95} and Tc^{97} have been studied by using high-resolution conversion-electron spectrographs, gamma-ray scintillation detectors, and coincidence techniques.

The half-life of the 74.6-kev excited state in Np^{239} has been measured by the delayed coincidence technique as 1.2 ± 0.1 mμsec.

The directional correlations of two gamma-ray cascades following the beta decay of U^{237} to Np^{237} have been studied and the results are consistent with previous assignments of the total angular momenta of the excited states. An upper limit on the half-life of the 332-kev excited state in Np^{237} was determined to be 1.0 mμsec.

Electron-electron coincidence measurements have been performed on the beta decay of Pa^{233}. This work removes some of the ambiguities between previous coincidence work and the previously proposed decay scheme.

The transmission of one half of the original electron-electron coincidence spectrometer has been increased by a factor of six without sacrificing resolution. This increased transmission was achieved by converting the original thin-lens magnetic field to a thick-lens triangular magnetic field.

8. FISSION OF GOLD WITH 112-Mev C^{12} IONS: A YIELD-MASS AND CHARGE-DISTRIBUTION STUDY

H. Marshall Blann

(Thesis)

Lawrence Radiation Laboratory
University of California
Berkeley, California

May 23, 1960

ABSTRACT

Fission-product cross sections have been measured radiochemically and mass-spectrometrically for gold bombarded with 112-Mev C^{12} ions. Cross sections for 43 nuclides have been measured for elements from nickel to barium. Thirty-six yields are either primary fission product yields (independent yields) or have been corrected (with less than 25% correction) so as to represent independent yields. The independent yields have been empirically systematized and a yield-mass curve has been constructed. The yield-mass curve is compared with the yield-mass curves obtained from the fission of bismuth with 22-Mev and 190-Mev deuterons. The yield systematics indicate that the sum of the mass numbers of complementary fission products is 13±1 amu less than that of the compound nucleus, and the sum of the charges of complementary fission products is two units less than that of the compound nucleus. It is postulated that 9±1 neutrons and an alpha particle must have been emitted. Evidence is presented that at least three and possibly more of the neutrons are emitted prior to fission.

The most probable charge of the fission products as a function of mass number has been determined empirically. It is shown that from mass number 80 to mass number 111 the Equal Charge Displacement (ECD) and Constant Charge Ratio (CCR) rules predict the empirical values equally well. For masses less than 80 and greater than 120 the ECD and CCR rules are shown to be equally poor, as the empirical distribution is

between them. The Minimum Potential Energy theory of charge distribution proposed by Present and modified and interpreted by Swiatecki is shown to predict the empirical points over the entire mass region studied (A = 66 to A=135) within experimental error (±0.2 charge unit).

9. SOME LOW-TEMPERATURE NUCLEAR ORIENTATION STUDIES

James Frederick Schooley

Lawrence Radiation Laboratory
University of California
Berkeley, California

July 19, 1960

ABSTRACT

Nuclear-orientation experiments were performed on promethium-144 included as the tripositive ion in the crystal $Nd(C_2H_5SO_4)_3 \cdot 9H_2O$. Theoretical predictions of Elliott and Stevens regarding the fine-structure splitting of the Pm^{+3} electronic state $^5I_4$ have been confirmed. The magnetic hyperfine-structure parameter has been measured and is $0.0063\ cm^{-1} \pm 0.0002\ cm^{-1}$ or $0.0055\ cm^{-1} \pm 0.0002\ cm^{-1}$ for the nuclear spin of Pm^{144} equal to 5 or 6, respectively. On the basis of theoretical prediction of the hyperfine-structure parameter, the nuclear magnetic moment can be calculated as $1.68 \pm .14$ nm or $1.75 \pm .14$ nm for the respective nuclear-spin choices. The John-Teller splitting parameter has been measured as $0.014\ cm^{-1}$.

Nuclear alignment experiments have been performed on neptunium-239 included as the NpO_2^{++} ion in the crystal $UO_2Rb(NO_3)_3$. The temperature of the crystal was reduced to $\sim 0.14\ ^oK$ by contact with magnetically cooled $MnSO_4 \cdot (NH_4)_2SO_4 \cdot 24H_2O$. Anisotropy was detected in the 106-kev gamma ray which depopulates the 392-kev level in Pu^{239}. This anisotropy indicates that the 10^{-7}-sec lifetime of the 392-kev level does not result in appreciable attenuation of the anisotropy or that the daughter state itself is aligned through its own hyperfine-structure interactions.

10. PERTURBATION OF ALPHA-GAMMA ANGULAR CORRELATIONS IN TRANSURANIUM ISOTOPES

Eileen Flamm

Lawrence Radiation Laboratory and Department of Chemistry
University of California, Berkeley, California

August 1960

ABSTRACT

The perturbation of alpha-gamma angular correlations has been studied in Am^{241}, Am^{243} and Cm^{243} by observing alpha particles in coincidence with gamma rays from daughter nuclei recoiling into vacuum, air, aluminum, silver, iron, Mylar, water and benzene. Attenuation coefficients below the hard core value for a static interaction were obtained in vacuum, indicating that fluctuating magnetic fields or electric field gradients are present at the daughter nuclei during the recoil motion. Significantly larger anisotropies were obtained in nonmagnetic metals than in iron or in insulators. The magnetic and electric moments of the intermediate nuclear states in the alpha-gamma cascades are estimated and the configuration of the electron shell following alpha decay is considered. Extra-atomic electric fields at the daughter nuclei during and after the recoil motion are discussed with reference to current theories of radiation damage and the chemical behavior of the actinides. The results and interpretations of previous alpha-gamma angular correlations are reviewed. From the observed correlations in Cm^{243}, a lower limit can be set for the E2/M1 mixing ratio δ^2 of the 278 kilovolt gamma ray in Pu^{239} and the sign of δ is determined.

11. SOME PROBLEMS OF CRYSTALLOGRAPHY

Quintin C. Johnson

Lawrence Radiation Laboratory
University of California
Berkeley, California
August 1960

ABSTRACT

Crystal Energy Calculations

Calculations of minimum-energy-structures have been made in an effort to ascertain the effectiveness of the Born expression for the energy of a crystal. This expression assumes an r^{-1} attractive potential due to charge separation and an r^{-n} repulsive force due to the Pauli effect. Application of this model to a number of problems of crystal chemistry indicates that ionic substances may be suitably described by the above potential. This is shown by a comparison of the minimum-energy-structures of LaOCl, YOCl, $SrBr_2$, brookite, and YF_3 to the acutal structures. Consideration of the $CdCl_2$ structure shows that van der Waals forces can not always be neglected.

The Crystal Structure of Semicarbazide Hydrochloride

The structure of semicarbazide hydrochloride, $H_2NHNCONH_2 \cdot HCl$, has been determined by single-crystal x-ray diffraction methods. The space group is $P2_12_12_1$ and the cell dimensions are a = 7.54 ± .02, b = 13.22 ± .03, and c = 4.67 ± .02 Å. The interesting nitrogen-nitrogen single-bond distance is 1.457 ± .007 Å.

A Redetermination of the Crystal Structure of Tetramethylammonium Bromide

In order to determine a fairly reliable carbon-nitrogen bond distance in a quaternary amine, a redetermination of the structure of tetramethylammonium bromide, $(CH_3)_4NBr$, was carried out by single crystal x-ray diffraction methods. The results are in close agreement with work done by previous researchers. The carbon-nitrogen bond distance is equal to 1.50 ± .02 Å. Attempts to localize the hydrogen atoms were unsuccessful.

12. THE CROSS SECTIONS FOR THE FORMATION OF ASTATINE ISOTOPES MADE BY THE BOMBARDMENT OF BISMUTH-209 WITH HELIUM-3

E. Thomas Strom
(Master's Thesis)

Lawrence Radiation Laboratory and Department of Chemistry
University of California, Berkeley, California

August 19, 1960

ABSTRACT

Bismuth 209 was bombarded with He^3 on the Berkeley Heavy-ion linear accelerator. Cross sections for the formation of astatine isotopes were measured. The experimental cross sections are compared with theoretical cross sections, calculated using the Jackson model.

The results of this work are compared with those of other workers and proposals for further research are made.

13. $N^{15}(p, p^{2n})N^{13}$ REACTION INDUCED BY PROTONS OF ENERGY 0.4 TO 6.2 Bev

Linda Chang Sah

Lawrence Radiation Laboratory and Department of Chemistry
University of California, Berkeley, California

August 1960

ABSTRACT

N^{14} and N^{15} were bombarded with protons in the energy range 0.4 to 6.2 Bev. Measured values of the absolute cross sections for $N^{14}(p, pn)N^{13}$ is 6 mb over the stated energy range, which agree and supplement the previous measurements up to 3.0 Bev. The (p, pn) yield is higher than the (p, p^{2n}) yield by a factor of 2 to 3 in the entire energy range of interest.

14. OXIDATION POTENTIAL OF THE Ce(III)-Ce(IV) COUPLE AS A FUNCTION OF TEMPERATURE IN PERCHLORIC ACID SOLUTIONS: THERMODYNAMIC PROPERTIES

Harry Lee Conley

Lawrence Radiation Laboratory
University of California
Berkeley, California

August 22, 1960

ABSTRACT

The temperature coefficient of the cerous-ceric oxidation potential has been measured in molal perchloric acid. E_f, dE_f/dT, ΔH, ΔF, ΔS, and ΔC_p

$$Ce(OH)^{+3} + 1/2\ H_2 = Ce^{+3} + H_2O), \quad (1)$$

$$Ce^{+4} + 1/2\ H_2 = Ce^{+3} + H^+ \quad (2)$$

at 25°C and a total cerium concentration of zero. E_f for Reaction (1) is in good agreement with the value found by Sherrill, King, and Spooner. ΔH, ΔF, and ΔS values for Reaction (1) at ceric perchlorate concentrations of 0.005 and 0.025 molal have also been determined and found to be in good agreement with the calorimetric values of Evans and Fontana. Evans and Fontana worked with ceric perchlorate concentrations of 0.005 and 0.025 molal, respectively, in half-molal perchloric acid.

From the temperature coefficient of the equilibrium constant K_D, ΔH, ΔF, and ΔS have been determined for the reaction

$$2\ Ce(OH)^{+3} = Ce\text{-}O\text{-}Ce^{+6} + H_2O \quad (8)$$

at 25°C. These results have been compared with those of Hardwick and Robertson.

UCRL-9566
(from UCRL-9079)

G

15. IONIC MASS TRANSPORT BY FREE CONVECTION TO HORIZONTAL ELECTRODES

Eugene Joseph Fenech
(Thesis)
Lawrence Radiation Laboratory and Department of Chemical Engineering
University of California, Berkeley, California

April 1960

ABSTRACT

Electrodeposition of copper from acid copper sulfate solutions onto horizontal electrodes facing upward is employed to investigate the mechanism and rate of mass transport under free-convection conditions. Mass-transfer rates are obtained by limiting-current measurements, and the distribution of current densities over the electrode surface is examined by the "sectioned-electrode" technique.

Solution properties (concentration, viscosity, and density) and geometry (shape and size) are varied between broad limits. A physical model involving two distinct types of free convection is postulated by which the effect of geometry on mass-transfer rates can be explained. In the absence of a suitable mathematical model the data are correlated by the equation:

$$Nu' = 0.122\ (Sc^{9/8}\ Gr)^{1/3}\ .d_n\ ,$$

where Nu', Sc, Gr, and d_n are respectively the Nusselt number for mass transfer, the Schmidt number, the Grashof number, and the correction factor for electrode size.

In the range of $2{,}000 < Sc < 50{,}000$ and $4\times10^6 < (Sc^{9/8}\ Gr) < 4\times10^{13}$, 95% of the experimentally obtained mass-transfer rates are within ±6.7% of the values predicted by this correlation.

16. LONGITUDINAL DISPERSION IN BEDS OF FINELY DIVIDED SOLIDS

Jerry Max Robinson

Lawrence Radiation Laboratory and Department of Chemical Engineering
University of California, Berkeley, California

June 1960

ABSTRACT

Experimental determinations of the longitudinal dispersion coefficient and the Peclet number were made for three binary gas systems. The experimental technique involved measuring the dispersion of a step function input to a column packed with glass beads.

The diffusional model was employed to obtain the differential equation describing longitudinal dispersion in a packed column. This equation was solved with suitable boundary conditions, and the solution was used in the analysis of the experimental dispersion data.

The experimental results show a variation in the Peclet number from 0.1 to 0.6, and in the eddy dispersion coefficient from 0.03 to 1.0 cm^2/sec for the Reynolds number range from 0.03 to 1.0.

UCRL-9566
(from UCRL-8926)

G

17. CHARGED-PARTICLE-INDUCED FISSION: A MASS SPECTROMETRIC YIELD STUDY

Yung Yee Chu

Lawrence Radiation Laboratory and Department of Chemistry
University of California, Berkeley, California

November, 1959

ABSTRACT

The products from the fission of uranium induced by charged particles were studied in a mass spectrometer. Both U^{238} and U^{235} were bombarded with 45.7- and 24-Mev helium ions, and U^{238} was also bombarded with 730-Mev protons and 100-Mev carbon ions. The total chain yields in the region of the rare earth elements (mass 140 to mass 155) for most of the above bombardments and a thermal-neutron bombardment of U^{235} were studied by using the isotopic-dilution technique. Independent yields were measured for all the above bombardments for several shielded nuclides.

The total chain yields in the mass region 140 to 155 constitute a smooth portion of the yield-mass curve, showing no obvious perturbations. The fractional-chain-yield results show that the charge distribution agrees best with the equal-charge-displacement rule, provided linear Z_A values are used. In other words, the obvious shell effect in the Z_A used in the fitting of thermal-neutron data is not appropriate in the medium-energy fission (24- and 45.7-Mev helium ions here). The indications are that this process is closer to the higher-energy fission mechanism. A more practical distinction between the low-energy fission and the high-energy fission would be required. It seems that the mechanism for the medium-energy fission should be somewhere between the equal-charge-displacement rule using "non-shell-affected Z_A" and the constant charge-to-mass ratio rule.

The broad and asymmetric-shaped independent yield distribution for higher-energy fission (730-Mev protons) with a given element was observed.

This can be explained by the multiplicity of fissioning nuclei. In 100-Mev carbon-ion fission of U^{238}, the distribution showed a similar effect, but not as striking.

The contribution of fission induced by secondary-neutrons in all the cyclotron bombardments was discussed. From the results of some other studies and the indications of this work, the contribution cannot be significant.

The composition of stable isotopes of Ce, Nd, and Sm formed in high-energy fission is discussed. It has been concluded that it is not impossible that the natural abundance of these elements may be, in part, due to some kind of high-energy fission of heavy elements.

18. SOME NUCLEAR AND ELECTRONIC GROUND-STATE PROPERTIES OF Pa^{233}, Am^{241} and 16-hr Am^{242}

Joseph Winocur

Lawrence Radiation Laboratory
University of California
Berkeley, California

April 13, 1960

ABSTRACT

The atomic-beam, magnetic-resonance method has been used to study some properties of the nuclear ground-state and the low-lying electronic states of three radioactive actinide isotopes. The following results were obtained:

Isotope	$T_{1/2}$	I	J	g_J	a(Mc)	b(Mc)
Pa^{233}	27.4d	3/2	11/2	0.8141(4)	+595(40)	-2400(300)
			9/2	0.8062(15)		
			7/2	0.7923(15)		
		μ_I(measured) = 3.4(1.2) nm				
Am^{241}	458 yr.	5/2*	7/2*	1.9371(10)	±17.144(8)	∓123.82(10)
Am^{242}	16 hr	1	7/2	1.9371(10)	±10.124(10)	± 69.639(40)

The starred results are confirmations of earlier measurements made by optical spectroscopy.

The observed electronic energy levels of protactinium very probably arise from the configuration $(5f)^2$ (6d) $(7s)^2$. Experimental transition intensities indicate that the ordering of these levels is probably inverted. From the observed hfs constants of Pa^{233} and detailed calculations involving the electronic wave functions, we infer the following values of the nuclear moments:

$\mu_I(Pa^{233}) = +2.1$ nm
$Q\ (Pa^{233}) = -\ 3.0$ barns.

From the ratios of the hfs constants of the two americium isotopes, together with the optically measured nuclear moments of Am^{241}, it follows that

$\mu_I(Am^{242}) = \pm\ 0.33$ nm

and

$Q\ (Am^{242}) = \mp\ 2.76$ barns.

A description of the experimental technique, and an analysis of the results are presented.

19. Part One: NUCLEAR SPECTROSCOPIC STUDIES IN THE HEAVIEST ELEMENT REGION

Part Two: AN ACCELERATING ELECTRON SPECTROGRAPH

Royal G. Albridge, Jr.
(Thesis)

Lawrence Radiation Laboratory and Department of Chemistry
University of California, Berkeley, California

April 1960

ABSTRACT

The decays of Np^{238} and Pa^{233} were studied by means of high-resolution spectroscopic instruments. The proposed decay schemes were tested by comparing the experimental data with predictions of the Bohr-Mottelson Theory of Deformed Nuclei. Previously unreported transitions were observed and some of these were used to assign new levels in the daughter nuclei, Pu^{238} and U^{233}. Gamma-gamma coincidence techniques were used to study the electron-capture decay of Cm^{241}. The decay scheme is discussed in the light of data obtained.

An accelerating permanent-magnet electron spectrograph for the detection of low-energy electrons was constructed. The instrument can be used as either a pre- or postaccelerating spectrograph. The equipment was used to study the low-energy electron spectrum of Pa^{233}.

H. AUTHOR INDEX OF UCRL REPORTS FOR 1960

Albert, R. D., Bloom, S. D., and Glendenning, N. K.
(p, n) Angular Distributions from Mirror Nucleus Targets: C^{13}, B^{11}, and Be^{9}.
UCRL-6199 November 1960

Albridge, R. G., and Hollander, J. M.
The Decay of Neptunium-238
UCRL-8034-Rev. June 1960
Nuclear Physics 21, 438 (1960)

Albridge, R. G., Hollander, J. M., Gallagher, C. J., and Hamilton, J. H.
The Energy Levels of U^{233}
UCRL-9438 November 1960
J. Nuclear Physics

Alexander, J. M. and Gallagher, M. F.
Recoil Properties of Fission Products
UCRL-8978-Rev. April 1960
Phys. Rev. 120, 874 (1960)

Alexander, J. M. and Winsberg, L.
Ranges and Range Straggling of Tb^{149}, At, and Po
UCRL-8997 April 1960
Phys. Rev.

Alexander, J. M. and Winsberg, L.
Recoil Studies of Nuclear Reactions Induced by Heavy Ions
UCRL-9118 August 1960
Phys. Rev.

Alexander, J. M. and Winsberg, L.
Recoil Studies of Heavy-Ion-Induced Nuclear Reactions
UCRL-9152 Abstract April 1960
Gatlinburg - May 1960

Alpert, S. S., Lipworth, E., and White, M. B.
Nuclear Moments of I^{133}
UCRL-9062 Abstract February 1960
APS, Washington - April 1960

Alpert, S. S. - (see White, M. B., UCRL-9069 Abstract)

Alpert, S. S., White, M. B., Smith, K. F., and Lipworth, E.
The Magnetic Dipole and Electric Quadrupole Interaction Constants of I^{132}
UCRL-9424 Abstract November 1960
BNL - November 1960

Alpert, S. S. - (see White, M. B., - UCRL-9429 Abstract)

Alpert, S. S., Lipworth, E., White, M. B., and Smith, K. F.
The Magnetic Dipole and Electric Quadrupole Interaction Constants of Bi^{210}
UCRL-9474 Abstract November 1960
Bull. APS - 6, 74 (1961)

Alster, J., and Conzett, H. E.
Elastic Scattering of C^{12} Ions from Several Nuclei
UCRL-9143 Abstract May 1960
Gatlinburg - May 1960

Alster, J., and Gonzalez-Vidal, J.
(p, α) Reactions on Li^6 and Li^7
UCRL-9432 Abstract October 1960
Bull. Am. Phys. Soc. 5, No. 7 (1960)

Appelman, E. H.
Chemical Properties of Astatine
UCRL-9025 February 1960
PhD Thesis

Appelman, E. H.
The Oxidation States of Astatine in Aqueous Solution
No UCRL number December 1960
J. Am. Chem. Soc.

Appelman, E. H.
Solvent Extraction Studies of Interhalogen Compounds of Astatine
No UCRL number December 1960
J. Phys. Chem.

Appelman, E. H.
The Half-Lives of At^{211} and Bi^{207}
No UCRL number August 1960
Phys. Rev.

Asaro, F.
Alpha-Particle Measurements and Standards
No UCRL number September 1960
Proceedings of International Conference on Nuclidic Masses

Asaro, F., Stephens, F. S., Hollander, J. M., and Perlman, I.
Anomalous Electric Dipole Conversion Coefficients in Odd-Mass Isotopes of the Heavy Elements
UCRL-8786 July 1960
Phys. Rev. 117, 492 (1960)

Asaro, F. - (see Stephens, F. S., - UCRL-8996)

Asaro, F., Perlman, I., Rasmussen, J. O., Thompson, S. G.,
The Isomers of Am^{242}
UCRL-9047 January 1960
Phys. Rev. 120, 934 (1960)

Asaro, F., Stephens, F. S., Thompson, S. G., and Perlman, I.
The Alpha Decay of Fm^{253}
UCRL-9305 September 1960
Kingston Conference

Asaro, F., Michel, M., Thompson, S., and Perlman, I.
Alpha Decay of Long-Lived Am^{242m}
UCRL-9306 Abstract July 1960
Kingston Conference

Asaro, F., Thompson, S., Stephens, F., and Perlman, I.
Decay Scheme of E^{253}
UCRL-9307 Abstract July 1960
Kingston Conference

Asaro, F., and Perlman, I.
Alpha Decay to Beta Vibrational States
UCRL-9308 September 1960
Kingston Conference

Asaro, F., Michel, M., Thompson, S. G., and Perlman, I.
Alpha Decay of Long-Lived Am^{242}
UCRL-9381 Abstract September 1960
Kingston Conference

Asaro, F., Thompson, S. G., Stephens, F. S., and Perlman, I.
Decay Scheme of E^{253}
UCRL-9382 Abstract August 1960
Kingston Conference

Asaro, F., and Perlman, I.
Decay-Energy Systematics of the Heavy Elements
UCRL-9524 November 1960
Handbook of Physics

Asprey, L. - (see McWhan, D. B. - UCRL-9115)

Axe, J. D., Kyi, R. T., and Stapleton, H. J.
Paramagnetic Resonance in Tetravalent Pa^{231}
UCRL-9010 December 1959
J. Chem. Phys. 32, 1261 (1960)

Axe, J.
The Electronic Structure of Octahedrally Coordinated Protactinium (IV)
UCRL-9293 August 1960
PhD Thesis

Benioff, P. A.
Nuclear Reactions of Low-Z Elements With 5.7-Bev Protons
UCRL-8780-Rev. Part I. November 1959
Phys. Rev. 119, 316 (1960)

Benioff, P. A.
Nuclear Structure and Simple Nuclear Reactions
UCRL-8780-Rev. Part II November 1959
Phys. Rev. 119, 324 (1960)

Blann, H. M.
Fission of Gold with 112 Mev C^{12} Ions; Mass and Charge Distribution Characteristics
UCRL-9190 June 1960
PhD Thesis

Bloom, S. D. - (see Albert, R. D. - UCRL-6199)

Bloom, S. D. - (see Glendenning, N. K. - UCRL-9165 Abstract)

Bosch, H. E.
Remarks on Properties of Even-Even Nuclei Related to the Asymmetric Rotor Theory of Davydov and Filippov
UCRL-9031 February 1960

Bosch, H. E.
Remarks on Excited States of Even-Even Nuclei and on the Existence of a Complex Vibrational Second Excited State
UCRL-9074 February 1960

Bosch, H. E.
Decay of Rh^{106}
UCRL-9385-Rev December 1960
Nuclear Physics

Bowman, H. R. - (see Muga, M. L. - UCRL-9044)

Brandt, R., Werner, F. G., Wakano, M., Fuller, R., and Wheeler, J. A.
Effect of a Composition Dependent Surface Tension Upon the Masses and Stability of Heavy Nuclei
No UCRL number September 1960
Proceedings of the International Conference on Nuclidic Masses

Burnett, D. S., and Thompson, S. G.
Fission Thresholds for Elements Lighter than Radium
UCRL-9321 November 1960

Cabezas, A., Lipworth, E., Marrus, R., and Winocur, J.
Nuclear Spin of Samarium-153
UCRL-8776 Rev. August 1959
Phys. Rev. 118, 233 (1960)

Cabezas, A. - (see Lindgren, I. - UCRL-9064 Abstract)

Cabezas, A., Lindgren, I., Lipworth, E., Marrus, R., and Rubinstein, M.
Nuclear Spins of Neodymium-147 and Promethium-147
UCRL-9122 May 1960
Nuclear Physics 20, 509 (1960)

Cabezas, A. Y. and Lindgren, I. P. K.
Atomic Beam Study of the Hyperfine Structure of Tb^{170}
UCRL-9163 May 1960
Phys. Rev.

Cabezas, A. - (see Lindgren, I. - UCRL-9184)

Cabezas, A. Y.
Electronic and Nuclear Properties of Some Radioactive Rare-Earth Elements
UCRL-9346 August 1960
PhD Thesis

Cabezas, A., Lindgren, I., Marrus, R., and Rubinstein, M.
Nuclear Spins of Pm^{149}, Pm^{151}, and Tb^{160}
UCRL-9425 Abstract October 1960
Bull. Am. Phys. Soc. Series II, Vol. 5, No. 7, p. 504 (1960)

Cerny, J. - (see Harvey, B. G. - UCRL-9081 Abstract)

Cerny, J. - (see Harvey, B. G. - UCRL-9259)

Cerny, J., Harvey, B. G., and Pehl, R. H.
The Reactions $Li^6(\alpha, d)Be^8$ and $Li^7(\alpha, d)Be^9$ with 48 Mev Helium Ions
UCRL-9427 Abstract October 1960
Bull. Am. Phys. Soc. Series II, Vol. 5, No. 7, p. 493 (1960)

Cerny, J. - (see Harvey, B. G. - UCRL-9428 Abstract)

Chiao, L. - (see Rasmussen, J. O. - UCRL-9301)

Clements, T. P., and Winsberg, L.
Direct Nuclear Collision Inside the Nucleus According to the Impulse Approximation
UCRL-8982 Rev November 1960

Clements, T. P. and Winsberg, L.
Polynomial Fits of Nucleon-Nucleon Scattering Data
UCRL-9043 January 1960

Conley, H. L.
Oxidation Potential of the Ce(III)-Ce(IV) Couple as a Function of Temperature in Perchloric Acid Solutions--Thermodynamic Properties
UCRL-9332 November 1960
MS thesis

Conway, J. G.
Emission Spectroscopy of Radioactive Elements
UCRL-8752 September 1959
Proceedings of the VIII Colloquim Spectroscopicum Internationale Switzerland

Conway, J. G. - (see Gruber, J. B. - UCRL-8839)

Conway, J. G. - (see Gruber, J. B. - UCRL-8869 Rev.)

Conway, J. G., and Gruber, J. B.
Luminescence Spectrum of $PmCl_3$
UCRL-9042 January 1960
J. Chem. Phys. Vol. 32, No. 5, 1586 (1960)

Conway, J. G., and Gruber, J. B.
Absorption Spectrum of Pm^{+3} in D_2O, DCl
UCRL-9116 April 1960
J. Inor. Nucl. Chem. 14, 303 (1960)

Conway, J. G. (see Gruber, J. B. - UCRL-9310)

Conzett, H. E. - (see Nir, A. - no UCRL number - Abstract)

Conzett, H. E. - (see Gonzalez-Vidal, J. - UCRL-9082 Abstract)

Conzett, H. E. - (see Alster, J. - UCRL-9143 Abstract)

Cranberg, L., and Glendenning, N. K.
Direct-Interaction Contributions to 3-Mev Neutron Inelastic Scattering from Fe and Pb
UCRL-9295 July 1960
Kingston Conference

Cunningham, B. B.
Submicrogram Methods Used in Studies of the Synthetic Elements
No UCRL number December 1960
Microchemical Journal

Cunningham, B. B.
Book Review on - "Soviet Research on the Lanthanide and Actinide Elements, 1949 - 1957"
No UCRL number April 1960
Chem. and Eng. News, June 1960, p. 68

Cunningham, B. B. - (see McWhan, D. B. - UCRL-9115)

Dauben, C. H. - (see Templeton, D. H. - UCRL-8923)

Diamond, R. M. - (see Tuck, D. G. - UCRL-8897 Rev)

Diamond, R. M. - (see Elbek, B. - UCRL-9156 Abstract)

Diamond, R. M., Elbek, B., Igo, G., and Stephens, F. S.
Coulomb Excitation of Vibrational Levels by Heavy Ions
UCRL-9302 July 1960
Kingston Conference

Diamond, R. M., Hollander, J. M., Horen, D., and Naumann, R.
Identification of Neutron-Deficient Iridium Isotopes Ir^{182}, Ir^{183} and Ir^{184}
UCRL-9467 Abstract November 1960
Bull. Am. Phys. Soc.

Diamond, R. M.
Coulomb Excitation
No UCRL number November 1960
Nuclear Reactions Symposium-St. Louis -March '61

Dodge, R. P., Templeton, D. H., and Zalkin, Z.
Crystal Structure of Vanadyl Bisacetylacetonate. Geometry of Vanadium in Five-Fold Coordination
UCRL-8225 Rev November 1960
J. Chem. Phys.

Donovan, P. F., Harvey, B. G., and Wade, W. H.
Recoil Studies of Heavy Element Nuclear Reactions. I.
UCRL-9060 February 1960
Phys. Rev. 119, 218 (1960)

Donovan, P. F. - (see Harvey, B. G. - UCRL-9061)

Dostrovsky, I., Fraenkel, Z., and Winsberg, L.
Monte Carlo Calculations of Nuclear Evaporation Processes; IV. The Spectra of Neutrons and Charged Particles from Nuclear Reactions
UCRL-8963 November 1959
Phys. Rev. 118, 781 (1960)

Elbek, B., Stephens, F. S., and Diamond, R. M.
Coulomb Excitation with Heavy Ions
UCRL-9156 Abstract April 1960
Gatlinburg - May 1960

Elbek, B. - (see Diamond, R. M. - UCRL-9302)

Elbek, B. and Nakamura M.
Multichannel Detector for Use in Particle Spectrometers
UCRL-9405 September 1960
Nuclear Instruments and Methods

Elbek, B.
On the Correlation Between the Nuclear Deformation and the Moment of Inertia
No UCRL number November 1960
Kingston Conference

Ellinger, F. H. - (see McWhan, D. B. - UCRL-9115)

Elliott, J. H.
Experimental Results with a Lithium Drifted Silicon Diode Radiation Detector
UCRL-9433 Abstract October 1960
Bull. Am. Phys. Soc., Ser.II, Vol. 5, No. 7, p. 501, Dec. 1960

Ericson, T.
Fluctuations of Nuclear Cross Sections in the "Continuum" Regions
UCRL-9314 July 1960
Phys. Rev. Letters 5, No. 9, 430 (1960)

Ericson, T.
The Compound Nucleus - (Abstract)
No UCRL number August 1960
International Conference on Nuclear Structure - September 1960

Fenech, E. J.
Ionic Mass Transport by Free Convection to Horizontal Electrodes
UCRL-9079 April 1960
PhD Thesis

Flamm, E.
Perturbation of Alpha-Gamma Angular Correlations in Transuranium Isotopes
UCRL-9325 August 1960
PhD Thesis

Fraenkel, Z. - (see Dostrovsky, I. - UCRL-8963)

Fried, S. - (see Ghiorso, A. - no UCRL number)

Fuller, R. - (see Brandt, R. - no UCRL number)

Gallagher, C. J. - (see Albridge, R. G. - UCRL-9438)

Gallagher, M. F. - (see Alexander, J. M. - UCRL-8978-Rev.)

Garvin, H. L. and Lipworth, E.
The Nuclear Spins of I^{126}, I^{132}, I^{133}, and I^{135}
UCRL-9038 January 1960
J. Nucl. Phys. 19, 140 (1960)

Garvin, H. L. - (see White, M. B. - UCRL-9429 Abstract)

Ghiorso, A. - no UCRL number
Diamond, H., Fields, P. R., Stevens, C. S., Studier, M. H., Fried, S. M., Inghram, M. G., Hess, D. C., Pyle, G. L., Mech, J. F., and Manning, W. M., from Argonne National Laboratory. Ghiorso, A., Thompson, S. G., Higgins, G. H., and Seaborg, G. T., from Lawrence Radiation Laboratory and the University of California. Browne, C. I., Smith, H. L., and Spence, R. W., from Los Alamos Scientific Laboratory.
Heavy Isotope Abundances in Mike Thermonuclear Device
No UCRL number August 1959
Phys. Rev. 119, 2000 (1960)

Ghiorso, A.
Modern Techniques in New Element Research
UCRL-9029 Abstract April 1960
ACS Meeting - Cleveland - April 1960

Ghiorso, A.
Recent Research with the Heaviest Elements
UCRL-9168 Abstract April 1960
Gatlinburg - May 1960

Gilmore, J.
The Effect of Angular Momentum on Fission Probability
UCRL-9304 August 1960
PhD Thesis

Glendenning, N. K. - (see Albert, R. D. - UCRL-6199)

Glendenning, N. K.
Theoretical Predictions for the Spectra of the Odd-Mass Xenon and Tellurium Isotopes
UCRL-8915 November 1959
Phys. Rev. 119, 213 (1960)

Glendenning, N. K. and Sawicki, J.
Nuclear Quadrupole Moments and Superfluidity
UCRL-9078 Abstract February 1960
APS Meeting - Washington - April 1960

Glendenning, N. K. and Bloom, S. D.
Proton-Neutron Interaction and the (p, n) Reaction in Mirror Nuclei
UCRL-9165 Abstract April 1960
Montreal Meeting - June 1960

Glendenning, N. K. and Sawicki, J.
Intrinsic Quadrupole Moments of Deformed Nuclei and Superfluidity
UCRL-9178 May 1960
Nuclear Physics 18, 596 (1960)

Glendenning, N. K. - (see Cranberg, L. - UCRL-9295)

Glendenning, N. K. and Sawicki, J.
Intrinsic Quadrupole Moments of Deformed Nuclei
UCRL-9303 July 1960
Kingston Conference

Gonzalez-Vidal, J., Conzett, H. C., and Wade, W. H.
(α, t) Differential Cross-Sections for Several Light Elements
UCRL-9082 Abstract February 1960
APS Meeting - Washington - April 1960

Gonzalez-Vidal, J. - (see Igo, G. - UCRL-9090 Abstract)

Gonzalez-Vidal, J., and Wade, W. H.
Survey of Tritium-Producing Nuclear Reactions
UCRL-9102 April 1960
Phys. Rev. 120, 1354 (1960).

Gonzalez-Vidal, J. - (see Alster, J. - UCRL-9432 Abstract)

Gordon, G. E., Larsh, A. E., and Sikkeland, T.
Angular Distribution of Fragments from Fission of Au^{197} with Carbon Ions
UCRL-9003 December 1959
Phys. Rev. 118, 1610 (1960)

Gordon, G. E., Kilian, G. W., Larsh, A. E., and Sikkeland, T.
Silicon P-N Junctions as Charged-Particle Detectors
UCRL-9052 January 1960
Phys. Rev. Letters

Gordon, G. E.
Fission and Spallation in Nuclear Reactions Induced by Heavy Ions
UCRL-9083 May 1960
PhD Thesis

Gordon, G. E. - (see Larsh, A. E. - UCRL-9139 Abstract)

Gordon, G. E. - (see Latimer, R. M. - UCRL-9217)

Gordon, G. E. - (see Larsh, A. E. - UCRL-9240)

Gordon, G. E., Larsh, A. E., Sikkeland, T., and Seaborg, G. T.
Fission of Gold by Carbon Ions
UCRL-9257 June 1960
Phys. Rev. 120, 1341 (1960)

Griffioen, R. D. and Rasmussen, J. O.
Analysis of Long Range Alpha-Emission Data
UCRL-9368 September 1960
Phys. Rev.

Gruber, J. B. and Conway, J. G.
Electronic Energy Levels and Crystal Quantum States of Tm (IV)
UCRL-8839 August 1959
J. Chem. Phys. 32, 1178 (1960)

Gruber, J. B., and Conway, J. G.
Crystal Field Splitting of Energy Levels of Thulium Ethylsulfate
UCRL-8869 September 1959
J. Chem. Phys. 32, 1531 (1960)

Gruber, J. B. - (see Conway, J. G. - UCRL-9042)

Gruber, J. B. - (see Conway, J. G. - UCRL-9116)

Gruber, J. B., and Conway, J. G.
Evaluation of Electrostatic Energy Levels of f^6
UCRL-9310 August 1960
J. Chem. Phys.

Haag, J. N., Johnson, C. E., Shirley, D. A., and Templeton, D. H.
Nuclear Moment of Ce^{137m} by Nuclear Alignment
UCRL-9299 July 1960
Phys. Rev.

Hamilton, J. H. - (see Albridge, R. G. - UCRL-9438)

Hamilton, J. H., Pettersson, B. G., and Hollander, J. M.
Beta- Gamma Directional Correlation in Rb^{86}
No UCRL number December 1960
Arkiv för Fysik

Hamilton, J. H., Pettersson, B. G., and Hollander, J. M.
Beta- Gamma Directional Correlation in Silver-111
No UCRL number December 1960
Arkiv för Fysik

Harvey, B. G. - (see Donovan, P. F. - UCRL-9060)

Harvey, B. G., Wade, W. H., and Donovan, P. F.
Recoil Studies of Heavy Element Nuclear Reactions. II.
UCRL-9061 February 1960
Phys. Rev. 119, 225 (1960)

Harvey, B. G., and Cerny, J.
Deuteron Spectra from Bombardment of C^{12}, N^{14}, and N^{15} with 48 Mev Helium Ions
UCRL-9081 Abstract February 1960
APS Meeting - Washington - April 1960

Harvey, B. G.
Recoil Techniques in Nuclear Reaction and Fission Studies
UCRL-9151 April 1960
Annual Review of Nuclear Science - Vol. 10 (1960)

Harvey, B. G., and Cerny, J.
The Reaction $C^{12}(\alpha, d)N^{14}$
UCRL-9259 June 1960
Phys. Rev. 120, 2162 (1960)

Harvey, B. G. - (see Cerny, J. - UCRL-9427 Abstract)

Harvey, B. G., Cerny, J., and Pehl, R. H.
Comparison of the Reactions $C^{12}(He^3, p)N^{14}$ and $C^{12}(\alpha, d)N^{14}$
UCRL-9428 Abstract October 1960
Bull. APS, Series II, 5, No. 7, p. 493 (1960)

Hoff, R. W., Hollander, J. M., and Michel, M. C.
The Neutron-Deficient Chain Sr^{80} - Rb^{80}
UCRL-5939-T(Livermore) April 1960
Physical Review

Hollander, J. M. - (see Hamilton, J. H. - no UCRL number)

Hollander, J. M. - (see Hamilton, J. H. - no UCRL number)

Hollander, J. M. - (see Hoff, R. W. - UCRL-5939-T)

Hollander, J. M. - (see Albridge, R. G. - UCRL-8034-Rev.)

Hollander, J. M. - (see Asaro, F. - UCRL-8786)

Hollander, J. M. - (see Albridge, R. G. - UCRL-9438)

Hollander, J. M. - (see Diamond, R. M. - UCRL-9467 Abstract)

Holmes, J. T.
Diffusion Coefficients in Multicomponent Solvents
UCRL-9145 April 1960
M. S. Thesis

Horen, D. - (see Bosch, H. E. - UCRL-9385-Rev.)

Horen, D. - (see Diamond, R. M. - UCRL-9467 Abstract)

Huffmann, E. H. - (see Jeung, E. UCRL-8739)

Hyde, E. K.
A Review of Nuclear Fission - Part I - Fission Phenomena at Low Energy
UCRL-9036 March 1960

Hyde, E. K.
A Review of Nuclear Fission - Part II - Fission Phenomena at Moderate and High Energy
UCRL-9065 March 1960

Hyde, E. K.
The Isotopes of Thorium, Protactinium, and Uranium
UCRL-9458 December 1960

Igo, G. - (see Nir, A. - No UCRL number)

Igo, G., Gonzalez-Vidal, J., and Markowitz, S.
The Elastic Scattering of 31 Mev He^3 Ions from Several Elements
UCRL-9090 Abstract February 1960
APS Meeting - Washington - April 1960

Igo, G.
Polarization of Nuclei in Direct Interactions
UCRL-9210 Abstract June 1960
Meeting - Bazel Switzerland - July-August 1960

Igo, G. - (see Diamond, R. M. - UCRL-9302)

Jeung, E. and Huffmann, E. H.
The Determination of Iodine in Thallium (I) Iodide Precipitates
UCRL-8739 May 1959
Analytical Chemistry 32, 152 (1960)

Johnson, C. E., Schooley, J. F., and Shirley, D. A.
Nuclear Orientation of Iodine by Electric HFS Alignment
UCRL-9216 May 1960
Phys. Rev. 120, 1777 (1960)

Johnson, C. E., Schooley, J. F., and Shirley, D. A.
Nuclear Alignment of Iodine by Quadrupole Coupling
UCRL-9241 May 1960
International Conference on Low Temperature Physics - Toronto, Canada

Johnson, C. E., Schooley, J. F., and Shirley, D. A.
Nuclear Orientation of Tb^{160}
UCRL-9267 July 1960
Phys. Rev. 120, 2108 (1960)

Johnson, C. E. - (see Haag, J. N. - UCRL-9299)

Johnson, Q. C. - (see Templeton, D. H. - UCRL-9195)

Johnson, Q. C.
Some Problems of Crystallography
UCRL-9350 November 1960
PhD Thesis

Johnson, Q. C., and Templeton, D. H.
Madelung Constants for Several Structures
UCRL-9439 November 1960
J. Chem. Phys.

Judd, B., and Lindgren, I.
Theory of Zeeman Effects in the Ground Multiplets of Rare Earth Atoms
UCRL-9188 May 1960
Phys. Rev.

Kaufman, W. J., Nir, A., and Parks, G.
Recent Advances in Low-Level Scintillation Counting of Tritium
No UCRL number - Abstract December 1960
IAEA Symposium on Detection and Use of Tritium in the Physical and Biological Sciences - Vienna, April 1961

Kilian, G. W. - (see Gordon, G. E. - UCRL-9052)

Kyi, R-T
Paramagnetic Resonance of Tetravalent Pa^{231}
UCRL-9109 April 1960
PhD Thesis

Kyi, R-T - (See Axe, J. D. - UCRL-9010)

Ladenbauer, I. M., and Winsberg, L.
Interaction of High-Energy Protons and Alpha Particles with Iodine-127
UCRL-8907 November 1959
Phys. Rev. 119, 1368 (1960)

Lang, S. B.
Use of Pyroelectric Devices for Measuring Small Temperature Changes
UCRL-9298 July 1960
Review of Scientific Instruments

Larsh, A. E. - (see Gordon, G. E. - UCRL-9003)

Larsh, A. E. - (see Gordon, G. E. - UCRL-9052)

Larsh, A. E., and Gordon, G. E.
Heavy Ion-Induced Nuclear Fission
UCRL-9139 Abstract May 1960
Gatlinburg - May 1960

Larsh, A. E., Gordon, G. E., and Sikkeland, T.
Use of Silicon p-n Junction Detectors in Studies of Nuclear Reactions Induced by Heavy Ions
UCRL-9240 June 1960
Review of Scientific Instruments 31, 1114 (1960)

Larsh, A. E. - (see Gordon, G. E. - UCRL-9257)

Latimer, R. M., Gordon, G. E., and Thomas, T. D.
Alpha-Particle Branching Ratios for Neutron-Deficient Astatine Isotopes
UCRL-9217 June 1960
J. Inorg. and Nuclear Chem.

Lessler, R. M., and Michel, M. C.
Identification of Np^{240} and Np^{241}
UCRL-8757 May 1959
Phys. Rev. 118, 263 (1960)

Lindgren, I., Cabezas, A., and Nierenberg, W.
Nuclear Spin and Hyperfine Structure of Tm^{170}
UCRL-9064 Abstract February 1960
APS Meeting - Washington - April 1960

Lindgren, I. - (see Cabezas, A. - UCRL-9122)

Lindgren, I. - (see Cabezas, A. - UCRL-9163)

Lindgren, I., Nierenberg, W., and Cabezas, A.
Relativistic and Diamagnetic Corrections of Atomic g-Values
UCRL-9184 May 1960

Lindgren, I. - (see Judd, B. - UCRL-9188)

Lindgren, I. - (see Cabezas, A. - UCRL-9425 Abstract)

Lipworth, E. - (see Cabezas, A. - UCRL-8776-Rev.)

Lipworth, E. - (see Garvin, H. L. - UCRL-9038)

Lipworth, E. - (see Alpert, S. S. - UCRL-9062 Abstract)

Lipworth, E. - (see White, M. B. - UCRL-9069 Abstract)

Lipworth, E. - (see Cabezas, A. - UCRL-9122)

Lipworth, E. - (see Alpert, S. S. - UCRL-9424 Abstract)

Lipworth, E. - (see White, M. B. - UCRL-9429 Abstract)

Lipworth, E. - (see Alpert, S. S. - UCRL-9474 Abstract)

Lovejoy, C. A., and Shirley, D. A.
Nuclear Orientation of Tb^{156}
UCRL-9236 May 1960
International Conference on Low Temperature Physics - Toronto, Canada

Lovejoy, C. A., Rasmussen, J. O., and Shirley, D. A.
Nuclear Orientation of Pm^{143}
UCRL-9452 November 1960
Phys. Rev.

Macfarlane, R. D.
Dysprosium-154, A Long-Lived Alpha Emitter
UCRL-9335 August 1960
J. of Inorg. and Nuclear Chem.

Macfarlane, R. D.
Concerning the Natural Occurrence of Samarium-146
UCRL-9352 October 1960
Nature

Mains, G. J., and Newton, A. S.
The Mercury-Sensitized Photolysis and Radiolysis of Methane
UCRL-9045-Rev. January 1960
J. Phys. Chem. 64, 511 (1960)

Mains, G. J., and Newton, A. S.
The Radiolysis of Biacetyl Vapor
UCRL-9363 September 1960

Mang, H. J.
Calculation of Alpha-Transition Probabilities
UCRL-8931-Rev. November 1959
Phys. Rev. 119, 1069 (1960)

Margulis, T. N., and Templeton, D. H.
Crystal and Molecular Structure of the Compound of Triethyl Phosphine and Carbon Disulfide
No UCRL number December 1960
J. Am. Chem. Soc.

Markowitz, S. - (see Igo, G. - UCRL-9090 Abstract)

Markowitz, S., and Chang, L.
$N^{14}(p, pn)N^{13}$ and $N^{15}(p, p2n)N^{13}$ Reactions Induced by Protons of Energy 0.4 to 6.2 Gev
UCRL-9468 Abstract November 1960
Bull. APS 6, February 1961

Marrus, R. - (see Cabezas, A. - UCRL-8776-Rev.)

Marrus, R. - (see Cabezas, A. - UCRL-9122)

Marrus, R., Nierenberg, W. A., and Winocur, J.
Hyperfine Structure of Americium-241
UCRL-9207 May 1960
Phys. Rev.

Marrus, R. - (see Cabezas, A. - UCRL-9425 Abstract)

Marshall, T.
I. Beta-Spectroscopic Studies in the Promethium Region
II. The Coriolis Interaction in Deformed Nuclei
UCRL-8740 May 1960
PhD Thesis

Michel, H. V.
Hindrance Factors for Alpha Decay
UCRL-9229 June 1960

Michel, M. C. - (see Naumann, R. A. - no UCRL number)

Michel, M. C. - (see Hoff, R. W. - UCRL-5939-T)

Michel, M. C. - (see Lessler, R. M. - UCRL-8757)

Michel, M. C. - (see Naumann, R. A. - UCRL-9206)

Michel, M. C., Power, J., and Naumann, R. A.
Preparation of Long-Lived Terbium-157 and Terbium-158
UCRL-9287 July 1960
J. Inorg. and Nuclear Chem.

Michel, M. C. - (see Asaro, F. - UCRL-9306 Abstract)

Michel, M. C. - (see Asaro, F. - UCRL-9381 Abstract)

Miyauchi, T., McMullen, A. K., and Vermeulen, T.
Longitudinal Dispersion in Two-Phase Continuous-Flow Operations: Calculation Methods
UCRL-3911-Rev. March 1960
Industrial and Engineering Chemistry - March 1960

Muga, M. L., Bowman, H. R., and Thompson, S. G.
Tripartition in the Spontaneuous-Fission Decay of Cf^{252}
UCRL-9044 October 1960
Phys. Rev.

McCarthy, I. E., and Pursey, D. L.
A Simple Treatment of Nuclear Direct Interaction Processes
No UCRL number July 1960
Kingston Conference - August/September 1960

McMullen, A. K. - (see Miyauchi, T. - UCRL-3911-Rev.)

McWhan, D. B., Wallmann, J. C., Cunningham, B. B., Asprey, L., Ellinger, F. H., and Zachariasen, W. H.
Preparation and Crystal Structure of Americium Metal
UCRL-9115 April 1960
J. Inorg. Nuclear Chem.

Nakamura, M. - (see Elbek, B. - UCRL-9405)

Naumann, R. A., Michel, M. C., and Power, J. L.
Mass Spectrometric Identification of Long-Lived Tb^{157}, Ho^{163}, Hf^{182}
No UCRL number December 1960
Bull. APS - Vol. 6, February 1961

Naumann, R. A., Michel, M. C., and Power, J. L.
The Preparation of Long Lived Holmium-163
UCRL-9206 May 1960
J. Inorg. and Nuclear Chem.

Naumann, R. A. - (see Michel, M. C. - UCRL-9287)

Naumann, R. A. - (see Diamond, R. M. - UCRL-9467 Abstract)

Nethaway, D. R., and Winsberg, L.
Interaction of High-Energy Protons with Indium
UCRL-8908 January 1960
Phys. Rev. 119, 1375 (1960)

Newby, N.
Tensor Force Effects in Off-Odd Nuclei
UCRL-9100 January 1960
Phys. Rev. 119, 747 (1960)

Newby, N.
Odd-Even Shifting in the K = 0 Band of Odd-Odd Deformed Nuclei
UCRL-9470 Abstract November 1960
APS Meeting - New York, February 1961

Newton, A. S.
The Radiation Chemistry of Organic Compounds Containing Electro-negative Groups
No UCRL number February 1960
Abstract - Meeting in Cleveland - March 1960

Newton, A. S. - (see Mains, G. J. - UCRL-9045-Rev.)

Newton, A. S. - (see Mains, G. J. - UCRL-9363)

Newton, J. O.
Auger Transitions in Re^{183} and the M3 Isomer in Os^{189}
UCRL-8798 June 1959
Phys. Rev. 117, 1529 (1960)

Newton, J. O.
The Decay of Os^{182} and Os^{183} (I) Gamma and Beta Spectroscopy
UCRL-8799 June 1959
Phys. Rev. 117, 1510 (1960)

Newton, J. O.
The Decay of Os^{182} and Os^{183} (II) Coincidences, Conversion Coefficients and Decay Schemes
UCRL-8800 June 1959
Phys. Rev. 117, 1520 (1960)

Nierenberg, W. - (see Lindgren, I. - UCRL-9064 Abstract)

Nierenberg, W. - (see Lindgren, I. - UCRL-9184)

Nierenberg, W. - (see Marrus, R. - UCRL-9207)

Nir, A. - (see Kaufmann, W. J. - No UCRL number - Abstract)

Nir, A., Conzett, H. E., and Igo, G.
Polarization in P-He^4 Scattering at 22-Mev
No UCRL number - Abstract October 1960
J. APS, Series II, Vol. 5, No. 7, p. 494, December 1960

Olovsson, I. - (see Ruben, H. - UCRL-8977)

Parks, G. - (see Kaufman, W. J. - no UCRL number - Abstract)

Pehl, R. H. - (see Cerny, J. - UCRL-9427 Abstract)

Pehl, R. H. - (see Harvey, B. G. - UCRL-9428 Abstract)

Perlman, I.
The History of Radioisotope Development
No UCRL number - Abstract February 1960
Western Industrial Radioisotopes Conference - San Francisco
Feb. 1960

Perlman, I. - (see Asaro, F. - UCRL-8786)

Perlman, I. - (see Stephens, F. S. - UCRL-8996)

Perlman, I. - (see Asaro, F. - UCRL-9047)

Perlman, I. - (see Asaro, F. - UCRL-9305)

Perlman, I. - (see Asaro, F. - UCRL-9306 Abstract)

Perlman, I. - (see Asaro, F. - UCRL-9307 Abstract)

Perlman, I. - (see Asaro, F. - UCRL-9308)

Perlman, I.
Comparison of Experimental Data on Energy Levels in the Deformed Medium and Heavy Nuclei with Nuclear Models, Particularly the Collective Model
UCRL-9369 Abstract August 1960
Kingston Conference

Perlman, I. - (see Asaro, F. - UCRL-9381 Abstract)

Perlman, I. - (see Asaro, F. - UCRL-9524)

Person, L. W., and Rasmussen, J. O.
Effect of Vibration-Rotation Interaction on E2 Transition Probabilities in Spheroidal Nuclei
UCRL-9230 August 1960

Pettersson, B. G. - (see Hamilton, J. H. - No UCRL number)

Pettersson, B. G. - (see Hamilton, J. H. - No UCRL number)

Power, J. L. - (see Naumann, R. A. - No UCRL number)

Power, J. L. - (see Naumann, R. A. - UCRL-9206)

Power, J. L. - (see Michel, M. C. - UCRL-9287)

Pursey, D. L. - (see McCarthy, I. E. - No UCRL number)

Rasmussen, J. O. (see Toth, K. S. - UCRL-8973)

Rasmussen, J. O. - (see Asaro, F. - UCRL-9047)

Rasmussen, J. O.
Theory of E0 Transitions of Spheroidal Nuclei
UCRL-9084 February 1960
Nuclear Physics 19, 85 (1960)

Rasmussen, J. O. - (see Person, L. W. - UCRL-9230)

Rasmussen, J. O. - (see Schooley, J. F. - UCRL-9232)

Rasmussen, J. O. - (see Shirley, D. A. - UCRL-9276)

Rasmussen, J. O., and Chiao, L.
Concerning the Magnetic Moments of Deformed Nuclei
UCRL-9301 July 1960
Kingston Conference

Rasmussen, J. O. - (see Griffioen, R. D. - UCRL-9368)

Rasmussen, J. O. - (see Lovejoy, C. A. - UCRL-9452)

Reddoch, A. H.
Nuclear Quadrupole Resonance in $TiCl_4$, and $ThCl_4$, $NdCl_5$, $TaCl_5$
UCRL-8972-Rev. December 1960
J. Chem. Phys.

Robinson, J. M.
Longitudinal Dispersion in Beds of Finely Divided Solids
UCRL-9193 May 1960
M. S. Thesis

Rosenstein, R. D. - (see Ruben, H. - UCRL-8977)

Ruben, H., Templeton, D. H., Rosenstein, R. D., and Olovsson, I.
Crystal Structure and Entropy of Sodium Sulfate Decahydrate
UCRL-8977 August 1960
J. Am. Chem. Soc.

Rubinstein, M. - (see Cabezas, A. - UCRL-9122)

Rubinstein, M. - (see Cabezas, A. - UCRL-9425 Abstract)

Sah, L. C.
$N^{15}(p, p2n)N^{13}$ Reaction Induced by Protons of Energy 0.4 to 6.2 Bev.
UCRL-9394 November 1960
M.S. Thesis

Sah, L. C. - (see Markowitz, S. S. - UCRL-9468 Abstract)

Sani, R.
Down Flow Boiling and Non-Boiling Heat Transfer in a Uniformly Heated Tube
UCRL-9023 January 1960
M. S. Thesis

Sawicki, J. - (see Glendenning, N. K. - UCRL-9078 Abstract)

Sawicki, J. - (see Glendenning, N. K. - UCRL-9178)

Sawicki, J. - (see Glendenning, N. K. - UCRL-9303)

Schooley, J. F. - (see Johnson, C. E. - UCRL-9216)

Schooley, J. F., Shirley, D. A., and Rasmussen, J. O.
Nuclear Orientation of Pm^{144}
UCRL-9232 May 1960
Meeting of International Conference on Low Temperature Physics, Toronto

Schooley, J. F. - (see Johnson, C. E. - UCRL-9241)

Schooley, J. F. - (see Johnson, C. E. - UCRL-9267)

Schooley, J. F. - (see Shirley, D. A. - UCRL-9276)

Schooley, J. F.
Some Low-Temperature Nuclear-Orientation Studies
UCRL-9296 July 1960
PhD Thesis

Seaborg, G. T. - (see Ghiorso, A. - No UCRL number)

Seaborg, G. T. - (see Gordon, G. E. - UCRL-9257)

Senko, M. E., and Templeton, D. H.
Unit Cells of Choline Halides and Structure of Choline Chloride
UCRL-3521-Rev. 2 January 1960
Acta. Cryst. 13, 281, (1960)

Shirley, D. A. - (see Johnson, C. E. - UCRL-9216)

Shirley, D. A. - (see Schooley, J. F. - UCRL-9232)

Shirley, D. A. - (see Lovejoy, C. A. - UCRL-9236)

Shirley, D. A. - (see Johnson, C. E. - UCRL-9241)

Shirley, D. A. - (see Johnson, C. E. - UCRL-9267)

Shirley, D. A., Schooley, J. F., and Rasmussen, J. O.
Gamma Ray Anisotropies from Oriented Pm^{144}
UCRL-9276 July 1960
Phys. Rev.

Shirley, D. A. - (see Haag, J. N. - UCRL-9299)

Shirley, D. A. - (see Lovejoy, C. A. - UCRL-9452)

Sikkeland, T. - (see Gordon, G. E. - UCRL-9003)

Sikkeland, T. - (see Gordon, G. E. - UCRL-9052)

Sikkeland, T. - (see Larsh, A. E. - UCRL-9240)

Sikkeland, T. - (see Gordon, G. E. - UCRL-9257)

Smith, K. F. - (see Alpert, S. S. - UCRL-9424 Abstract)

Smith, K. F. - (see Alpert, S. S. - UCRL-9474 Abstract)

Stapleton, H. J. - (see Axe, J. D. - UCRL-9010)

Stephens, F. S. - (see Asaro, F. - UCRL-8786)

Stephens, F. S., Asaro, F., and Perlman, I.
States of Even-Even Nuclei in the Near-Harmonic Region: Spectra of Rn-218, Rn-220, and Rn-222
UCRL-8996 February 1960
Phys. Rev. 119, 796 (1960)

Stephens, F. S. - (see Elbek, B. - UCRL-9156 Abstract)

Stephens, F. S. - (see Diamond, R. M. - UCRL-9302)

Stephens, F. S. - (see Asaro, F. - UCRL-9305)

Stephens, F. S. - (see Asaro, F. - UCRL-9307 Abstract)

Stephens, F. S. - (see Asaro, F. - UCRL-9382 Abstract)

Strom, E. T.
The Cross-Sections for the Formation of Astatine Isotopes made by the Bombardment of Bi^{209} with He^3
UCRL-9372 November 1960
M. S. Thesis

Templeton, D. H. - (see Margulis, T. N. - No UCRL number)

Templeton, D. H. - (see Senko, M. E. - UCRL-3521-Rev. 2)

Templeton, D. H. - (see Dodge, R. P. - UCRL-8225-Rev.)

Templeton, D. H.
Least Squares and Choice of Origin in Polar Space Groups
UCRL-8751 August 1959
Zeitschrift fur Kristallographie 113, 234 (1960)

Templeton, D. H., and Dauben, C. H.
Polarized Octahedra in Barium Tetratitanate
October 1959
J. Chem. Phys.

Templeton, D. H. - (see Ruben, H. - UCRL-8977)

Templeton, D. H.
Hydrogen Bonding in Zirconium Sulfate Tetrahydrate
UCRL-9051 January 1960
Acta Cryst 13, 684 (1960)

Templeton, D. H.
The Crystal Structure of Hydrogen Peroxide Dihydrate
UCRL-9101 Abstract February 1960
Proceedings of the Meeting of the International Congress of the International Union of Crystallography, Cambridge, England, August 1960

Templeton, D. H.
Dispersion Corrections for Atomic Scattering Factors
UCRL-9146 April 1960
International Tables for X-Ray Crystallography - Vol. III

Templeton, D. H. and Johnson, Q. C.
Computation of Madelung Sums and Crystal Energies
UCRL-9195 May 1960
Proceedings of the Conference on Computing Methods and Phase Problems in X-Ray Crystal Analysis - Glasgow, Scotland, August 1960

Templeton, D. H. - (see Haag, J. N. - UCRL-9299)

Templeton, D. H. - (see Johnson, Q. C. - UCRL-9439)

Thomas, T. D. - (see Latimer, R. M. - UCRL-9217)

Thompson, S. G. - (see Ghiorso, A. - No UCRL number)

Thompson, S. G. - (see Muga, M. L. - UCRL-9044)

Thompson, S. G. - (see Asaro, F. - UCRL-9047)

Thompson, S. G. - (see Asaro, F. - UCRL-9305)

Thompson, S. G. - (see Asaro, F. - UCRL-9306 Abstract)

Thompson, S. G. - (see Asaro, F. - UCRL-9307 Abstract)

Thompson, S. G. - (see Burnett, D. S. - UCRL-9321)

Thompson, S. G. - (see Asaro, F. - UCRL-9381 Abstract)

Thompson, S. G. - (see Asaro, F. - UCRL-9382 Abstract)

Toth, K. S., and Rasmussen, J. O.
Systematics of Alpha-Radioactivity in the Rare Earth Region
UCRL-8973 December 1959
Nuclear Physics 16, 474 (1960)

Tuck, D. G., and Diamond, R. M.
The Primary Solvation of the Proton in the Solvent Extraction of Mineral Acid
UCRL-8897-Rev. December 1960
Journal of Physical Chemistry

Unik, J. P.
Coincidence Measurements in Nuclear Decay Scheme Studies
UCRL-9105 April 1960
PhD Thesis

Unik, J. P.
Electron-Electron Coincidence Spectrometer BRS-IV
UCRL-9423 November 1960

Vermeulen, T. - (see Miyauchi, T. - UCRL-3911-Rev.)

Vanderveen, J. H.
Coalescence and Dispersion Rates in Agitated Liquid-Liquid Systems
UCRL-8733 December 1960
M. S. Thesis

Wade, W. H. - (see Donovan, P. F. - UCRL-9060)

Wade, W. H. - (see Harvey, B. G. - UCRL-9061)

Wade, W. H. - (see Gonzalez-Vidal, J. - UCRL-9082 Abstract

Wade, W. H. - (see Gonzalez-Vidal, J. - UCRL-9102)

Wakano, M. - (see Brandt, R., - No UCRL number)

Wallmann, J. C. - (see McWhan, D. B. - UCRL-9115)

Werner, F. G. - (see Brandt, R. - No UCRL number)

Wheeler, J. A. - (see Brandt, R. - No UCRL number)

White, M. B. - (see Alpert, S. S. - UCRL-9062 Abstract)

White, M. B. - (see Alpert, S. S. - UCRL-9424 Abstract)

White, M. B., Alpert, S. S., and Lipworth, E.
Nuclear Spin of Lu^{176m}
UCRL-9069 Abstract February 1960
APS Meeting - Washington - April 1960

White, M. B., Alpert, S. S., Garvin, H. L., and Lipworth, E.
Nuclear Moments of I^{132}
UCRL-9429 Abstract October 1960
Bull. APS, Series II, Vol. 5, No. 7, p. 504, December 1960

White, M. B. - (see Alpert, S. S. - UCRL-9474 Abstract)

Wilcox, W. R.
Fractional Crystallization from Melts
UCRL-9213 June 1960
PhD Thesis

Winocur, J. - (see Cabezas, A. - UCRL-8776-Rev.)

Winocur, J.
Some Nuclear and Electronic Ground State Properties of Pa^{233}, Am^{241}, and 16-hour Am^{242}
UCRL-9174 April 1960
PhD Thesis

Winocur, J. - (see Marrus, R. - UCRL-9207)

Winsberg, L. - (see Ladenbauer, I. M. - UCRL-8907)

Winsberg, L. - (see Nethaway, D. R. - UCRL-8908)

Winsberg, L. - (see Dostrovsky, I. - UCRL-8963)

Winsberg, L. - (see Clements, T. P. - UCRL-8982-Rev.)

Winsberg, L. - (see Alexander, J. - UCRL-8997)

Winsberg, L. - (see Clements, T. P. - UCRL-9043)

Winsberg, L. - (see Alexander, J. - UCRL-9118)

Winsberg, L. - (see Alexander, J. - UCRL-9152 Abstract)

Zachariasen, W. H. - (see McWhan, D. B. - UCRL-9115)

Zalkin, A. - (see Dodge, R. P. - UCRL-8225-Rev.)

Zietz, C. M.
A Mass-Spectrometric Investigation of Sulfur Vapor as a Function of Temperature
UCRL-9277 June 1960
PhD Thesis

AUTHOR INDEX

Albridge, R. G., Jr. 19, 22, 303
Alexander, J. M. 145, 174
Alpert, S. S. 220, 221, 222
Alster, J. 153
Appelman, E. H. 286
Asaro, F. 12, 28, 32, 39, 42, 46, 50, 57
Axe, J. D. 245, 246, 284
Axel, P. 89

Bjørnholm, S. 46
Blann, H. M. 289
Bowman, H. R. 184
Brandt, R. 120
Bromley, L. A. 270
Brown, M. 99
Burnett, D. S. 124

Cabezas, A. Y. 222, 279
Cerny, J. 133, 138
Chiao, L. 53, 65
Chu, Y. Y. 299
Conley, H. L. 296
Conway, J. G. 222, 228, 237
Conzett, H. E. 153, 174
Cunningham, B. B. 210, 218

Diamond, R. M. 25, 96, 208
Dodge, R. P. 203

Elbek, B. 25

Fenech, E. J. 297
Flamm, E. 292
Futrell, J. H. 196

Gallagher, C. J. 19
Garvin, H. L. 221
Gatti, R. 184
Gazdik, M. F. 145
Gibson, L. E. 99
Gilmore, J. 111
Glendenning, N. K. 143
Gonzalez-Vidal, J. 148, 177
Gordon, G. E. 101, 115, 248, 287
Goulding, F. S. 256
Griffioen, R. D. 17, 147
Gruber, J. B. 222, 228, 237

Haag, J. N. 84
Haines, E. 106
Hamilton, J. H. 19
Hansen, W. L. 256
Harvey, B. G. 133, 138
Hennico, A. 272
Hoff, R. W. 95
Hollander, J. M. 11, 19, 22, 57, 95, 96
Holmes, J. T. 265, 267
Horen, D. J. 53, 57, 96
Hubbard, E. L. 260
Huizenga, J. R. 128
Hultberg, S. 57

Igo, G. 25, 126, 128, 158, 174

Jeffries, C. M. 245
Johnson, C. E. 70, 73, 84
Johnson, Q. C. 293
Judd, B. R. 235

Kaplan, M. 89
Kaufman, W. J. 152
Kyi, R. 246

Larsh, A. E. 101, 115, 248
Lemmon, R. M. 189
Leres, R. G. 254
Lindgren, I. 222
Lipworth, E. 220, 221, 222

Macfarlane, R. D. 46
Mains, G. J. 190, 193
Margulis, T. N. 198
Markowitz, S. S. 158
Marrus, R. 219, 220, 222
Marshall, T. V. 285
Meredith, R. E. 264, 272
Michel, M. C. 32, 95
Miyauchi, T. 273
Mosier, D. F. 254
Mullen, R. T. 189
McMullen, K. 273
McWhan, D. B. 218

Naumann, R. A. 96
Navarro, Q. O. 79
Newby, N. D., Jr. 63, 64
Newton, A. S. 190, 193, 196
Nierenberg, W. A. 220
Nir, A. 152, 174

Olander, D. R. 265, 267, 276
Olovsson, I. 200

Parks, G. 152
Pehl, R. H. 138
Perlman, I. 12, 28, 32, 39, 42, 50, 57, 111
Phillips, L. 184

Rasmussen, J. O. 17, 32, 62, 65, 80
Reddoch, A. H. 247
Reynolds, F. L. 11, 189, 204
Robinson, J. M. 298
Rubenstein, M. 222
Ruiz, C. 42

Sah, L. C. 295
Sani, R. L. 270
Scheer, J. A. 99
Schooley, J. F. 70, 73, 80, 291
Shirley, D. A. 70, 73, 75, 79, 80, 84, 89
Sikkeland, T. 101, 115, 248
Smith, K. F. 220
Stapleton, H. J. 245, 246
Stephens, F. S., Jr. 12, 25, 28, 39, 57
Strom, E. T. 294

Templeton, D. H. 84, 198, 200, 203
Thompson, S. G. 28, 32, 39, 99, 111, 120, 124, 184
Tobias, C. W. 264, 272

Unik, J. P. 288

Vanderveen, J. H. 269
Vermeulen, T. 269, 272, 273
Viola, V. 109

Wade, W. H. 177
Wallmann, J. C. 11, 218
Westenbarger, G. A. 75
White, M. B. 220, 221, 222
Whitney, D. C. 208
Wilcox, W. R. 264
Wilke, C. R. 264, 265, 267
Wilkins, B. 126
Winocur, J. 220, 301
Winsberg, L. 145, 174
Wydler, A. A. 258

Zalkin, A. 203
Zietz, M. C. 283

This report was prepared as an account of Government sponsored work. Neither the United States, nor the Commission, nor any person acting on behalf of the Commission:

A. Makes any warranty or representation, expressed or implied, with respect to the accuracy, completeness, or usefulness of the information contained in this report, or that the use of any information, apparatus, method, or process disclosed in this report may not infringe privately owned rights; or

B. Assumes any liabilities with respect to the use of, or for damages resulting from the use of any information, apparatus, method, or process disclosed in this report.

As used in the above, "person acting on behalf of the Commission" includes any employee or contractor of the Commission, or employee of such contractor, to the extent that such employee or contractor of the Commission, or employee of such contractor prepares, disseminates, or provides access to, any information pursuant to his employment or contract with the Commission, or his employment with such contractor.